Source Contributions to the Size and Composition Distribution of Urban Particulate Air Pollution

Thesis by

Michael John Kleeman

In Partial Fulfillment of the Requirements

for the Degree of

Doctor of Philosophy

California Institute of Technology

Pasadena, California

1999

(Submitted October 5, 1998)

Acknowledgements

This thesis summarizes more than five years of research which could not have been completed without the support of colleagues, friends and family. I would like to take this opportunity to thank those people who have helped me during my time at Caltech.

The underlying foundation of this work is due in large part to the vision of my advisor, Glen Cass. His experience, encouragement, and commitment to excellence have not only improved the quality of my research but have made me a better scientist in the process.

The contributions to atmospheric aerosol modeling which I have made during my graduate career build upon the hard work of many previous students at Caltech. Special thanks are due to Rob Harley, who was principally responsible for the last major revision of the CIT trajectory and airshed models, and Annmarie Eldering who did much of the preliminary work to remove errors from the particulate emissions inventory and to incorporate aerosol calculations in the CIT trajectory model. The latest version of the module to calculate the formation of secondary organic aerosol species was developed in close collaboration with Jay Odum. Jay was a gifted researcher and a good friend. I know that I will miss him in the years to come.

The sampling portion of my research could not have been completed without the help of Jamie Schauer who coordinated all of the tests, ran the upstream sampling equipment, and provided a lot of sound engineering advice through all of my years at Caltech. Many other Cass group members

also provided a variety of assistance during the source sampling work including Mike Hannigan, Matt Fraser, and Phil Fine. I would like to thank Lara Hughes for all of her work in running the 1996 field sampling campaign, as well as Jonathon Allen, Christos Christoforou, Rob Johnson, Kimberley Prather and the entire Prather research group who were also involved in that work. Thanks are due to Bob Cary (Sunset Labs) for aerosol carbon analyses, Ilhan Olmez, Michael Ames, and Jec Gone (MIT) for neutron activation analysis of trace metals, and Lynn Salmon (Caltech) for ion chromatography / colorimetric analyses.

Dr. Mark Bassett and Dr. Xinqiu Zhang of the South Coast Air Quality Management District provided help with the emissions inventories and emissions control strategies which were used in the modeling studies described in Chapter 4 and Chapter 8. Model results shown in much of this work were produced using a Beowulf class parallel computer developed and supported by Thomas Sterling, Jan Lindheim, John Salmon, Paul Angelino and other members of the Center for Advanced Computer Research at Caltech.

Research is hard work, and it can seldom be maintained for long without the companionship of friends. I would like to thank Frank, Matt, Pat, Linda, Denis, Anne, Don, Courtney, Jay, Mike, Neil, Paul and Yvette with whom I have played basketball, soccer, softball, and football, with whom I have gone camping, hiking, skiing, and mountain biking, and with whom I have shared the excitement, joy, and pain of being a graduate student.

I would like to end by thanking the person who has been the single biggest influence on my life throughout all my years at Caltech. Thank you Lisa for your love, support and encouragement through the good times and the bad. This work is dedicated to you.

Abstract

A mechanistic air quality model is developed that represents the atmospheric aerosol as a source-oriented external mixture of particles. A source-oriented external mixture is created when particles are released to the atmosphere from sources having distinctly different particle size and composition distributions. These particles evolve separately in the atmosphere while interacting with a common gas phase distribution of pollutants. The model represents advection, turbulent diffusion, gas-phase photochemistry, diffusion of reactants and products to and from the particles, aerosol thermodynamics, heterogeneous chemical reactions within fogs, and dry deposition. Calculations track individual particles from specific sources and then quantify the contribution which each source makes to the size and composition distribution of ambient suspended particulate matter at downwind receptor sites. Model results that simulate the August 28, 1987, episode of the Southern California Air Quality Study (SCAQS) experiments show that hygroscopic background particles advected into the Los Angeles area are transformed significantly by secondary chemical reactions in the urban atmosphere in a way that shapes the largest peak in the ambient fine particle (PM2.5) size distribution. Source contributions from more than 50 separate types of primary particle emissions sources also are revealed through a new technique for displaying model outputs.

The air quality model is used to calculate the effects that alternative specific emissions control measures would have on air quality. Calculations show

that a control plan which combines nearly all available emissions reduction techniques for gas- and particle-phase pollutants could have cut atmospheric fine particle (PM2.5) concentrations approximately in half at Claremont, CA, on August 28, 1987, in the absence of any other changes.

Source tests are conducted to measure the size and chemical composition distribution of particles released from diesel vehicles, catalyst-equipped gasoline-powered vehicles, non-catalyst-equipped gasoline vehicles, meat cooking, wood burning, and cigarette smoke. These improved emissions data are combined with the air quality model, which then is used to determine the source origin of particulate matter in the Southern California atmosphere during field experiments conducted for purposes of model evaluation in September, 1996.

Contents

List of Tables

List of Figures

1 Introduction

1.1 Motivation

Particulate air pollution has been the focus of increasing attention during recent years due to studies which have linked elevated mortality rates to high levels of ambient fine particulate matter [1]. Based on this evidence, the United States Environmental Protection Agency (USEPA) has revised the National Ambient Air Quality Standard (NAAQS) for airborne particulate matter to regulate the ambient concentrations of particles with a diameter less the 2.5μm. Classification of particulate matter into "fine" (diameter, $d_p < 2.5\mu m$) and "coarse" (diameter, $d_p > 2.5\mu m$) fractions does not fully characterize the nature of the particles present in an urban atmosphere, however. Particle chemical composition is also an important factor since it influences the light scattering properties of particles [2] and possibly also the effects which inhaled particles have on human health. While many of the mechanisms that trigger respiratory and cardiac problems in response to airborne particle exposure remain unknown, evaluation of several of the hypotheses advanced to explain the health effects observed depends on being able to account for either the absolute number concentration and composition of ultrafine particles (diameter, $d_p < 0.1\mu m$; [3]) or specific details of individual particle chemical composition such as particle acidity [4] or trace metals content [5]. Thus, it is important to understand the factors which influence both the size and composition distribution of particulate matter in an urban atmosphere.

In large urban locations such as Los Angeles, the atmospheric aerosol is composed of a complicated mixture of many types of particles. Mechanistic air quality models have been developed that predict how these particles will evolve in the atmosphere in the presence of dilution, chemical reaction, gas-to-particle conversion processes, and deposition at the Earth's surface [6, 7, 8, 9, 10, 11, 12]. Despite the experimental evidence which shows that particles co-exist in the atmosphere that have the same diameter but very different chemical compositions [13, 14, 15], all of the air quality models which have been demonstrated to date represent the ambient particles as if they have the same chemical composition if they have the same diameter at any given time and location. This simplification not only distorts the calculated effect which the model aerosol will have on visibility and human health, but it also may modify the calculated evolution of the aerosol as it undergoes gas-to-particle conversion processes, since calculations of this type are influenced by the initial chemical composition and hygroscopic behaviour of the particles under consideration. As mechanistic air quality models become more sophisticated in representing aqueous kinetic reactions and gas-to-particle conversion processes (for both inorganic and organic compounds), improvements must also be made to the way in which the atmospheric aerosol itself is represented if the accuracy of the overall calculation is to be increased.

Strategies to improve ambient air quality in large urban centers typically involve the reduction of emissions from primary pollutant sources. When undertaking the preliminary design of control strategies to limit airborne particle concentrations, it is useful to be able to observe the separate contributions that different emissions sources make to the ambient particle size distribution and chemical composition. Traditional methods for separately visualizing source contributions to particulate air quality rely on receptor-

oriented statistical models [16] or non-reactive transport models [17]. These techniques have several limitations. Receptor-oriented statistical models can only separate the contributions from a limited number of sources, cannot calculate the effect of source contributions on different parts of the ambient particle size distribution, and do not show the association between secondary particulate matter (formed from gaseous precursors by chemical reactions in the atmosphere) and primary particulate matter (released in the particle phase directly from a source). Non-reactive transport models cannot calculate the concentration of secondary particulate matter that is formed by atmospheric chemical reactions, which may constitute a significant fraction of the atmospheric aerosol in heavily populated regions.

Mechanistic air quality models can be developed that solve an initial value problem in which the size and composition of particles are specified at the time of release to the atmosphere followed by transformation of the particles as they participate in atmospheric chemical reaction processes. With detailed attention to this process, the particles emitted from different sources which therefore have different emitted chemical compositions could be tracked separately through the atmosphere, thereby preserving both the chemical details of the particles that may be important to public health as well as the information that indicates which sources should be controlled in order to reduce the public's exposure to elevated particle concentrations. The accuracy of model results is limited by the weakest link in the chain of calculations; historically this has been the data which describe the size and composition distribution of particles as they are released from the emissions sources.

1.2 Research Objectives

The research summarized in this thesis has three primary objectives:

1) Create an air quality model in which the individual particles emitted from characteristically different source types evolve separately in the atmosphere based on their initial size and composition distribution as they undergo gas-to-particle conversion processes. In previous models, particles once emitted to the atmosphere have been mixed into the ambient aerosol size and composition distribution in a way that knowledge of the source origin of the particles is lost and in a way that assumes that all particles of the same size have exactly the same chemical composition. The new model envisioned here will provide a valuable tool which allows for the examination of the contributions from different emissions sources to the size and composition distribution of ambient particulate matter and in the future will also permit the predicted heterogeneity of atmospheric particle chemical composition to be compared to observations of single particle composition acquired by aerosol time of flight mass spectrometers [13]. Proposed emissions control programs to improve air quality can then be evaluated in advance of their adoption with a greater understanding of their expected effect on the atmospheric aerosol.

2) Characterize experimentally the size and composition distribution of particulate matter emitted from contemporary sources of urban particulate air pollution. Improved data of this type will increase the accuracy of the overall chain of mechanistic modeling calculations.

3) Combine the improvements to mechanistic modeling calculations and improved input data to demonstrate the ability of the new modeling system to predict air quality parameters measured during field studies conducted in the South Coast Air Basin of Southern California during the summer of 1996.

1.3 Approach

This section provides an overview of the research presented in the rest of this thesis. Chapter 2 describes the development of a mechanistic air quality model which can represent the atmospheric aerosol as an internal mixture or as a source-oriented external mixture. In an internally mixed aerosol, all particles of the same size are represented as if they have exactly the same chemical composition. In contrast, in a model that represents the aerosol as a source-oriented external mixture, particles are released to the atmosphere having the characteristically different size and composition distributions determined at their source. These particles evolve separately in the atmosphere while interacting with a common gas phase distribution of pollutants. The result is an externally mixed aerosol in which many particles having different chemical compositions exist at any particle size. Model components are tested using both approaches in order to quantify the extent of distortion of the aerosol size and composition distribution which results from the use of the internal mixture approximation. The source-oriented external mixture model is then applied using data from the August 28, 1987, episode of the Southern California Air Quality Study (SCAQS) in order to predict ambient air quality at Claremont, CA. Model results are compared to ambient data collected using electronic particle size distribution monitors, filter-based samplers, and cascade impactors.

In Chapter 3, the source-oriented external mixture model is employed to calculate the separate contribution that emissions from different types of air pollution sources make to ambient particle concentrations. Model performance is illustrated by calculating source contributions to the size and composition distribution of the ambient aerosol at Claremont, CA. During

this work, the model is modified to distinguish between particles having different ages since their time of release to the atmosphere, and the secondary aerosol coatings that accumulate on primary particles over time are quantified.

In Chapter 4 the source-oriented external mixture model is used to examine how the ambient aerosol size distribution and chemical composition would be affected by individual and combined emissions control strategies. 11 primary particle control measures and 79 control measures applicable to gaseous sources of aerosol precursors are examined to determine their effects on air quality in Southern California.

The computational burden imposed when tracking an externally mixed aerosol increases linearly as the number of different types of particles that must be tracked separately through the governing differential equations in the model increases. In Chapter 5, a technique is developed that greatly enhances the ability of the source-oriented external mixture model to separate the airborne particle contribution due to individual emissions sources from each other without significantly increasing the computational burden required to exercise the model.

Chapters 6 and 7 describe a source testing program undertaken to better characterize the size and chemical composition distribution of particulate matter released from present-day sources of urban air pollution. This information is needed to model recent air quality episodes. Chapter 6 describes the characterization of particulate matter released from catalyst-equipped gasoline-powered vehicles, non-catalyst gasoline-powered vehicles, and medium-duty diesel trucks. The relative release rate of particulate matter during cold start, hot running, and the hot start portion of the standard Federal Test Procedure urban driving cycle are examined. Chapter 7 de-

scribes the characterization of particulate matter released from wood burning, meat charbroiling, and cigarette smoke.

In Chapter 8, the newly acquired data on source emissions are applied through the source-oriented external mixture model to study an air quality episode that occurred in Southern California over the period September 24-25, 1996. Comparisons are made between model results and measurements made by filter-based samplers and cascade impactors. Data on single particle size and chemical composition also were taken by aerosol time of flight mass spectrometers during the September 1996 field experiments. The aerosol time of flight mass spectrometers measure single particle characteristics in much the same way that the source-oriented external mixture model predicts single particle chemical composition. Analysis of the data from the September 1996 experiments is thus a prerequisite step toward eventually comparing single particle measurements to the predictions of single particle chemical composition that are derived by the air quality model developed here.

Finally, in Chapter 9 the major results of this research are summarized. Important accomplishments are highlighted, and areas for future research are identified.

Bibliography

[1] Douglas W. Dockery, C. Arden Pope, Xinping Xu, John D. Spengler, James H. Ware, Martha E. Fay, Benjamin G. Ferris, and Frank E. Speizer. An association between air pollution and mortality in six U.S. cities. *The New England Journal of Medicine*, 329(24):1753–1759, 1993.

[2] NRC (National Research Council). *Protecting Visibility in National Parks and Wilderness Areas.* National Academy Press, Washington, DC, 1993.

[3] G. Oberdorster, R. M. Gelein, J. Ferin, and B. Weiss. Association of particulate air pollution and acute mortality, involvement of ultrafine particles? *Inhalation Toxicology*, 7:111–124, 1995.

[4] R. B. Schlesinger. Factors affecting the response of lung clearance systems to acid aerosols - Role of exposure concentration, exposure time and relative acidity. *Environ. Health Perspect.*, 79:121–126, 1989.

[5] K. L. Dreher, R. H. Jaskot, J. R. Lehmann, J. H. Richards, J. K. McGee, A. J. Ghio, and D. L. Costa. Soluable transition metals mediate residual oil fly ash induced acute lung injury. *Journal of Toxicology and Environ. Health*, 50:285–305, 1997.

[6] C. Seigneur, A. B. Hudischewskyj, John H. Seinfeld, K. T. Whitby, J. R. Brock, and H. M. Barnes. Simulation of aerosol dynamics - a compar-

ative review of mathematical-models. *Aerosol Sci. Technol.*, 5:205–222, 1986.

[7] A. B. Hudischewskyj and C. Seigneur. Mathematical modeling of the chemistry and physics of aerosols in plumes. *Environ. Sci. Technol.*, 23:413–421, 1989.

[8] Spyros N. Pandis, Anthony S. Wexler, and John H. Seinfeld. Secondary organic aerosol formation and transport – II. Predicting the ambient secondary organic aerosol size distribution. *Atmos. Environ.*, 27A:2403–2416, 1993.

[9] Annmarie Eldering and Glen R. Cass. Source–oriented model for air pollutant effects on visibility. *J. Geophys. Res.*, 101(D14):19343–19369, 1996.

[10] F. S. Binkowski and U. Shankar. The regional particulate matter model 1. Model description and preliminary results. *J. Geophys. Res.*, 100(D12):26191–26209, 1995.

[11] P. Middleton and S. Burns. Denver air quality modeling study. In *Annual International Meeting*, Air and Waste Management Association, Vancouver, B.C., Canada, 1991.

[12] Christodoulos Pilinis and John H. Seinfeld. Development and evaluation of an Eulerian photochemical gas–aerosol model. *Atmos. Environ.*, 22:1985–2001, 1988.

[13] Christopher A. Noble and Kimberly A. Prather. Real-time measurement of correlated size and composition profiles of individual atmospheric aerosol particles. *Environ. Sci. Technol.*, 30(9):2667–2680, 1996.

[14] X. Q. Zhang, P. H. McMurry, S. V. Hering, and G. S. Casuccio. Mixing characteristics and water content of submicron aerosols measured in Los Angeles and at the Grand Canyon. *Atmos. Environ.*, 27A:1593–1607, 1993.

[15] Mary P. Ligocki, Harvey I. H. Liu, Glen R. Cass, and Walter John. Measurements of particle deposition rates inside southern California museums. *Aerosol Sci. Technol.*, 13:85–101, 1990.

[16] James J. Schauer, Wolfgang Rogge, Lynn M. Hildemann, Monica A. Mazurek, Glen R. Cass, and Bernd R. T. Simoneit. Source apportionment of airborne particulate matter using organic compounds as tracers. *Atmos. Environ.*, 30(22):3837–3855, 1996.

[17] H. Andrew Gray and Glen R. Cass. Source contributions to atmospheric carbon particles. *Atmos. Environ.*, in press, 1998.

2 Modeling the Airborne Particle Complex as a Source-Oriented External Mixture

[1]

2.1 Introduction

Mechanistic air quality models are presently being formulated that track primary emissions of particles and gases in the atmosphere as these pollutants undergo dilution, chemical reaction, gas-to-particle conversion processes, and deposition at the Earth's surface [1, 2, 3, 4, 5, 6, 7]. These models seek to predict the size distribution and chemical composition of ambient particles, and from such information, predictions of radiative transfer through the atmosphere can be made. Accurate calculations of the effect of source emissions on particle size and composition are important for understanding how to control urban/regional visibility problems [8] as well as the large-scale effects that air pollutants can have, such as climate forcing [9, 10]. Another important application of detailed aerosol calculations is related to the adverse health effects associated with inhalation of airborne fine particles. While many of the mechanisms that trigger respiratory and cardiac problems in response to airborne particle exposure remain unknown, evaluation of several of the

[1]Reference: Kleeman, M. J.; Eldering, A.; Cass, G. R. Modeling the Airborne Particle Complex as a Source-oriented External Mixture. *J. Geophys. Res.*, **102**, 1997: 21355-21372.

hypotheses advanced to explain the health effects observed depends on being able to account for either the absolute number concentration and composition of ultrafine particles (diameter, $d_p < 0.1$ μm) [11] or the specific details of individual particle chemical composition such as particle acidity or trace metals content [12, 13].

An internally mixed aerosol is defined as one in which all particles of the same size have exactly the same chemical composition. The atmospheric aerosol processes air quality models that have been demonstrated to date all represent the particles as an internal mixture even though several experiments have shown that this assumption may not be accurate. Zhang et al. [14] used a tandem differential mobility analyzer to demonstrate that the ambient aerosol at Claremont, California, contains particles having different hygroscopic characteristics at the same particle size, suggesting that particles of the same size have different chemical compositions. Ligocki et al. [15] examined the chemical composition of particles deposited from the atmosphere using a scanning electron microscope equipped with an X-ray spectrometer and also found significant variability in the chemical composition of particles with the same diameter. While previous air quality models using moving size sections to represent the aerosol may develop situations where particles in adjacent size bins begin to overlap in size because of differences in the rate of gas-to-particle conversion processes, the degree of heterogeneity between particles of the same size in those models is still small compared with that measured in the atmosphere by aerosol time-of-flight mass spectrometers [16].

The purpose of this chapter is to demonstrate the properties of an aerosol processes air quality model in which the airborne particles are represented as a source-oriented external mixture. An externally mixed aerosol is one in which different particles of the same size can have different chemical com-

positions. In the extreme an external mixture would consist of particles containing only model pure substances, such as pure ammonium sulfate in many particles of one type separated from other particles made entirely of organic compounds or pure elemental carbon. However, such complete segregation of chemical substances is no more realistic than the idealization that all particles are internally mixed. Instead, we conceive of the aerosol as a source-oriented external mixture in which the individual chemical composition of the primary seed particles emitted at their source reflects the possibly complex chemical composition of the effluent from that source. The aerosol then contains particles with different chemical compositions at the same size as seed particles from characteristically different emissions source types enter into the same air parcel and evolve over time.

2.2 Model Formulation

In the present study, the Lagrangian aerosol processes trajectory models developed previously by Eldering and Cass [4], Russell et al. [17], and Russell and Cass [18] are expanded to produce a model capable of representing the ambient aerosol either as an internal or as a source-oriented external mixture of particles. In the model of Eldering and Cass a countable number of discrete particles, having initial sizes and chemical compositions determined by the source from which they were emitted, are inserted into a vertical stack of computational cells as it is advected across the airshed. Along a typical trajectory crossing the South Coast Air Basin of California and terminating at Claremont on August 28, 1987, approximately 10^{20} particles are emitted into the model. Air parcel trajectories and mixing depths are determined from three-dimensional wind fields and mixing depth fields interpolated from observational data by the methods of Goodin et al. [19]. Within each computa-

tional cell, atmospheric gas-phase chemical reactions are modeled according to the chemical mechanism of Carter [20] with extensions to track condensible organic gases that may form secondary organic aerosol [21]. Diffusion of gases to and from particles is calculated according to the AIM computer code of Wexler and Seinfeld [22]. Dry deposition of particles as a function of size is calculated from atmospheric boundary layer theory, as is dry deposition of reactive gases. An approximate fog model is used to track sulfate formation within fog droplets due to SO_2 oxidation in the aqueous phase by dissolved hydrogen peroxide, dissolved ozone, or dissolved oxygen in the presence of trace metal catalysts.

The processes listed above may be described by a Lagrangian trajectory form of the atmospheric diffusion equation

$$\begin{aligned} \frac{\partial G_j}{\partial t} &= \frac{\partial}{\partial z}(K_{zz}\frac{\partial G_j}{\partial z}) - \sum_k L_{ij}^k(G, P^k, T, \mathrm{RH}) \\ &\quad + R_j(G, T, \mathrm{RH}); \quad \mathrm{j} = 1, 2, ..., \mathrm{n} \end{aligned} \tag{2.1}$$

$$\begin{aligned} \frac{\partial P_i^k}{\partial t} &= \frac{\partial}{\partial z}(K_{zz}\frac{\partial P_i^k}{\partial z}) + \sum_j L_{ij}^k(G, P^k, T, \mathrm{RH}) \\ &\quad + M_i^k(P^k, T, \mathrm{RH}); \quad \mathrm{i} = 1, 2, ..., \mathrm{m} \end{aligned} \tag{2.2}$$

where G_j is the gas-phase concentration of species j, P_i^k is the concentration of chemical species i present in particles of type k, K_{zz} is the turbulent eddy diffusivity in the vertical direction z, L_{ij}^k is the gas-to-particle conversion rate for gas-phase species j which form aerosol-phase species i on particles of type k, R_j is the rate of production of gas-phase species j due to gas-phase reaction, M_i^k is the rate of production of species i within particles of type k

due to aqueous-phase chemical reaction, T is the absolute temperature, and RH is the ambient relative humidity. Pollutant emissions and dry deposition processes are incorporated into the boundary conditions for the ground level cell in the model. Coagulation and nucleation are neglected relative to other processes for the case of the relatively dilute atmospheric systems of interest to regional air pollution problems. Test calculations applied to self-coagulation of an urban aerosol like that studied during the applications in this chapter show that the time scale for coagulation is greater than 17 hours, much longer than for other processes in the model. If conditions are encountered elsewhere in which coagulation and nucleation should not be neglected, then these processes can be added to the model.

In the original model of Eldering and Cass [4], particle-phase emissions from each source are internally mixed into the preexisting ambient aerosol when they enter the atmosphere. The purpose of the research described in the present study is to create a source-oriented external mixture of particles by continuing to differentiate between particles emitted from different sources even after they are released into the atmosphere. This formulation greatly increases the computational burden of the problem, and so efficiency improvements also are necessary to make calculations tractable. Each major feature of the model which differs significantly from the description given by Eldering and Cass [4] is discussed in the following sections.

2.2.1 Emissions Model

The model of Eldering and Cass [4] represents particles emitted from a single source type as if they had a discrete distribution where the initial diameters of the primary particles occur at 15 discrete sizes centered at equally spaced logarithmic size intervals spanning the diameter range from 0.01 μm to 10

μm. The number of particles emitted at a given size is calculated using the mass emission rate within each logarithmic size interval for the source under consideration and the particle density calculation method described by Larson et al. [23]. The size distribution and chemical composition of the particles from each of the major emission source types that occur in an urban area are principally obtained from the source test program conducted by Hildemann et al. [24, 25] supplemented by other data sources as described by Eldering and Cass [4].

In the present chapter, a source-oriented external mixture of particles is created by differentiating the primary particles emitted from the following source types: catalyst-equipped gasoline engines, non-catalyst-equipped gasoline engines, diesel engines, meat cooking, paved road dust, crustal material from sources other than paved road dust, and acidic aerosol from industrial processes. Particulate emissions from the remaining sources are combined to produce a single lumped source category having a chemical composition equivalent to the weighted average composition of the many remaining small sources that are grouped together. The individual particles emitted from each of the source types listed above are described in terms of their content of the following chemical components: elemental carbon, organic carbon, sodium, chloride, ammonium, sulfite, sulfate, nitrate, iron (oxidation states II and III), manganese (oxidation states II and III), copper (oxidation states I and II), all remaining metals as a single group, and all other nonmetallic species as a single group. The distribution of iron between oxidation states is represented according to the data of Erel et al. [26] as Fe(II)/Fe(III) = 51/49 based on analysis of fog water samples taken in the Los Angeles area. The distribution of manganese and copper between possible oxidation states is taken from Jacob et al. [27] based on measure-

ments made at Bakersfield, California. This distribution is Cu(I)/Cu(II) = 10/90 and Mn(II)/Mn(III) = 600/1. The relative chemical composition of all particles from the same source is assumed to be identical since data that distinguish differences in the composition of particles of different sizes from the same source are not available in general.

Gas-to-particle conversion processes represented within the model require that gaseous pollutant emission data for oxides of nitrogen, volatile organic species, ammonia, and SO_2 be supplied to the model. These emissions are represented as described by Harley et al. [28, 29, 30] and Eldering and Cass [4].

2.2.2 Vertical Transport and Dry Deposition

Vertical transport due to turbulent diffusion is specified between five computational cells with thicknesses (beginning at ground level and proceeding upward) of 34.5 m, 105.5 m, 140 m, 330 m, and 390 m resulting in a modeling region 1000 m thick. Calculation of the dry deposition of gas-phase pollutants is based on boundary layer theory and land-use specific surface resistances as described by Russell et al. [31]. Vertical transport of particle-phase species is based on particle number concentrations per cubic meter of air exchanged and is calculated numerically using the Crank-Nicholson method [32].

Dry deposition of particles follows the method described by Slinn and Slinn [33] and Seinfeld [34] with appropriate modifications to account for the effect of changes in atmospheric stability conditions. The resultant equation for the deposition velocity of particles of type k, v_p^k, may be written as

$$v_p^k = \frac{1}{r_C^k + r_D^k + r_C^k r_D^k v_s^k(a_d^k)} + v_s^k(a_d^k) \tag{2.3}$$

with

$$(r_D^k)^{-1} = u_*[(Sc^k)^{-2/3} + 10^{-3/St^k}] \tag{2.4}$$

where r_C^k is is the resistance to deposition in the constant flux layer, r_D^k is the resistance in the sublayer immediately adjacent to the ground, u_* is the friction velocity, Sc^k is the Schmidt number for particles of size k, St^k is the Stokes number for particles of size k, and v_s^k is the gravitational settling velocity of particles with aerodynamic diameter a_d^k. In the present study, representation of the resistance term r_C^k has been improved and depends on atmospheric stability conditions as described by McRae et al. [35]:

Stable conditions

$$r_C^k = \frac{0.74}{k_V u_*} \ln(\frac{z_r}{z_0}) + \frac{4.7}{L k_V u_*}(z_r - z_0) \tag{2.5}$$

Neutral conditions

$$r_C^k = \frac{0.74}{k_V u_*} \ln(\frac{z_r}{z_0}) \tag{2.6}$$

Unstable conditions

$$r_C^k = \frac{0.74}{k_V u_*} \left\{ \ln\left[\frac{\gamma_1 - 1}{\gamma_1 + 1}\right] - \ln\left[\frac{\gamma_2 - 1}{\gamma_2 + 1}\right] \right\} \tag{2.7}$$

where $\gamma_1 = \sqrt{1 - 9\frac{z_r}{L}}$, $\gamma_2 = \sqrt{1 - 9\frac{z_0}{L}}$, k_V is the Von Karman constant, z is elevation above ground level, z_r is the pollutant measurement reference height (10 m), z_0 is the surface roughness height, and L is the Monin-Obukhov length. Values of the surface roughness height z_0 are obtained from detailed land-use maps as described by Russell et al. [31].

2.2.3 Gas-to-Particle Conversion: Large Aerosol Water Content

In the present study, the approximate fog model of Eldering and Cass [4] is replaced by a more exact treatment. The model used to describe liquid-phase chemical conversion under these conditions follows the approach of Jacob [36] and Jacob et al. [27]. Dissolution of gas-phase species into the aqueous phase is considered for NH_3, HCl, CH_3OH, HCOOH, CH_3O_2, CH_3OOH, $CH_3C(O)OOH$, OH, HNO_3, H_2O_2, HO_2, O_3, NO, NO_2, NO_3, HNO_4, HCHO, CHOCHO, $CH_3C(O)CHO$, SO_2, HONO, and CH_3COOH. The rate equation that describes transport between the gas phase and the particle or droplet phase within the fog module is

$$\frac{\partial P_i^k}{\partial t} = 4\pi N_k D_i r_k \alpha_i (G_i^\infty - G_i^s) \tag{2.8}$$

where P_i^k is the concentration (μmole m^{-3} air) of the i^{th} chemical species within the liquid phase associated with particles of type k, N_k is the ambient number concentration of particles of type k, D_i is the gas-phase molecular diffusivity of chemical species i, r_k is the radius of particles of type k, α_i is the accommodation coefficient for collision of gaseous chemical species i with the aqueous phase, G_i^∞ is the ambient gas-phase concentration of chemical species i, and G_i^s is the gas-phase concentration of chemical species i at the droplet surface. Gas-phase molecular diffusivities are estimated by the method of Wilke and Lee [37], when data on boiling points are available, and the method of Fuller, Schettler, and Giddings [37], when no data on boiling points are available. The accommodation coefficient for all chemical species is assumed to be 0.1.

The exchange of NH_3 between the gas and the aqueous phases requires special attention at high pH because the aqueous concentrations of NH_4^+ and H^+ become closely coupled. Since an extremely small time step is required for

integration under these conditions, this calculation is done separately from the rest of the equation set to improve numerical efficiency. An explicit form of Euler's method is used to integrate equation (2.8) for NH_3 along with the following equation describing the evolution of aqueous hydrogen ion:

$$\frac{\partial[H^+]}{\partial t} = \frac{\partial[H^+]}{\partial[N(-III)]} \frac{\partial[N(-III)]}{\partial t} \tag{2.9}$$

where $[H^+]$ is the concentration of hydrogen ion in solution, and [N(-III)] is the aqueous concentration of NH_3 plus NH_4^+. The gas-phase concentration of NH_3 at the particle surface needed in equation (2.8) is related to aqueous-phase NH_3 concentrations via Henry's law for ammonia according to the treatment of Jacob [36]. The term $\frac{\partial[H^+]}{\partial[N(-III)]}$ is calculated using perturbation analysis every time the pH of a particular droplet shifts by more than 0.5 units.

Species in aqueous solution are acted on by a kinetic reaction mechanism focusing on the oxidation of sulfur via pathways including iron, manganese and copper catalysis in addition to reaction with dissolved O_3 and H_2O_2. The mechanism consists of 58 active chemical species undergoing 177 reactions while constrained by 29 equilibrium relationships. Temperature corrections to rate and equilibrium constants are made using thermodynamic data from Jacob [36], Jacob et al. [27], and Wagman et al. [38]. Ionic strength corrections to equilibrium calculations are made using the Davies method as described by Stumm and Morgan [39]. The simultaneous nonlinear equations describing the equilibrium system are solved using the MICROQL technique described by Westall [40].

When meteorological observations indicate that the air parcel studied is entering a fog, the critical radius and critical saturation ratio for each particle is calculated according to the Kohler equation as described by Pruppacher

and Klett [41]. Those particles with a critical saturation ratio less than the ambient saturation ratio are activated to form fog droplets, while particles with a higher critical saturation ratio are not activated and thus remain as interstitial aerosol. Droplet growth occurs by condensation of water vapor which is calculated according to the method described by Pruppacher and Klett [41] with data on osmotic coefficients from Robinson and Stokes [42].

2.2.4 Gas-to-Particle Conversion: Small Aerosol Water Content

In the absence of fog, aerosol liquid water content is small but nonzero during periods when the ambient relative humidity is greater than the relative humidity of deliquescence for the particles in the atmosphere. The gas-to-particle conversion calculations for particles under these conditions are based on the framework of the computer code AIM developed by Wexler and Seinfeld [22]. During the construction of the model described in this study, it was discovered that the original AIM algorithm does not permit the crystallization of solid-phase species as aerosol water content decreases below the point where this should occur under conditions where particles contain more than one possible solid-phase component. This problem was corrected and the convergence criteria for particle-phase equilibrium were altered to ensure that the driving potential for the formation of an additional amount of each solid-phase species was zero at equilibrium.

The original version of AIM considers gas-phase water concentrations to be in equilibrium with particle-phase concentrations using the Zdanovskii, Stokes, and Robinson (ZSR) method described by Wexler and Seinfeld [22]. During model development it was discovered that if aerosol water content is treated in a kinetic fashion then the efficiency of the overall solution method could be improved. The equations describing the kinetic exchange of wa-

ter between the gas and the particle phases are taken from Pruppacher and Klett [41]. Data on osmotic coefficients are obtained from the original version of AIM with modifications for the electrolytes $(NH_4)_2SO_4$, NH_4HSO_4, $(NH_4)_3H(SO_4)_2$, Na_2SO_4, $NaHSO_4$, and $NaNO_3$ based on the data of Tang and Munkelwitz [43]. The original version of AIM uses the Kusik and Meissner method to calculate binary activity coefficients for ion pairs in solution and then uses an alternative approximation to calculate activity coefficients in multicomponent solutions. The method used to estimate the multicomponent activity coefficients was modified to more closely follow the treatment shown by Kusik and Meissner [44].

2.2.5 Gas-to-Particle Conversion: Zero Aerosol Water Content

During periods of low relative humidity the liquid water shell surrounding atmospheric particles may disappear entirely, leaving a solid particle core exposed to the gas phase. Gas-to-particle conversion may still occur under these conditions, but the flux of acidic gas-phase species to and from the particle must be balanced by the flux of ammonia so that no dissociated species exist in the particle phase. The equations used to describe this process are the same as those used in the original version of AIM, but the conditions when they are applied are modified. The original version of AIM uses equations requiring that the flux of ammonia to the particle exactly balance the net flux of strong acids whenever the ambient relative humidity falls below 78%. In the revised version of AIM, this flux-matching requirement is not imposed until the particle becomes completely solid. The thickness of the liquid water shell surrounding the particle is calculated at each time step. If the water shell becomes thinner than the approximate thickness of 20 water molecules (5.6 nm), the remaining water is expelled from the particle and the

equations for zero water content are used. This modification is important since many particles retain a significant aqueous shell even after the relative humidity falls below 78%.

2.2.6 Solution Technique

The most complicated and time-consuming operations performed during model calculations involve the integration of sets of simultaneous ordinary differential equations describing such processes as gas-phase kinetics / transport / deposition, aqueous-phase kinetics / gas-to-particle conversion, and gas-to-particle conversion during periods of low relative humidity. The numerical solution technique used for all these tasks is based on the hybrid method described by Young and Boris [45] with several modifications.

The Young and Boris algorithm classifies individual equations in the simultaneous set as either stiff or nonstiff. Nonstiff equations are solved with an implicit form of Euler's method. This technique is simple and easy to apply but suffers from stability problems when the characteristic time for an equation becomes small relative to the time step used by the solution method. To minimize this effect, stiff equations are modeled with the form

$$\frac{dC(t)}{dt} = a - \frac{C(t)}{\tau} \tag{2.10}$$

where $C(t)$ is the concentration of a chemical species at time t, a is the rate of production for the chemical species, and τ is the time constant for chemical species rate of destruction. If a and τ are constant with respect to time, this equation can be solved analytically to give

$$C(t + \Delta t) = a\tau + (C(t) - a\tau)\exp(\frac{-\Delta t}{\tau}) \tag{2.11}$$

This leads to an implicit numerical technique to solve for $C(t+\Delta t)$

$$C(t+\Delta t) = \beta + (C(t) - \beta) \cdot \exp\left(\frac{-2\Delta t}{\tau(t) + \tau(t+\Delta t)}\right) \tag{2.12}$$

where

$$\beta = \left(\frac{a(t) + a(t+\Delta t)}{2}\right) \cdot \left(\frac{\tau(t) + \tau(t+\Delta t)}{2}\right) \tag{2.13}$$

Young and Boris recognize that evaluation of the exponential is computationally expensive and so they derive an approximate solution for $C(t + \Delta t)$ as

$$C(t+\Delta t) = \beta + (C(t) - \beta) \cdot \left[\frac{\tau(t+\Delta t) + \tau(t) - \Delta t}{\tau(t+\Delta t) + \tau(t) + \Delta t}\right] \tag{2.14}$$

When the time step Δt is large compared with the characteristic time τ for the equation, the error introduced by this approximation converges to

$$\text{error} = \text{C(t)} - \beta \tag{2.15}$$

Thus the Young and Boris technique applies a more stable solution to stiff equations, but application is limited to equations for which the error term defined by equation (2.15) is small. Performance analysis undertaken in the current study indicates that within the present application, the majority of the computational time is spent evaluating equilibrium conditions in the particle phase, and these calculations benefit from increased stability in the kinetic solver. As a result, use of equation (2.12) instead of equation (2.14) does not significantly increase the computational burden of each iteration. Furthermore, because equation (2.12) does not introduce an extra error term into the calculation, it can be applied to a larger fraction of the equation set,

leading to increased stability and efficiency improvements in the equilibrium solution. To take advantage of these features, the numerical solution technique was modified to use equation (2.12) when integrating stiff equations. The definition of a stiff equation was also relaxed to include more of the equation set being integrated. Overall, these changes increase the stability of the solution technique, allowing larger time steps to be taken, which leads to improved computational efficiency.

2.3 Testing of Individual Model Components

Gas-to-particle conversion and aqueous-phase chemical reaction processes are influenced by the composition of the particles on which those processes are initiated. Thus the model components describing these processes are tested to illustrate their sensitivity to the representation of the aerosol particles as an internal mixture vs. a source-oriented external mixture. Model components describing physical processes such as emissions, transport and deposition are not directly affected by the representation of the airborne particles as a source-oriented external mixture, so no further tests of these algorithms beyond those reported earlier are required.

2.3.1 Gas-to-Particle Conversion in the Absence of Clouds or Fog

Gas-to-particle conversion in the absence of clouds or fog is calculated with a modified form of the computer code AIM as described in Section 2.4. Kim et al. [46] present a comparison of the results produced by the original version of AIM to the results obtained from the gas/aerosol equilibrium model SCAPE by initializing both models with the same gas- and particle-phase chemical species concentrations and then running the original version of AIM until equilibrium is reached. This analysis is repeated using the revised version of

AIM so that all three sets of results can be compared directly. In SCAPE calculations, activity coefficient estimates obtained by Kusik and Meissner's method will be used in the present work since this is the activity coefficient calculation method used in both the original and the revised version of AIM.

Test case 3 from Kim et al. [46] represents an example where all of the ionic species considered by AIM are present in significant amounts. Intial particle-phase concentrations are 48.97 μg m^{-3} of $SO_4^=$, 29.52 μg m^{-3} of NO_3^-, 9.1 μg m^{-3} of Cl^-, 10.59 μg m^{-3} of NH_4^+, 5.9 μg m^{-3} of Na^+, and 0.91 μg m^{-3} of H^+, while all gas phase species are initialized to zero. Gaseous species then evolve from the particles until equilibrium is reached. For the purposes of illustration an external mixture calculation will be conducted in which this system is split into two groups of particles both with initial diameters of 1.0 μm. The first set of particles contains all the sodium/chloride, while the second set of particles contains all the sulfate/nitrate/ammonium as may be expected to be the case if freshly generated sea spray aerosol is mixed with sulfates and nitrates produced previously during long-distance transport of aged air pollution. Hydrogen ion is distributed appropriately to obtain charge balance. The equilibrium concentrations of volatile components in the particle phase predicted by each of the three aerosol process models at a temperature of 298 K and various relative humidities are summarized in Table 2.1.

The predictions made by all three aerosol process models appear to be very similar for the case of an internally mixed aerosol. Nonvolatile sulfate dominates this test system, pulling all available ammonia into the particle phase. This leaves insufficient ammonia in the gas phase to form either NH_4NO_3(s) or NH_4Cl(s) in the particle phase. As a result, nitrate and chlo-

Table 2.1: Results for Test of Alternative Aerosol Thermodynamics Models

	Relative Humidity, %					
	90	80	70	60	50	40
	Nitrate as NO_3^- ($\mu g\ m^{-3}$)					
Internal mixture						
SCAPE[a]	4.8	1.9	0.9	0.4	0.1	0.2
original AIM[a]	1.2	0.4	1.6	1.2	0.5	0.2
revised AIM[b]	1.1	0.25	0.03	0.01	0.02	0.01
revised AIM[c]	1.5	0.3	0.04	0.03	0.02	0.02
External Mixture						
revised AIM[c,d]	14.3	14.6	16.4	15.9	15.9	15.9
	Ammonia as NH_4^+ ($\mu g\ m^{-3}$)					
Internal mixture						
SCAPE[a]	10.5	10.5	10.5	10.5	10.5	10.5
original AIM[a]	10.6	10.6	10.5	10.5	10.5	10.5
revised AIM[b]	10.6	10.6	10.6	10.6	10.5	10.5
revised AIM[c]	10.5	10.6	10.6	10.6	10.5	10.5
External Mixture						
revised AIM[c,d]	10.6	10.6	10.6	10.6	10.6	10.6
	Chloride as Cl^- ($\mu g\ m^{-3}$)					
Internal Mixture						
SCAPE[a]	0.7	0.2	0.1	0.0	0.0	0.0
original AIM[a]	0.1	0.0	0.0	0.0	0.0	0.0
revised AIM[b]	0.11	0.01	0.0	0.0	0.0	0.0
revised AIM[c]	0.11	0.01	0.0	0.0	0.0	0.0
External Mixture						
revised AIM[c,d]	2.17	1.44	6.02	7.03	7.7	8.2
	Water ($\mu g\ m^{-3}$)					
Internal Mixture						
SCAPE[a]	218	110	74.4	55.9	15.3	4.61
original AIM[a]	188	102	75.1	54.1	37.7	29.5
revised AIM[b]	173	81.2	7.3	1.4	0.6	0.44
revised AIM[c]	175	81.4	6.5	1.7	0.6	0.44

See text for initial gas and particle-phase composition. [a] Results for case 3 of Kim et al. [46]. [b] Thermodynamic data for NH_4NO_3 from Wagman et al. [38]. [c] Thermodynamic data for NH_4NO_3 from Stelson and Seinfeld [47]. [d] Na^+ and SO_4^{2-} present in separate particles.

ride exist in the gas phase as HNO_3 and HCl and as free ions in the aqueous shell surrounding the particles but never crystallize to form part of the solid core of the particle. The aerosol water content predicted by the original version of AIM matches predictions made by the revised version of AIM and the SCAPE model at high relative humidity but significantly overpredicts water content at low relative humidity, reflecting the inability of that model to crystallize solids under certain conditions.

In the case of an externally mixed aerosol, dramatic differences are seen for the predicted aerosol composition at equilibrium made by the revised version of AIM relative to the internally mixed aerosol representation of the same chemical system. The particle group containing the nonvolatile sulfate still draws all of the available ammonia into the particle phase, but separate particles containing the nonvolatile sodium also draw nitrate and chloride into the particle phase in an analogous fashion. This leads to a great increase in the predicted nitrate and chloride concentrations in the particle phase relative to the internally mixed aerosol calculation. This example illustrates one possible distortion of the atmospheric aerosol concentrations that could be produced by employing an internal mixture model under conditions where secondary formation processes are active.

2.3.2 Gas-to-Particle Conversion in the Presence of Fog or Clouds

The degree to which the ambient aerosol at Claremont, California, is externally mixed has been studied experimentally by Zhang et al. [14]. This experiment involved selecting a narrow range of particle sizes using a differential mobility analyzer (DMA), humidifying this classified aerosol and then measuring the modified size distribution of particles using a second DMA. Upon humidification, one group of particles grew rapidly to larger sizes while

a second group containing more hydrophobic particles grew by a smaller amount, thereby creating a bimodal size distribution from initially monodisperse seed particles. The results of this experiment indicated that ambient submicron particles of the same size typically have distinctly different hygroscopic characteristics, strongly suggesting that the ambient particles consist of an external mixture. In order to test the operation of the fog model in the presence of an internally versus externally mixed representation of the atmospheric aerosol, a numerical experiment motivated by that conducted by Zhang et al. [14] was performed. Gas- and particle-phase pollutant concentrations based on ambient conditions near the coast of Los Angeles at 0000 PST on August 28, 1987, were obtained from one of the trajectory simulations that will be presented in section 4 of this study. A narrow slice of the aerosol size distribution in the diameter range 0.3 μm to 0.5 μm was then selected and exposed to an atmosphere with a water vapor supersaturation of 0.08%, in one case with the aerosol represented as an internal mixture and in the second case with the aerosol represented as a source-oriented external mixture. The captured air parcel studied was spiked with 0.15 ppm SO_2 in order to allow heterogenous sulfate formation to occur. Gas-phase photochemistry, gas and particle-phase deposition, and continuing emissions were not enabled during this test so that the effect of the internally versus externally mixed representations of the aerosol on the gas-to-particle conversion and aqueous-phase physical and chemical transformations during fog events could be examined directly. The initial particle-phase concentrations and major gas-phase concentrations specified for this test are found in Table 2.2. The initial size distribution of material in the particle phase and the evolution of this size distribution after 1 hour and 2 hours with no further inputs or losses is shown in Figure 2.1. Although water is not explicitly shown in

Table 2.2: Initial Conditions for Box Model of Fog Initiated on Nearly Monodisperse Aerosol in the Diameter Range 0.3 μm-0.5 μm

Particle-Phase Species[a]	Concentration[b] μg m^{-3} air	Gas-Phase Species[a]	Concentration[b] ppm
$NH_4^+(aq)$	14.3	$NH_3(g)$	8.73×10^{-4}
$Cl^-(aq)$	17.0	$HCl(g)$	7.33×10^{-4}
$NO_3^-(aq)$	57.3	$HNO_3(g)$	1.63×10^{-3}
$SO_4^=(aq)$	129.7	$SO_2(g)$	1.55×10^{-1}
$H_2SO_3(aq)$	2.38×10^{-7}	$OH(g)$	2.71×10^{-9}
$Na^+(aq)$	1.55×10^{-1}	$H_2O_2(g)$	7.97×10^{-4}
Cu(I)(aq)	2.10×10^{-4}	$O_3(g)$	2.18×10^{-6}
Cu(II)(aq)	1.80×10^{-3}	$NO(g)$	3.29×10^{-2}
Fe(II)(aq)	1.11×10^{-1}	$NO_2(g)$	6.62×10^{-2}
Fe(III)(aq)	1.11×10^{-1}	$NO_3(g)$	1.32×10^{-11}
Mn(II)(aq)	1.74×10^{-2}	$HNO_4(g)$	1.63×10^{-6}
Mn(III)(aq)	3.48×10^{-5}	$HCHO(g)$	6.23×10^{-3}
Elemental carbon	7.50×10^{-2}	$CHOCHO(g)$	8.12×10^{-5}
Primary organics	1.56	$CH_3(O)CHO(g)$	1.53×10^{-4}
Secondary organics	2.39×10^{-1}	$HONO(g)$	1.79×10^{-4}
Other	1.58×10^{-1}	$HO_2(g)$	2.50×10^{-8}

[a] Species not listed have initial concentration equal to zero. [b] Concentrations represent SO_2 spiked air as it would exist near the Los Angeles coastline at 0000 PST on August 28, 1987, before raising the relative humidity to produce a fog.

these graphs, the size distributions of particle-phase chemical components are plotted at the equivalent wet particle diameters.

The results of this numerical experiment show that the internally mixed aerosol grows due to condensation of water, but the size distribution of particles remains nearly monodisperse since all particles of the same size have the same chemical composition and hygroscopic properties. The externally mixed aerosol splits into two distinct modes when exposed to the supersaturated air, reflecting different hygroscopic properties between particles of the same diameter. The mode with the smaller diameter consists of particles

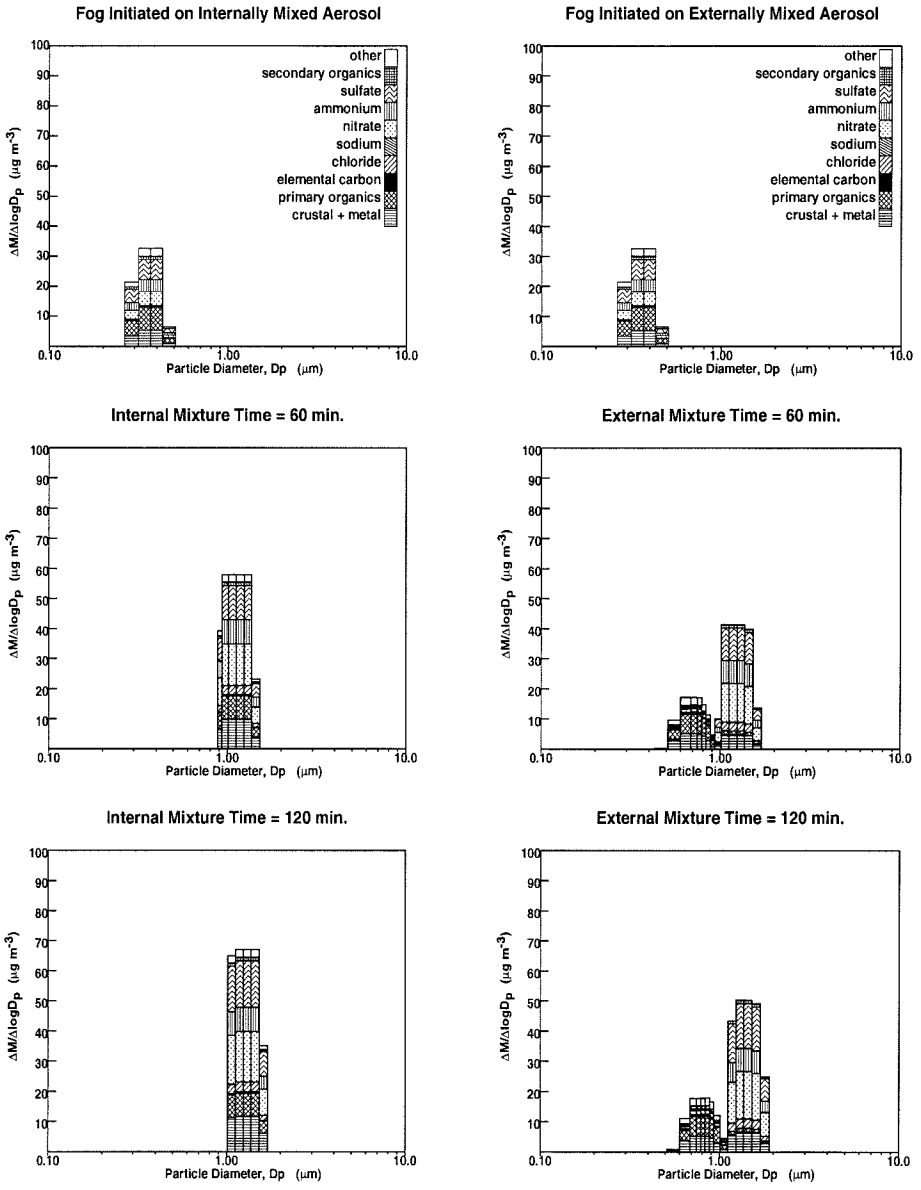

Figure 2.1:
Initial size distribution of a nearly monodisperse aerosol separated from a representative Los Angeles coastal ambient aerosol and the evolution of its size distribution within a box model after 1 hour and 2 hours in the presence of fog and additional SO_2 (see Table 2.2 for initial conditions). External mixture calculations produce a size distribution that is bimodal because of the different hygroscopic properties of particles having the same initial diameter. Particles are shown at their equivalent wet diameter, but water is not shown explicitly.

composed largely of less hygroscopic material such as primary organics and crustal material, while the mode with the larger diameter is comprised mainly of more hygroscopic material such as ammonium, sulfate, and nitrate. Such bimodal behavior during conditions when the atmosphere is supersaturated with respect to water vapor would affect particle removal by gravitational sedimentation, urban/regional visibility calculations during fogs, as well as global scale radiative transfer calculations involving clouds.

Aqueous phase chemical transformations lead to production of sulfate in the particle phase. No significant difference is seen between the total amount of sulfate produced within a fog seeded by an internally versus externally mixed aerosol under the conditions of the particular test case examined here.

2.4 Trajectory Model Evaluation

A comparison of the results produced by the external versus internal mixture models applied to the same air pollution episode requires an episode for which detailed information is available which describes meteorological conditions, gas and particulate-phase emissions, and ambient air quality. Because complete data sets of this type are extremely difficult and expensive to obtain, few air quality episodes have been characterized in such detail. The Southern California Air Quality Study (SCAQS) was a large cooperative air quality measurement program carried out in the South Coast Air Basin of California to collect information for the design and evaluation of air quality models [48]. Eldering and Cass [4] examined the SCAQS data taken during the summer of 1987 and determined that the data collected during the episode of August 27-28, 1987, at Claremont, California, are relatively complete and self-consistent. They then used a trajectory model having an internally mixed representation of the aerosol to predict the evolution of the particle size and composition

distribution as well as visibility-related parameters for this episode. Since the present study builds on this previous work, trajectories ending at Claremont during the August 27-28, 1987, SCAQS episode also are used here as the basis for comparison of the results of calculations that use alternative representations of the extent of aerosol mixing. Air parcels are tracked over a period of 2 days, starting over the ocean and terminating at Claremont on August 28, 1987. Although the trajectory paths and model inputs used in this study are virtually identical with those used by Eldering and Cass [4], the representation of the aerosol as a source-oriented external mixture and other model improvements result in different predictions for ambient air quality.

2.4.1 Meteorological Inputs

The construction of meteorological inputs used for the August 27-28, 1987, episode closely follows the treatment described by Harley et al. [29] and Eldering and Cass [4] except in the construction of the gridded fields describing fog events. In the present study, airports reporting fog were assigned a probability of 1.0 that fog was present, while airports reporting that fog was not present were assigned a fog probability of 0.0. The probability that a fog event occurred at a given time and location was then computed by spatial interpolation between these locations according to the method of Goodin et al. [19]. If a model grid square had a fog probability greater than 0.5 and an interpolated relative humidity value greater than 70%, it was concluded that fog was present at that time and location between the ground and the base of the inversion layer. During periods when a fog event occurred, particles located below the inversion base were activated by exposure to an environment with a water vapor supersaturation of 0.08%, while particles above the

inversion base were assumed to be exposed to a high relative humidity that is nevertheless below the saturated conditions needed to form fog.

2.4.2 Particulate-Phase Emission Inventory

Mass emission rates, source locations, and temporal variation for 455 separate primary particle source types in Southern California are provided by the California Air Resources Board (CARB) for the August 27-28, 1987, episode. Source activity levels (e.g., vehicle miles traveled by location, quantities of fuel burned, etc.) are retained but the mass emission rates per unit activity or the chemical composition profiles for 90% of the primary particle emissions are replaced by better information. Modifications to this inventory are made to account for the results of the source test program of Hildemann et al. [24, 25]. More recent information concerning the emission rates for paved road dust and dust from construction and demolition sites is used as described by Eldering and Cass [4]. In addition, emission rates for mobile sources are subdivided into rates for catalyst-equipped light-duty autos, catalyst-equipped light-duty trucks, catalyst-equipped medium-duty trucks, catalyst-equipped heavy-duty trucks, motorcycles, noncatalyst light-duty autos, noncatalyst light duty trucks, noncatalyst medium-duty trucks, noncatalyst heavy-duty trucks, diesel heavy-duty trucks, diesel urban buses, and tire wear to allow detailed emission profiles to be applied for each of these sources. The diurnal profile used for commercial food-cooking operations was modified to match that described by Gray [49]. Once the total particulate mass emission rates for each source were specified, the chemical composition and size distribution of the emitted material was calculated using the emissions processing model described in Section 2.1.

2.4.3 Gas-Phase Emission Inventory

Mass emission rates and source locations for major gas-phase emission sources relevant to the August 27-28, 1987, SCAQS episode were once again obtained from the California Air Resources Board. This inventory includes a description of NO_x, SO_x, CO, and volatile organic compound (VOC) emissions along with the diurnal variation of each source. Carbon monoxide and organic gas hot exhaust emissions from on-road vehicles were scaled to three times the levels shown in the official CARB inventory based on the results of experiments conducted in a highway tunnel as described by Harley et al. [30]. The 1982 spatially and temporally resolved ammonia emission inventory for the South Coast Air Basin prepared by Gharib and Cass [50], as summarized by Russell and Cass [18], was used to represent NH_3 emissions for the episode studied. Once the gas-phase mass emission rates of NO_x, SO_x, CO, VOCs and NH_3 for each source were specified, speciation of the VOC emissions was calculated using the gas-phase emission model described in Section 2.1.

2.4.4 Initial Conditions

Particle-phase initial conditions for the episode modeled are substantially identical to those shown by Eldering and Cass [4] except for rearrangement of material within the size distribution to ensure charge balance for particles of all sizes. The species mass concentrations contained within the initial conditions are based on filter measurements made at San Nicolas Island during the August 27-28, 1987, period. The initial concentrations for various aerosol chemical species are 3 μg m^{-3} Cl^-, 2 μg m^{-3} Na^+, 1 μg m^{-3} NO_3^-, 1.4 μg m^{-3} NH_4^+, 3 μg m^{-3} $SO_4^=$, and 1 μg m^{-3} of organic material. The relative size distribution of the ionic species is based on impactor measurements made at Long Beach during SCAQS. The particles present due to initial conditions

are injected into the trajectory model as the air mass crosses the coastline by setting the background concentrations in the model equal to the measured marine background values at that point in time. In the external mixture model, the particle-phase initial conditions are split into particles of two types to separate the freshly generated sodium chloride aerosol produced by sea spray from the aged ammonium nitrate and ammonium sulfate aerosol as shown in Figure 2.2. Initial conditions for relevant gas-phase pollutants were taken to be 113 ppb CO, 5 ppb NO, 40 ppb O_3, 11 ppb MEK, 3.8 ppb HCHO, and 3.5 ppb CH_3CHO based on measurements made over the ocean during SCAQS [30].

2.4.5 Results

Model results for the 24 trajectories arriving hourly at Claremont on August 28, 1987, predict the ambient concentration of major gas-phase pollutants as well as the concentration, size distribution, and chemical composition of particle-phase species. In the following sections, results calculated using the source-oriented external mixture representation of the aerosol will be compared to ambient measurements and then to results produced when the aerosol is represented as an internal mixture.

Gas-phase species

Gas-phase concentrations for O_3, NO_2, NH_3, and HNO_3, calculated using the source-oriented external mixture model, are substantially identical to those calculated using the internal mixture model. Both calculations underpredict peak O_3 concentrations, matching the general trend for the August 28, 1987, Claremont SCAQS episode noted by Eldering and Cass [4] and Harley et al. [29]. Predicted NO_2 concentrations fall between the range of values reported by two collocated NO_2 monitors with some overprediction during

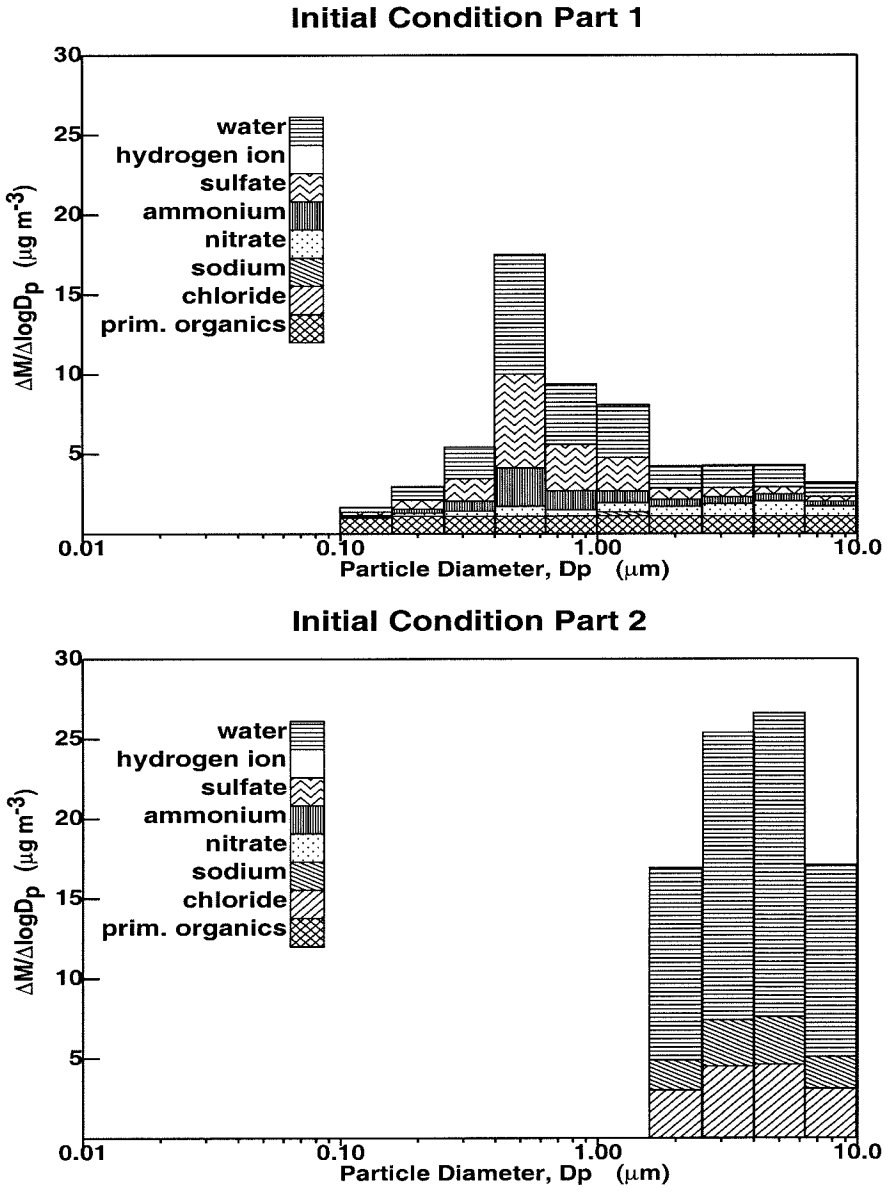

Figure 2.2:
Aerosol mass distributions, $\Delta M/\Delta \log D_p$, describing initial conditions over the ocean for trajectories ending at Claremont, CA, on August 28, 1987. During external mixture calculations, aged ammonium nitrate and ammonium sulfate aerosol is tracked as existing in particles that are separate from the freshly generated sodium chloride aerosol produced by sea spray.

the nighttime hours. HNO_3 measurements are 0 to 5 ppb during the early morning and late night hours and reach a peak value of approximately 20 ppb during the 0900-1300 PST SCAQS sampling period. This trend is generally well matched by model predictions. Both measured and predicted NH_3 concentrations are of the order of a few parts per billion, with modeled results slightly higher than the measurements for all sampling periods. See Eldering and Cass [4] for a graphical display of typical gas-phase species results.

Particle-phase species

Measurements of particle-phase pollutant concentrations at Claremont during the August 28, 1987, SCAQS episode were made using a filter-based SCAQS sampler [51], a nine stage Berner impactor [52], and a micro-orifice uniform deposit impactor [14]. The SCAQS sampler was operated over the full 24 hour period in five discrete time intervals of 0000-0500 PST, 0500-0900 PST, 0900-1300 PST, 1300-1700 PST, and 1700-2400 PST. The impactors were operated during all but the first of these sampling periods. Model results are presented at the particle sizes obtained after removing all particle-phase water, recalculating the particle density based on the remaining chemical components, and then adjusting the particle diameter so that particle-phase mass, number count, density, and volume are in agreement. This is done because it has been previously determined that the instruments used to measure particle size distributions at Claremont dried out the aerosol while making their measurements [53].

Bulk chemical composition

A comparison of the observed particle-phase concentrations to the model results produced by the internal and source-oriented external mixture models is shown in Table 2.3. Model results for total particulate matter smaller than

Table 2.3: Comparison of Model Results to Filter-Based Ambient Measurements From the SCAQS Sampler at Claremont on August 28, 1987

Case	PM2.5 EC [mean][a] bias[b] (s.d.)[c]	OC (PM2.5)	$SO_4^=$ (PM2.5)	NH_4^+ (PM2.5)	NO_3^- (PM2.5)	Na^+ (PM10)	Mass (PM2.5)	Mass (PM10)
Observed mean	[3.17]	[20.80]	[7.06]	[6.71]	[14.10]	[1.45]	[60.18]	[96.26]
Internal mixture	[3.69]	[23.10]	[5.60]	[4.75]	[10.75]	[0.90]	[73.61]	[109.09]
	0.52	2.31	-1.46	-1.96	-3.35	-0.55	13.43	12.84
	(1.71)	(11.96)	(2.68)	(2.50)	(7.77)	(0.16)	(31.11)	(46.50)
External mixture	[3.69]	[23.15]	[6.04]	[4.90]	[11.50]	[1.12]	[74.97]	[108.97]
	0.52	2.36	-1.02	-1.82	-2.60	-0.33	14.79	12.71
	(1.70)	(11.92)	(1.86)	(2.33)	(7.83)	(0.16)	(30.14)	(44.88)

SCAQS, Southern California air quality study. [a] Unweighted mean of five pairs of predictions and observations corresponding to the five sampling periods (μg m^{-3}). [b] Predicted-observed (μg m^{-3}). [c] Standard error of residuals (μg m^{-3}).

10 μm diameter (PM10 mass) and smaller than 2.5 μm diameter (PM2.5 mass) produced by using both models differ by less than 1.8%. The elemental carbon (EC) and organic carbon (OC) results shown in Table 2.3 overpredict observed values by a small amount, 0.52 μg m^{-3} for EC and 2.31 μg m^{-3} for OC. The mean PM10 concentration is also overpredicted but is within 13% of the observed value.

Predictions for $SO_4^=$, NH_4^+, NO_3^-, and Na^+ made by the internal mixture and source-oriented external mixture models are slightly lower than observations. The internal mixture and external mixture model results differ by 0.75 μg m^{-3} for NO_3^- to 0.15 μg m^{-3} for NH_4^+ with the external mixture results always closer to the observed values. The underprediction of Na^+ concentrations is most likely related to imperfect initial conditions supplied to the model as described by Eldering and Cass [4]. Overall, the predicted bulk concentrations of all the particle-phase ionic species appear to be in good agreement with measurements made with the SCAQS sampler for the

episode under consideration.

Impactor results

A comparison of the source-oriented external mixture model results to the impactor measurements for the 0900-1300 PST sampling period is shown in Figure 2.3. Internal mixture model results are also shown for chemical species where they differ from the source-oriented external mixture calculations at that time period.

Impactor measurements and model predictions for elemental carbon during the 0900-1300 PST sampling period agree well, a result consistent with that obtained by Eldering and Cass [4]. Both the predicted and the measured elemental carbon mass distribution has a single mode located between 0.1 μm and 1.0 μm with a peak located at approximately 0.2 μm to 0.3 μm diameter. Model predictions for organic carbon also match observations in terms of the shape of the size distribution and location of the peak, but model results show significantly more organic carbon than that measured by the impactor. Eldering and Cass [4] describe a similar trend in their results and go on to note that the measurements for organic carbon made by the impactor are significantly lower than the measurements made by the SCAQS sampler, indicating an inconsistency in the measured data.

Impactor measurements for sodium show increasing mass concentrations with increasing particle diameter, reflecting the sea-salt origin of this chemical component. Model predictions match observations fairly well when it is considered that initial conditions for sodium over the ocean are known on the average for this day but not for each separate trajectory.

The sulfate and ammonium ion size distributions measured by the Berner impactors each have a single mode in the 0.1 μm - 1.0 μm range with a peak

located at approximately 0.5 μm - 0.7 μm diameter. Model results are in good agreement with these observations except for a slight underprediction of values right at the peak in the size distribution.

Nitrate aerosol concentration predictions for the source-oriented external mixture model and internal mixture model differ from each other. Both models underpredict nitrate aerosol in particles larger than 1 μm diameter in part because the Na^+ concentration prediction in the largest particle sizes is too low due to the imprecision with which the marine aerosol initial conditions are known. The Na^+ concentrations in the initial conditions are due to NaCl aerosol produced by sea spray. The production rate of these particles is expected to be a strong function of wind speed and therefore is likely to vary from hour to hour and from trajectory to trajectory in ways that cannot be represented exactly by the 24 hour average Na^+ value computed from the SCAQS data. Nitrate aerosol concentrations in the external mixture case overall are higher than those for the internal mixture, and this advantage of the external mixture calculation would be expected to be even more pronounced if the larger amount of Na^+ actually present in the atmosphere were present in the model, as the test case of section 2.3.1 of this chapter shows.

Aerosol size and composition distribution

A comparison of the model results to plots of $\Delta V/\Delta \log d_p$ obtained from electronic particle size distribution measurement instruments and filter samplers at 0700 PST and 1200 PST is shown in Figure 2.4. The ambient measurements shown here over the size range from 0.01 μm to 1 μm particle diameter are a composite constructed from TSI electrical aerosol analyzer (EAA), and laser optical particle counter (OPC) data as described by Eldering et al. [53]. The response of those instruments falls off above 1 μm particle

diameter; the measured aerosol volume shown between 2.5 μm and 10 μm is obtained from the difference between SCAQS sampler PM10 versus PM2.5 filters and conveys no information other than the total aerosol volume in that size range. The chemically resolved size distributions predicted by both the internal and the source-oriented external mixture models are shown by grouping all particles having a diameter that falls within the particle diameter intervals reported by the electronic size distribution monitors. For both the hours under consideration the ambient data clearly show a bimodal mass distribution in the size range between 0.1 μm and 1.0 μm as described by John et al. [52] and Hering et al. [54]. The external mixture model predicts this bimodal feature routinely as seen for both 0700 PST and 1200 PST, but the internal mixture calculation predicts only a single separate peak in the 0.1 μm - 1 μm diameter range for 1200 PST.

Degree of external mixing

The big difference between the source-oriented external mixture model and the internal mixture model is that only the external mixture model can predict chemical composition differences between particles of the same general size. Figure 2.5 shows the source-oriented external mixture model representation of the ambient aerosol at Claremont, California, on August 28, 1987, at 1200 PST. Each of the pie charts in Plate 1 illustrates the composition of a single particle from one of the independent particle groups tracked by the source-oriented external mixture model. The size of each pie chart is proportional to the log of the actual particle diameter. The diameter of each particle is shown below the plot, while the number concentration of all particles of that type and size is shown above. The particle types are sorted such that the most numerous particles of each size appear toward the top of each

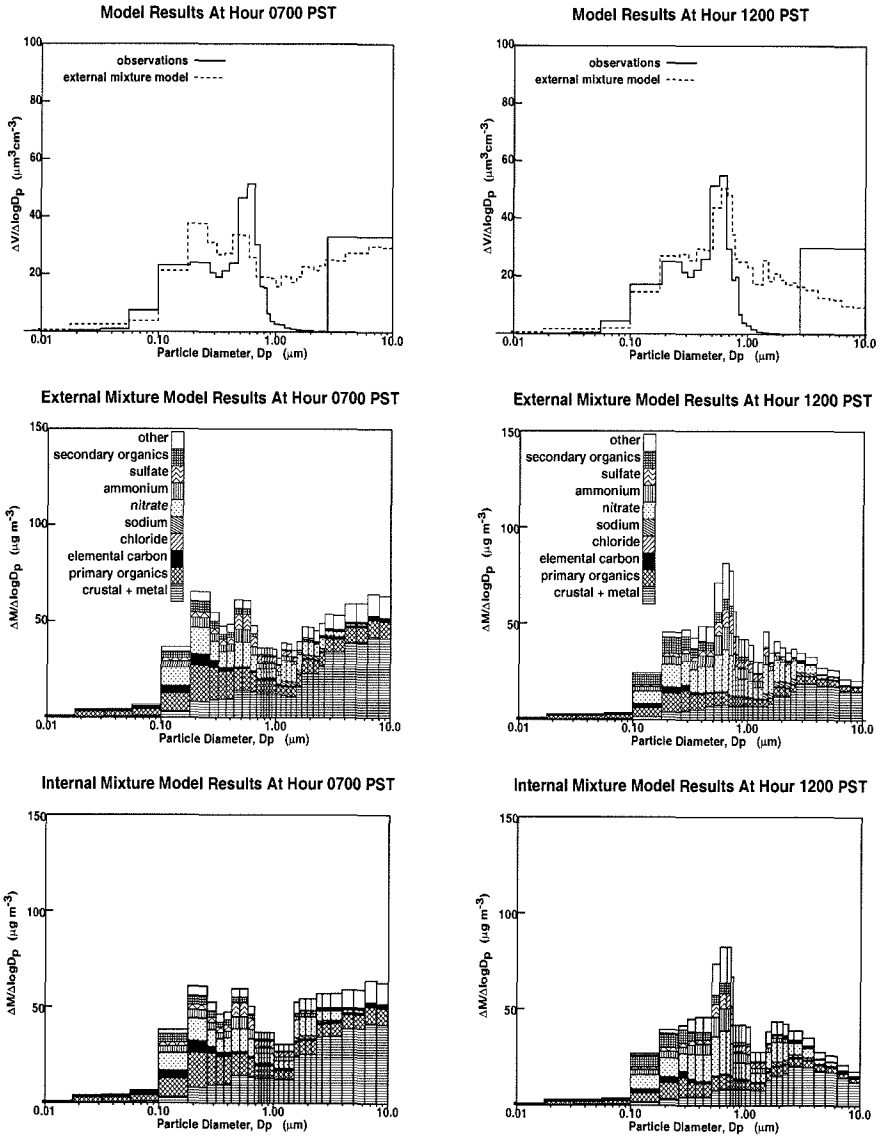

Figure 2.4:
Comparison of measured and predicted size and composition distributions produced by the source-oriented external mixture model and the internal mixture model for 0700 PST and 1200 PST on August 28, 1987, at Claremont, CA. Observed aerosol size distributions were measured using electrical aerosol analyzers, optical particle counters, and filter samplers. Comparison of results produced using internal mixture and source-oriented external mixture models show loss of the peak at a diameter of approximately 0.3 μm at 1200 PST in the internal mixture model.

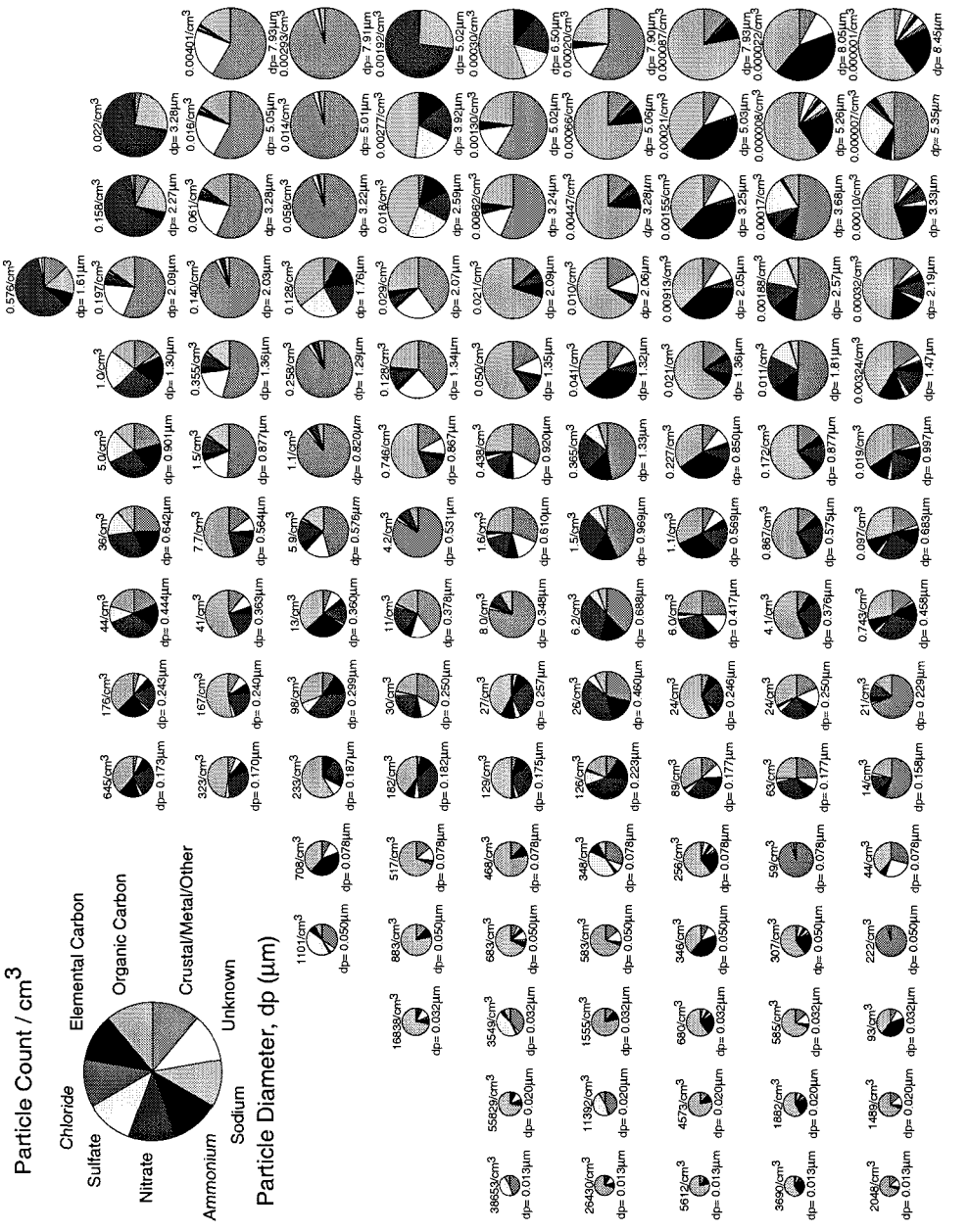

Figure 2.5:
Source-oriented external mixture model representation of the ambient aerosol at Claremont, CA, on August 28, 1987, at 1200 PST. Each pie chart characterizes a single group of particles that are tracked separately by the model. The particle atmospheric concentration (number per cm^3 air) is shown above each pie chart while the particle diameter (μm) is shown below.

column in Figure 2.5.

Figure 2.5 shows that the source-oriented external mixture calculation represents ambient particles with a diameter of approximately 0.013 μm using five types of particles with unique chemical composition. Number concentrations for some of these very small particles may be above $10^4 cm^{-3}$. Some of these very fine particles are composed mainly of elemental/organic carbon, while other particles of the same size have significant sulfate and metals concentration. Particles in the diameter range from 0.1 μm to 10.0 μm show the greatest diversity in terms of chemical composition and degree of external mixing with up to 10 unique particle types existing at the same approximate diameter. Some particles in this size range are seen to be composed primarily of organic carbon and crustal/metal material, while others have a large ionic species content. Particles with an inert core and a coating of ammonium / nitrate / sulfate are common between 0.1 μm - 1.0 μm particle diameter. At larger sizes, particles containing sodium/nitrate are seen to exist separately from particles composed primarily of crustal material.

2.5 Conclusions

An atmospheric aerosol processes model has been constructed which is capable of representing the airborne particle complex as a source-oriented external mixture in which particles of the same size have different chemical compositions determined by the source from which they were initially emitted. These particles evolve separately in the atmosphere as they are affected by transport, deposition, gas-to-particle conversion, and aqueous phase chemical reaction. Tests cases presented in Figure 2.1 and Table 2.1 indicate that representation of the atmospheric aerosol as an internal mixture in which all particles of the same size have the same chemical composition can distort

aerosol size and composition distributions during conditions when significant amounts of sulfate and sodium exist in externally mixed particles of the same size and when externally mixed particles containing material with different hygroscopic properties are exposed to high relative humidity.

Model evaluation against ambient data taken at Claremont, California, during the August 28, 1987, episode of the Southern California Air Quality Study indicates that ambient concentrations of particle-phase species can be successfully predicted both in terms of bulk properties and size-resolved chemical composition. Source-oriented external mixture calculations predict small differences in particle-phase concentrations of NH_4^+, NO_3^-, and Na^+ relative to internal mixture results. The source-oriented external mixture model routinely produces an aerosol volume distribution at Claremont which is distinctly bimodal within the accumulation mode size range from 0.1 μm to 1.0 μm particle diameter, which matches field experimental observations, while the same model employing an internal mixture representation of the aerosol at times does not retain the observed bimodal distribution.

At very fine particle sizes close to 0.01 μm diameter, numbers of largely carbonaceous particles are predicted to coexist at Claremont with separate particles containing largely sulfates and metals. In the size range between 0.1 μm and 1.0 μm particle diameter, a very large number of particles of highly diverse composition are found to accumulate as sulfate, nitrate, and secondary organic aerosol components lay coatings down onto seed particles having different initial core compositions. In relatively large particle sizes above 1.0 μm diameter, marine aerosol is transformed to produce $NaNO_3$-containing particles that exist separately from mineral particles. The ability to predict the composition of individual particles is expected to have applications including explanation of the particle-to-particle differences seen

by time-of-flight mass spectrometers that measure single-particle composition, the design of realistic test atmospheres for inhalation toxicology studies, support of accurate light scattering and absorption calculations, and more accurate predictions of aerosol response to changes in relative humidity.

The method described in the current study is theoretically applicable in an Eulerian grid-based model provided that the particle categories are defined so narrowly that particles with the same core properties (e.g., source), same approximate diameter, and possibly same age since emission to the atmosphere are present in adjacent grid cells. Whether or not one finds this formulation practical within a grid model depends on the availability of sufficient computational resources. Since computers are advancing very rapidly, we believe that such models will soon be practical.

Bibliography

[1] C. Seigneur, A. B. Hudischewskyj, John H. Seinfeld, K. T. Whitby, J. R. Brock, and H. M. Barnes. Simulation of aerosol dynamics - a comparative review of mathematical-models. *Aerosol Sci. Technol.*, 5:205–222, 1986.

[2] A. B. Hudischewskyj and C. Seigneur. Mathematical modeling of the chemistry and physics of aerosols in plumes. *Environ. Sci. Technol.*, 23:413–421, 1989.

[3] Spyros N. Pandis, Anthony S. Wexler, and John H. Seinfeld. Secondary organic aerosol formation and transport – II. Predicting the ambient secondary organic aerosol size distribution. *Atmos. Environ.*, 27A:2403–2416, 1993.

[4] Annmarie Eldering and Glen R. Cass. Source–oriented model for air pollutant effects on visibility. *J. Geophys. Res.*, 101(D14):19343–19369, 1996.

[5] F. S. Binkowski and U. Shankar. The regional particulate matter model 1. Model description and preliminary results. *J. Geophys. Res.*, 100(D12):26191–26209, 1995.

[6] P. Middleton and S. Burns. Denver air quality modeling study. In *Annual International Meeting*, Air and Waste Management Association, Vancouver, B.C., Canada, 1991.

[7] Christodoulos Pilinis and John H. Seinfeld. Development and evaluation of an Eulerian photochemical gas–aerosol model. *Atmos. Environ.*, 22:1985–2001, 1988.

[8] NRC (National Research Council). *Protecting Visibility in National Parks and Wilderness Areas.* National Academy Press, Washington, DC, 1993.

[9] R. J. Charlson, S. E. Schwartz, J. M. Hales, R. D. Cess, J. A. Coakley, J. E. Hansen, and D. J. Hofmann. Climate forcing by anthropogenic aerosols. *Science*, 255:423–430, 1992.

[10] J. E. Penner, R. J. Charlson, J. M. Hales, N. S. Laulainen, R. Leifer, T. Novakov, J. Ogren, L. F. Radke, and S. E. Schwartz. Quanitifying and minimizing uncertainty of climate forcing by anthropogenic aerosols. *Bulletin of the American Meteorological Society*, 75:375–400, 1994.

[11] G. Oberdorster, R. M. Gelein, J. Ferin, and B. Weiss. Association of particulate air pollution and acute mortality, involvement of ultrafine particles? *Inhalation Toxicology*, 7:111–124, 1995.

[12] R. B. Schlesinger. Factors affecting the response of lung clearance systems to acid aerosols - Role of exposure concentration, exposure time and relative acidity. *Environ. Health Perspect.*, 79:121–126, 1989.

[13] K. L. Dreher, R. H. Jaskot, J. R. Lehmann, J. H. Richards, J. K. McGee, A. J. Ghio, and D. L. Costa. Soluable transition metals mediate residual oil fly ash induced acute lung injury. *Journal of Toxicology and Environ. Health*, 50:285–305, 1997.

[14] X. Q. Zhang, P. H. McMurry, S. V. Hering, and G. S. Casuccio. Mixing characteristics and water content of submicron aerosols measured in Los Angeles and at the Grand Canyon. *Atmos. Environ.*, 27A:1593–1607, 1993.

[15] Mary P. Ligocki, Harvey I. H. Liu, Glen R. Cass, and Walter John. Measurements of particle deposition rates inside southern California museums. *Aerosol Sci. Technol.*, 13:85–101, 1990.

[16] Christopher A. Noble and Kimberly A. Prather. Real-time measurement of correlated size and composition profiles of individual atmospheric aerosol particles. *Environ. Sci. Technol.*, 30(9):2667–2680, 1996.

[17] Armistead G. Russell, Gregory J. McRae, and Glen R. Cass. Mathematical modeling of the formation and transport of ammonium nitrate aerosol. *Atmos. Environ.*, 17:949–964, 1983.

[18] Armistead G. Russell and Glen R. Cass. Verification of a mathematical model for aerosol nitrate and nitric acid formation and its use for control measure evaluation. *Atmos. Environ.*, 20:2011–2025, 1986.

[19] William R. Goodin, Gregory J. McRae, and John H. Seinfeld. A comparison of interpolation methods for sparse data: Application to wind and concentration fields. *J. Appl. Met.*, 18:761–771, 1979.

[20] William P. L. Carter. A detailed mechanism for the gas–phase atmospheric reactions of organic compounds. *Atmos. Environ.*, 24A:481–518, 1990.

[21] Spyros N. Pandis, Robert A. Harley, Glen R. Cass, and John H. Seinfeld. Secondary organic aerosol formation and transport. *Atmos. Environ.*, 26A:2269–2282, 1992.

[22] Anthony S. Wexler and John H. Seinfeld. Second-generation inorganic aerosol model. *Atmos. Environ.*, 25A:2731–2748, 1991.

[23] Susan M. Larson, Glen R. Cass, Kevin J. Hussey, and Frederick Luce. Verification of image processing based visibility models. *Environ. Sci. Technol.*, 22:629–637, 1988.

[24] Lynn M. Hildemann, Gregory R. Markowski, and Glen R. Cass. Chemical composition of emissions from urban sources of fine organic aerosol. *Environ. Sci. Technol.*, 25:744–759, 1991.

[25] Lynn M. Hildemann, Gregory R. Markowski, Michael C. Jones, and Glen R. Cass. Submicrometer aerosol mass distributions of emissions from boilers, fireplaces, automobiles, diesel trucks, and meat–cooking operations. *Aerosol Sci. Technol.*, 14:138–152, 1991.

[26] Yigal Erel, Simo O. Pehkonen, and Michael R. Hoffmann. Redox chemistry of iron in fog and stratus clouds. *J. Geophys. Res.*, 98:18423–18434, 1993.

[27] Daniel J. Jacob, Elaine W. Gottlieb, and Michael J. Prather. Chemistry of a polluted boundary layer. *J. Geophys. Res.*, 94(D10):12975–13002, 1989.

[28] Robert A. Harley, Michael P. Hannigan, and Glen R. Cass. Respeciation of organic gas emissions and the detection of excess unburned gasoline in the atmosphere. *Environ. Sci. Technol.*, 26:2395–2408, 1992.

[29] Robert A. Harley, Armistead G. Russell, and Glen R. Cass. Mathematical modeling of the concentrations of volatile organic compounds: Model performance using a lumped chemical mechanism. *Environ. Sci. Technol.*, 27:1638–1649, 1993.

[30] Robert A. Harley, Armistead G. Russell, Gregory J. McRae, Glen R. Cass, and John H. Seinfeld. Photochemical modeling of the Southern California Air Quality Study. *Environ. Sci. Technol.*, 27:378–388, 1993.

[31] Armistead G. Russell, Darrell A. Winner, Kenneth F. McCue, and Glen R. Cass. Mathematical modeling and control of the dry deposition flux of nitrogen-containing air pollutants. *Environ. Sci. Technol.*, 27:2772–2782, 1993.

[32] Steven C. Chapra and Raymond P. Canale. *Numerical Methods For Engineers.* McGraw Hill Publishing Company, New York, 2^{nd} edition, 1988.

[33] S. A. Slinn and W. G. N. Slinn. Predictions for particle deposition on natural waters. *Atmos. Environ.*, 14:1013–1016, 1980.

[34] John H. Seinfeld. *Atmospheric Chemistry and Physics of Air Pollution.* John Wiley and Sons, New York, 1986.

[35] Gregory J. McRae, William R. Goodin, and John H. Seinfeld. Development of a second–generation mathematical model for urban air pollution – I. Model formulation. *Atmos. Environ.*, 16:679–696, 1982.

[36] Daniel J. Jacob. Chemistry of OH in remote clouds and its role in the production of formic acid and peroxymonosulfate. *J. Geophys. Res.*, 91(D9):9807–9826, 1986.

[37] Robert C. Reid, John M. Prausnitz, and Bruce E. Poling. *The Properties of Gases and Liquids.* McGraw-Hill, New York, 4^{th} edition, 1987.

[38] D. D. Wagman, W. H. Evans, V.B. Parker, R. H. Schumm, R. H. Harlow, S. M. Baily, K. L. Churney, and R. L. Nuttall. The NBS tables of chemical thermodynamic properties: selected values for inorganic and C_1 and C_2 organic substances in SI units. *J. Phys. Chem. Ref. Data*, 11(Suppl2), 1982.

[39] Werner Stumm and James J. Morgan. *Aquatic Chemistry. An Introduction Emphasizing Chemical Equilibria in Natural Waters.* John Wiley and Sons, 2^{nd} edition, 1981.

[40] John Westall. *MICROQL. A Chemical Equilibrium Program in Basic.* Technical Report CH-8600, Swiss Federal Institute of Technology EAWAG, Duebendorf Switzerland, June 1979.

[41] Hans R. Pruppacher and James D. Klett. *Microphysics of Clouds and Precipitation.* D. Reidel Publishing Company, Boston, Mass., 1978.

[42] R. A. Robinson and R. H. Stokes. *Electrolyte Solutions.* Academic Press Inc., New York, 1955.

[43] I. N. Tang and H. R. Munkelwitz. Water activities, densities, and refractive indices of aqueous sulfates and sodium nitrate droplets of atmospheric importance. *J. Geophys. Res.*, 99(D9):18801–18808, 1994.

[44] C. L. Kusik and H. P. Meissner. Electrolyte activity coefficients in inorganic processing. *Fundamental Aspects of Hydrometallurgical Processes AIChE Symposium Series*, 74(173):14–20, 1978.

[45] T.R. Young and J.P. Boris. A numerical technique for solving stiff ordinary differential equations associated with the chemical kinetics of reactive flow problems. *J. Phys. Chem.*, 81:2424–2427, 1977.

[46] Yong Pyo Kim, John H. Seinfeld, and Pradeep Saxena. Atmospheric gas-aerosol equilibrium II. Analysis of common approximations and activity coefficient calculation methods. *Aerosol Sci. Technol.*, 19:182–198, 1993.

[47] Arthur W. Stelson and John H. Seinfeld. Relative humidity and temperature dependence of the ammonium nitrate dissociation constant. *Atmos. Environ.*, 5:983–992, 1982.

[48] Douglas R. Lawson. The Southern California Air Quality Study. *J. Air Waste Manage. Assoc.*, 40:156–165, 1990.

[49] H. Andrew Gray. *Control of Atmospheric Fine Primary Carbon Particle Concentrations.* PhD dissertation, also published as Environmental Quality Laboratory Report 23, California Institute of Technology, Pasadena, 1986.

[50] S. Gharib and G.R. Cass. *Ammonia Emissions in the South Coast Air Basin, Open file report 84–2.* Environmental Quality Laboratory, Calif. Inst. of Technol., Pasadena, 1984.

[51] D. R. Fitz, M. Chan, G. R. Cass, D. R. Lawson, and L. Ashbaugh. A multi-component size-classifying aerosol and gas sampler for ambient air monitoring. 1989. Paper No. 89-140.1, presented at the Air and Waste Management Association 82nd Annual Meeting.

[52] Walter John, Stephen M. Wall, Joseph L. Ondo, and Wolfgang Winklmayr. Modes in the size distribution of atmospheric inorganic aerosol. *Atmos. Environ.*, 24A:2349–2359, 1990.

[53] Annmarie Eldering, Glen R. Cass, and K. C. Moon. An air monitoring network using continuous size distribution monitors: Connecting pollutant properties to visibility via Mie scattering calculations. *Atmos. Environ.*, 28:2733–2749, 1994.

[54] Susanne Hering, Annmarie Eldering, and John H. Seinfeld. Bimodal character of accumulation mode aerosol mass distribution in southern California. *Atmos. Environ.*, 31:1–11, 1997.

3 Source Contributions to the Size and Composition Distribution of Urban Particulate Air Pollution

[1]

3.1 Introduction

Strategies to improve ambient air quality in large urban centers typically involve the reduction of emissions from primary pollutant sources. When undertaking the preliminary design of control strategies to limit airborne particle concentrations it is useful to be able to observe the separate contributions that different emissions sources make to the ambient particle size distribution and chemical composition. Traditional methods for separately visualizing source-contributions to particulate air quality rely on receptor-oriented statistical models or non-reactive transport models since previous mechanistic aerosol processes models that follow the evolution of particle size and composition in the presence of atmospheric chemical reactions have not been structured to reveal the sources from which the particles originated. The purpose of the present chapter is to illustrate how a mechanistic aerosol

[1]Reference: Kleeman, M. J.; Cass, G. R. Source Contributions to the Size and Composition Distribution of Urban Particulate Air Pollution *Atmos. Environ.*, **32**, 1998: 2803-2816.

processes model can be structured to reveal the source contributions to the size and composition distribution of the airborne particle complex. In the following sections, the formulation of this model is discussed. The model then is exercised to predict source contributions to the size and composition distribution of the atmospheric particulate matter observed at Claremont, California, during the August 28, 1987, episode of the Southern California Air Quality Study (SCAQS).

3.2 Model Description

The Lagrangian aerosol processes trajectory model used in the current study is descended from previous formulations developed by Eldering and Cass [1] and Kleeman et al. [2]. It examines the evolution of the size-and chemically-resolved ambient aerosol when gas-to-particle conversion processes are active. This model includes a description of all aerosol processes relevant to regional air pollution problems including emissions, transport, deposition, gas-to-particle conversion and fog chemistry. In the present application, the atmospheric aerosol is represented as a source-oriented external mixture [2] in which particles emitted from the different major source types in the airshed are tracked separately as they interact with the surrounding gas phase. By this means the separate contributions that particles from each source make to ambient air quality can be determined.

3.2.1 Major Features

Transport of gas-phase and particle-phase pollutants is represented within an air column that is advected by the wind across the airshed of interest. Meteorological fields that describe air motion, mixing depths, temperature, relative humidity and the spatial extent of fog events are calculated based on inter-

polation of observed data using the methods of Goodin et al. [3]. Air parcel trajectories then are integrated through these meteorological fields. Transport in the vertical direction is described within a stack of computational cells with thicknesses (beginning at ground level and proceeding upwards) of 34.5 m, 105.5 m, 140 m, 330 m, and 390 m producing a modeling region 1000 m thick. Dry deposition of gas-phase species is based on boundary layer theory and land-use specific surface resistances as described by Russell et al. [4]. Deposition of particles to the earth's surface is calculated according to the method of Slinn and Slinn [5] with modifications to account for the effect of changes in atmospheric stability conditions [2]. The gas-phase mechanism used within the model is based on the chemical mechanism of Carter [6] with extensions to track the formation of secondary organic aerosol as described by Pandis et al. [7]. Gas-phase chemical reactions within all of the vertical cells are directly coupled to the transport and deposition equations and are propagated simultaneously using a modified form of the Young and Boris solver [8, 2]. To increase computational efficiency, operator splitting techniques are used to couple gas-to-particle conversion calculations to particle-phase transport and gas-phase transport and reaction as described by Eldering and Cass [1]. In the absence of fog conditions, the exchange of chemical species between the gas phase and the particle phase is calculated using the computer code AIM [9] with modifications to improve the accuracy and efficiency of the calculation [2]. During periods of fog, exchange of chemical species between the gas phase and droplet phase and subsequent modification of aqueous species by oxidation processes is calculated using the fog model described by Jacob [10] and Jacob et al. [11] as implemented by Kleeman et al. [2].

The processes listed above may be described by a Lagrangian trajectory

form of the atmospheric diffusion equation

$$\frac{\partial G_j}{\partial t} = \frac{\partial}{\partial z}(K_{zz}\frac{\partial G_j}{\partial z}) - \sum_k L_{ij}^k(G, P^k, T, RH) + R_j(G, T, RH); \quad j = 1, 2, ...n \tag{3.1}$$

$$\frac{\partial P_i^k}{\partial t} = \frac{\partial}{\partial z}(K_{zz}\frac{\partial P_i^k}{\partial z}) + \sum_j L_{ij}^k(G, P^k, T, RH) + M_i^k(P^k, T, RH); \quad i = 1, 2, ...m \tag{3.2}$$

where G_j is the gas-phase concentration of species j, P_i^k is the concentration of chemical species i present in particles of type k, K_{zz} is the turbulent eddy diffusivity in the vertical direction z, L_{ij}^k is the gas-to-particle conversion rate for gas-phase species j that form aerosol-phase species i on particles of type k, R_j is the rate of production of gas-phase species j due to gas-phase reaction, M_i^k is the rate of production of species i within particles of type k due to aqueous-phase chemical reaction, T is the absolute temperature, and RH is the ambient relative humidity. Initial conditions for the problem may be stated as:

$$G_j(z, t) = G_j^o(z), \quad t = 0 \tag{3.3}$$

$$P_i^k(z, t) = P_i^{ko}(z), \quad t = 0 \tag{3.4}$$

Boundary conditions have the form:

$$(K_{zz}\frac{\partial G_j}{\partial z}) = 0, \quad z = H \tag{3.5}$$

$$(K_{zz}\frac{\partial P_i^k}{\partial z}) = 0, \quad z = H \tag{3.6}$$

$$[v_{gj}G_j - K_{zz}\frac{\partial G_j}{\partial z}] = E_{gj}, \quad z = 0 \tag{3.7}$$

$$[v_p^k P_i^k - K_{zz}\frac{\partial P_i^k}{\partial z}] = E_{pi}^k, \quad z = 0 \tag{3.8}$$

where H is the height of the top of the air column represented by the stack of computational cells, v_{gj} is the deposition velocity for gas-phase species j, v_p^k

is the deposition velocity for particles of type k, E_{gj} is the gas-phase emission rate of species j, and E_{pi}^{k} is the emission rate for species i present on particles of type k. Coagulation and nucleation processes are neglected because calculations show that these processes cannot compete with condensation onto atmospheric particles under typical urban conditions.

3.2.2 Emissions Model

Information on the emission rate of oxides of nitrogen, volatile organic compounds (VOC), carbon monoxide, sulfur dioxide, ammonia and total particulate matter mass first is gathered for each source of interest. This information is then transformed into a statement of the emission rates of individual gas-phase organic species and particle-phase chemical species using a system of source profiles that describe in detail the organic composition of VOC emissions and the size and composition of particulate matter emissions. The emissions model used for gas-phase species follows the treatment of Harley et al. [12, 13, 14] and Eldering and Cass [1]. Particle-phase emissions are created using the emissions model of Eldering and Cass [1]. The model uses the total particulate emission rate for a specified source along with the size and composition profile assigned to that source to create a chemical profile for particles emitted to the atmosphere in terms of the following components: elemental carbon, organic carbon, sodium, chloride, ammonium, sulfite, sulfate, nitrate, iron (oxidation states II and III), manganese (oxidation states II and III), copper (oxidation states I and II), all remaining metals as a single group, and all other non-metallic species as a single group. The size distribution of particles emitted from each source is represented by 15 discrete particle diameters centered within equally spaced logarithmic size intervals spanning the diameter range from 0.01μm to 10μm. The initial relative chem-

ical composition of particles of all sizes from the same source is assumed to be identical since data that distinguish differences in the composition of particles of different sizes from the same source are not available in general. To create a source-oriented mixture of particles, primary particle emissions from the following source types are tracked separately after their release to the atmosphere: catalyst-equipped gasoline engines, non-catalyst equipped gasoline engines, diesel engines, meat cooking, paved road dust, crustal material from sources other than paved road dust, and sulfur-bearing particles from fuel burning and industrial processes. These sources typically account for 85% to 90% of the anthropogenic primary particulate matter (with particle diameter less than or equal to 10μm) emitted in an urban location such as Los Angeles. Particulate emissions from the remaining sources are combined to produce a single lumped source category.

3.2.3 Particle Aging

In reality, the size and chemical composition of individual particles emitted into the atmosphere are transformed over time by gas-to-particle conversion processes. However, all of the atmospheric aerosol processes models which have been demonstrated to date mix the fresh particle-phase emissions from each source into the pre-existing ambient aerosol on a particle-by-particle basis. This creates a reduced number of individual computational particles, each of which have averaged properties somewhere between those of the fresh particle emissions and an aged ambient aerosol. Since particle composition influences gas-to-particle conversion processes, it is expected that averaging freshly emitted particle characteristics into the pre-existing ambient aerosol will affect the transfer of material between the gas and particle phases. In the current application, the source-oriented mixture model described by Kleeman

et al. [2] is expanded to allow particles to age in a more realistic fashion. Each source emits particles to the atmosphere at the rate, size, and chemical composition determined by the source strength and the emissions processing model described previously. All particles emitted from the same source type during the same hour are tracked separately from all other particles in the model. An external mixture of particles is created in which all particles interact with the same gas phase conditions, but aged particles differ from freshly emitted particles even though they may have been emitted originally from the same source type. By this method, particles are allowed to age in a more realistic fashion without distortion due to the effects caused by averaging two particle groups with different chemical compositions. For example, hydrophobic freshly emitted diesel soot particles are distinguished from aged diesel particles that have become coated with sulfates and nitrates over time, which in turn affects the hygroscopic properties of these older particles and thus their interaction with the gas phase.

3.3 Model Application

Application and evaluation of the aerosol processes model described in the current study requires a well characterized air pollution event since detailed information on meteorological conditions and emissions rates are needed as model inputs while measurements of ambient air quality (including size resolved chemical composition of particulate matter) are needed for model evaluation. The Southern California Air Quality Study (SCAQS) was a large cooperative air quality measurement program carried out in the South Coast Air Basin of California to collect information for the application and evaluation of air quality models [15]. The data collected during the SCAQS episode of August 27-28, 1987, at Claremont, California, has been used extensively in

previous investigations including both the model evaluation studies of Eldering and Cass [1] and Kleeman et al. [2]. To allow a comparison of the effects of the revised particle aging calculation to this previous work, data from the August 27-28, 1987, SCAQS episode also will be used in the current study to verify model performance against ambient data and to illustrate source contributions to the ambient particle size and composition distribution.

3.3.1 Model Inputs

Model inputs specific to the August 27-28, 1987, SCAQS episode have been described previously by Eldering and Cass [1] and by Kleeman et al. [2] and so only a brief summary is presented here. Meteorological inputs are interpolated based on observational data using the method of Goodin et al. [3]. Twenty-four trajectories of 48 hours duration each start over the Pacific Ocean and terminate at Claremont, CA, at each hour of the day on August 28, 1987. Claremont is a photochemical smog receptor site located approximately 70km inland from the Santa Monica Bay coastline of Los Angeles County; a map showing its location relative to a trajectory path followed during this episode is given in Figure 2 of Eldering and Cass [1]. Particle-phase initial conditions for the episode modeled are identical to those shown by Kleeman et al. [2] and are based on filter samples taken at San Nicolas Island during SCAQS, with their size distribution shaped according to impactor samples taken near the ocean. Gas-phase initial conditions are the same as those presented by Eldering and Cass [1] based on measurements made over the ocean during SCAQS. Source locations and estimated mass emissions rates for major gas and particle-phase emissions sources relevant to the August 27-28, 1987, SCAQS episode were obtained from the California Air Resources Board (ARB). This inventory includes a description of NO_x,

SO_x, CO volatile organic compounds (VOC) and total particulate matter emissions along with the diurnal variation of each source. Carbon monoxide and organic gas hot exhaust emissions from on-road vehicles are scaled to three times the levels shown in the official ARB inventory based on the results of experiments conducted in a Los Angeles area highway tunnel as described by Harley et al. [14]. More recent information concerning the particulate emission rates for motor vehicles, paved road dust and dust from construction and demolition sites also is used as described by Eldering and Cass [1], and the diurnal profile used for commercial food cooking operations is modified to match that described by Gray [16]. Ammonia emissions for the episode studied are represented using the 1982 spatially and temporally resolved NH_3 emission inventory for the South Coast Air Basin [17, 18]. Emission rates for total VOC's and particulate matter mass then are used as inputs to an emissions processing model which calculates the detailed organic gas speciation and particle-phase size and chemical composition distribution for each source as described in Section 2.2. Through that emissions processing model, data on VOC composition and particle size and composition originally supplied by the ARB are replaced with newer information for the most important source types [1].

3.3.2 Results

Model results for the 24 trajectories arriving hourly at Claremont on August 28, 1987, predict the ambient concentration of major gas-phase pollutants as well as the concentration, size distribution and chemical composition of particle-phase species. Gas-phase species such as ozone and oxides of nitrogen show little variation from the values reported previously by Eldering and Cass [1] and thus will not be discussed in the current analysis. All model

results for particulate matter shown in the following sections are illustrated at the corresponding dry particle diameters [2] since it has been previously determined that the instruments used to measure particle size distributions at Claremont during SCAQS dried out the aerosol while making their measurements [19].

Comparison to Ambient Filter Samples

Measurements of particle-phase pollutant concentrations at Claremont on August 28, 1987, were made using a filter-based SCAQS sampler [20], during five discrete sampling periods: 0:00-5:00 PST, 5:00-9:00 PST, 9:00-13:00 PST, 13:00-17:00 PST, and 17:00-24:00 PST. A comparison of the average concentration and bulk chemical composition of the aerosol as measured by filter-based sampling to the results produced by the source-oriented external mixture model with particle aging is sufficiently similar to that shown in Table 2.3 of Chapter 2 without particle aging that the table will not be repeated here. The predictions are in reasonable agreement with observations across a broad range of particle chemical species. Results for elemental carbon (EC) and organic carbon (OC) found in particles with diameter less than 2.5 μm overpredict observed values by only 0.52μg m^{-3} and 2.32μg m^{-3} respectively. Predicted concentrations of the ionic species $SO_4^=$, NH_4^+, NO_3^-, and Na^+ fall below observed values by only 1.0, 1.8, 2.6 and 0.33μg m^{-3}, respectively. The mean PM10 concentration is overpredicted but is within 13% of the observed value of 96μg m^{-3}.

Comparison to Ambient Impactor Samples

Comparisons of model predictions at Claremont, CA, on August 28, 1987, are made to ambient measurements taken with a 9 stage Berner impactor [21] and a micro orifice uniform deposit impactor [22]. The impactor data at

Claremont, CA, on August 28, 1987, were collected in four discrete sampling periods from 5:00-9:00 PST, 9:00-13:00 PST, 13:00-17:00 PST and 17:00-24:00 PST. A comparison of model results averaged over the 13:00-17:00 PST sampling period to the impactor measurements during this interval is shown in Figure 3.1 for particle-phase elemental carbon, organic carbon, sodium, ammonium, nitrate, and sulfate. These results generally show excellent agreement with the observations both in terms of the shape of the species size distributions and the location/magnitude of the peak in the size distribution for each of the chemical species, with the possible exception of coarse particle organics. Predicted organic carbon concentrations in the larger particle sizes are higher than those measured by the impactor. This result may be due in part to the fact that this impactor was preceded by a cyclone separator used to remove particles with a diameter greater than approximately 2μm in order to suppress particle bounce. Model predictions are consistent with the results of fine paved road dust source tests which show at least some organic carbon in the particle size range between 0.5-2μm [23].

Predicted sodium concentrations are low relative to observations for particles larger than approximately 4μm diameter, matching the trend noted previously by Eldering and Cass [1] and Kleeman et al. [2]. This is likely due to the use of a single set of initial conditions for all trajectories arriving at Claremont on August 28, 1987. Virtually all of the sodium in the atmosphere is associated with the background marine aerosol. If the initial conditions were known more exactly, it is expected that the sodium deficiency in the model predictions would be corrected. It is interesting to note that if additional sodium was present in the particle size range between 4-10μm diameter, increased nitrate would also be expected at these particle sizes, probably correcting the remaining discrepancy between the predicted and

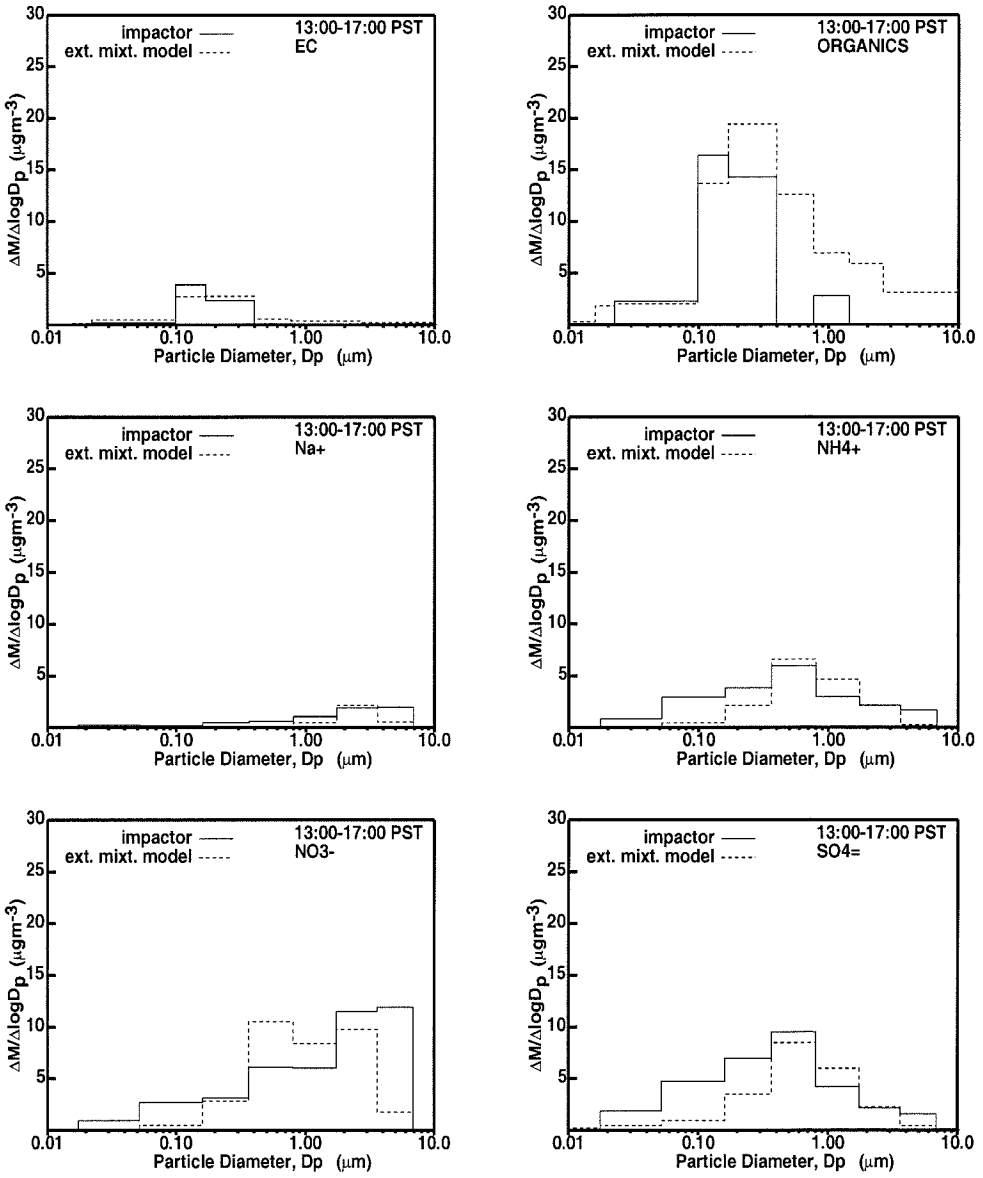

Figure 3.1:
Model predictions of the mass distribution, $\Delta M/\Delta \log Dp$, of individual chemical species compared to impactor measurements made during the sampling period 13:00-17:00 PST on August 28, 1987, at Claremont, CA.

observed nitrate size distributions for this sampling period.

Comparison to Ambient Size Distribution Measurements

Ambient particle size distributions at Claremont, CA, on August 28, 1987, were measured over the size range from 0.01μm to 1μm particle diameter using a TSI electrical aerosol analyzer (EAA), and a laser optical particle counter (OPC) as described by Eldering et al. [19]. The response of those instruments falls off above 1μm particle diameter; the aerosol volume present between 2.5μm and 10μm particle diameter can be obtained from the difference between SCAQS sampler PM10 vs PM2.5 filters, but no information other than the total aerosol volume in that size range is known. A comparison of model predictions and measured values for hour 13:00 PST on August 28, 1987, at Claremont, CA, is shown is Figure 3.2, along with the predicted size and composition information from the air quality model. Hour 13:00 PST was chosen for detailed analysis because it is an hour in the peak photochemical smog period of the day that is different from the hours for which model results have been displayed in previous papers (Eldering and Cass, 1996; Kleeman et al., 1997). Model predictions for the particle size distribution show good agreement with electronic instrument measurements both in terms of the profile shape and the peak locations. Chemically resolved model predictions indicate that a significant fraction of the PM10 mass is composed of secondary formation products at this time and location. It has been noted previously [21, 19, 24] that the ambient aerosol measured during SCAQS typically exhibited two peaks in the submicron size range: one at approximately 0.7μm particle diameter plus a smaller mode located at about 0.2μm particle diameter. The present model captures both modes in the size distribution at hour 13:00 PST on August 28, 1987, at Claremont, CA.

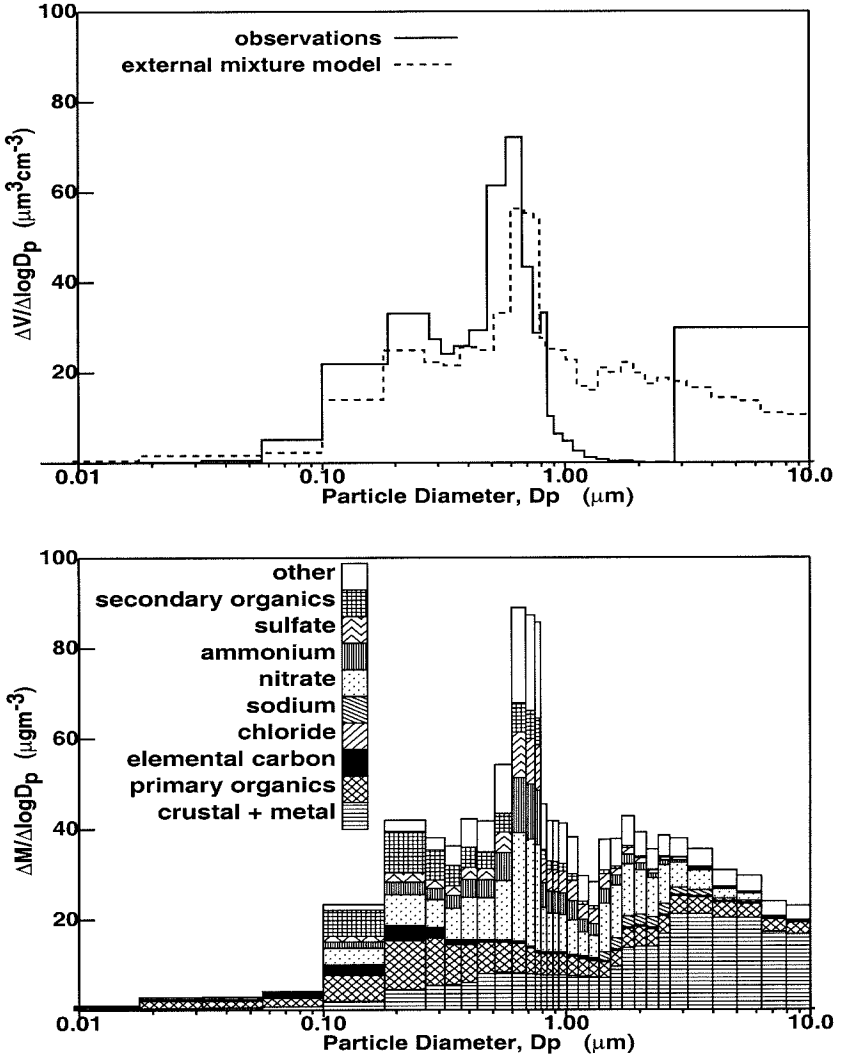

Figure 3.2:
Comparison of measured and predicted size and composition distributions at 13:00 PST on August 28, 1987, at Claremont, CA. Observed aerosol size distributions were measured using electrical aerosol analyzers, optical particle counters and filter samplers. Observations generally do not exist between 1.0 and 2.5μm particle diameter; the aerosol volume in sizes between 2.5-10μm particle diameter is based on the difference between PM2.5 and PM10 filter samples and conveys no information about the shape of the particle size distribution in that range.

Model performance in comparison to observations is favorable. Nevertheless, it is important to note that there are inherent limitations in the trajectory model formulation of atmospheric transport processes (see [25]) and that emissions inventories required for particle formation modeling are undergoing rapid review and improvement. In order to assess the sensitivity of model results to changes in emissions, a different 1987 emissions inventory recently prepared by the South Coast Air Quality Management District was processed through the model, and the diurnal variation of NH_3 emissions into the model was perturbed. These changes did not significantly alter the conclusions of the present study.

Source Contributions to Ambient Concentrations

The purpose of the study described in this chapter is to investigate the contribution to the ambient particle mixture made by different emission sources using a mechanistic, size-resolved model. Figure 3.3 shows the size- and chemically-resolved ambient predictions for particles in the atmosphere at Claremont, CA, on August 28, 1987, at 13:00 PST as predicted by the time- and source-separated external mixture model. Each of the graphs in Figure 3.3 shows the concentration, chemical composition and size distribution of the primary seed particles released into the model from a separate major source type plus those gas-to-particle conversion products that have accumulated on those seed particles over time. For each primary particle source type, particles of all ages are summed to create the sub-plots shown in Figure 3.3.

Model results indicate that particles emitted from paved road dust sources and crustal sources other than paved road dust dominate particle concentrations in sizes larger than $1\mu m$ diameter. Very little secondary aerosol accumulates on these generally hydrophobic dust particles. The somewhat

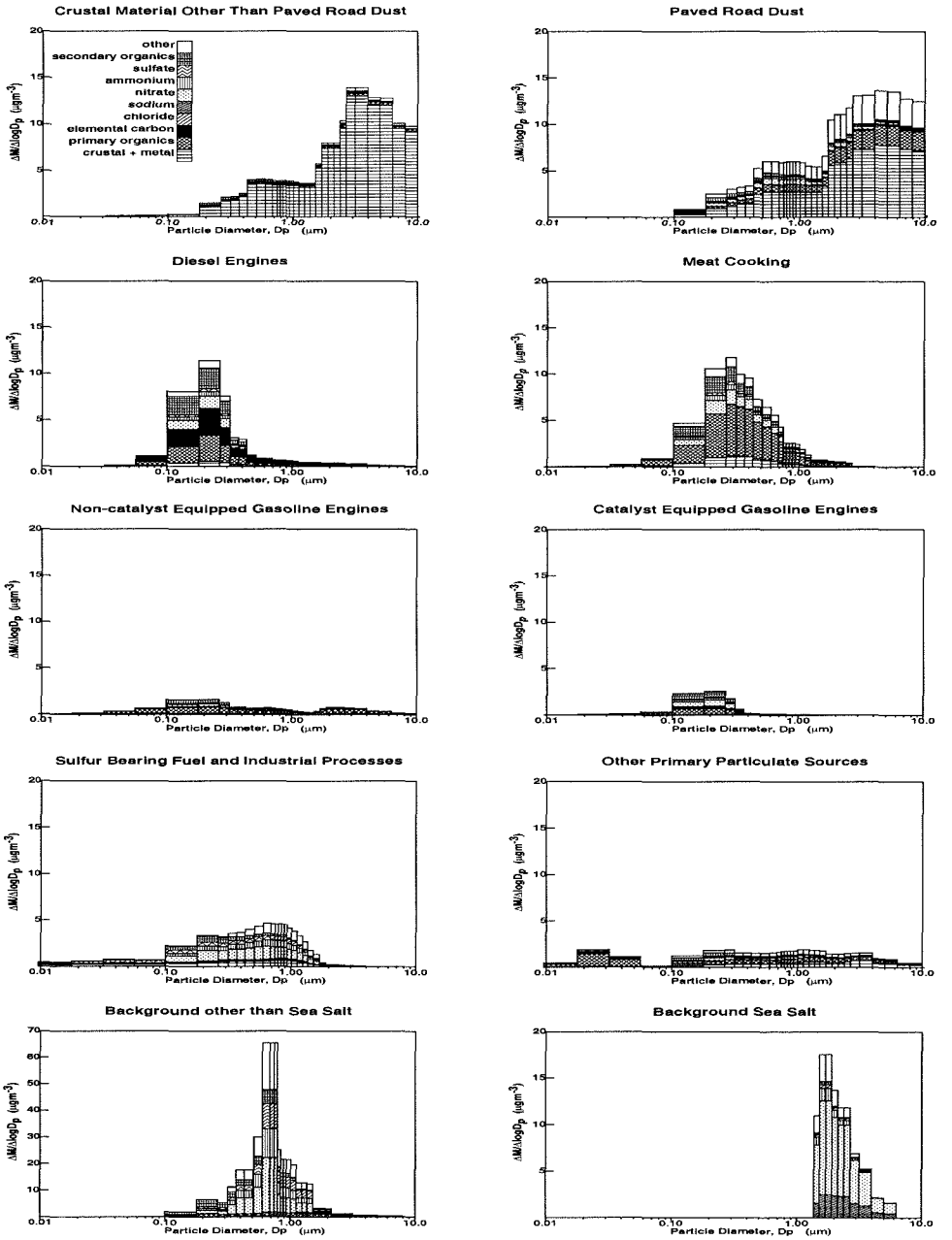

Figure 3.3:
Individual source contributions to the particle size and chemical composition distributions predicted at 13:00 PST on August 28, 1987, at Claremont, CA. Each subplot represents the primary seed particles of many ages emitted from the indicated source along with the associated gas-to-particle conversion products that have accumulated on those seed particles over time.

more complex composition of paved road dust particles reflects the fact that they contain more primary organic material and other materials at the time of emission to the atmosphere. Particles emitted by diesel engines and meat cooking operations dominate the smaller primary particles in the atmosphere at Claremont, CA, on August 28, 1987, at 13:00 PST. Both types of particles have a single mode centered between 0.2-0.3μm particle diameter. Meat cooking particles are composed primarily of organic material, while diesel engine particles have greater elemental carbon content. The older particles of these types have accumulated coatings of secondary formation products such as ammonium nitrate and secondary organic carbon. Particles from the tail pipes of catalyst- and non-catalyst equipped gasoline engines make only a minor contribution to the ambient particle-phase complex at this time and location. Emissions of sulfur-bearing primary particles from fuel burning and from industrial sources show evidence of significant transformation through gas-to-particle conversion processes, reflecting the hygroscopic nature of these particles. Likewise, background marine particles (both sea salt and aged long distance transport of ammonium/sulfate/nitrate - containing particles) show very significant evidence of further processing by gas-to-particle conversion processes within the air basin. Particles which started out as NaCl over the ocean are converted entirely to $NaNO_3$ with trace amounts of S(IV)-carbonyl products by the time they reach Claremont. Background particles originally composed of ammonium, sulfate and nitrate show significant further accumulation of ammonium, nitrates, sulfates and S(IV)-carbonyl products present within the "other" category in Figure 3.3. The presence of this latter species indicates that these particles underwent significant fog processing in the presence of gas phase formaldehyde and SO_2. The extent to which the S(IV)-carbonyl reaction products remain in the particle phase upon fog evaporation

is an open question at present; Jacob [11] assumes that these chemical species become associated with ammonium and remain in the particle phase as the aerosol dries out after the fog.

Figure 3.4 shows the atmospheric size distribution broken down according to source type. Primary particles emitted from the different sources tracked by the model become coated by gas-to-particle conversion products over time. The contribution that the primary particles from specific sources make to the atmospheric particle size and composition distribution can be graphed either with or without the secondary aerosol coatings that have accumulated on those particles. In the upper frame of Figure 3.4, source contributions are grouped according to primary seed particle type and include the secondary aerosol material accumulated on those seed particles, while in the lower frame of Figure 3.4, all sulfates, nitrates, ammonium ion and secondary organics are grouped separately from the rest of the primary seed particles on which they are present. Model predictions indicate that particles larger than approximately 2μm diameter are primarily associated with paved road dust sources, crustal material sources other than paved road dust, and the transformation products of background sea salt. The small particle mode in the size distribution located between 0.2-0.3μm particle diameter is created primarily by emissions from diesel vehicles and meat cooking operations. Finally, the large peak in the size distribution located at 0.7μm particle diameter is created by the further accumulation of gas-to-particle conversion products onto the aged non-NaCl background aerosol originating from long distance transport. These "background" particles are altered significantly as they are advected across the air basin in the presence of fog and increased sulfur dioxide, ammonia and nitric acid gas phase concentrations.

The predicted source contributions to PM2.5 and PM10 particle mass

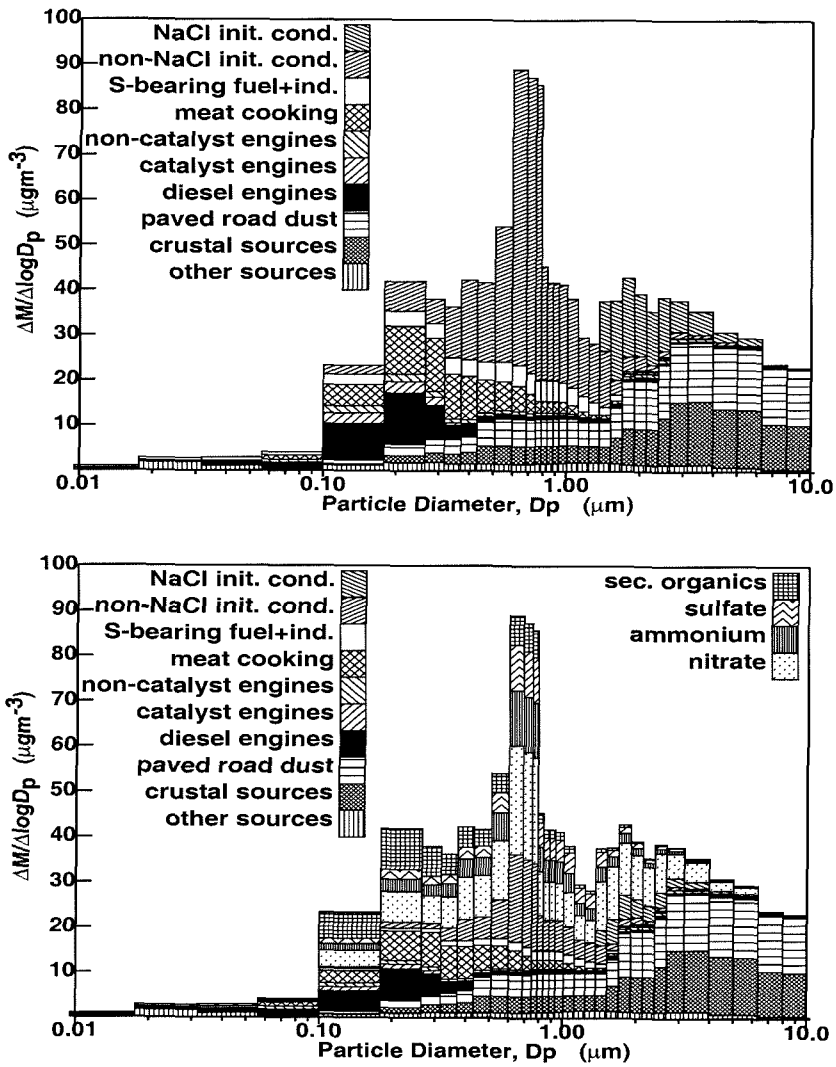

Figure 3.4:
Source contributions to the aggregate particle distribution predicted at 13:00 PST on August 28, 1987, at Claremont, CA. The upper frame in this figure is graphed according to primary seed particle source type and includes the secondary material accumulated on the seed particles. The lower frame is also graphed according to primary seed particle source type, but all sulfates, nitrates, ammonium ion, and secondary organic aerosol are separated from the primary seed particles.

concentrations at Claremont, CA, averaged over each hour of August 28, 1987, are shown in the first columns of Table 3.1 and Table 3.2 respectively. The concentration increments shown in these columns are those due to the primary seed particles from each source type studied plus the gas-to-particle conversion products that have accumulated on those seed particles over time. Transformed background particles that originally were composed primarily of $(NH_4)_2SO_4$ within the non-NaCl initial condition and that accumulate additional sulfates, nitrates, organics and other secondary reaction products during transit across the air basin are the largest single contributor to PM2.5 concentrations. Significant contributions to PM2.5 mass are also made by diesel engines, meat cooking operations, paved road dust, and crustal material from sources other than paved road dust. Model results predict that 45% of the PM10 mass concentration is contributed by paved and unpaved road dust.

The air quality model also can be used to closely examine the distinction between primary contributions versus secondary aerosol formation for those chemical species that could be either emitted directly in primary particles or formed by atmospheric reaction. In the second and subsequent columns of Tables 3.1 and 3.2, the predicted concentrations of sulfates, ammonium, nitrates, chloride and organic aerosol in the PM2.5 and PM10 fractions of the ambient aerosol are listed and separated into an amount present on each particle type initially at its source plus an increment due to the net effect of atmospheric chemical reactions. Other species (e.g., elemental carbon, metals) are excluded from the tables; hence the difference between total mass concentrations and the sum of the listed species. Of the fine particle sulfate at Claremont, CA, on August 28, 1987, the model predicts that 43% was due to pre-existing sulfate within the background aerosol, 19% was due

to primary particulate sulfate emissions into the trajectories within the air basin, and 38% was due to atmospheric oxidation of SO_2 within air parcel trajectories crossing the air basin (of course the pre-existing background itself is due in part to both primary sulfates plus SO_2 oxidation over longer transport times). Fine particle ammonium is divided into 21% present due to the marine background plus 79% due to secondary formation within the trajectory model. Fine particle nitrate ion is almost entirely due to secondary formation, with only 4% contributed by the pre-existing atmospheric background aerosol and 1.5% due to primary nitrate emissions. The primary chloride is almost completely stripped from the aerosol by atmospheric reaction (negative amount of secondary formation). Secondary organic aerosol is by definition formed by atmospheric reactions. Secondary organics on average account for 20% of the entire (pre-existing plus primary and secondary) fine organic aerosol concentration.

Modification of Source Profiles with Age

The time- and source-separated external mixture model categorizes particles according to the emission source from which primary seed particles are emitted. In the present study, several source categories are defined with the property that only a single source profile or two very similar source profiles contribute to particles of that type. These categories include catalyst-equipped gasoline engines, non-catalyst equipped gasoline engines, diesel engines, meat cooking, paved road dust, and crustal material from sources other than paved road dust. It is possible to examine particles of different ages within each of these categories and directly view the effect of the atmospheric transformation processes which have acted on them. Figures 3.5 and 3.6 show the size distributions and chemical compositions of particles of various age (since the

Table 3.1: Source Contributions to 24-hour Average PM2.5 Particulate Matter Concentrations at Claremont, CA, August 28, 1987

Source type	PM2.5[a]	$SO_4^=$		NH_4^+		NO_3^-		Cl^-		Organics	
	(μg m^{-3})	Prim[b]	Sec[c]	Prim[b]	Sec[c]	Prim[b]	Sec[c]	Prim[b]	Sec[c]	Prim[b]	Sec[c]
Paved road dust	11.64	0.13	0.08	0.00	0.20	0.03	0.40	0.02	-0.01	1.75	0.15
Other crustal material	7.18	0.01	0.05	0.00	0.07	0.01	0.18	0.01	-0.01	0.16	0.12
Diesel engines	10.13	0.01	0.45	0.01	0.58	0.02	1.41	0.02	-0.01	2.57	1.08
Meat cooking	11.67	0.06	0.25	0.00	0.37	0.01	0.95	0.21	-0.19	6.79	0.51
Catalyst gasoline engines	2.01	0.05	0.07	0.00	0.12	0.02	0.30	0.03	-0.02	0.82	0.18
Non-cat gasoline engines	2.56	0.01	0.05	0.00	0.08	0.01	0.20	0.02	-0.01	1.65	0.14
S-bearing fuel+ind	4.34	0.61	0.31	0.03	0.54	0.01	0.97	0.02	-0.02	0.23	0.27
Other sources	8.10	0.30	0.14	0.00	0.19	0.08	0.41	0.08	-0.01	3.35	0.32
NaCl initial cond.	3.52	0.00	0.07	0.00	0.25	0.00	2.41	0.97	-0.96	0.00	0.05
non-NaCl initial cond.	15.56	2.61	0.88	1.09	1.74	0.51	4.57	0.00	0.01	1.42	1.80
Total	76.70	3.79	2.35	1.12	4.14	0.72	11.80	1.38	-1.24	18.75	4.60

[a] Concentration increment includes both primary particle core plus net accumulation of secondary aerosol due to atmospheric chemical reactions. Source contributions without secondary reaction products can be computed by subtracting secondary components listed in columns 3, 5, 7, 9, and 11. [b] Concentration increment due to primary particle emissions or pre-existing aerosol (μg m^{-3}). [c] Net concentration increment due to atmospheric chemical reaction within trajectories crossing the air basin (μg m^{-3}).

Table 3.2: Source Contributions to 24-hour Average PM10 Particulate Matter Concentrations at Claremont, CA, August 28, 1987

Source type	PM10[a]	$SO_4^=$		NH_4^+		NO_3^-		Cl^-		Organics	
	(μg m^{-3})	Prim[b]	Sec[c]	Prim[b]	Sec[c]	Prim[b]	Sec[c]	Prim[b]	Sec[c]	Prim[b]	Sec[c]
Paved road dust	31.88	0.37	0.09	0.00	0.33	0.08	0.57	0.05	-0.04	4.98	0.15
Other crustal material	17.44	0.03	0.05	0.00	0.09	0.02	0.23	0.02	-0.02	0.41	0.12
Diesel engines	10.30	0.01	0.45	0.01	0.58	0.02	1.41	0.02	-0.01	2.63	1.08
Meat cooking	11.67	0.06	0.25	0.00	0.37	0.01	0.95	0.21	-0.19	6.79	0.51
Catalyst gasoline engines	2.02	0.05	0.07	0.00	0.12	0.03	0.30	0.03	-0.02	0.83	0.18
Non-cat gasoline engines	3.03	0.01	0.05	0.00	0.08	0.02	0.21	0.02	-0.02	2.01	0.14
S-bearing fuel+ind.	4.36	0.61	0.31	0.03	0.54	0.01	0.97	0.02	-0.02	0.23	0.27
Other sources	9.40	0.31	0.14	0.00	0.20	0.09	0.42	0.08	-0.01	3.82	0.32
NaCl initial cond.	4.73	0.00	0.11	0.00	0.31	0.00	3.21	1.36	-1.33	0.00	0.05
Non-NaCl initial cond.	15.90	2.67	0.88	1.14	1.74	0.61	4.55	0.00	0.01	1.55	1.80
Total	110.73	4.13	2.42	1.18	4.36	0.88	12.83	1.81	-1.65	23.26	4.62

[a] Concentration increment includes both primary particle core plus net accumulation of secondary aerosol due to atmospheric chemical reactions. Source contributions without secondary reaction products can be computed by subtracting secondary components listed in columns 3, 5, 7, 9, and 11. [b] Concentration increment due to primary particle emissions or pre-existing aerosol (μg m^{-3}). [c] Net concentration increment due to atmospheric chemical reaction within trajectories crossing the air basin (μg m^{-3}).

time of their emission from different sources) as they arrive at Claremont, CA, at 13:00 PST on August 28, 1987. All size distribution plots are normalized to a common peak height in order to remove the effect of source strength and focus on the effects of atmospheric transformation processes.

Figures 3.5 and 3.6 show that the older particles from all source categories have altered size distributions that reflect the preferential removal of larger particles from the atmosphere by deposition processes. This trend is most noticeable in those particle categories whose emissions contained a greater fraction of large particles at the time of initial release to the atmosphere, such as paved road dust, crustal material from sources other than paved road dust, and non-catalyst equipped gasoline engines. Figures 3.5 and 3.6 also show that non-volatile secondary species such as sulfates accumulate progressively as particles increase in age. The same trend is not apparent for volatile secondary formation products, since these species can redistribute themselves between the gas and particle phases as aerosol properties evolve over time. Thus, concentrations of particle-phase species such as nitrate, ammonium and chloride are not necessarily always greater on older particles relative to more recently emitted particles even though both sets of particles experience the same gas-phase conditions during the lifetime of the newer particles.

In addition to describing the effects of particle aging on emissions from crustal sources other than paved road dust and meat cooking, Figure 3.6 shows the transformation of the background marine particles that act as model initial conditions. Only the initial and final size and composition distributions are shown for these particle types, since there are no further emissions of these particles once particle-phase concentrations are initialized. As discussed previously, that part of the intial conditions originally composed

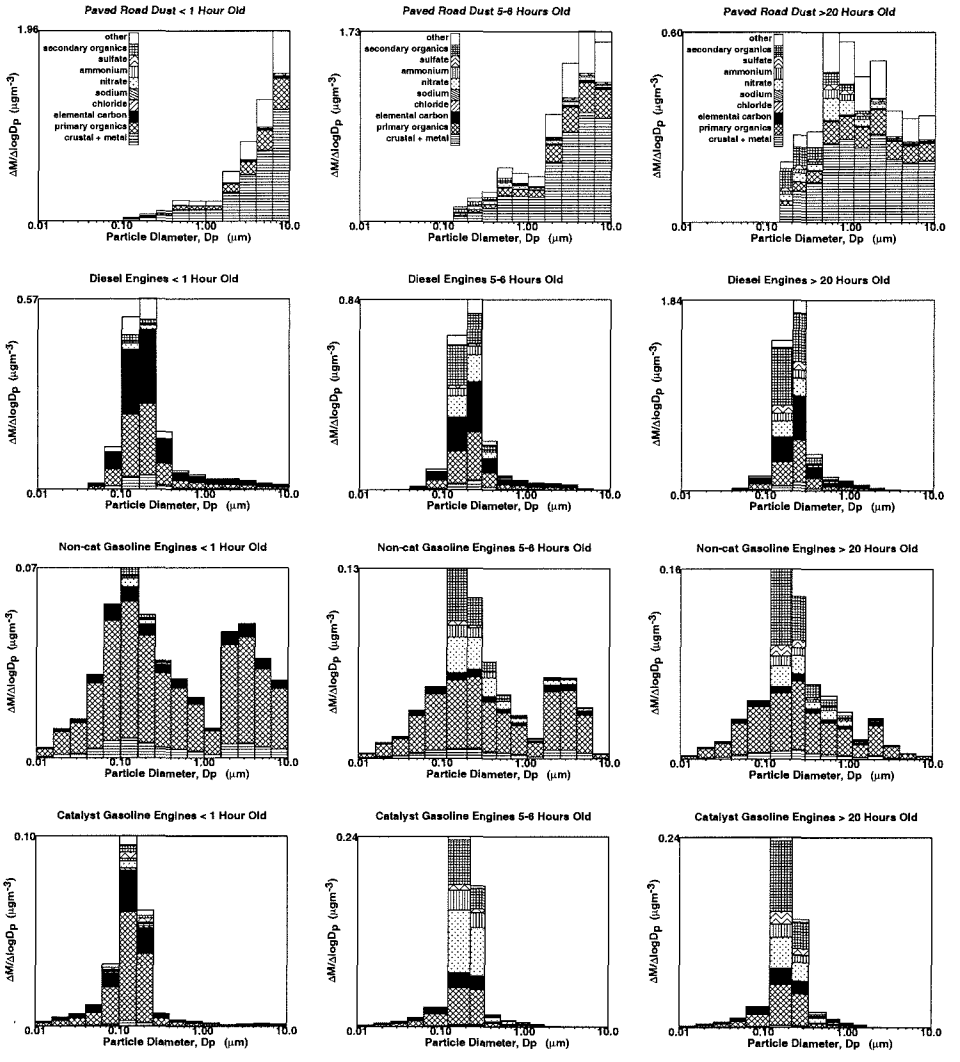

Figure 3.5:
Comparison of particle size and composition distributions for particles of different ages (relative to their release to the atmosphere) as they arrive at Claremont, CA, at 13:00 PST on August 28, 1987. Particles in the left column are less than 1 hour old, particles in the middle column are 5-6 hours old and particles in the right column are greater than 20 hours old.

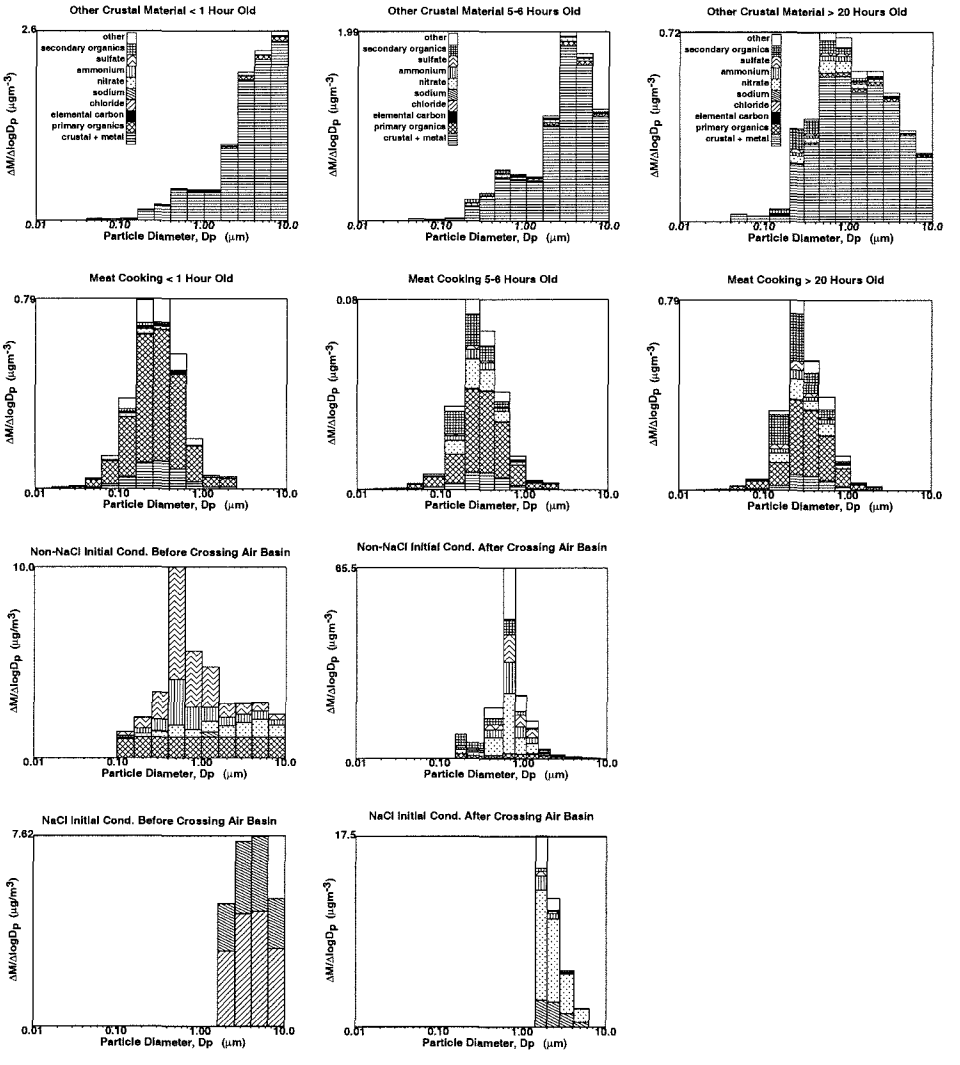

Figure 3.6:
Comparison of particle size and composition distributions for particles of different ages (relative to their release to the atmosphere) as they arrive at Claremont, CA, at 13:00 PST on August 28, 1987. Particles in the left column are less than 1 hour old, particles in the middle column are 5-6 hours old and particles in the right column are greater than 20 hours old. For the background aerosol shown in the lower two sets of frames, only the initial composition at the coast and the final size and composition distribution at Claremont are shown since there are no continuing emissions of particles of these types over land.

of coarse particle sodium chloride aerosol is transformed to sodium nitrate, while the fine particle background originally composed mainly of ammonium nitrate and sulfate shows significant further ammonium and nitrate addition, as well as the accumulation of other material including S(IV)-carbonyl adducts.

3.4 Conclusions

The source- and age-separated external mixture model successfully predicts the size and composition distribution of ambient particle-phase concentrations at Claremont, CA, on August 28, 1987, given data on initial conditions, emissions, and meteorological conditions. Major features of the predicted aerosol size and composition distribution match observations, including the bimodal distribution of the submicron aerosol. Model results indicate that the mode in the particle size distribution that is located between 0.2-0.3μm particle diameter is shaped by transformed primary emissions from sources such as diesel engines and meat cooking operations with lesser contributions from gasoline powered motor vehicles and other combustion sources burning sulfur-bearing fuel. The larger mode in the size distribution located between 0.7-0.8μm particle diameter is caused by fine particle background aerosol (initially containing largely $(NH_4)_2SO_4$) which has been transformed by fog and gas-to-particle conversion processes until it contains much greater quantities of secondary reaction products. Primary contributors to coarse particle concentrations larger than 2.5μm particle diameter consist, not surprisingly, of paved and unpaved road dust particles and transformed sea salt particles. Major primary particle source contributions to fine particle concentrations at Claremont, CA, on August 28, 1987, arise from diesel engine exhaust, food cooking operations, and the fine particle portion of paved and unpaved road

dust. Sources making smaller contributions to fine particulate concentrations include gasoline-powered engines and sources burning sulfur-bearing fuels.

Transformed background particles make a significant contribution to PM2.5 concentrations at Claremont, CA, on August 28, 1987. These results indicate that control of gas-phase pollutant emissions that interact with this background aerosol probably will play an important role in future strategies for control of fine particle concentrations in the Los Angeles area, and that the origin of the fine particle background aerosol itself merits serious investigation.

Bibliography

[1] Annmarie Eldering and Glen R. Cass. Source–oriented model for air pollutant effects on visibility. *J. Geophys. Res.*, 101(D14):19343–19369, 1996.

[2] Michael J. Kleeman, Annmarie Eldering, and Glen R. Cass. Modeling the airborne particle complex as a source-oriented external mixture. *J. Geophys. Res.*, 102(D17):21355–21372, 1997.

[3] William R. Goodin, Gregory J. McRae, and John H. Seinfeld. A comparison of interpolation methods for sparse data: Application to wind and concentration fields. *J. Appl. Met.*, 18:761–771, 1979.

[4] Armistead G. Russell, Darrell A. Winner, Kenneth F. McCue, and Glen R. Cass. Mathematical modeling and control of the dry deposition flux of nitrogen-containing air pollutants. *Environ. Sci. Technol.*, 27:2772–2782, 1993.

[5] S. A. Slinn and W. G. N. Slinn. Predictions for particle deposition on natural waters. *Atmos. Environ.*, 14:1013–1016, 1980.

[6] William P. L. Carter. A detailed mechanism for the gas–phase atmospheric reactions of organic compounds. *Atmos. Environ.*, 24A:481–518, 1990.

[7] Spyros N. Pandis, Robert A. Harley, Glen R. Cass, and John H. Seinfeld. Secondary organic aerosol formation and transport. *Atmos. Environ.*, 26A:2269–2282, 1992.

[8] T.R. Young and J.P. Boris. A numerical technique for solving stiff ordinary differential equations associated with the chemical kinetics of reactive flow problems. *J. Phys. Chem.*, 81:2424–2427, 1977.

[9] Anthony S. Wexler and John H. Seinfeld. Second-generation inorganic aerosol model. *Atmos. Environ.*, 25A:2731–2748, 1991.

[10] Daniel J. Jacob. Chemistry of OH in remote clouds and its role in the production of formic acid and peroxymonosulfate. *J. Geophys. Res.*, 91(D9):9807–9826, 1986.

[11] Daniel J. Jacob, Elaine W. Gottlieb, and Michael J. Prather. Chemistry of a polluted boundary layer. *J. Geophys. Res.*, 94(D10):12975–13002, 1989.

[12] Robert A. Harley, Michael P. Hannigan, and Glen R. Cass. Respeciation of organic gas emissions and the detection of excess unburned gasoline in the atmosphere. *Environ. Sci. Technol.*, 26:2395–2408, 1992.

[13] Robert A. Harley, Armistead G. Russell, and Glen R. Cass. Mathematical modeling of the concentrations of volatile organic compounds: Model performance using a lumped chemical mechanism. *Environ. Sci. Technol.*, 27:1638–1649, 1993.

[14] Robert A. Harley, Armistead G. Russell, Gregory J. McRae, Glen R. Cass, and John H. Seinfeld. Photochemical modeling of the Southern California Air Quality Study. *Environ. Sci. Technol.*, 27:378–388, 1993.

[15] Douglas R. Lawson. The Southern California Air Quality Study. *J. Air Waste Manage. Assoc.*, 40:156–165, 1990.

[16] H. Andrew Gray. *Control of Atmospheric Fine Primary Carbon Particle Concentrations.* PhD dissertation, also published as Environmental Quality Laboratory Report 23, California Institute of Technology, Pasadena, 1986.

[17] S. Gharib and G.R. Cass. *Ammonia Emissions in the South Coast Air Basin, Open file report 84–2.* Environmental Quality Laboratory, Calif. Inst. of Technol., Pasadena, 1984.

[18] Armistead G. Russell and Glen R. Cass. Verification of a mathematical model for aerosol nitrate and nitric acid formation and its use for control measure evaluation. *Atmos. Environ.*, 20:2011–2025, 1986.

[19] Annmarie Eldering, Glen R. Cass, and K. C. Moon. An air monitoring network using continuous size distribution monitors: Connecting pollutant properties to visibility via Mie scattering calculations. *Atmos. Environ.*, 28:2733–2749, 1994.

[20] D. R. Fitz, M. Chan, G. R. Cass, D. R. Lawson, and L. Ashbaugh. A multi-component size-classifying aerosol and gas sampler for ambient air monitoring. 1989. Paper No. 89-140.1, presented at the Air and Waste Management Association 82nd Annual Meeting.

[21] Walter John, Stephen M. Wall, Joseph L. Ondo, and Wolfgang Winklmayr. Modes in the size distribution of atmospheric inorganic aerosol. *Atmos. Environ.*, 24A:2349–2359, 1990.

[22] X. Q. Zhang, P. H. McMurry, S. V. Hering, and G. S. Casuccio. Mixing characteristics and water content of submicron aerosols measured in Los Angeles and at the Grand Canyon. *Atmos. Environ.*, 27A:1593–1607, 1993.

[23] Lynn M. Hildemann, Gregory R. Markowski, and Glen R. Cass. Chemical composition of emissions from urban sources of fine organic aerosol. *Environ. Sci. Technol.*, 25:744–759, 1991.

[24] Susanne Hering, Annmarie Eldering, and John H. Seinfeld. Bimodal character of accumulation mode aerosol mass distribution in southern California. *Atmos. Environ.*, 31:1–11, 1997.

[25] M. K. Liu and John H. Seinfeld. On the validity of grid and trajectory models of urban air pollution. *Atmos. Environ.*, 9:555–574, 1975.

4 Effect of Emissions Control Strategies on the Size and Composition Distribution of Urban Particulate Air Pollution

4.1 Introduction

The size and chemical composition distribution of suspended particles influences their light scattering properties [1] and is expected to affect the health consequences of exposure to ambient concentrations of fine particulate matter [2, 3, 4]. Recently, a mechanistic air quality model has been developed which is capable of directly studying source contributions to the size and chemical composition distribution of particles suspended in an urban atmosphere [5, 6]. This model represents the ambient aerosol as a source-oriented external mixture in which particles emitted from different sources interact with a common gas phase but are not lumped into a single ambient size distribution. By this method, the primary particles emitted from major source types in an urban area are tracked separately in the atmosphere as they accumulate coatings of gas-to-particle conversion products. Because the separate contributions that individual source types make to the construction of the ambient particle mixture is revealed directly, this modeling procedure is ideally suited to studying the effect that proposed combinations of emissions controls would have on the size and composition distribution of airborne particles.

Previous calculations using the source-oriented external mixture model

have shown that, in Los Angeles, the characteristic peak in the aerosol size distribution at 0.2-0.3 μm particle diameter is shaped by primary combustion particles (from sources such as diesel engines and meat cooking) while the characteristic peak in the size distribution at 0.7-0.8 μm particle diameter is formed by the further accumulation of secondary atmospheric reaction products onto sulfate-containing background particles advected into the urban area from the upwind polluted marine environment [6]. The purpose of the study summarized in this paper is to examine how the multi-modal urban aerosol described above will change in response to various components of specific emissions control strategies which have been proposed for the Los Angeles area. In the sections below, the formulation of the model used for this analysis will be discussed and the study period used for control measure evaluation will be defined. Changes in the size and composition distribution of airborne particles predicted to occur in response to specific emissions control techniques then will be presented.

4.2 Model Formulation and Extension

The Lagrangian aerosol processes trajectory model used in the current study is virtually identical to that used in previous work to examine the effect of the internal mixture approximation on aerosol model predictions [5] and to identify source contributions to the size and composition distribution of the ambient aerosol [6]. This model represents airborne particles as a source-oriented external mixture in which each particle is labelled according to the emissions source type from which it was emitted at the time of release to the atmosphere. Particles emitted from different sources do not influence one another except through interaction with a common gas phase as they are transported in the vertical direction by turbulent diffusion, acted on by sec-

ondary atmospheric chemical reactions, removed at the earth's surface by dry deposition and advected to downwind receptor sites. This formulation more accurately represents the processes occurring in an urban atmosphere than is the case for models that represent airborne particles as an internal mixture in which particles emitted from different sources with different chemical compositions are blended together into a single size and composition distribution in the atmosphere as if all particles have the same chemical composition at any given particle size.

The source-oriented external mixture model includes a full description of heterogenous fog chemistry based on the chemical mechanisms of Jacob [7] and Jacob et al. [8] with extensions to allow for rigorous calculation of fog droplet water content using the method described by Pruppacher and Klett [9]. Condensation of inorganic species onto particles is calculated using a modified form of the AIM program developed by Wexler and Seinfeld [10] as described in Kleeman et al. [5].

A description of gas-phase photochemistry relevant to urban locations is included in the current model based on the work of Carter [11] with extensions to track the reaction of organic gases that may form condensible products based on the work of Pandis et al. [12]. The actual formation of secondary organic aerosol species in the current model application has been modified from the original SOAM mechanism proposed by Pandis. Recent work by Odum et al. [13, 14] has indicated that the formation of secondary organic aerosol is best represented using an absorption model similar to that proposed by Pankow [15, 16] in which semi-volatile gas-phase organic species absorb into the organic material contained in atmospheric particles. Organic precursor species first are oxidized to form semi-volatile organic products

according to reactions having the form:

$$HC_a + ox \rightarrow \alpha_i B_i + \alpha_j B_j \tag{4.1}$$

where HC_a is the concentration of the organic vapor precursor, ox is the concentration of the relevant oxidizing species (e.g., OH, O_3, NO_3); B_i and B_j are semi-volatile reaction products that are produced with stoichiometric coefficients α_i and α_j, respectively, relative to one molecule of HC_a. α_i and α_j are determined experimentally [13, 14]. Semi-volatile species then partition into an absorbing organic phase associated with all particles of a given type at a rate limited by the kinetic equation:

$$\frac{dA_{om,i}}{dt} = \frac{4\pi N D_i R_p}{\beta + 1}(B_{i,\infty} - B_{i,surf}) \tag{4.2}$$

where $A_{om,i}$ is the concentration of product i in the organic aerosol matrix, $B_{i,\infty}$ is the gas-phase concentration of semi-volatile species i far from the particle, $B_{i,surf}$ is the gas-phase concentration of semi-volatile species i at the particle surface, N is the particle number concentration, D_i is the diffusivity of the semi-volatile species of interest in air, R_p is the particle radius, $\beta = D_i/a_i c_i R_p$, a_i is the surface accommodation coefficient of species i (taken here to be 0.1 for all species), and c_i is the molecular velocity of species i [10]. The concentration of each semi-volatile gas-phase species at the particle surface is calculated using the equation:

$$B_{i,surf} = \frac{A_{om,i}}{K_{om,i} M_o} \tag{4.3}$$

where $K_{om,i}$ is a partitioning coefficient (measured experimentally), and M_o is the total organic aerosol mass concentration within the particle of interest [13, 14]. Table 4.1 lists the organic precursor species included in the lumped photochemical mechanism used by the air quality model, the symbols given

to the semi-volatile oxidation products produced by that mechanism, the reaction product stoichiometric coefficient, and the value of the partitioning coefficients used to calculate the rate at which these species partition between the gas and particle phases.

4.3 Model Application

Calculations preformed by Eldering and Cass [19], Kleeman et al. [5] and Kleeman and Cass [6] have verified the ability of the source-oriented external mixture model used here to reproduce aerosol properties observed at Claremont, California, on August 28, 1987, during the Southern California Air Quality Study (SCAQS) experiments. Since the purpose of the research summarized in the current paper is to build on this previous work by examining how aerosol properties are expected to change in response to emissions controls, the same episode will serve as the basis for the current model application. Briefly, 24 air parcel trajectories terminating at Claremont, California, on consecutive hours of the day on August 28, 1987, are integrated backward for 48 hours to their starting positions over the Pacific Ocean. Model calculations are then performed within air masses as they are advected inland along these trajectory paths, stagnate overnight and then continue onward to reach Claremont. Emissions of gas-phase and particle-phase pollutants from the complex array of sources in Southern California are inserted into the air parcels as they move over the sources. These emissions undergo vertical mixing and dry deposition while being transformed by chemical reaction in the atmosphere.

Table 4.1: Parameters Used in the Calculation of Secondary Organic Aerosol Concentrations[a]

Gas-phase Precursor[b]	First Semi-Volatile Oxidation Product B_1			Second Semi-Volatile Oxidation Product B_2		
HC_a	Species Name	α_i^c	K_1 (μg^{-1} m^3)[d]	Species Name	α_2^c	K_2 (μg^{-1} m^3)[d]
AAR1	AEA1	0				
AAR2	AEA2	0				
AAR3	AEA3	0				
AAR4	AEA4a	0.083	0.093	AEA4b	0.22	0.001
AAR5	AEA5a	0.083	0.093	AEA5b	0.22	0.001
AAR6	AEA6a	0.038	0.042	AEA6b	0.167	0.0014
AAR7	AEA7a	0.083	0.093	AEA7b	0.22	0.001
OLE1	AEO1	9.2	1000			
OLE2	AEO2	0				
OLE3	AEO3a	0.048	0.171	AEO3b	0.595	0.004
APIN	AEAPa	0.048	0.171	AEAPb	0.595	0.004
BPIN	AEBPa	0.048	0.171	AEBPb	0.595	0.004
C7OL	AEC7	78	1000			
C8OL	AEC8	227	1000			
C9OL	AEC9	304	1000			
TOLU	AETLa	0.083	0.093	AETLb	0.22	0.001
BALD	AEBA	5	1000			
PBZN	AEPB	5	1000			
PHEN	AEPH	0				
CRES	AECR	0				
NPHE	AENP	0				

[a] Secondary organic aerosol formation calculations follow the treatment of Odum et al. [17]. [b] Gas-phase precursor symbols correspond to the organic species used in the lumped photochemical mechanism by Pandis et al. [12]. [c] α_1 and α_2 are the stoichiometric coefficients that apply to the first and second semi-volatile reaction products, B_1 and B_2 respectively, from the reaction of one molecule of gaseous precursor HC_a [18]. [d] K_1 and K_2 are the gas / particle partitioning coefficients used in the calculation of equation 4.3. In those cases where there are no data on gas / particle partitioning of reaction products, K_1 is set to a very high value and the value of α_1 is set to the yield estimated by Pandis et al. [12] such that the model effectively reverts to the treatment of Pandis et al. [12] for that species.

4.3.1 Initial Conditions

Initial conditions used in the current study are identical to those used by Kleeman et al. [5] and Kleeman and Cass [6]. Aerosol initial conditions are based on chemical analysis of cascade impactor samples collected during the Southern California Air Quality Study. These data define two (externally mixed) types of background particles. The first type of particle has a size distribution which peaks in the size range greater than 1.0 μm particle diameter and is composed primarily of sodium chloride produced by the action of breaking waves at the coast. The second type of background particle has a size distribution which peaks between 0.5-1.0 μm particle diameter and is composed of organic species, sulfates, nitrates and ammonium ion. Background particles of this type are thought to be advected into the study area by long range transport processes. In previous applications of the source-oriented external mixture model, both types of background particles were injected into the air mass over the ocean at the start of each trajectory simulation. In the current study, background sulfate particles are initialized far out over the Pacific ocean (at the beginning of each trajectory calculation), but sea salt particles are not injected into the air mass until each trajectory actually crosses the coastline.

4.3.2 Meteorological Inputs

Meteorological inputs for the August 28, 1987, period are interpolated based on observational data using the methods of Goodin et al. [20] as described in Eldering and Cass [19] and Kleeman et al. [5]. During daylight hours in Southern California, solar radiation heats the ground which in turn heats the atmosphere from below. At night, the ground radiates energy to space, cooling the atmosphere from below. This diurnal cycle produces a dynamic

structure where both temperature and relative humidity in the atmosphere are a function of elevation and time of day. Temperature and relative humidity are of critical importance for aerosol calculations because they strongly influence the volatility of secondary inorganic aerosol species such as ammonium nitrate. In the present application, vertical sounding data are combined with ground-based observations to reconstruct the vertical profile of temperature and relative humidity at each grid location in the study area for each hour of the day on August 27-28, 1987. These vertical temperature and humidity profiles are then used to help calculate improved estimates of the vertical gradients in aerosol formation processes.

4.3.3 Base Emissions Inventory

The base emissions inventory used in the present analysis is nearly identical to that used by Eldering and Cass [19], Kleeman et al. [5], and Kleeman and Cass [6], and so only a brief description is provided here. Source locations and estimated mass emissions rates for major gas- and particle-phase emissions sources relevant to the August 27-28, 1987, SCAQS episode were obtained from the California Air Resources Board (ARB). This inventory describes the spatial and temporal distribution of the emissions of NO_x, SO_x, CO volatile organic compounds (VOC) and total particulate matter in the South Coast Air Basin which surrounds Los Angeles. In order to perform the mechanistic modeling calculations described in the current study, it is necessary to apply detailed organic gas speciation profiles to the reported total VOC emissions rates to convert this surrogate species into the estimated emissions of specific organic gases. Similarly, total particulate matter emissions rates are converted to detailed size- and chemically-resolved particulate emissions through the emissions processing modeling described by Eldering and Cass

[19]. Ammonia emissions for the episode studied are represented using the 1982 spatially and temporally resolved NH_3 emission inventory for the South Coast Air Basin [21, 22]. An additional 11 tons day^{-1} of ammonia produced by gasoline-powered vehicles also are added to the ammonia inventory based on the results of experiments conducted in a Los Angeles highway tunnel as described by Fraser and Cass [23]. Modifications to the emissions processing software described in Eldering and Cass [19] were made to correct a two hour bias in the diurnal variation of ammonia emissions.

As in previous calculations, several modifications were made to the emissions inventory described above to incorporate information from more recent studies. Carbon monoxide and organic gas exhaust emissions from on-road vehicles during the hot running portion of their driving cycle are scaled to 3 times the levels shown in the official ARB 1987 emissions inventory for the South Coast Air Basin based on the results of experiments conducted in a Los Angeles area highway tunnel as described by Harley et al. [24]. More recent information concerning the particulate emission rates for motor vehicles, paved road dust and dust from construction and demolition sites also is used as described by Eldering and Cass [19], and the diurnal profile used for commercial food cooking operations is modified to match that described by Gray [25]. A summary of the base emissions inventory for the South Coast Air Basin used in the current study is shown in Table 4.2; the emissions are stated in metric tons per day.

4.3.4 Source Control Strategies

Emission control measures for the improvement of particulate air quality can be divided into two general classes. The first class of controls focuses on the primary particles that are emitted directly from sources. The sec-

Table 4.2: Emissions Inventory Summary for the South Coast Air Basin on August 28, 1987[a]

Category Code	ROG[b] ton day^{-1}	NO_x ton day^{-1}	CO ton day^{-1}	SO_x ton day^{-1}	PM10 ton day^{-1}	PM2.5 ton day^{-1}
Fuel Combustion						
Agricultural	0.00	0.01	0.00	0.00	0.00	0.00
Oil and Gas Production	2.21	24.85	4.23	0.16	0.35	0.35
Petroleum Refining	1.45	30.33	3.09	2.46	0.53	0.53
Other Manufacturing/Industrial	3.50	60.38	18.88	5.49	2.37	2.32
Electric Utilities	1.31	35.44	7.64	0.44	1.11	1.10
Other Service and Commerce	3.50	40.31	13.80	9.00	2.56	2.54
Residential	0.41	22.02	5.52	0.12	1.10	1.10
Other	2.38	12.20	9.02	0.98	0.60	0.60
	14.76	225.54	62.18	18.65	8.62	8.53
Waste Burning						
Agricultural Debris	0.06	0.00	0.35	0.00	0.04	0.04
Range Management	0.00	0.00	0.00	0.00	0.00	0.00
Forest Management	0.00	0.00	0.00	0.00	0.00	0.00
Incineration	0.01	0.84	0.08	0.05	0.43	0.31
Other	0.82	0.63	0.17	0.38	0.33	0.32
	0.89	1.47	0.60	0.43	0.79	0.67
Solvent Use						
Dry Cleaning	17.87	0.01	0.00	0.00	0.00	0.00
Degreasing	79.67	0.02	0.00	0.00	0.03	0.02
Architectural Coating	101.91	0.00	0.00	0.00	0.00	0.00
Other Surface Coating	277.73	0.20	0.00	0.00	1.95	1.57
Asphalt Paving	5.68	0.00	0.00	0.00	0.00	0.00
Printing	10.15	0.10	0.00	0.00	0.01	0.01
Consumer Products	81.92	0.00	0.00	0.00	0.00	0.00
Industrial Solvent Use	22.97	0.00	0.00	0.00	0.01	0.01
Other	12.13	0.00	0.00	0.00	0.05	0.04
	610.04	0.33	0.01	0.00	2.05	1.65
Petroleum Process, Storage & Transfer						
Oil and Gas Extraction	29.39	1.26	0.16	2.09	0.33	0.23
Petroleum Refining	18.93	4.98	4.55	14.26	2.28	1.68
Petroleum Marketing	44.62	0.21	0.03	0.09	0.08	0.06
Other	2.86	0.03	0.21	0.00	0.11	0.09
	95.81	6.48	4.95	16.44	2.80	2.06
Industrial Processes						
Chemical	14.27	1.35	0.78	2.47	1.81	1.44
Food and Agricultural	23.53	0.41	0.01	0.00	23.21	22.54
Mineral Processes	0.57	7.42	1.46	3.28	4.65	1.83
Metal Processes	1.14	1.87	4.86	0.73	8.29	7.39
Wood and Paper	0.09	0.00	0.00	0.00	4.36	2.05
Other	16.58	0.10	0.00	0.00	0.52	0.36
	56.18	11.14	7.11	6.48	42.82	35.61

Table 4.2 (continued): Emissions Inventory Summary for the South Coast Air Basin on August 28, 1987[a]

Category Code	ROG[b] ton day^{-1}	NO_x ton day^{-1}	CO ton day^{-1}	SO_x ton day^{-1}	PM10 ton day^{-1}	PM2.5 ton day^{-1}
Miscellaneous Processes						
Pesticide Application	15.27	0.00	0.00	0.00	0.00	0.00
Farming Operations	33.40	0.00	0.00	0.00	32.35	4.32
Construction and Demolition	0.00	0.00	0.00	0.00	126.77	27.75
Entrained Road Dust - Paved	0.00	0.00	0.00	0.00	132.68	24.77
Entrained Road Dust - Unpaved	0.00	0.00	0.00	0.00	42.29	9.26
Unplanned Fires	11.95	2.66	170.69	0.00	0.66	0.63
Fugitive Windblown Dust	0.00	0.00	0.00	0.00	81.30	17.80
Waste Disposal	4.83	0.13	0.00	0.00	0.01	0.00
Other	3.13	0.51	0.06	0.08	0.86	0.51
	68.59	3.29	170.75	0.08	416.92	85.04
On-Road Vehicles						
Light-Duty Passenger	684.75	296.73	5609.27	13.01	10.27	8.91
Light- and Medium-Duty Trucks	324.42	180.61	2919.96	7.87	3.88	3.36
Heavy-Duty Gas Trucks	21.57	16.01	362.00	0.72	3.76	3.26
Heavy-Duty Diesel Trucks	21.61	103.53	77.48	6.14	8.08	7.01
Motorcycles	13.89	1.35	33.19	0.07	0.20	0.17
Heavy-Duty Diesel - Urban Bus	0.98	6.03	1.45	0.38	1.53	1.33
	1067.22	604.27	9003.35	28.19	27.71	24.05
Other Mobile						
Off-Road Vehicles	19.97	4.62	96.25	0.38	0.15	0.13
Commericial Boats	1.12	6.37	2.75	0.98	0.70	0.67
Trains	1.17	24.43	3.65	1.71	0.55	0.52
Ships	0.67	21.53	1.55	23.42	1.70	1.62
Aircraft - Government	7.56	2.78	13.08	0.40	2.60	2.57
Aircraft - Other	7.90	11.55	63.21	0.85	0.24	0.24
Mobile Equipment	19.87	74.09	206.96	3.13	6.79	6.37
Utility Equipment	9.67	1.73	112.12	0.16	0.18	0.13
	67.93	147.09	499.57	31.03	12.91	12.25
Biogenic Organics	72.83	0.00	0.00	0.00	0.00	0.00
TOTALS FOR ALL CATEGORIES:	2054.26	999.61	9748.51	101.30	514.63	169.86

[a] Inventory presented here includes only emissions within the South Coast Air Basin (SoCAB) and excludes emissions in portions of the Southeast Desert Air Basin and Ventura County that are within the modeling grid but outside of the formal boundaries of the SoCAB; the 3x hot exhaust correction to the gasoline-powered motor vehicle emissions is included in the totals shown. [b] Refers to Reactive (non-methane) Organic Gases.

ond class of controls targets the emissions of pollutant gases that react in the atmosphere to produce secondary aerosol species including sulfates, nitrates, ammonium ion and secondary organic aerosol. These include direct reductions in emissions of gaseous oxides of sulfur (SO_x), gaseous ammonia (NH_3), reactive organic gases (ROG) and oxides of nitrogen (NO_x). The current analysis will consider the effects of specific emissions control measures in each of these categories as if they had been in place on August 28, 1987; no attempt will be made to forecast air quality in future years.

Primary Particle Controls

The most obvious method available to reduce ambient particulate concentrations in an urban area is to reduce the direct emission rate of primary particles from anthropogenic sources. The primary particle control technologies considered in this analysis are selected from the stationary source control measures described in the 1997 Air Quality Management Plan (AQMP) for the Los Angeles area prepared by the South Coast Air Quality Management District (SCAQMD). In addition, conversion of non-catalyst gasoline-powered vehicles to catalyst-equipped gasoline-powered vehicles and conversion of sources using diesel engines to newer technology (lowering emitting) diesel engines is considered. A brief description of the primary particle source controls considered in the current analysis, the emissions to which they apply, and their effect on the particulate emission rates in the South Coast Air Basin if those measures had been in use on August 28, 1987, is shown in Table 4.3. The net effect of these primary particle controls is to reduce PM10 emissions by 201 tons day^{-1} and PM2.5 emissions by 70 tons day^{-1}.

Table 4.3: Specific Emissions Control Measures for Primary Particulate Matter

	Source - Control Measure	PM10 emissions before control tons day^{-1}	PM2.5 emissions before control tons day^{-1}	Fraction PM Remaining
1	Refinery Fluid Catalytic Cracking Units - Electrostatic Precipitators; Cyclones	0.47	0.44	0.60
2	Wood Working - Baghouse Filters	4.15	1.93	0.05
3	Restaurant Cooking - Catalytic Converters; Carbon Adsorption; Afterburners; Grill Re-design Electrostatic Precipitators	21.85	21.84	0.29[a]
4	Agricultural Operations - Restrict Hay Grinding; Treat Unpaved Access Roads	29.50	3.69	0.53
5	Paved Roads - Clean; Treat Unpaved Access Roads	132.68	24.77	0.71
6	Unpaved Roads - Treat; Restrict Speed to 15 km/hr	42.29	9.26	0.71
7	Agricultural Dust - Better Tilling Practices	2.85	0.63	0.81
8	Construction & Demolition Dust - Methods Described in Rule 403 Implementation Handbook	126.77	27.75	0.26
9	Light Duty Non-Catalyst Vehicles - Convert to Catalyst Vehicles	5.71	4.14	0.08[b]
10	On-Road Diesel Engines - Use New Technology	14.50	13.77	0.14[c]
11	Off-Road Diesel Engines - Use New Technology	6.42	6.10	0.13[d]

[a] Fraction remaining reflects complete control of the specific emitter named within a larger class of sources. [b] Fraction remaining represents the difference between emissions factors for catalyst-equipped gasoline-powered vehicles and non-catalyst equipped gasoline-powered vehicles. [c] Based on emissions factors of 1.82 g kw^{-1} hr^{-1} and 0.25 g kw^{-1} hr^{-1} for old technology and new technology on-road diesel engines respectively (26). [d] Based on emissions factors of 0.95 g kw^{-1} hr^{-1} and 0.12 g kw^{-1} hr^{-1} for old technology and new technology off-road diesel engines respectively (27).

SO_x Controls

Virtually all sources of SO_x in the South Coast Air Basin were heavily controlled prior to 1987 (the base year for the current analysis) in an ongoing effort to reduce particulate sulfate concentrations. Table 4.2 indicates that the major sources of SO_x remaining in 1987 included emissions from fuel combustion in on-road vehicles and ships in the Los Angeles and Long Beach harbors with lesser contributions from stationary fuel combustion and petroleum processing, transfer and storage.

The 1997 AQMP specifies further controls for stationary sources of SO_x within the South Coast Air Basin under the Regional Clean Air Incentives Market (RECLAIM) program. The RECLAIM program establishes an emissions cap and an annual rate of reduction for facilities emitting targeted pollutants (SO_x in this case). Each facility is free to meet annual emissions reductions through adoption of techniques such as installation of pollution control devices, use of reformulated products, implementation of process change, or reduction of output. Facilities are also free to trade emissions credits with other participants in the program to achieve their annual emission reduction targets in the most efficient manner possible. The future-year emissions inventories listed in the 1997 AQMP suggest that the net effect of the RECLAIM program will be a further 67% reduction in SO_x emissions from stationary sources within the South Coast Air Basin.

SO_x emissions from on-road mobile sources in future years will be affected by many factors including a reduction in the sulfur content of liquid fuels and the incorporation of electric vehicles into the motor vehicle fleet. All of these parameters are represented in the future year mobile source emissions inventories prepared by the SCAQMD as part of the 1997 AQMP. This inventory provides information on both vehicle miles travelled per day (VMT) as well

as total emissions for different vehicle classes (e.g., light-duty passenger car, heavy-duty truck, etc.) and engine type (e.g., catalyst-equipped gasoline, diesel, etc.). With this information, it is possible to calculate total vehicle emissions factors (g/mile) in the presence of proposed emissions controls for each vehicle class/engine type combination for all of the pollutants of interest, including SO_x. These emission factors can then be used with VMT information available for August 27-28, 1987, to estimate what the emissions of SO_x from on-road mobile sources would have been during the study period if the future controls had been in place in 1987. The net result of this calculation indicates that emissions of SO_x from non-marine mobile sources would have been reduced by 74% on August 27-28, 1987, if the technology assumed in the 1997 AQMP had been in place at that time.

As shown in Table 4.2, the largest source of off-road mobile SO_x emissions in the South Coast Air Basin is from ships in or around the Los Angeles and Long Beach harbors. Emissions of SO_x from these sources in future-year inventories prepared by the SCAQMD show little variation relative to the 1987 values, indicating that few controls are currently envisioned. This apparent omission is largely due to the inability of local governments to control the sulfur content of fuel purchased by ships engaged in international commerce before they enter the Los Angeles area. In spite of these regulatory difficulties, the present study will consider the effect of a further reduction of 74% in SO_x emissions from off-road mobile sources (including ships) achieved through a reduction in the sulfur content of the liquid fuels burned. In addition, a direct reduction of 12% of the SO_x emitted from ships berthed in the Los Angeles and Long Beach harbors will be specified due to the use of supplementary electrical power from on-shore to replace some of the fuel burning aboard the ships.

Table 4.4: Specific Emissions Control Measures for SO_x

	Source - Control Measure	SO_x emissions before control tons day^{-1}	Fraction SO_x Remaining
1	Stationary Sources - RECLAIM[a]	42.08	0.33
2	On-Road Mobile Sources - Reduce Sulfur Content of Fuel; Electric Vehicles	28.19	0.26
3	Off-Road Mobile Sources - Reduce Sulfur Content of Fuel	31.03	0.26
4	Ships at Berth - Electrification	23.42	0.88[b]

[a] Regional Clean Air Incentives Market. [b] Fraction remaining reflects complete control of the specific emitter named within a larger class of sources.

The net effect of the control program described above is to reduce SO_x emissions in the South Coast Air Basin to 29 tons day^{-1}, which is just over 5% of the SO_x emissions in this area in 1973 (see [26]). A brief description of the controls used to achieve this reduction, their individual control efficiencies, and the SO_x emissions which they would affect in the South Coast Air Basin on August 28, 1987, is given in Table 4.4.

NH_3 Controls

Under base case 1987 pre-control conditions, 176 tons day^{-1} of ammonia are estimated to have been released into the South Coast Air Basin atmosphere. Ammonia in the Los Angeles atmosphere serves as the principal base which neutralizes acids such as H_2SO_4 and HNO_3 as they condense onto particles. By reducing emissions of ammonia in the South Coast Air Basin, concentrations of secondary aerosol nitrate are reduced. The control program considered in the present analysis cuts the ammonia emitted from mobile sources by 50% relative to the base case inventory described in Section 4.3.3 resulting in a decrease of 11 tons day^{-1} in the South Coast Air Basin. This emissions reduction is consistent with the motor vehicle fleet achieving a target ammonia emission rate of 0.022 g km^{-1} (0.035 g $mile^{-1}$) and could be achieved by better vehicle maintenance that reduced the number of vehicles

with malfunctioning three-way or dual-bed catalysts. In addition, controls were specified that remove agricultural livestock from the South Coast Air Basin. This measure reduces ammonia emissions from livestock waste decomposition by 75 tons day^{-1} primarily in the eastern portion of the greater Los Angeles area.

ROG AND NO_x CONTROLS

In addition to the controls aimed at the reduction of ambient particulate levels described in the previous sections, significant effort has been expended in the Los Angeles area to control emissions of reactive organic gases (ROG) and oxides of nitrogen (NO_x) in an effort to meet the national ambient air quality standard for ozone. Control of ROG and NO_x also will affect the formation of secondary aerosol components, and so a control program for these species was considered in the current analysis. The control measures examined here incorporate the tier I and tier II stationary source ROG and NO_x controls that are defined in the 1991 AQMP for the Los Angeles area with the exception of the rule which would totally eliminate farming activities from the South Coast Air Basin. Partial control of farming activities consistent with the controls discussed above for PM10 and NH_3 emissions were considered instead. Fleet average emissions of ROG and NO_x from on-road motor vehicles in the presence of further emission controls were calculated in a fashion analogous to on-road mobile SO_x emissions as described in Section 4.3.4 (i.e., the emission rate per vehicle km traveled given control technology expected in the year 2006 according to the 1997 AQMP was calculated and then used to replace the emission factors used in the 1987 base case emissions inventory). In addition, non-catalyst-equipped gasoline-powered on-road vehicles were converted to catalyst-equipped gasoline powered vehicles while retaining the

same number of vehicle kilometers traveled.

The net effect of the ROG portion of the control plan examined is to reduce emissions of reactive organic gases by 70% from the base case August 28, 1987, value of 2054 tons day^{-1} to a new lower value of 617 tons day^{-1} in the South Coast Air Basin, primarily through controls on motor vehicles, solvent use and petroleum processing and storage. The effect of the NO_x portion of the control plan is to reduce emissions of oxides of nitrogen from the August 28, 1987, base case value of 1000 tons day^{-1} to new lower value of 436 tons day^{-1} in the South Coast Air Basin, primarily through controls on motor vehicles and stationary source fuel combustion. A brief description of the controls used to achieve these reductions, the ROG or NO_x emissions which they affect, and the fraction of emissions remaining after their application is shown in Table 4.5.

4.4 Results

The base case (precontrol) gas-phase and particle-phase model results for the episode at Claremont, CA, on August 28, 1987, are similar to those presented by Eldering and Cass [19], Kleeman et al. [5], and Kleeman and Cass [6]. Differences do exist between the base case results produced in the current analysis relative to those presented in these previous studies due to the incorporation of an updated secondary organic aerosol formation mechanism within the model (described in Section 4.2), the use of an updated ammonia inventory which accounts for increased NH_3 emissions from catalyst-equipped automobiles (described in Section 4.3.3), and the correction of a minor error related to the diurnal variation of ammonia emissions. The net effect of these changes on model results is manifested as a shift in aerosol nitrate concentrations from a small under predicition to a small over prediciton relative

Table 4.5: Specific Emissions Control Measures for ROG and NOx

	Source - Control Measure	ROG emissions before control tons day^{-1}	NOx emissions before control tons day^{-1}	Fraction ROG Remaining	Fraction NOx Remaining
1	Eliminate Planned Fires	16.0	2.54	0.00	0.00
2	Electrify Stationary Non-generating Internal Combustion Engines and Turbines		64.0		0.29[a]
3	Controls on Small Engines & Heaters		2.10		0.85
4	Petrol Dry Cleaning - Solvent Recovery	0.897		0.67	
5	Domestic Products - Reformulate	88.2		0.82	
6	Control of Commercial Bakery Fugitive Emissions	6.01		0.49	
7	Further Controls on Metal Cleaning & Degreasing	76.2		0.43	
8	Substitue Solvents for Surface Coating Clean Up	64.1		0.91	
9	Reduced Solvents in Domestic Products	88.2		0.63	
10	Fail-Safe Gasoline Transfer : Phase I	4.88		0.85	
11	Licensing of Vapor Recovery System Installations	4.66		0.91	
12	Boat Gasoline Refueling Operations Improvements	19.3		0.99[a]	
13	Gasoline Dispensing Facilities - Tank Vents Control	5.66		0.10	
14	Small Engine Refueling - Reduce Spillage	5.49		0.10	
15	Req Fuel Shutoff to Prevent Topping-Off	4.66		0.50	
16	Active Drain Measure - Organic Vapors	2.34		0.10	
17	Commercial Charbroiling - Catalytic Converters; Carbon Adsorption	3.26		0.10	
18	Control of Deep Fat Frying	8.05		0.10	
19	Commercial Energy Conservation - Natural Gas	0.581	7.28	0.80	0.80
20	Control of Misc. Combustion Sources		14.1		0.50
21	Control of Res. & Com. Water Heating		14.0		0.50
22	Residential Energy Conservation - Natural Gas	0.628	18.4	0.70	0.70
23	Control of Pesticide Formulation and Use	9.04		0.60	
24	Control of Livestock Wastes [ROG]	111.		0.75	
25	Gas Space Heat Boilers - BARCT[b]		1.27		0.80
26	Miscellaneous Solvent Use - BARCT[b]	42.2		0.60	
27	Miscellaneous Sources - BARCT[b] Assume 20%	252.	13.3	0.80	0.80
28	Metal Parts & Products Coatings - BARCT[b]	32.0		0.90	
29	Fixed and Floating Roof Refinery Tanks-BARCT[b]	4.72		0.90	
30	Oil Field Storage Tanks - BARCT[b]	4.99		0.90	

Table 4.5 (continued): Specific Emissions Control Measures for ROG and NOx

	Source - Control Measure	ROG emissions before control tons day^{-1}	NOx emissions before control tons day^{-1}	Fraction ROG Remaining	Fraction NOx Remaining
31	Breweries - BARCT[b]	0.106		0.50	
32	Automobile Assembly Coating - Higher Transfer Efficiency; Exhaust Controls; Alt. Solvents	20.5		0.80	
33	Paper, Fabric & Film Coating - Low Solvent Coatings; Recordkeeping	21.9		0.99	
34	Perchloroethylene Dry Cleaning - Dry-to-Dry Transfer System; Eliminate Exemptions	17.0		0.75	
35	Petroleum Refinery FCC [NO_x] - Selective Catalytic Reduction		3.71		0.30
36	Bulk Gasoline Terminals - Carbon Adsorption; Refrigeration; Incineration	4.67		0.30	
37	Rubber Product Mfg. - Electrostatic Precip.; Carbon Adsorber	2.79		0.25	
38	Small Boilers & Process Heaters - Radient Burners; Alternative Fuels		3.79		0.25
39	Metal Melting Furnaces - Combustion Modif.; Alternative Fuels; Electric Melting		1.75		0.50
40	Curing and Drying Ovens - Combustion Modif.; Alternative Fuels		4.18		0.25
41	Glass Melting Furnaces - Electric Melting; Advanced Furnaces; Flue Gas Treatment; Alt. Fuel		5.27		0.05
42	Cement Kilns - Selective Catalytic Reduction; Scrubbing		7.76		0.15
43	Glass Recycling		5.27		0.87
44	Control of POTW Fugitive Emissions	0.054		0.66	
45	Phase-out Stationary Oil & Solid Fuel Use		34.3		0.40[a]
46	Ships at Berth - Electrification		25.3		0.88[a]
47	Lower Emission Standards on New Jet Aircraft Engines	5.07	10.6	0.50	0.50
48	Marine Vessel Tank Fugitive Emissions - Add on Control Devices; Operational Requirements	3.97		0.05	
49	Marine Diesel - Reduce Speed; Restrict Access		25.3		0.83

Table 4.5 (continued): Specific Emissions Control Measures for ROG and NOx

	Source - Control Measure	ROG emissions before control tons day^{-1}	NOx emissions before control tons day^{-1}	Fraction ROG Remaining	Fraction NOx Remaining
50	Military Aircraft - Engine Redesign; Reduce Taxi and Idle Times	8.35	2.74	0.50	0.50
51	Ban Leaf Blowers	10.7	1.73	0.90[a]	0.98[a]
52	Reduce Petrol Refining to Incl. ZEV VMT	21.4	28.3	0.83	0.83
53	Reduce MV Fuel Distribution to ZEV VMT	15.0	0.00	0.83	0.83
54	Emissions Stds for New Heavy Duty Construction & Farm Equipment	22.0	74.1	0.81	0.58
55	Emissions Standards for Off-Road Motorcycles	1.78		0.10	
56	Locomotive Emission Control	1.21	24.4	0.84	0.68
57	Emission Standards for Utility Engines	10.7	1.73	0.13	1.20
58	Emission Standards for Marine Vessels	1.85	27.9	0.59	0.39
59	Control of Off-Highway Vehicles	22.0	74.1	0.88	0.96
60	Control of Airport & Ground Service Vehicles	8.74	11.6	0.88[a]	0.82[a]
61	Centralized Airport Ground Power System	8.74	11.6	0.99[a]	0.97[a]
62	Restrictions on High-Emitting Jet Aircraft	8.74	11.6	0.69[a]	0.80[a]
63	General Aviation Vapor Recovery	8.74		0.98[a]	
64	Railroad Consolidation, Xings Regs. and Seps.	1.21	24.4	0.70[a]	0.70[a]
65	Electrify Railroad Line-Haul Operations	1.21	24.4	0.10[a]	0.10[a]
66	High Speed Rail Substitute for Airline Travel	8.74	11.6	0.95[a]	0.91[a]
67	Reduce Petrol Refining to SCAG VMT (2010)	21.4	28.3	0.83[a]	0.83[a]
68	Reduce MV Fuel Distribution to SCAG VMT	15.0	0.00	0.83	0.83
69	50% Elimination of Reactive Solvents and CO	626.	0.326	0.50	0.50
70	Emissions Standards on New Pleasure Boat Engines	19.3		0.80	
71	Reduce Petroleum Refining to Southern California Demand	21.4	28.3	0.75[a]	0.75[a]
72	Stricter BARCT Requirements (50% Misc Source)	453.	44.7	0.50	0.50
73	Further NO_x Reductions from Fuel Combustion		48.0		0.50
74	Further Control of NO_x from Electric Utilities		28.1		0.15
75	On-Road Vehicles - Meet Emissions Target Suggested by EMFAC7G for Year 2006	1067.	604.	0.13	0.49

[a] Fraction remaining reflects complete control of the specific emitter named within a larger class of sources. [b] Stands for Best Available Retrofit Control Technology.

to measured values. A decrease in secondary organic aerosol concentration predictions also is observed.

4.4.1 Basecase Model Results

Figure 4.1 shows the source contributions to the predicted 24-hour average size- and chemical-composition distribution of particles in the atmosphere at Claremont, CA, on August 28, 1987, for the situation prior to the application of the emission controls studied here. Each of the smaller graphs in this figure shows the size and composition distribution of the primary seed particles from specific emissions source types as they exist in the ambient atmosphere after the particles have been released from their source and then advected to the downwind site while being transformed by atmospheric chemical reactions. As was the case for Figure 3 of Kleeman and Cass [6], model results indicate that particles emitted from paved road dust sources and crustal material other than paved road dust dominate the 24-hour average size distribution of particles larger than 1 μm particle diameter. Transformed particles originally released from diesel engines and meat cooking operations are the largest contributors to the 24-hour average particle size distribution in the range from 0.1-0.3 μm particle diameter. The peak in the ambient particle size distribution that occurs in the range from 0.6-0.8 μm particle diameter is associated with non-sea salt background particles which are advected into the Los Angeles area from upwind and then are transformed greatly by interaction with pollutant gases in the urban atmosphere. The degree to which this transformation occurs is apparent in Figure 6 of Kleeman et al. [6] which shows the size and composition distribution of these non-sea salt background particles at the start of a trajectory simulation over the ocean compared to their condition after they have been advected across the air basin to Clare-

mont. That figure indicates that, for trajectories arriving at Claremont at 1300 PST, there is a six-fold increase in the height of the peak in the particle size distribution associated with non-sea salt background particles due to the accumulation of secondary gas-to-particle conversion products on these water-soluble background particles. The focus of the analysis presented in the sections below will be to evaluate how the base case results described above change in response to the emissions control programs described in Section 4.3.4.

4.4.2 Effect of Emissions Controls

The predicted effect that the control measures described in Section 4.3.4 would have had on ambient fine particle (PM2.5) concentrations at Claremont, CA, if they had been in effect on August 27-28, 1987, is summarized in Table 4.6. This table includes a description of the 24-hour average PM2.5 concentration predicted after the separate application of each package of emission controls as well as for all control packages applied simultaneously. In each case, the calculated primary and secondary aerosol concentrations of $SO_4^=$, NO_3^-, NH_4^+, Cl^-, and organic compounds are displayed as well.

Primary particle controls applied to the base emissions inventory reduce fine particle mass concentrations by 20.5 μg m^{-3} with 9.2 μg m^{-3} of this reduction due to reduced emissions of primary organic compounds. Little or no change is observed for the predicted fine particle mass concentrations of secondary aerosol species in response to primary particle emissions controls.

SO_x controls applied to the base emissions inventory reduce the predicted average PM2.5 concentrations at Claremont, CA, on August 28, 1987, by 1.2 μg m^{-3}. The magnitude of this effect is not surprising since secondary $SO_4^=$ formation accounts for only 2.3 μg m^{-3} of the predicted base case am-

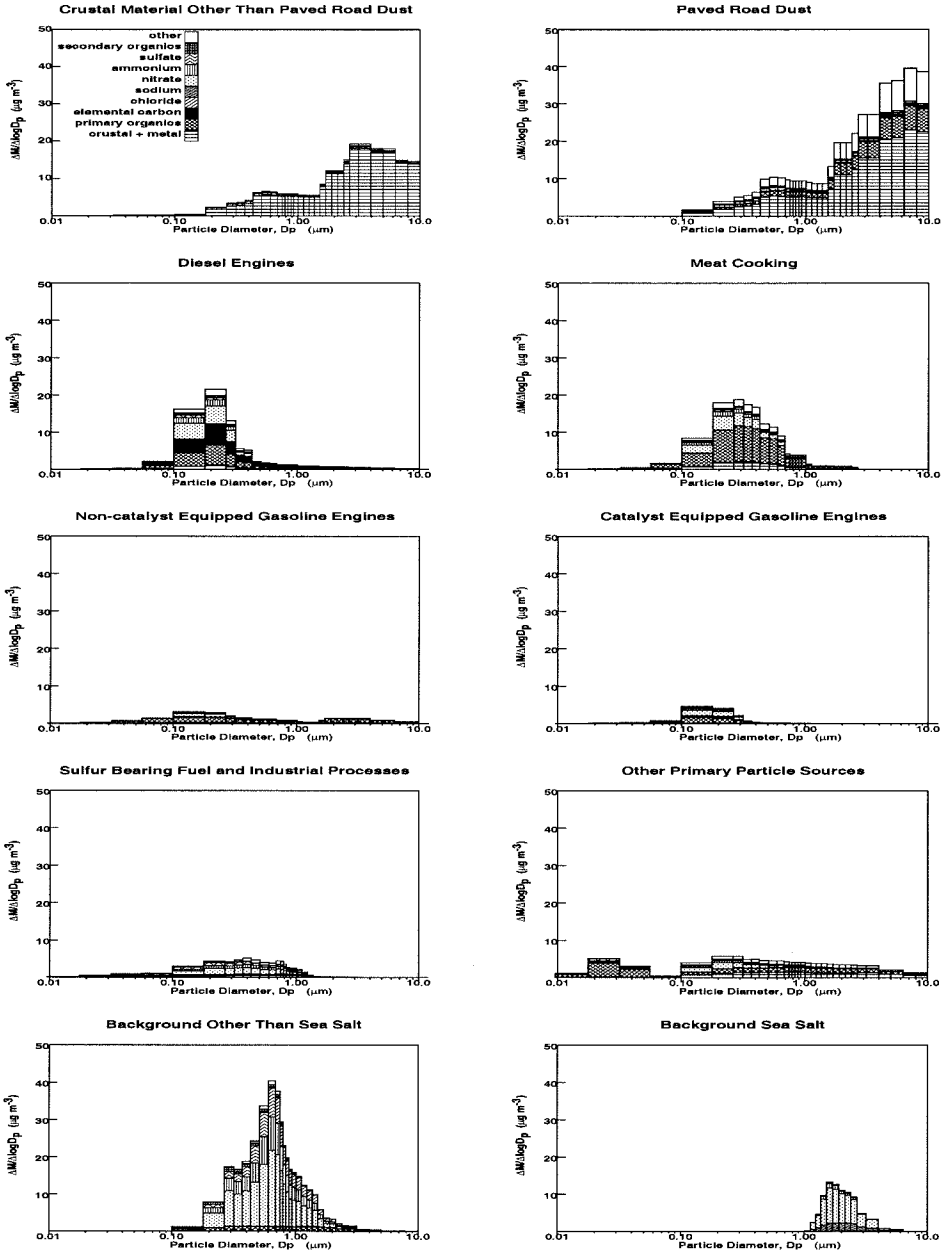

Figure 4.1:
Individual source contributions to the daily average particle size and chemical composition distributions predicted at Claremont, CA, on August 28, 1987, using base case emissions. Each subplot shows the primary seed particles emitted from the indicated source along with the associated gas-to-particle conversion products that have accumulated on those seed particles over time.

bient aerosol mass. It is interesting to note that the reduction in $SO_4^=$ concentrations resulting from SO_x emissions controls is partially offset by an increase in the amount of aerosol NO_3^-. Ammonia remaining in the gas phase when aerosol $(NH_4)_2SO_4$ concentrations decrease combines with gas phase nitric acid vapor to produce additional NH_4NO_3 in the particle phase.

The ammonia control measures described in Section 4.3.4 result in a decrease in daily PM2.5 concentrations of 10.9 μg m^{-3} relative to the base case concentrations primarily through reduction in aerosol NH_4^+ and NO_3^- concentrations. The ROG and NO_x control program, if applied alone, would lower PM2.5 concentrations by reducing the concentrations of gas-phase aerosol precursors such as HNO_3 and organic gases which lead to the formation of secondary aerosol NO_3^- and organic compounds, respectively.

The final row of Table 4.6 indicates the effect on aerosol PM2.5 concentrations that would have occurred at Claremont, CA, on August 28, 1987, if all of the control measures described above had been applied to the base emissions inventory simultaneously. Predicted PM2.5 mass concentrations are reduced by 46% to 46 μg m^{-3} through the combination of all of the individual control measures.

Source Contributions to PM2.5 Aerosol Concentrations

Since aerosol calculations for the current study were conducted using a source-oriented external mixture model that separately tracks the primary particles emitted from each major emission source type, it is possible to directly examine source contributions to the PM2.5 concentrations shown in Table 4.6. Table 4.7 lists the response to emissions controls of PM2.5 concentrations separated according to the source from which the primary particles were originally emitted. Changes in the secondary $SO_4^=$, NO_3^-, NH_4^+, and organic

Table 4.6: Net Effect of Different Packages of Control Measures on 24-hour Average PM2.5 Particulate Matter Concentrations at Claremont, CA, August 28, 1987

Control Strategy	PM2.5[a] (μg m^{-3})	$SO_4^=$		NH_4^+		NO_3^-		Cl^-		Organics	
		Prim[b]	Sec[c]	Prim[b]	Sec[c]	Prim[b]	Sec[c]	Prim[b]	Sec[c]	Prim[b]	Sec[c]
Basecase	84.21	3.61	2.34	1.04	6.48	0.69	20.04	1.43	-1.20	19.16	1.17
Primary Particle Control	63.72	3.50	2.33	1.04	6.47	0.65	20.11	1.25	-1.07	9.95	1.07
SO_x Control	83.04	3.64	0.82	1.05	6.15	0.69	20.90	1.43	-1.21	19.30	1.19
NH_3 Control	73.30	3.63	2.30	1.05	3.98	0.69	11.71	1.43	-1.27	19.22	1.18
ROG & NO_x Control	76.19	3.61	2.79	1.05	5.00	0.71	14.56	1.46	-1.22	19.13	0.50
Combine All Controls	45.79	3.54	0.93	1.06	2.62	0.68	8.95	1.27	-1.13	10.00	0.45

[a] Concentration increment includes both primary particle core plus net accumulation of secondary aerosol due to atmospheric chemical reactions. Source contributions without secondary reaction products can be computed by subtracting secondary components listed in columns 3, 5, 7, 9, and 11. [b] Concentration increment due to primary particle emissions plus pre-existing background aerosol (μg m^{-3}). [c] Net concentration increment due to atmospheric chemical reaction within trajectories crossing the air basin (μg m^{-3}).

compounds that have accumulated on the primary particles from each source are indicated as well. The sum of all the small concentration increments given in Table 4.7 produces the totals shown in Table 4.6. Concentrations of primary $SO_4^=$, NO_3^-, NH_4^+ and organic compounds that are emitted directly in the particle phase are not shown in this table since they are included within the effect of the primary particle controls.

Table 4.7 shows that the primary particle controls summarized in Table 4.3 significantly reduce PM2.5 concentrations from paved road dust and crustal material other than paved road dust. Ambient concentrations of particles associated with diesel engines and meat cooking operations also are reduced significantly by the primary particle controls studied here. Table 4.7 indicates that primary particle controls reduce the concentrations of secondary aerosol NO_3^- that forms on diesel engine and meat cooking particles, but an equivalent amount of aerosol nitrate is seen to accumulate on non-sea salt background particles instead, which leads to changes in the overall fine particle size distribution. The implications of this behavior are considered in greater detail in Section 4.4.3

Table 4.7 shows that control of gas-phase emissions of SO_x, NH_3 and ROG and NO_x in the absence of further primary particle control reduces the concentrations of secondary aerosol $SO_4^=$, NH_4^+, NO_3^- and organic species with little or no preferential redistribution of material between the particles emitted from different sources.

A plot of the size and composition distribution of the ambient aerosol that results from the combined effect of all control measures applied simultaneously is shown in Figure 4.2. Comparison of these results to the base case values shown in Figure 4.1 illustrates the effect of controls on primary particulate emissions from sources such as diesel engines and meat cooking

Table 4.7: Change in Source Contributions to 24-hour Average PM2.5 Particulate Matter Concentrations at Claremont, CA, August 28, 1987, in Response to Different Packages of Control Measures

Control Strategy	PM2.5[a] ($\mu g\ m^{-3}$)	Secondary Concentrations[b] $SO_4^=$	NH_4^+	NO_3^-	Organics	PM2.5[a] ($\mu g\ m^{-3}$)	Secondary Concentrations[b] $SO_4^=$	NH_4^+	NO_3^-	Organics
	Paved road dust					**Other crustal material**				
Basecase	11.64	0.08	0.27	0.67	0.05	7.29	0.04	0.14	0.42	0.04
Primary Particle Control	8.50	0.08	0.25	0.62	0.05	4.14	0.03	0.08	0.23	0.02
SO_x Control	11.68	0.02	0.26	0.71	0.05	7.34	0.01	0.14	0.46	0.04
NH_3 Control	11.28	0.09	0.18	0.35	0.05	7.03	0.05	0.08	0.21	0.04
ROG & NO_x Control	11.36	0.10	0.23	0.52	0.02	7.09	0.05	0.10	0.28	0.02
Combine All Controls	7.92	0.03	0.12	0.27	0.02	3.93	0.01	0.03	0.09	0.01
	Diesel engines					**Meat cooking**				
Basecase	10.95	0.31	0.79	2.28	0.29	12.79	0.27	0.70	2.05	0.18
Primary Particle Control	2.98	0.12	0.31	0.89	0.10	4.19	0.12	0.31	0.89	0.08
SO_x Control	10.99	0.09	0.78	2.52	0.29	12.84	0.07	0.70	2.29	0.18
NH_3 Control	9.21	0.30	0.39	0.94	0.29	11.47	0.28	0.39	0.98	0.18
ROG & NO_x Control	9.79	0.34	0.57	1.51	0.11	11.87	0.34	0.54	1.41	0.07
Combine All Controls	1.92	0.04	0.08	0.22	0.04	3.26	0.04	0.11	0.31	0.03
	Non-cat gasoline engines					**Catalyst gasoline engines**				
Basecase	3.09	0.06	0.16	0.46	0.05	2.54	0.08	0.23	0.65	0.06
Primary Particle Control	1.35	0.04	0.09	0.28	0.03	3.63	0.15	0.41	1.15	0.12
SO_x Control	3.10	0.02	0.16	0.51	0.05	2.55	0.02	0.22	0.71	0.07
NH_3 Control	2.76	0.06	0.08	0.20	0.05	2.07	0.07	0.12	0.29	0.06
ROG & NO_x Control	2.87	0.07	0.12	0.32	0.02	2.29	0.11	0.18	0.46	0.02
Combine All Controls	1.05	0.01	0.03	0.09	0.01	2.35	0.05	0.14	0.37	0.04

Table 4.7 (continued): Change in Source Contributions to 24-hour Average PM2.5 Particulate Matter Concentrations at Claremont, CA, August 28, 1987, in Response to Different Packages of Control Measures

Control Strategy	PM2.5[a] ($\mu g\ m^{-3}$)	Secondary Concentrations[b] $SO_4^=$	NH_4^+	NO_3^-	Organics	PM2.5[a] ($\mu g\ m^{-3}$)	Secondary Concentrations[b] $SO_4^=$	NH_4^+	NO_3^-	Organics
	S-bearing fuel+ind					**Other sources**				
Basecase	4.92	0.37	0.68	1.36	0.08	8.65	0.14	0.37	1.00	0.11
Primary Particle Control	5.22	0.40	0.75	1.58	0.11	8.49	0.20	0.51	1.45	0.16
SO_x Control	4.38	0.20	0.58	1.29	0.07	8.71	0.06	0.37	1.10	0.11
NH_3 Control	4.02	0.31	0.47	0.76	0.07	7.91	0.14	0.19	0.41	0.11
ROG & NO_x Control	4.15	0.43	0.56	0.95	0.03	8.11	0.16	0.27	0.64	0.04
Combine All Controls	3.45	0.25	0.40	0.65	0.04	6.89	0.09	0.17	0.41	0.06
	NaCl background particles					**non-NaCl background particles**				
Basecase	3.55	0.04	0.25	2.54	0.00	18.78	0.95	2.90	8.62	0.32
Primary Particle Control	3.64	0.05	0.27	2.61	0.01	21.58	1.15	3.49	10.43	0.40
SO_x Control	3.57	0.02	0.26	2.59	0.00	17.88	0.31	2.68	8.72	0.32
NH_3 Control	3.43	0.04	0.22	2.47	0.00	14.10	0.97	1.86	5.11	0.32
ROG & NO_x Control	3.39	0.05	0.21	2.41	0.00	15.26	1.13	2.21	6.06	0.18
Combine All Controls	3.22	0.02	0.17	2.33	0.00	11.80	0.39	1.37	4.19	0.20

[a] Concentration increment includes both primary particle core plus net accumulation of secondary aerosol due to atmospheric chemical reactions. Source contributions without specific secondary reaction products can be computed by subtracting secondary components listed in the four columns to the right; the NaCl initial condition also is affected by loss of Cl^- from the aerosol as shown in Table 4.6. [b] Net concentration increment due to accumulation of secondary atmospheric chemical reaction products onto the primary particles from each source type during transport across the air basin ($\mu g\ m^{-3}$).

operations. The concentrations of elemental carbon and primary organic compounds in the size range from 0.1-0.3 μm particle diameter are virtually eliminated through the use of the control measures studied here. Similarly, controls on emissions from coarse particle sources such as paved road dust and crustal material other than paved road dust reduce ambient particulate matter concentrations in the larger particle size range. Control of gas-phase pollutants is seen to be effective at reducing the concentrations of secondary aerosol nitrates, although there is still a significant fraction of secondary material seen to be associated with the non-sea salt background particles which are advected into the Los Angeles area and then processed by reactions in the urban atmosphere. Particles of this type still dominate the 24-hour average size distribution between 0.5-0.8 μm particle diameter, even though the magnitude of the peak concentration is reduced. Just over half of the 11.8 μg m^{-3} of fine particle mass associated with the non-sea salt background particles arriving at Claremont in the combined control case is due to accumulation of secondary reaction products on these particles during transit across the air basin (see also Table 4.7).

4.4.3 Redistribution of Volatile Material in Response to Primary Particle Controls

The results summarized in Table 4.7 indicate that control of primary particle emissions can alter the distribution of particle solubility and surface area in the ambient aerosol size distribution in a manner which leads to a redistribution according to particle size of secondary aerosol species such as NO_3^- and NH_4^+. To illustrate this effect more clearly, model calculations were performed under more extreme conditions. Figure 4.3 shows the results of model calculations predicting the size and composition distribution of the

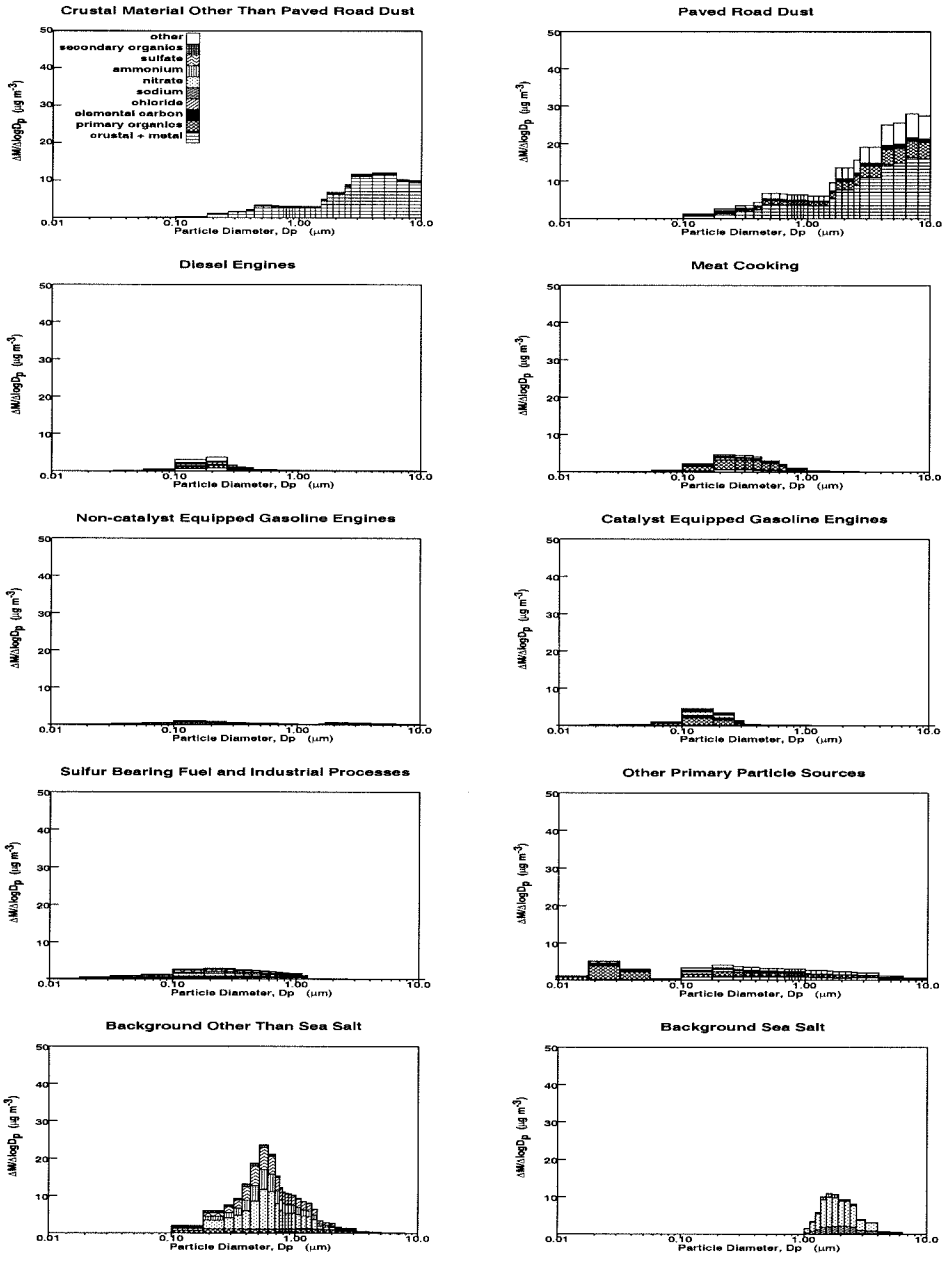

Figure 4.2:
Individual source contributions to the daily average particle size and chemical composition distributions predicted at Claremont, CA, on August 28, 1987, after applying all of the control measures studied to reduce base case emissions. Each subplot illustrates the primary seed particles emitted from the indicated source along with the associated gas-to-particle conversion products that have accumulated on those seed particles over time.

ambient aerosol at Claremont, CA, on August 28, 1987, at 1000 PST. Subgraphs are grouped in pairs of two, with the upper panel of each pair displaying the calculated and measured volume distribution of the ambient aerosol while the panel immediately below shows the corresponding size and chemical composition distribution of particles in the atmosphere. The observed aerosol volume distribution in the range below approximately 1 μm particle diameter results from electronic size distribution measurements made by an electrical aerosol analyzer and an optical particle counter (OPC) during the SCAQS experiments. Above 1 μm particle diameter, a data gap exists because larger particles fail to negotiate the inlet to the OPC. The rectangle in the volume distribution between 2.5 μm and 10 μm particle diameter reflects the aerosol volume estimated from the differences between PM2.5 and PM10 filter samples.

The results of four different emissions control situations are illustrated in Figure 4.3. The two sub-plots shown in the upper left illustrate model results using base case emissions and initial conditions which will be used for comparison to the other results shown in this figure. The observed bimodal nature of the ambient submicron aerosol is reproduced well by model predictions, with the mode at 0.1-0.3 μg m^{-3} attributable largely to particles originating from diesel engines and meat cooking sources while the mode at 0.6-0.8 μm particle diameter is caused largely by transformed non-sea salt background particles.

The two sub-plots shown in the upper right quadrant of Figure 4.3 show the results of model calculations in which it is assumed that there are no emissions of primary particles in the study region (particle initial conditions and gas-phase emissions remain at their base case values). As this figure shows, ambient particles with diameters greater than 2.5 μm or smaller than

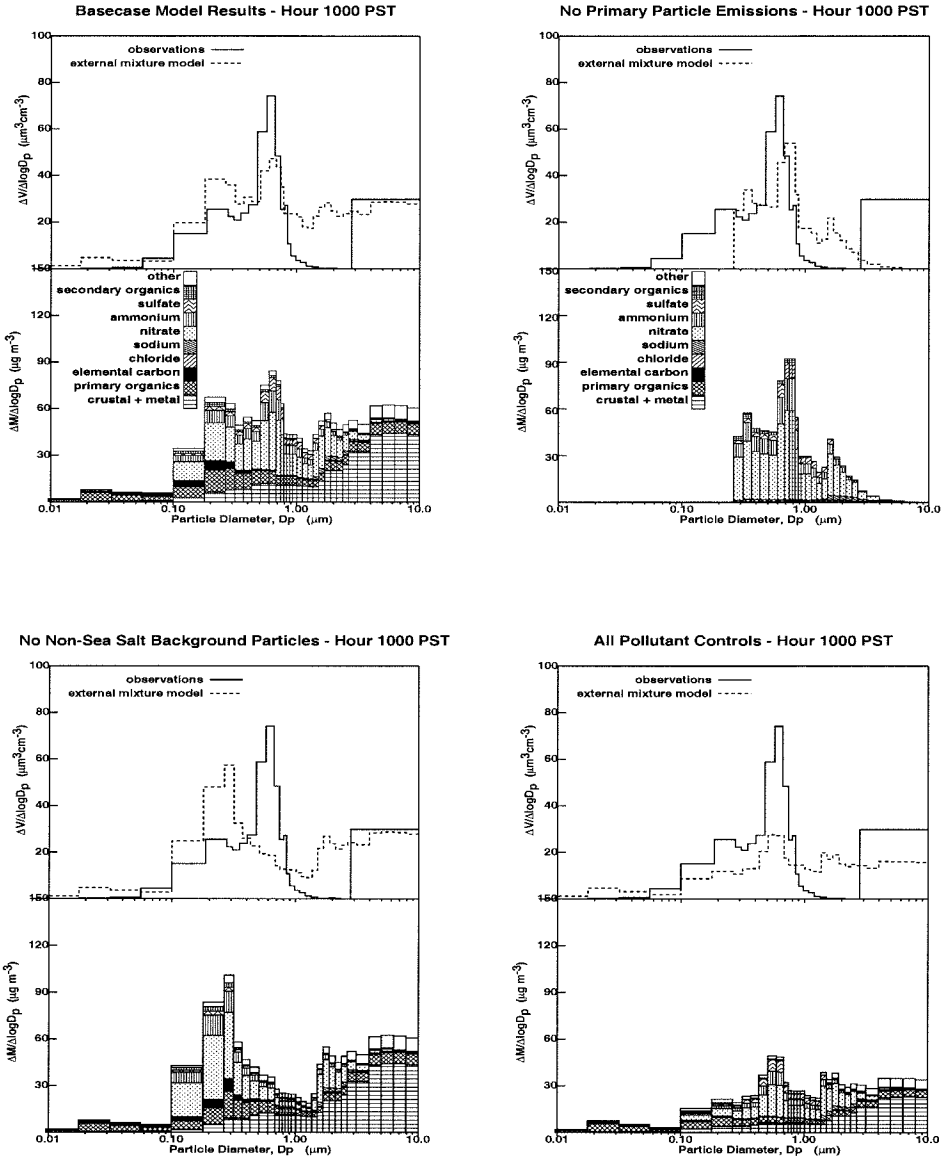

Figure 4.3:

Model predictions illustrating the redistribution of secondary aerosol within the particle size- and composition-distribution at Claremont, CA, on August 28, 1987, at 1000 PST in response to specific emissions changes. Upper left quadrant: base case with no controls. Upper right quadrant: complete elimination of particle emissions (initial conditions at basecase values). Lower left quadrant: remove background non-sea salt particles. Lower right quadrant: all control measures in Tables 4.3-4.5.

0.2 μm are virtually eliminated by this form of extreme control, but significant particulate mass is still apparent between 0.3-1.0 μm particle diameter. This is due to the fact that background particles are still advected into the study region where they participate in heterogeneous chemistry in the urban atmosphere. Despite the removal of the underlying primary particle emissions at approximately 0.7 μm particle diameter, the peak in the aggregate size distribution for particles of this size is even larger than in the base case simulation due to the accumulation of additional secondary reaction products onto the non-sea salt background particles. This behaviour should be examined in the future through light scattering calculations because the results may hold strong implications for visibility improvement. Particles of this size are chiefly responsible for light scattering in the atmosphere. The ability of the non-sea salt background particles to act as a sink for secondary reaction products in this critical light scattering size range may mean that visibility improvement will have to be attained primarily through abatement of gaseous secondary aerosol precursors even though primary particle control alone would be expected to reduce fine particle mass concentrations significantly.

The set of sub-plots shown in the lower left quadrant of Figure 4.3 illustrate the predicted size and composition distribution of the ambient aerosol at Claremont, CA, at 1000 PST on August 28, 1987, in the event that the non-sea salt background particles could be removed from the atmosphere before they are advected into the study region (local particle-phase and gas-phase emissions in the Los Angeles area were kept at their base case values). The sub-plots show that under these conditions, the secondary ammonium nitrate which would have been associated with the non-sea salt background particles now condenses onto particles in the size range from 0.1-0.3 μm par-

ticle diameter. This behavior is not totally unexpected, since the particles with 0.1-0.3 μm diameter dominate the distribution of surface area in the ambient aerosol. The peak in the size distribution formerly located between 0.6-0.8 μm particle diameter is completely eliminated if the non-sea salt background particles are removed. At present, no one knows how to reduce those non-sea salt background particles or even where they come from, but clearly it would be useful to study that question directly since it may be at the heart of the development of the Los Angeles visibility problem.

The final set of sub-plots shown in the lower right quadrant of Figure 4.3 illustrate the predicted size and chemical composition distribution of the ambient aerosol at Claremont, CA, at 1000 PST on August 28, 1987, when all of the controls described in Section 4.3.4 are applied simultaneously to the base emissions inventory. These results indicate that primary particle controls are very effective at reducing the concentrations of ambient particles at the small and large ends of the size distribution, while gas-phase emissions controls effectively reduce the concentrations of secondary material on most types of particles. This behavior emphasizes the need for a combined control strategy to reduce ambient particulate matter concentrations. Primary particle controls by themselves lead to the redistribution secondary aerosol formation products within the ambient particle size distribution, and this effect should be examined further because it might cause increased visibility impairment. Control of gas-phase pollutant emissions effectively reduces the concentrations of secondary aerosol species; however, this strategy does nothing to mitigate the abundance of primary aerosol pollutants (such as trace metals emitted from combustion sources) which may contribute to the health effects caused by fine particle exposure [3].

4.5 Conclusions

A wide variety of emissions control measures exist that could be employed to further reduce fine particle concentrations in the Los Angeles area atmosphere. Through the use of a detailed model for particle emission, transport and chemical transformation, it is seen that the available approaches to control will affect different portions of the atmospheric fine particle size distribution, which in turn may mean that not all approaches will be equally effective at reducing light scattering and visibility impairment.

The primary particle controls examined here were found to preferentially affect the smallest and largest ends of the fine particle size distribution. Reduction in motor vehicle tailpipe particulate matter emissions and particles emitted from food cooking operations will principally reduce primary carbon particle concentrations in the size range from 0.1-0.3 μm particle diameter while fugitive dust controls will affect mainly particles larger than 1 μm particle diameter. These primary particle controls, if used alone, will alter the surface area distribution of the aerosol, thereby causing gas-to-particle conversion products to preferentially accumulate on the non-sea salt background aerosol which peaks in the 0.5-0.8 μm size range where visibility could be affected.

Controls applied to ROG and NO_x alone according to plans that were originally designed to reduce ozone concentrations in the Los Angeles area would reduce fine particle mass concentrations at Claremont, CA, on August 28, 1987, by 9.5% under the conditions studied here, primarily by reducing aerosol nitrate concentrations. Addition of controls on ammonia emissions will suppress aerosol nitrate formation further.

The combined use of all available gas-phase and particle-phase emissions

controls would reduce ambient fine particle concentrations at Claremont, CA, by 46% relative to base case conditions during the 1987 summer smog episode studied here.

Bibliography

[1] NRC (National Research Council). *Protecting Visibility in National Parks and Wilderness Areas.* National Academy Press, Washington, DC, 1993.

[2] G. Oberdorster, R. M. Gelein, J. Ferin, and B. Weiss. Association of particulate air pollution and acute mortality, involvement of ultrafine particles? *Inhalation Toxicology*, 7:111–124, 1995.

[3] K. L. Dreher, R. H. Jaskot, J. R. Lehmann, J. H. Richards, J. K. McGee, A. J. Ghio, and D. L. Costa. Soluable transition metals mediate residual oil fly ash induced acute lung injury. *Journal of Toxicology and Environ. Health*, 50:285–305, 1997.

[4] R. B. Schlesinger. Factors affecting the response of lung clearance systems to acid aerosols - Role of exposure concentration, exposure time and relative acidity. *Environ. Health Perspect.*, 79:121–126, 1989.

[5] Michael J. Kleeman, Annmarie Eldering, and Glen R. Cass. Modeling the airborne particle complex as a source-oriented external mixture. *J. Geophys. Res.*, 102(D17):21355–21372, 1997.

[6] Michael J. Kleeman and Glen R. Cass. Source contributions to the size and composition distribution of urban particulate air pollution. *Atmos. Environ.*, 32:2803–2816, 1998.

[7] Daniel J. Jacob. Chemistry of OH in remote clouds and its role in the production of formic acid and peroxymonosulfate. *J. Geophys. Res.*, 91(D9):9807–9826, 1986.

[8] Daniel J. Jacob, Elaine W. Gottlieb, and Michael J. Prather. Chemistry of a polluted boundary layer. *J. Geophys. Res.*, 94(D10):12975–13002, 1989.

[9] Hans R. Pruppacher and James D. Klett. *Microphysics of Clouds and Precipitation.* D. Reidel Publishing Company, Boston, Mass., 1978.

[10] Anthony S. Wexler and John H. Seinfeld. Second-generation inorganic aerosol model. *Atmos. Environ.*, 25A:2731–2748, 1991.

[11] William P. L. Carter. A detailed mechanism for the gas–phase atmospheric reactions of organic compounds. *Atmos. Environ.*, 24A:481–518, 1990.

[12] Spyros N. Pandis, Robert A. Harley, Glen R. Cass, and John H. Seinfeld. Secondary organic aerosol formation and transport. *Atmos. Environ.*, 26A:2269–2282, 1992.

[13] Jay R. Odum, Tim P. W. Jungkamp, Robert J. Griffin, Halli J. L. Forstner, Richard C. Flagan, and John H. Seinfeld. Aromatics, reformulated gasoline, and atmospheric organic aerosol formation. *Environ. Sci. Technol.*, 31(7):1890–1897, 1997.

[14] Jay R. Odum, Tim P. W. Jungkamp, Robert J. Griffin, Richard C. Flagan, and John H. Seinfeld. The atmospheric-aerosol forming potential of whole gasoline vapor. *Science*, 276:96–99, 1997.

[15] J. F. Pankow. An absorption-model of gas-particle partitioning of organic-compounds in the atmosphere. *Atmos. Environ.*, 28:185–188, 1994.

[16] J. F. Pankow. An absorption-model of the gas aerosol partitioning involved in the formation of secondary organic aerosol. *Atmos. Environ.*, 28:189–193, 1994.

[17] Jay R. Odum, Donald Dabdub, and John H. Seinfeld. Observations on modeling and measuring ambient carbonaceous aerosol. *Environ. Sci. Technol.*, submitted for publication, 1998.

[18] Jay R. Odum. personal communication to Michael J. Kleeman, 1997.

[19] Annmarie Eldering and Glen R. Cass. Source–oriented model for air pollutant effects on visibility. *J. Geophys. Res.*, 101(D14):19343–19369, 1996.

[20] William R. Goodin, Gregory J. McRae, and John H. Seinfeld. A comparison of interpolation methods for sparse data: Application to wind and concentration fields. *J. Appl. Met.*, 18:761–771, 1979.

[21] S. Gharib and G.R. Cass. *Ammonia Emissions in the South Coast Air Basin, Open file report 84–2.* Environmental Quality Laboratory, Calif. Inst. of Technol., Pasadena, 1984.

[22] Armistead G. Russell and Glen R. Cass. Verification of a mathematical model for aerosol nitrate and nitric acid formation and its use for control measure evaluation. *Atmos. Environ.*, 20:2011–2025, 1986.

[23] Mathew P. Fraser and Glen R. Cass. Detection of excess ammonia emissions from in-use vehicles and the implications for fine particle control. *Environ. Sci. Technol.*, 32(8):1053–1057, 1998.

[24] Robert A. Harley, Armistead G. Russell, Gregory J. McRae, Glen R. Cass, and John H. Seinfeld. Photochemical modeling of the Southern California Air Quality Study. *Environ. Sci. Technol.*, 27:378–388, 1993.

[25] H. Andrew Gray. *Control of Atmospheric Fine Primary Carbon Particle Concentrations.* PhD dissertation, also published as Environmental Quality Laboratory Report 23, California Institute of Technology, Pasadena, 1986.

[26] Glen R. Cass. Sulfate air quality control strategy design. *Atmos. Environ.*, 15:1227–1249, 1981.

[27] R. F. Sawyer and J. H. Johnson. In *Diesel Exhaust: A Critical Analysis of Emissions, Exposure and Health Effects.* Technical Report, Health Effects Institute, Cambridge, MA, 1995.

[28] U.S. Environmental Protection Agency. *Nonroad Engine and Vehicle Emission Study – Report.* Technical Report EPA 21A – 2001, Office of Air and Radiation (ANR-443), U. S. Environmental Protection Agency, Washington, DC, 1991.

5 Identifying the Effect of Individual Emissions Sources on Particulate Air Quality Within a Photochemical Aerosol Processes Trajectory Model

5.1 Introduction

Design of emission control strategies for improvement of particulate air quality requires a detailed understanding of the relative contribution of many different types of emissions sources to ambient pollutant concentrations. Aerosol processes air quality models have been developed that are capable of separately tracking the contribution of the primary particles from distinct emission source categories as they are affected by atmospheric transport, heterogeneous chemical reactions, and dry deposition [1, 2, 3]. In such models, the ambient aerosol is represented as a source-oriented external mixture in which the particles emitted from different source categories (e.g., diesel engines, gasoline engines, meat cooking, etc.) evolve separately in the atmosphere based on their initial size distribution and chemical composition. By following the fate of particles emitted from different source types, the contribution which each group of similar sources makes to ambient air quality at community receptor sites can be calculated for use in the design of emission control programs.

Although the source-oriented external mixture model can reveal the contributions which different general source categories make to ambient particulate concentrations, the number of source types that can be tracked separately as a practical matter has been limited to about 10 by the computational burden of the problem. The cost of the calculation has been directly proportional to the number of source types whose particle emissions are tracked separately through the system of differential equations that describe atmospheric transport, chemical reaction, and diffusion of chemical species to and from the particles. To reduce the burden of these calculations, it has been the practice to group together all sources that emit particles having a common size distribution and chemical composition that thus will be viewed identically by the chemical calculations in the model. Therefore, as an example, it is efficient computationally to treat all diesel engine exhaust particles as arising from a single lumped source category in the model, and likewise all particles emitted from non-catalyst gasoline-powered engines would be lumped together as a group. The underlying contributions made by different types of diesel engine sources (such as highway vehicles, railroad locomotives, ships, etc.) cannot be seen when the emissions data are treated in this manner. In theory, the source-oriented external mixture model could be expanded to separately track the emissions from every specific source of interest, but the computational burden of the problem is directly proportional to the number of externally mixed source categories that are defined within the model. Since there are literally thousands of different sources in a typical urban area, the computational burden associated with greater source resolution within the model can quickly become overwhelming.

The purpose of this chapter is to illustrate a technique which can be used to calculate the contribution that the individual sources within a lumped

source category make to ambient particle concentrations without significantly increasing the computational burden of the problem. In the sections below, the formulation of this technique first is discussed. Then air quality model results for August 28, 1987, at Claremont, CA, obtained previously in Chapter 4 are post-processed to separate the contributions which more than 50 individual source types make to ambient particulate air quality.

5.2 Procedure

The source-oriented external mixture model developed by Kleeman and Cass [2] separately tracks groups of particles released to the atmosphere from different sources and follows them while they accumulate coatings of gas-to-particle conversion products as they age in the atmosphere. This model is cast in a Lagrangian photochemical trajectory model format. Because location and time are synonymous in a Lagrangian model, knowledge of the length of time that a particle has been in the atmosphere also identifies the location of the source from which the particle was emitted. Figure 5.1 shows the trajectory path followed by the air mass arriving at Claremont, CA, at 1200 PST on August 28, 1987. Highlighted sections of this trajectory path mark the locations where particles were released into the target air mass between 1100-1200 PST on August 27, 1987, and between 1100-1200 PST on August 28, 1987. Obviously, those particles emitted at the earlier time must have originated from marine sources, since the target air mass was over the Pacific Ocean at this time.

Figure 5.2 shows the size and composition distribution of diesel engine particles which were released between 1100-1200 PST on August 27, 1987, as they arrive at Claremont, CA, on August 28, 1987, at 1200 PST as calculated by the modeling procedure of Kleeman and Cass [2]. Examination of the

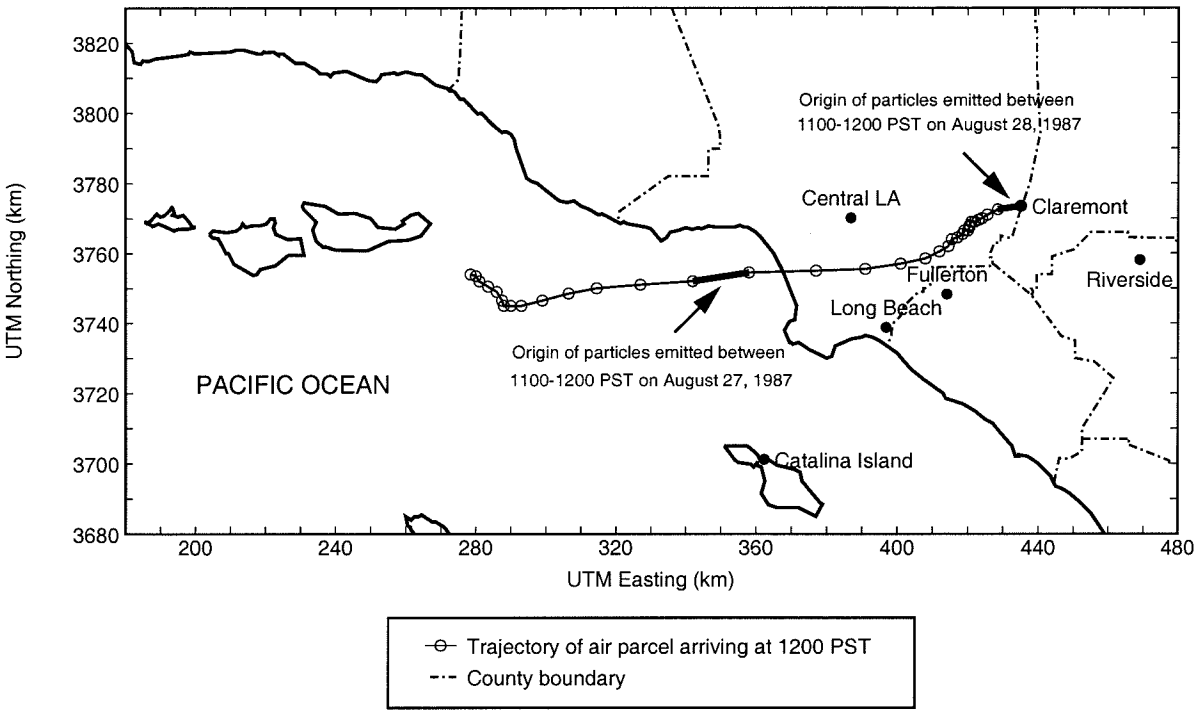

Figure 5.1:
Trajectory followed by air parcel arriving at 1200 PST on August 28, 1987, at Claremont, CA. Highlighted sections indicate the location of sources which emitted particles into the target air mass between 1100-1200 PST on August 27, 1987, and between 1100-1200 PST on August 28, 1987.

emissions inventory at the point of origin of those particles over the ocean reveals that two specific types of diesel engine uses contributed to particles of this type and age: American registered motor ships in transit and foreign motor ships in transit. The atmospheric concentrations of these day-old diesel engine particles can be apportioned between the two contributing types of ships in proportion to their relative emission rates along the trajectory segment since in all other respects the particles have been treated equally in the model.

Figure 5.3 shows the size and composition distribution of freshly emitted diesel engine particles released between 1100-1200 PST on August 28, 1987, as they arrive at Claremont, CA, on the same day at 1200 PST. These particles have aged less than 1 hour in the atmosphere before arriving at the receptor site. By examining the emissions inventory along the trajectory segment during which those particles were emitted, it is seen that many urban sources release diesel engine particles to the atmosphere at this time and location, including on-road diesel vehicles, off-road heavy-duty diesel vehicles (non-farm), mobile diesel refrigeration units, light duty industrial equipment, and railroad locomotives. Once again, the atmospheric burden of diesel engine particles of this age can be subdivided between the contributing emission sources in proportion to their relative emission rates at the location of initial particle insertion into the atmosphere. By repeating this analysis for all locations along the trajectory path, it is possible to subdivide the single lumped diesel engine particle type in the model into the separate contribution from dozens of different types of diesel engine uses.

The examples illustrated in Figures 5.2 and 5.3 can easily be extended to disaggregate the contribution from any specific sub-category of emissions source to particles of each type, age and size tracked by the source-oriented

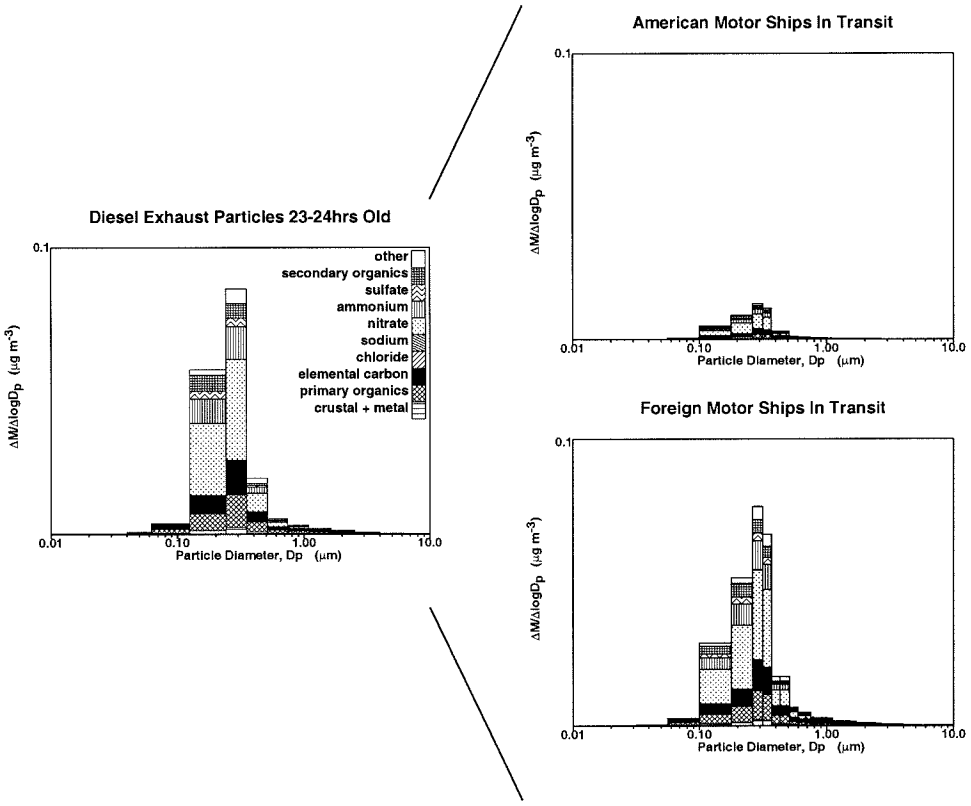

Figure 5.2:
Specific source contributions to diesel engine particles arriving at Claremont, CA, at 1200 PST on August 28, 1987, due to particles released to the atmosphere 23-24 hours earlier.

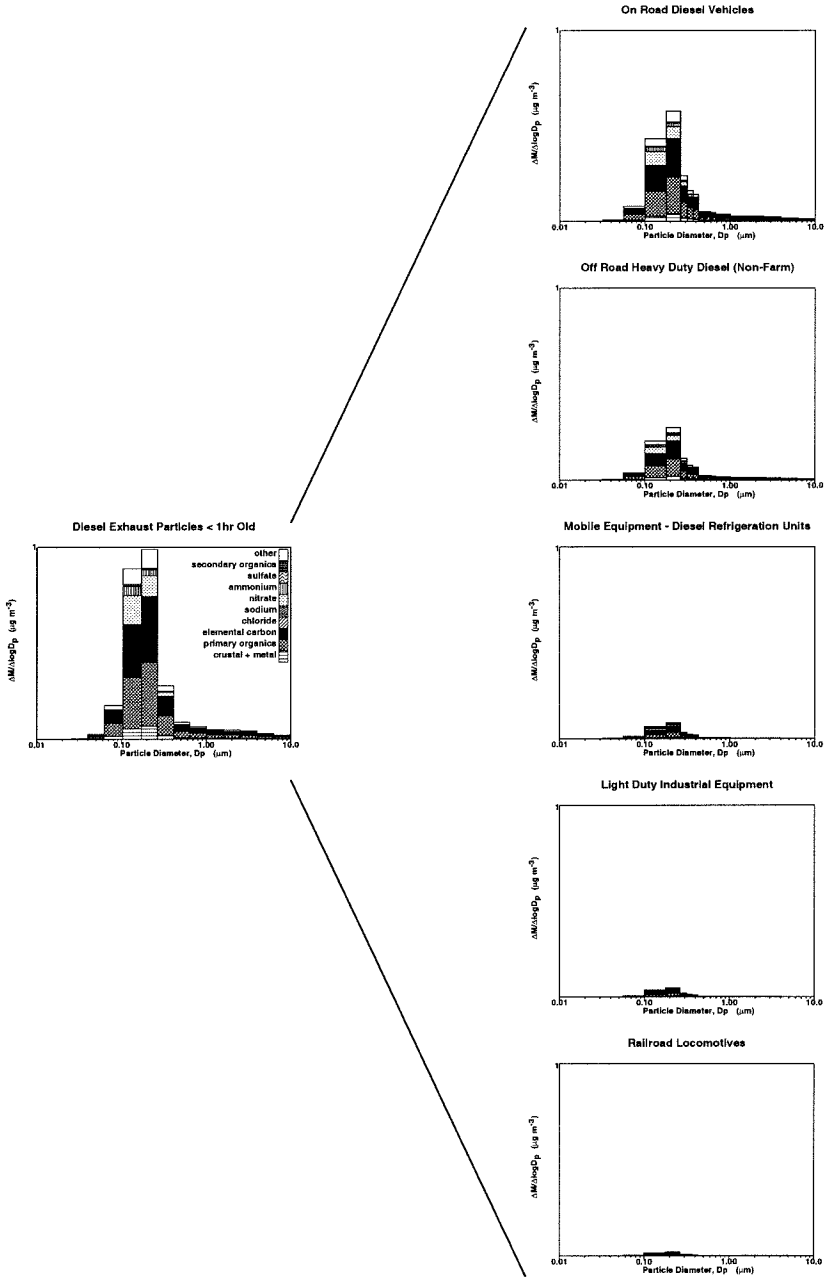

Figure 5.3:
Specific source contributions to diesel engine particles arriving at Claremont, CA, at 1200 PST on August 28, 1987, due to particles released to the atmosphere 0-1 hours earlier.

external mixture model without actually re-running the model. It is then a simple matter to aggregate this information across particles of different ages to calculate the overall contribution which any specific emissions source makes to ambient particulate concentrations. All of the necessary values for the calculations described above (particle age, type and size) are available as standard output from the source-oriented external mixture model, and further source separation can be obtained through simple processing of the emissions inventory with knowledge of the trajectory paths followed by each air parcel. As a result, the techniques just described which are used to obtain very detailed information on the contribution of individual sources to ambient particulate concentrations can be applied during the post-processing phase of the modeling exercise with comparatively little additional computational burden.

5.3 Trajectory Model Application

Basecase output from the source-oriented external mixture modeling study described by Kleeman and Cass [3] will be used to demonstrate the application of the analysis techniques described in Section 5.2. Twenty-four air parcel trajectories were tracked backward through time to their starting positions over the Pacific Ocean near Los Angeles on August 27, 1987. Each air parcel was then followed as it was advected inland across the South Coast Air Basin of Southern California and arrived at the target receptor site (Claremont, CA) at consecutive hours on August 28, 1987. Gas- and particle-phase initial conditions over the Pacific Ocean were based on measurements made during the study period as described by Kleeman and Cass [3]. Emissions of gas- and particle-phase pollutants were represented using a modified version of the emissions inventory provided by the California Air Resources Board

for the South Coast Air Basin of Southern California during the study period. Source location and activity level information from this inventory was retained, but the information describing particle size distributions and the chemical speciation of the gas- and particle-phase emissions was replaced using more recent data. Gas-phase VOC emissions were speciated into detailed organic compound classes following the treatment of Harley et al. [4, 5, 6]. Particle-phase emissions were speciated using the size and chemical composition information derived from the source test program of Hildemann et al. [7, 8] along with modifications to the emissions inventory as described by Eldering and Cass [9].

In the source-oriented external mixture model application described above, the hundreds of actual emissions source types in Southern California are aggregated into eight lumped groups of similar sources that are tracked during the computationally intensive gas-to-particle conversion calculations: paved road dust, crustal material other than paved road dust, food cooking, diesel engines, catalyst-equipped gasoline engines, non-catalyst gasoline engines, high sulfur content particles emitted from fuel combustion or industrial processes, and all remaining anthropogenic particles. Model calculations predict the size and composition distribution of particles emitted from each of these eight groups of sources as a function of particle age as they arrive at Claremont, CA, on August 28, 1987, after being modified by gas-to-particle conversion, deposition, and fog processes. The contribution which particles in each category make to the daily average particle size and chemical composition distribution predicted at Claremont, CA, on August 28, 1987, is shown in Figure 1 of Kleeman and Cass [3]. In the sections below, model results will be further processed using the techniques described in Section 5.2 to reveal the contribution to the size and composition distribution of the ambi-

ent aerosol from specific sub-categories of individual sources within the eight larger groups.

5.4 Specific Source Contributions

The contributions which specific emissions sources make to the ambient size- and composition distribution of particles associated with six of the eight categories tracked by the source-oriented external mixture model are illustrated in Figures 5.4-5.6. Only the largest specific contributors within each lumped source category are shown. The information describing the contributions from the hundreds of additional sources which are a part of several of these categories is available and will be used in Section 5.6.

The upper set of plots shown in Figure 5.4 illustrates the size and composition distribution of ambient particles associated with sources that contribute diesel engine particles in the atmosphere at Claremont, CA, at 1200 PST on August 28, 1987. The majority of diesel engine particles are seen to originate from on-road diesel vehicles with additional contributions from off-road heavy duty diesel (non-farm) equipment, mobile diesel-powered refrigeration units, and railroad locomotives involved in hauling operations. Most of the secondary ammonium, nitrate, and organic material associated with diesel engine particles is present on the diesel particles originating from on-road mobile sources.

The lower set of plots included in Figure 5.4 shows the four specific sources which make the largest contribution to particles originating from non-catalyst gasoline engines as these particles arrive at Claremont, CA, at 1200 PST on August 28, 1987. On-road mobile sources once again make the largest single contribution to particles within this lumped source category, with much smaller contributions from mobile gasoline-powered refrigeration units, com-

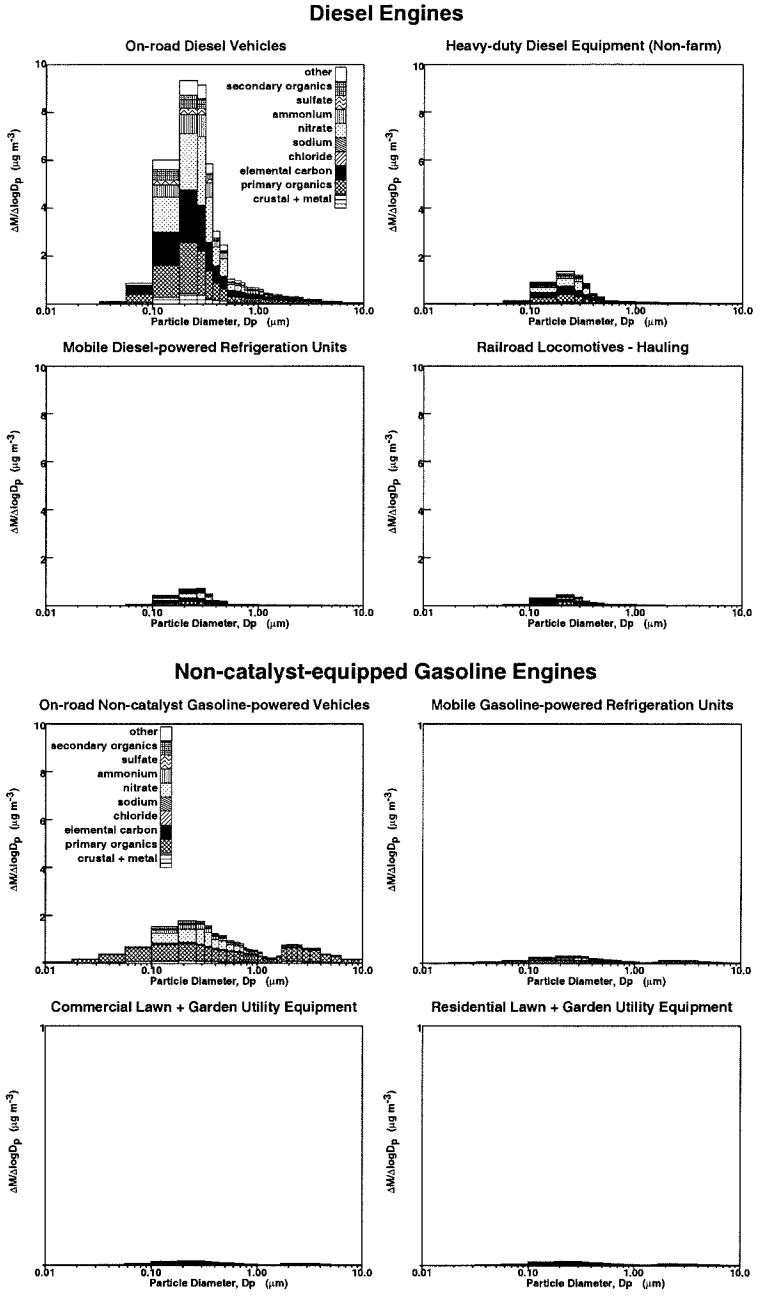

Figure 5.4:
Specific source contributions to diesel engine exhaust particles and non-catalyst-equipped gasoline engine exhaust particles arriving at Claremont, CA, at 1200 PST on August 28, 1987.

mercial lawn and garden utility equipment, and residential lawn and garden utility equipment. As was the case for diesel engine particles, the majority of the secondary ammonium, nitrate, and organic material associated with particles emitted from non-catalyst-equipped gasoline engines is present on particles emitted from on-road mobile sources.

The ambient size and composition distribution of particles released from sources which contribute to crustal particles other than paved road dust is shown in the upper half of Figure 5.5. Construction and demolition of commercial, residential, and industrial buildings as well as travel on unpaved city and county roads make the largest contributions to crustal particles other than paved road dust in the atmosphere at 1200 PST on August 28, 1987 at Claremont, CA. Crustal particles other than paved road dust are generated by mechanical abrasion and so are dominated by particles with diameters larger than 2.5 μm. Virtually no particle-phase nitrate or ammonium ion is associated with particles originally released from these sources due to their large particle size (hence small surface area to mass ratio) and due to their hydrophobic nature.

The lower plots included in Figure 5.5 reveal that particles originally released from industrial landfill waste gas flares, aluminum smelters, gas-fired petroleum refinery process heaters, and the combustion of distillate oil all contribute significantly to ambient aerosol associated with sources emitting high sulfur content particles. All of these particles accumulate significant quantities of ammonium and nitrate aerosol due to their hygroscopic nature.

Figure 5.6 shows the ambient size and composition distribution of particles released from sources included in the food cooking and other anthropogenic sources categories that are tracked by the source-oriented external mixture model. Sources contributing to food cooking particles include com-

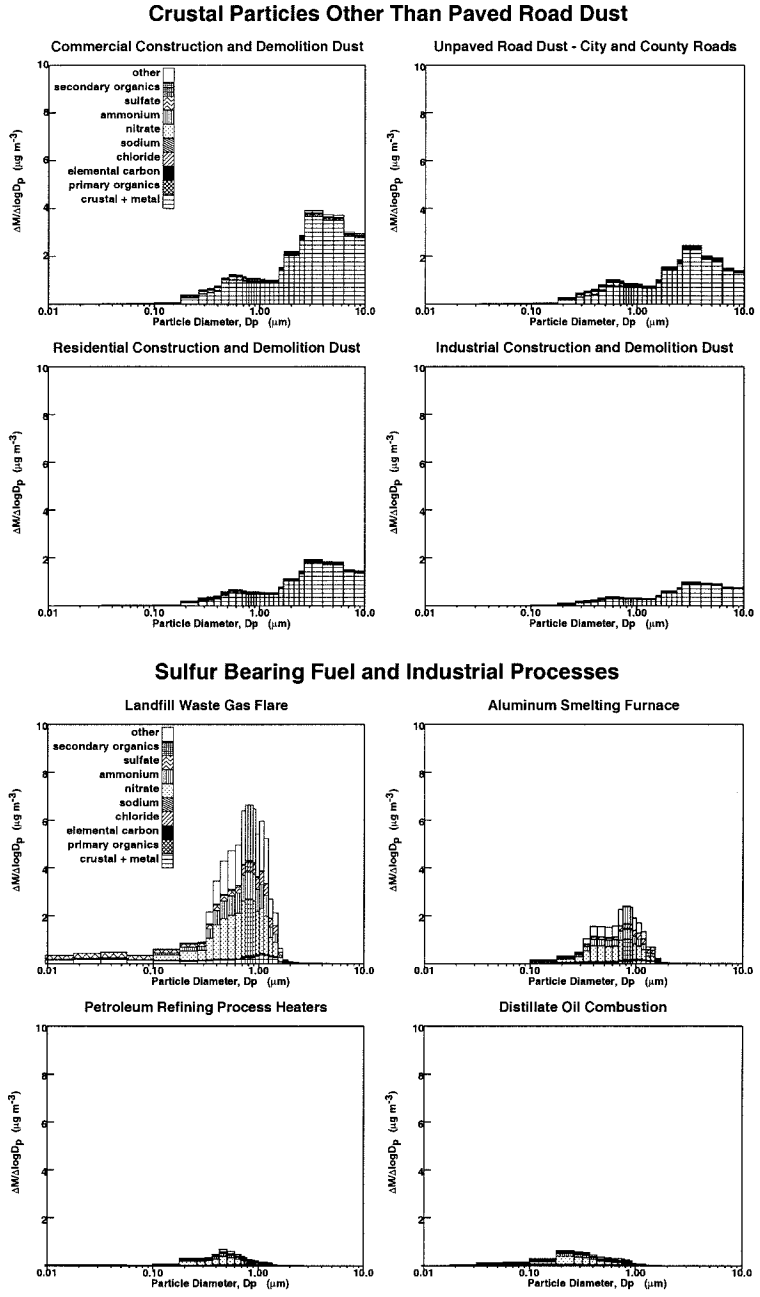

Figure 5.5:
Specific source contributions to crustal particles (other than paved road dust) and particles from sulfur bearing fuel and industrial processes arriving at Claremont, CA, at 1200 PST on August 28, 1987.

mercial charbroiling, commercial deep fat frying, and other commercial cooking (unspecified). Ambient particles originally released from these sources are composed largely of organic carbon that accumulates coatings of secondary ammonium nitrate during transit across the air basin.

The lower plots included in Figure 5.6 show the ambient size and composition distribution of particles released from sources included in the "other anthropogenic sources" category that is tracked by the source-oriented external mixture model. Source separation within this category is possible despite the diverse range of input particle sizes and compositions that contribute to this category because the technique described in Section 5.2 is separately applied to particles of each different size and age. As a result, particles of very small size emitted from one of the "other" sources at a particular grid square in the model are tracked separately from larger particles of a different age contributed by a different type of "other" source at a different location. Wood and paper processing losses are seen to generate particles which contribute to the coarse fraction of the ambient size distribution, as does cattle feedlot dust. Natural gas-fired turbines used in the production of electricity emit ultra-fine particles (Dp < 0.1 μm) which contribute to atmospheric concentrations at Claremont, CA, at 1200 PST on August 28, 1987. Particles released from spray drying of detergents also are seen to contribute to this source category.

Two of the lumped categories tracked by the source-oriented external mixture model had only one specific contributing source in the present study. Particles within the paved road dust category were emitted exclusively from entrainment of paved road dust, while particles within the catalyst-equipped gasoline-powered vehicles category were released only from on-road catalyst-equipped gasoline-powered vehicles.

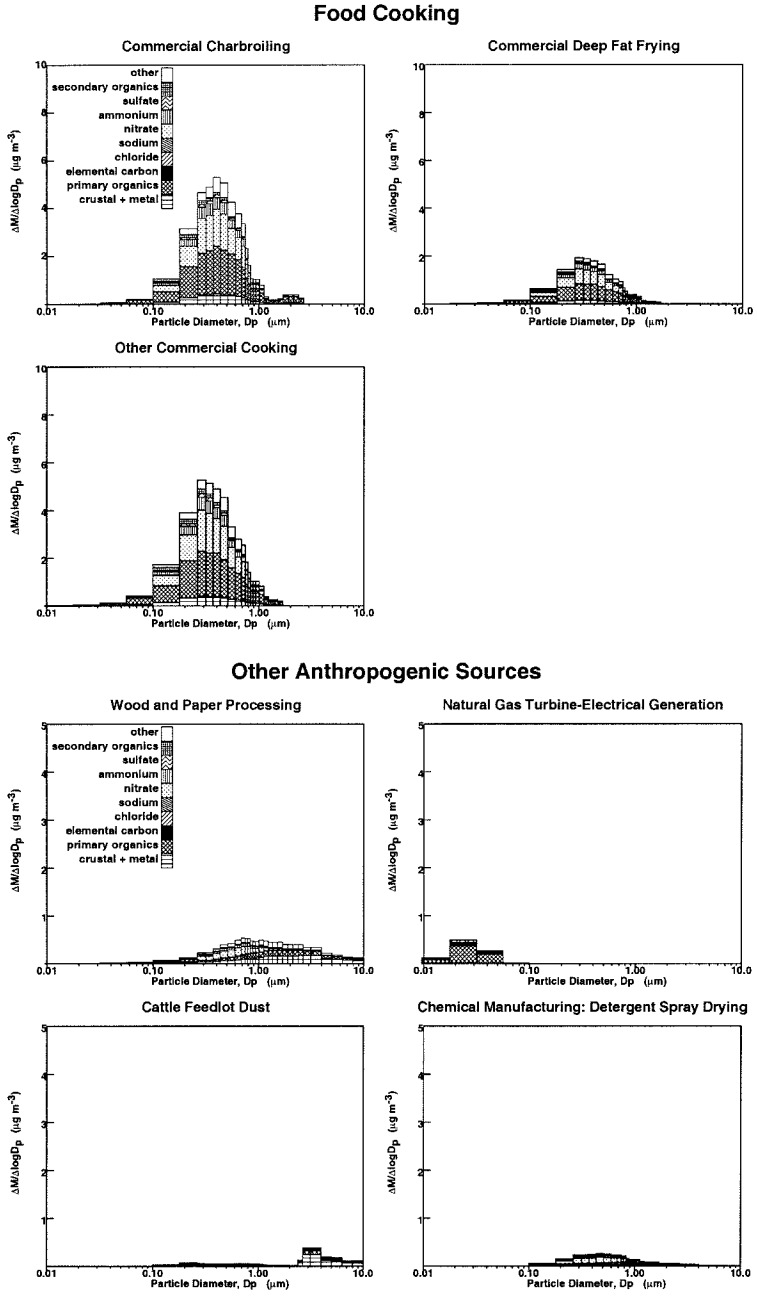

Figure 5.6:
Specific source contributions to food cooking particles and particles released from other anthropogenic sources arriving at Claremont, CA, at 1200 PST on August 28, 1987.

5.5 Specific Source Contributions as a Function of Location

When constructing Figures 5.4-5.6, the contributions to ambient particulate air quality at Claremont, CA, at a specific time from specific sources at all upwind locations were grouped together. This information identifies the important types of sources, but does not show the location of these sources. Information describing source location would be useful both to identify significant point sources and to determine the spatial distribution of the contributions from area sources.

The technique described in Section 5.2 can easily be used to show the contributions which particles from specific sources at different locations make to particulate air quality at a downwind receptor site. Table 5.1 shows the 20 largest contributions which particles from specific sources at different locations make to ambient PM2.5 concentrations at Claremont, CA, on August 28, 1987, at 1200 PST. The results show that the emissions from point sources such as industrial waste gas flares and aluminum smelting furnaces located at map coordinates UTM (420,3770) and UTM (420,3765) respectively in Figure 5.1 along with their accumulated coatings of gas-to-particle conversion products account for 5.45 μg m^{-3} (7.7%) of the PM2.5 mass at Claremont at the target time. The size and composition distribution of particles originally released from these facilities as they arrive at Claremont are shown in the lower portion of Figure 5.5.

Important area sources identified in Table 5.1 include on-road diesel vehicles, entrained paved road dust, commercial charbroiling, and commercial cooking (unspecified). Generally speaking, Table 5.1 indicates that the area sources located underneath the 1200 PST trajectory as it stagnates overnight

on August 27-28, 1987, make the largest contribution to ambient air quality at Claremont at noon the next day (compare Table 5.1 and Figure 5.1).

5.6 Reorganization of Source Contributions According to Regulated Emissions Categories

The eight source categories that are followed through the system of differential equations within the particle mechanics calculations of the source-oriented external mixture model application described by Kleeman et al. [1] and Kleeman and Cass [2, 3] are chosen to group those sources that emit particles with similar (or identical) initial size and composition. This approach is logical because particles with the same size and composition will undergo the same transformations as they are acted on by gas-to-particle conversion processes, deposition, and fog processing. When designing an emissions control program, however, it would be more convenient to view the results of the modeling calculation in terms of those source categories that will be regulated separately. Table 1 of Kleeman et al. [3] summarizes the basecase emissions inventory used by the source-oriented external mixture model in the present study. This inventory is broken down according to the emissions of reactive organic gases, NO_x, CO, SO_x, PM10, and PM2.5 in 55 categories similar to those used in the current governmental plan for emissions control in the Los Angeles area prepared by the South Coast Air Quality Management District as part of their 1997 Air Quality Management Plan (AQMP). The technique described in Section 5.2 of the current chapter can be used to break the results of the air quality model calculation of Kleeman and Cass [3] down to the format of the source resolution included in the emissions inventory summary described above, and likewise could be used to break the contribution down

Table 5.1: Location of 20 Largest Specific Sources Contributing to Ambient PM2.5 Concentrations at Claremont, CA, at 1200 PST on August 28, 1987

Description	UTM Location[a] East	UTM Location[a] North	PM2.5 Concentration[b] $\mu g\ m^{-3}$	PM2.5 Concentration[b] %
Industrial Landfill Waste Gas Flare	420	3770	4.23	6.0
Aluminum Smelting Furnace	420	3765	1.22	1.7
On-road Diesel Vehicles	400	3760	0.81	1.1
On-road Diesel Vehicles	405	3760	0.55	.8
On-road Diesel Vehicles	425	3770	0.50	.7
On-road Diesel Vehicles	425	3775	0.41	.6
On-road Diesel Vehicles	415	3765	0.37	.5
Entrained Paved Road Dust	425	3770	0.70	1.0
Entrained Paved Road Dust	405	3760	0.62	.9
Entrained Paved Road Dust	410	3760	0.60	.8
Entrained Paved Road Dust	400	3760	0.56	.8
Entrained Paved Road Dust	395	3760	0.52	.7
Entrained Paved Road Dust	420	3770	0.45	.6
Entrained Paved Road Dust	425	3775	0.40	.6
Commercial Charbroiling	405	3760	0.62	.9
Commercial Charbroiling	410	3760	0.56	.8
Commercial Charbroiling	435	3775	0.42	.6
Commercial Cooking - Unspecified	410	3760	0.60	.8
Commercial Cooking - Unspecified	405	3760	0.50	.7
Commercial Cooking - Unspecified	435	3775	0.47	.7

[a] Coordinates used refer to the Universal Transverse Mercator (UTM) system; the geographical region of interest falls into UTM zone 11. See Figure 5.1 to locate grid coordinates on a map of Southern California.

[b] Contribution to total ambient PM2.5 mass at Claremont, CA, at 1200 PST on August 28, 1987, including secondary gas-to-particle conversion products accumulated on the particles during transit across the air basin. The contribution due solely to the primary particle core without the gas-to-particle conversion products also can be computed easily (see [2]).

to the level of the many hundreds of different source types contained in the underlying computer-based version of the emissions inventory (although it would be impractical to reprint such a table here).

Table 5.2 shows the PM2.5 mass associated with ambient particles at 1200 PST on August 28, 1987, at Claremont, CA, according to the origin of the primary particle core of each particle reorganized into the 55 categories used to summarize the emissions inventory. The quantities of $SO_4^=$, NH_4^+, NO_3^-, Cl^-, and organics present in those particles are listed separately in Table 5.2, and are subdivided into material of primary vs secondary origin such that the secondary aerosol material can be separated from the primary particle core of each particle type if desired. Ambient PM2.5 concentrations associated with particles having primary cores emitted from anthropogenic sources at this time and location total 43.81 μg m^{-3} with roughly equal contributions from industrial processes (11.62 μg m^{-3}), miscellaneous processes (11.75 μg m^{-3}), and on-road vehicles (10.20 μg m^{-3}). Particles from industrial processes are dominated by food and agricultural sources (8.61 μg m^{-3}) which are largely composed of food cooking operations. Particles within the miscellaneous processes category include contributions from sources such as construction and demolition dust (3.16 μg m^{-3}), entrained paved road dust (6.71 μg m^{-3}), and entrained unpaved road dust (1.31 μg m^{-3}). Particles within the on-road mobile source category are chiefly associated with light-duty passenger vehicles (3.76 μg m^{-3}) and heavy-duty diesel trucks (3.67 μg m^{-3}).

Table 5.2: Source Contributions to Ambient PM2.5 Concentrations at Claremont, CA, at 1200 PST on August 28, 1987

Category Code	PM2.5[a]	$SO_4^=$		NH_4^+		NO_3^-		Cl^-		Org	
	$\mu g\ m^{-3}$	Prim[b]	Sec[c]	Prim[b]	Sec[c]	Prim[b]	Sec[c]	Prim[b]	Sec[c]	Prim[b]	Sec[c]
Fuel Combustion											
Agricultural	0.00	0.00	0.00	0.00	0.00	0.00	0.00	0.00	0.00	0.00	0.00
Oil and Gas Production	0.15	0.01	0.00	0.00	0.02	0.00	0.06	0.00	0.00	0.02	0.00
Petroleum Refining	0.64	0.06	0.02	0.00	0.10	0.00	0.27	0.00	0.00	0.02	0.01
Other Manufact./Ind.	0.83	0.08	0.01	0.00	0.04	0.02	0.12	0.02	0.00	0.39	0.01
Electric Utilities	0.03	0.00	0.00	0.00	0.00	0.00	0.00	0.00	0.00	0.02	0.00
Other Service and Commerce	0.82	0.09	0.02	0.01	0.09	0.01	0.24	0.01	0.00	0.11	0.02
Residential	0.19	0.02	0.00	0.00	0.00	0.01	0.00	0.01	0.00	0.13	0.00
Other	0.43	0.03	0.01	0.00	0.05	0.00	0.14	0.00	0.00	0.08	0.01
	3.09	0.28	0.06	0.01	0.30	0.03	0.83	0.04	0.00	0.78	0.05
Waste Burning											
Agricultural Debris	0.00	0.00	0.00	0.00	0.00	0.00	0.00	0.00	0.00	0.00	0.00
Range Management	0.00	0.00	0.00	0.00	0.00	0.00	0.00	0.00	0.00	0.00	0.00
Forest Management	0.00	0.00	0.00	0.00	0.00	0.00	0.00	0.00	0.00	0.00	0.00
Incineration	0.01	0.00	0.00	0.00	0.00	0.00	0.00	0.00	0.00	0.00	0.00
Other	4.33	0.40	0.10	0.00	0.61	0.01	1.30	0.01	-.01	0.08	0.05
	4.34	0.40	0.10	0.00	0.61	0.01	1.30	0.01	-.01	0.08	0.05
Solvent Use											
Dry Cleaning	0.00	0.00	0.00	0.00	0.00	0.00	0.00	0.00	0.00	0.00	0.00
Degreasing	0.00	0.00	0.00	0.00	0.00	0.00	0.00	0.00	0.00	0.00	0.00
Architectural Coating	0.00	0.00	0.00	0.00	0.00	0.00	0.00	0.00	0.00	0.00	0.00
Other Surface Coating	0.23	0.00	0.01	0.00	0.02	0.00	0.05	0.00	0.00	0.04	0.01
Asphalt Paving	0.00	0.00	0.00	0.00	0.00	0.00	0.00	0.00	0.00	0.00	0.00
Printing	0.00	0.00	0.00	0.00	0.00	0.00	0.00	0.00	0.00	0.00	0.00
Consumer Products	0.00	0.00	0.00	0.00	0.00	0.00	0.00	0.00	0.00	0.00	0.00
Industrial Solvent Use	0.02	0.00	0.00	0.00	0.00	0.00	0.00	0.00	0.00	0.00	0.00
Other	0.01	0.00	0.00	0.00	0.00	0.00	0.00	0.00	0.00	0.00	0.00
	0.26	0.00	0.01	0.00	0.02	0.00	0.06	0.00	0.00	0.04	0.01
Petrol. Proc., Storage & Trans											
Oil and Gas Extraction	0.00	0.00	0.00	0.00	0.00	0.00	0.00	0.00	0.00	0.00	0.00
Petroleum Refining	0.44	0.02	0.01	0.00	0.05	0.00	0.15	0.00	0.00	0.04	0.01
Petroleum Marketing	0.00	0.00	0.00	0.00	0.00	0.00	0.00	0.00	0.00	0.00	0.00
Other	0.01	0.00	0.00	0.00	0.00	0.00	0.00	0.00	0.00	0.00	0.00
	0.45	0.02	0.01	0.00	0.05	0.00	0.15	0.00	0.00	0.04	0.01
Industrial Processes											
Chemical	0.29	0.00	0.01	0.00	0.03	0.00	0.10	0.00	0.00	0.05	0.01
Food and Agricultural	8.61	0.03	0.17	0.00	0.69	0.01	2.11	0.10	-.09	3.22	0.23
Mineral Processes	0.31	0.01	0.01	0.00	0.02	0.00	0.07	0.00	0.00	0.05	0.01
Metal Processes	1.85	0.07	0.08	0.00	0.26	0.00	0.61	0.01	-.01	0.10	0.03
Wood and Paper	0.51	0.00	0.01	0.00	0.04	0.00	0.10	0.00	0.00	0.11	0.01
Other	0.06	0.00	0.00	0.00	0.00	0.00	0.01	0.00	0.00	0.01	0.00
	11.62	0.12	0.27	0.00	1.05	0.01	3.00	0.11	-.10	3.53	0.29

Table 5.2 (continued): Source Contributions to Ambient PM2.5 Concentrations at Claremont, CA, at 1200 PST on August 28, 1987

Category Code	PM2.5[a]	$SO_4^=$		NH_4^+		NO_3^-		Cl^-		Org	
	$\mu g\ m^{-3}$	Prim[b]	Sec[c]	Prim[b]	Sec[c]	Prim[b]	Sec[c]	Prim[b]	Sec[c]	Prim[b]	Sec[c]
Miscellaneous Processes											
Pesticide Application	0.00	0.00	0.00	0.00	0.00	0.00	0.00	0.00	0.00	0.00	0.00
Farming Operations	0.08	0.00	0.00	0.00	0.00	0.00	0.01	0.00	0.00	0.01	0.00
Construct. and Demolition	3.16	0.01	0.02	0.00	0.07	0.00	0.22	0.00	0.00	0.07	0.03
Road Dust - Paved	6.71	0.06	0.07	0.00	0.32	0.01	0.91	0.01	-.01	0.81	0.08
Road Dust - Unpaved	1.31	0.00	0.01	0.00	0.04	0.00	0.11	0.00	0.00	0.03	0.01
Unplanned Fires	0.30	0.00	0.01	0.00	0.03	0.00	0.09	0.00	0.00	0.05	0.01
Fugitive Windblown Dust	0.10	0.00	0.00	0.00	0.00	0.00	0.01	0.00	0.00	0.00	0.00
Waste Disposal	0.00	0.00	0.00	0.00	0.00	0.00	0.00	0.00	0.00	0.00	0.00
Other	0.09	0.00	0.00	0.00	0.01	0.00	0.02	0.00	0.00	0.02	0.00
	11.75	0.07	0.11	0.00	0.47	0.02	1.36	0.01	-.01	0.98	0.13
On-Road Vehicles											
Light-Duty Passenger	3.76	0.03	0.09	0.00	0.33	0.02	1.00	0.02	-.02	1.07	0.15
Light- and Med-Duty Trucks	1.35	0.01	0.03	0.00	0.12	0.01	0.37	0.01	-.01	0.40	0.05
Heavy-Duty Gas Trucks	0.69	0.00	0.01	0.00	0.05	0.00	0.14	0.00	0.00	0.33	0.02
Heavy-Duty Diesel Trucks	3.67	0.01	0.08	0.00	0.27	0.01	0.82	0.01	-.01	0.78	0.17
Motorcycles	0.04	0.00	0.00	0.00	0.00	0.00	0.01	0.00	0.00	0.02	0.00
Heavy-Duty Diesel Urban Bus	0.69	0.00	0.02	0.00	0.05	0.00	0.16	0.00	0.00	0.15	0.03
	10.20	0.05	0.23	0.00	0.83	0.03	2.49	0.04	-.03	2.75	0.43
Other Mobile											
Off-Road Vehicles	0.03	0.00	0.00	0.00	0.00	0.00	0.00	0.00	0.00	0.01	0.00
Commericial Boats	0.00	0.00	0.00	0.00	0.00	0.00	0.00	0.00	0.00	0.00	0.00
Trains	0.28	0.00	0.01	0.00	0.02	0.00	0.05	0.00	0.00	0.06	0.01
Ships	0.05	0.00	0.00	0.00	0.01	0.00	0.02	0.00	0.00	0.01	0.00
Aircraft - Government	0.00	0.00	0.00	0.00	0.00	0.00	0.00	0.00	0.00	0.00	0.00
Aircraft - Other	0.23	0.01	0.01	0.00	0.04	0.00	0.11	0.00	0.00	0.01	0.01
Mobile Equipment	1.45	0.00	0.03	0.00	0.10	0.00	0.31	0.00	0.00	0.34	0.06
Utility Equipment	0.04	0.00	0.00	0.00	0.00	0.00	0.01	0.00	0.00	0.02	0.00
	2.09	0.02	0.05	0.00	0.17	0.00	0.50	0.00	0.00	0.44	0.09
Non-NaCl Background	22.84	2.61	0.75	1.09	3.22	0.51	10.09	0.00	0.00	1.43	0.72
Sea Salt Background	4.18	0.00	0.06	0.00	0.28	0.00	2.99	1.20	-1.20	0.00	0.01
CATEGORY TOTALS:	70.83	3.57	1.64	1.11	7.00	0.62	22.78	1.42	-1.36	10.09	1.79

[a] Concentration increment includes both primary particle core plus net accumulation of secondary aerosol due to atmospheric chemical reactions. Source contributions without secondary reaction products can be computed by subtracting secondary components listed in columns 3, 5, 7, 9, and 11. [b] Concentration increment due to primary particle emissions or pre-existing aerosol ($\mu g\ m^{-3}$). [c] Net concentration increment due to atmospheric chemical reaction within trajectories crossing the air basin ($\mu g\ m^{-3}$).

In addition to particles with core material released from the anthropogenic sources listed above, background particles advected into the study region also make a significant contribution to ambient PM2.5 mass at Claremont, CA, on August 28, 1987, at 1200 PST. Model calculations predict that 22.84 μg m^{-3} of the ambient PM2.5 mass is attributable to sulfur-containing non-sea salt background particles which are advected into the study region from upwind over the ocean and which then pick up large quantities of ammonium nitrate through secondary processing during transit across the air basin.

Figure 5.7 shows the ambient particle size and composition distribution predicted for Claremont, CA, at 1200 PST on August 28, 1987, broken down according to the major source categories used to produce Table 5.2. The upper panel of Figure 5.7 shows the size and composition distribution of all aerosol material associated with particles having core material released from each source category. Model results predict that the majority of particles with diameter greater than 2.5 μm are originally released from sources included within the miscellaneous processes category of Table 5.2. Ambient concentrations within this category are dominated by particles originating from construction and demolition activities, as well as paved and unpaved road dust. Particles released from on-road vehicle exhaust and industrial processes chiefly contribute to the ambient size distribution between 0.1-1.0 μm particle diameter. Fuel burning activities are seen to dominate the ambient concentrations of ultra-fine particles (Dp $<$ 0.1 μm). Primary particle sources within the solvent use and petroleum processing categories do not contribute significantly to atmospheric particulate concentrations at Claremont, CA, on August 28, 1987, at 1200 PST. Background sulfate particles (identified in Figure 5.7 as the non-NaCl initial conditions to the model) which are advected into the study region and which are then transformed

by heterogeneous atmospheric reactions make a large contribution to the ambient particle size distribution between 0.2-1.0 μm particle diameter at 1200 PST on August 28, 1987, at Claremont, CA.

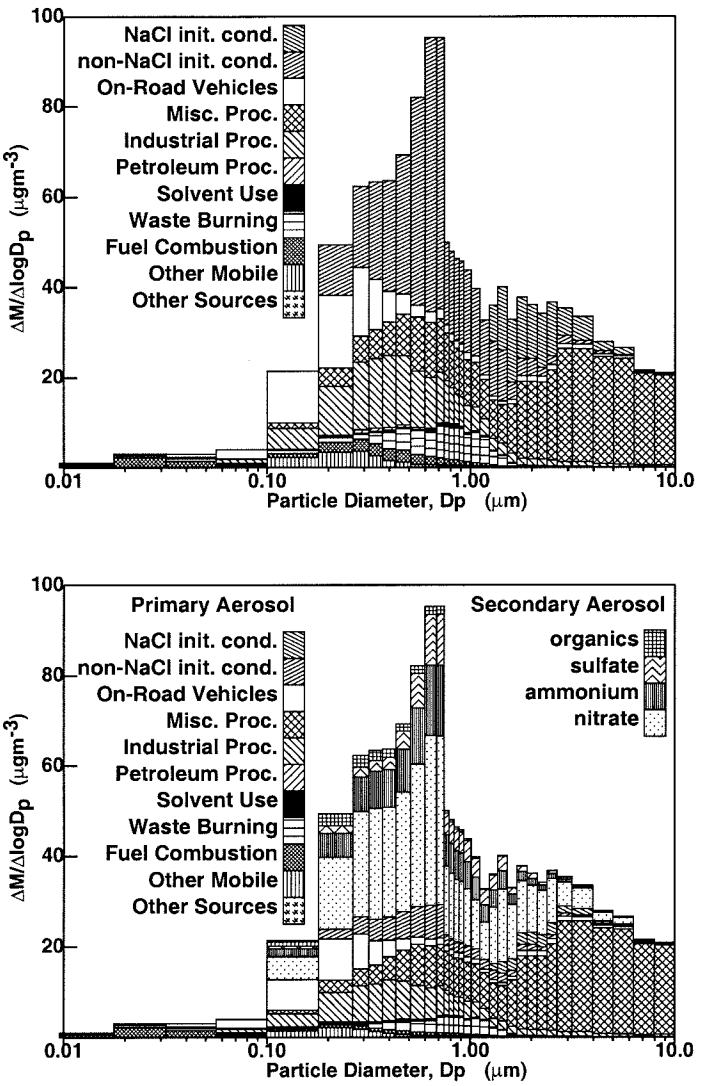

Figure 5.7:
Reorganization of specific source contributions to the ambient size and composition distribution into regulated emissions control categories for Claremont, CA, at 1200 PST on August 28, 1987. The upper panel displays the size and composition distribution of primary particles plus gas-to-particle conversion products which have accumulated on those particles associated with each of the major source categories shown in Table 2. The lower panel displays the size and composition distribution of primary particulate material associated with each source category plotted separately from the concentrations of secondary organics, sulfate, ammonium ion, and nitrate that have accumulated on the particles during transit across the air basin.

The lower panel of Figure 5.7 shows the size and composition distribution of the primary particulate material released from sources included within the major categories used in Table 5.2, with the secondary sulfate, nitrate, ammonium, and organic aerosol coatings removed from those particles and then plotted separately. A significant amount of the aerosol associated with particles originating from all source categories except miscellaneous processes is seen to be composed of species formed by secondary atmospheric chemical reactions. As discussed previously, particles within the miscellaneous processes category are chiefly associated with paved road dust, unpaved road dust, and construction / demolition dust. Since these particles are large and hydrophobic, little secondary nitrate formation occurs on these particles.

5.7 Conclusions

The output from Lagrangian trajectory-based aerosol processes models that represent particles as a source-oriented external mixture can be post-processed at little additional computational expense to greatly expand the separate identification of specific source contributions to the ambient particle size and composition distribution at a downwind receptor site. The resolution of the technique is limited only by the resolution of the emissions inventory used as the input to the mechanistic modeling calculations. The technique can be used to distinguish between ambient particles emitted from different sources having the same general size and composition profile (e.g., on-road diesel vehicles vs diesel railroad locomotives), and to distinguish between ambient particles originally released by the same specific source type but at different locations.

Model calculations illustrate that crustal particles in the atmosphere at Claremont, CA, at 1200 PST on August 28, 1987, are chiefly associated

with commercial, residential and industrial construction and demolition activities, as well as road dust from traffic on paved and unpaved city and county roads. Ambient diesel engine exhaust particles are primarily associated with on-road diesel engines, with lesser contributions from off-road heavy-duty diesel equipment (non-farm), mobile diesel-powered refrigeration units, and railroad locomotives involved in hauling operations. Particles released from non-catalyst equipped gasoline engines in the atmosphere at Claremont, CA, on August 28, 1987, at 1200 PST are largely attributable to on-road non-catalyst gasoline-powered vehicles with smaller contributions from lawn and garden equipment. Specific sources which contribute to particles from food cooking at Claremont include commercial charbroiling, deep fat frying, and other commercial cooking operations. Particles with high sulfur content originally released from landfill waste gas flares, aluminum smelting furnaces, petroleum refinery process heaters, and distillate oil combustion all contribute to ambient particulate concentrations associated with industrial processes and combustion of sulfur-bearing fuels. Finally, significant sources affecting Claremont within the "other anthropogenic sources" category tracked by the source oriented external mixture model include wood and paper processing, natural gas-fired turbine engines, cattle feedlot dust, and spray drying of detergent powders.

Bibliography

[1] Michael J. Kleeman, Annmarie Eldering, and Glen R. Cass. Modeling the airborne particle complex as a source-oriented external mixture. *J. Geophys. Res.*, 102(D17):21355–21372, 1997.

[2] Michael J. Kleeman and Glen R. Cass. Source contributions to the size and composition distribution of urban particulate air pollution. *Atmos. Environ.*, 32:2803–2816, 1998.

[3] Michael J. Kleeman and Glen R. Cass. Effect of emission control strategies on the size and composition distribution of urban particulate air pollution. *Environ. Sci. Technol.*, submitted for publication, 1998.

[4] Robert A. Harley, Michael P. Hannigan, and Glen R. Cass. Respeciation of organic gas emissions and the detection of excess unburned gasoline in the atmosphere. *Environ. Sci. Technol.*, 26:2395–2408, 1992.

[5] Robert A. Harley, Armistead G. Russell, and Glen R. Cass. Mathematical modeling of the concentrations of volatile organic compounds: Model performance using a lumped chemical mechanism. *Environ. Sci. Technol.*, 27:1638–1649, 1993.

[6] Robert A. Harley, Armistead G. Russell, Gregory J. McRae, Glen R. Cass, and John H. Seinfeld. Photochemical modeling of the Southern California Air Quality Study. *Environ. Sci. Technol.*, 27:378–388, 1993.

[7] Lynn M. Hildemann, Gregory R. Markowski, and Glen R. Cass. Chemical composition of emissions from urban sources of fine organic aerosol. *Environ. Sci. Technol.*, 25:744–759, 1991.

[8] Lynn M. Hildemann, Gregory R. Markowski, Michael C. Jones, and Glen R. Cass. Submicrometer aerosol mass distributions of emissions from boilers, fireplaces, automobiles, diesel trucks, and meat–cooking operations. *Aerosol Sci. Technol.*, 14:138–152, 1991.

[9] Annmarie Eldering and Glen R. Cass. Source–oriented model for air pollutant effects on visibility. *J. Geophys. Res.*, 101(D14):19343–19369, 1996.

6 Size and Composition Distribution of Fine Particulate Matter Emitted From Motor Vehicles

6.1 Introduction

Particulate matter emissions from motor vehicles are among the major contributors to fine particle concentrations in the urban atmosphere [1, 2]. In order to construct and exercise advanced air quality models that seek to predict the evolution of the size and composition distribution of fine particles in the atmosphere, it is necessary to be able to specify both the size distribution and the chemical composition of the direct particle emissions as they occur at their source. Data on the combined mass emission rate, size distribution and chemical composition distribution of primary particle emissions from motor vehicles are rare and need to be updated periodically as fuels, engines, and vehicle technologies evolve.

In the mid-1980's, Hildemann et al. [3, 4] conducted a series of motor vehicle particulate emissions source tests using a dilution tunnel source sampling system. Consumer-owned catalyst-equipped gasoline-powered vehicles and non-catalyst gasoline-powered vehicles were tested on a chassis dynamometer over the Federal Test Procedure (FTP) urban driving cycle, while heavy-duty diesel vehicles were tested over a specially selected transient driving cycle. Particulate matter emitted during these experiments was

collected using fine particle filters and analyzed to determine mass emissions rate, elemental carbon, organic carbon, water soluble ions including sulfate, nitrate, ammonium and chloride, and trace elements. Particle size distributions were measured with an electrical aerosol analyzer. In order to use these data to represent both the size distribution and the chemical composition of the emitted particles within air quality models that seek to predict ambient particle size and composition, it is necessary to assume that all of the fine particles have a chemical composition equal to that of the bulk fine particle filter sample.

In recent work, the size-resolved emissions of polycyclic aromatic hydrocarbons (PAH) emitted from diesel and gasoline vehicles have been studied based on samples collected within roadway tunnels using cascade impactors [5, 6]. A series of tests on a diesel-powered light-duty passenger vehicle operated under constant speed conditions using a dynamometer facility has been reported by Kerminen et al. [7]. Particle composition was characterized as a function of particle size using samples collected with a cascade impactor and analyzed for elemental carbon, organic carbon, and water soluable ions including sulfate, nitrate, chloride, ammonium, sodium, potassium, magnesium, and calcium. Trace element concentrations could not be determined, however, since the aluminum foil impaction substrates used in these experiments had large blank levels with high variation. No gasoline-powered vehicles or medium / heavy-duty diesel vehicles were considered in the experiments conducted by Kerminen et al.

The purpose of the present chapter is to report the results of a source testing program undertaken in order to better quantify the size and chemical composition of particulate matter emitted from present day light-duty catalyst-equipped gasoline vehicles, non-catalyst gasoline vehicles, and medium-

duty diesel vehicles. The dilution source sampling system of Hildemann et al. [3, 4] is used in these tests, and is augmented by high resolution particle size and chemical composition measurements made with two micro-orifice uniform deposit impactors (MOUDIs), a laser optical particle counter (OPC), and a scanning differential mobility analyzer (DMA) / condensation nucleus counter (CNC) system. All of the vehicles studied were tested on a chassis dynamometer using the Federal Test Procedure (FTP) urban driving cycle. The experimental methods employed during each source test and results that show the size-resolved chemical composition of the fine particulate matter emitted from these vehicles are described below.

6.2 Experimental Methods

Size-resolved particulate matter emissions from catalyst-equipped gasoline-powered vehicles were measured at the California Air Resources Board (CARB) Haagen-Smit laboratory in El Monte, CA. Vehicles were tested on a twin-roll hydraulic dynamometer while being driven through the standard Federal Test Procedure (FTP) urban driving cycle by CARB operations staff. A plot of vehicle speed as a function of time during the FTP cycle is shown in Figure 2a of Hildemann et al. [4]. The cycle consists of a cold start followed by a period of accelerations and decelerations typical of an urban driving pattern. Vehicles are shut off during a hot soak period that lasts for approximately 8 minutes during the middle of the test, and are then restarted while hot so that driving can continue. Sampling during the hot soak period was suspended until driving resumed to minimize the losses that otherwise might be induced by passing clean filtered air over the impactor substrates while the engine was not running.

The catalyst-equipped gasoline-powered vehicle exhaust samples analyzed

in the current study were collected from a 1981 Honda Accord (1.8L, 4 cylinder engine), a 1992 Toyota pick-up truck (3.0L, 6 cylinder engine), and a 1992 Chevrolet Astrovan (5.0L, 8 cylinder engine). Accumulated mileage for each of these vehicles was 106,722 miles, 41,283 miles, and 49,439 miles respectively. The fuel used during the tests was commercially available California reformulated Phase II unleaded gasoline. A complete account of the catalyst-equipped gasoline-powered vehicle source test procedures along with a detailed description of the overall mass emissions rates, organic species emitted as well as the elemental analysis of filter samples collected from this test is provided by Schauer et al. [8].

The size and composition distribution of particles emitted from non-catalyst-equipped gasoline-powered vehicles also was measured. Samples were collected from a 1970 Volkswagon Vancamper (1.6L, 4 cylinder engine) and a 1969 Chevrolet Camaro (5.0L, 8 cylinder engine) fueled by commercially available California Phase II reformulated unleaded gasoline. The Volkswagon van was powered by a rebuilt engine with only 30,000 miles of accumulated driving while the Camaro had its original engine with a total of 371,780 accumulated miles.

Test procedures employed to measure the size and composition distribution of particles emitted from medium-duty diesel trucks were similar to those described for automobiles and light-duty trucks. Because of safety considerations at the dynamometer facility, the trucks had to be driven rather than pushed onto the dynamometer, and thus these vehicles could not be started cold at the beginning of the FTP urban driving cycle. Therefore, each of the vehicles tested was warmed up by being driven for approximately 10 minutes on the dynamometer prior to the beginning of the test. The engine was then stopped and restarted to follow the hot start and hot running portions of the

FTP urban driving cycle. The inertial dynamometer load used in each test was 7500 pounds and an Actual Horse Power value of 17.5 was specified.

Diesel-powered vehicle samples analyzed in the current study were collected from a 1995 Isuzu Van (3.8L, 4 cylinder turbocharged diesel engine, 130Hp) and a 1995 GMC Vandura 3500 Van (6.5L, 8 cylinder diesel engine, 160Hp) powered with commercially available diesel fuel. Total accumulated mileage for the vehicles was 39,993 miles and 30,560 miles, respectively. Again, a more complete description of the diesel-powered vehicle source test procedures along with the overall mass emissions rates and the results of the chemical analysis of the bulk fine particle filter samples collected during this test are presented by Schauer et al. [9].

The dilution source sampling system used in the current study begins with the dilution tunnel described by Hildemann et al. [3, 4, 10]. In the present series of source tests, four separate sampling trains designed to characterize the particulate- and gas-phase emissions from motor vehicles are added to the test apparatus. The first two sampling trains focus on the collection of semi-volatile and fine particle-phase organic compounds using annular denuders, quartz fiber filters, and polyurethane foam (PUF) cartridges. The third sampling train collects fine particulate matter, carbonyls, organic acids, and gas-phase hydrocarbons using quartz fiber filters, Teflon filters, KOH impregnated quartz fiber filters, dintrophenylhydrazine (DNPH) impregnated C_{18} cartridges, and a 6-liter polished stainless steel SUMA canister. A complete description of the design of the first three sampling trains used in the source testing procedure is given by Schauer et al. [11, 9, 12, 8, 13]. The purpose of this chapter is to summarize the measurements made by the fourth sampling train designed to characterize the size-resolved properties of the particulate matter emitted from motor vehicles. Equipment used for this task includes

an optical particle counter, a scanning differential mobility analyzer / condensation nucleus counter combination, and two cascade impactors.

Measurements of aerosol size distributions are made from the residence time chamber of the dilution source sampler using a Particle Measuring Systems ASASP-100X laser optical particle counter (OPC) and a Thermal Systems Incorporated 3071 differential mobility analyzer (DMA) coupled with a Thermal Systems Incorporated 3760 condensation nucleus counter (CNC). The OPC is operated over the nominal size range of 0.09-3.0 μm particle diameter while the differential mobility analyzer was used over a size range between 0.020-0.25 μm particle diameter. The DMA is operated in continuous scan mode throughout each test so that a complete sweep of the indicated size range is completed every 60 sec.

Samples for measurement of the size distribution of chemical species in the vehicle exhaust particles smaller than 1.8 μm particle diameter are collected using a pair of micro orifice uniform deposit impactors (MOUDIs; MSP Corporation). Before each source test, the MOUDIs are disassembled and cleaned by rinsing vigorously in baths of deionized water, methanol and hexane. A small amount of silicone-based lubricant then is applied to the appropriate O-rings in order to properly assemble and operate the instruments. Two impactors are used during each test to facilitate the full range of desired chemical analyses. The first impactor is dedicated to the measurement of inorganic species and trace elements using collection on Teflon substrates. The second impactor is dedicated to the analysis of carbon-containing species using collection on aluminum substrates prepared by baking at 550°C for 48 hours to reduce the carbon blank levels. Each substrate is weighed several times before and after a sample is collected using a Mettler micro balance (Model M-55-A) in a temperature and humidity controlled room (20-24°C,

35-40% RH). The samples collected on foil substrates are analyzed for elemental and organic carbon using the thermal-optical carbon analysis method of Huntzicker et al. [14] as modified by Birch and Cary [15]. Pyrolysis effects are accounted for using the methodology described in [16]. Samples collected on Teflon substrates are divided in half after weighing. One half of each sample undergoes analysis for sulfate, nitrate and chloride using ion chromatography (Model 2020i, Dionex Corp.), and for ammonium ion using a modified indophenol colorimetric method [17] with a rapid-flow analyzer (Model RFA-300, Alpkem Corp.). The second half of each sample collected on Teflon substrates is subjected to neutron activation analysis for trace elements [18].

An AIHL-design cyclone separator [19] is operated upstream of each MOUDI impactor in order to remove particles larger than approximately 1.8 μm from the gas stream to reduce the occurrence of particle bounce. Impactor substrates are not coated with grease in order to avoid organic carbon contamination of the samples; the fine combustion particles entering the instrument are oily and likely to stick to an impaction surface. Only the lower six stages and the after filter of each MOUDI sampler that collected fine particles smaller than 1.8 μm aerodynamic diameter are analyzed for chemical species content since particles which would have accumulated on the upper stages are removed by the cyclone separator.

6.3 Comparison to Filter-Based Measurements

Measurements of particle-phase chemical species concentrations made using the MOUDI impactors can be summed across all stages to calculate bulk fine particle concentrations for each source test. These values may then be compared to fine particle filter-based measurements taken at the same time

in order to evaluate the performance of the impactors and related analysis methods. Figure 6.1 shows a comparison of data taken using MOUDI impactors and filter-based samplers for potassium, sulfate, nitrate, chloride, ammonium, total carbon, organic carbon, and elemental carbon. The data shown in Figure 6.1 involve source tests of the emissions from meat charbroiling, wood combustion and cigarette smoke in addition to the vehicle tests discussed here in order to provide a wider range of pollutant species concentrations [16]. Filter-based measurements of particles smaller than 2 μm particle diameter are collected from the dilution source sampler using one 47 mm diameter quartz fiber filter (Pallflex Tissuequartz 2500 QAO) and two Teflon membrane (Gelman Teflo, 2 μm pore size) filters operating in parallel downstream of a fine particle cyclone separator at a flow rate of 10 L min^{-1} per filter as described by Schauer et al. [11, 9, 12, 8, 13].

Regression analysis applied to the data shown in Figure 6.1 reveals that impactor-based measurements are nearly equal to the results obtained from filter samples for non-volatile potassium even though impactor samples were quantified by neutron activation analysis while filter samples were analyzed by X-ray fluorescence. No gas-phase sorption artifact is expected for this species since potassium exists exclusively in the particle phase. A comparison of sulfate, chloride and ammonium measured with the impactors to filter-based measurements shows that the impactor measurements are typically about 20% lower than the filter-based values. At least part of this small discrepancy could be due to the fact that the particle size range sampled by the impactor (0-1.8 μm particle diameter) is smaller than the size range covered by the filter samples (0-2 μm particle diameter). Particulate nitrate concentrations measured by the impactor were 39% lower than analogous filter-based measurements. The larger discrepancy between impactor-based

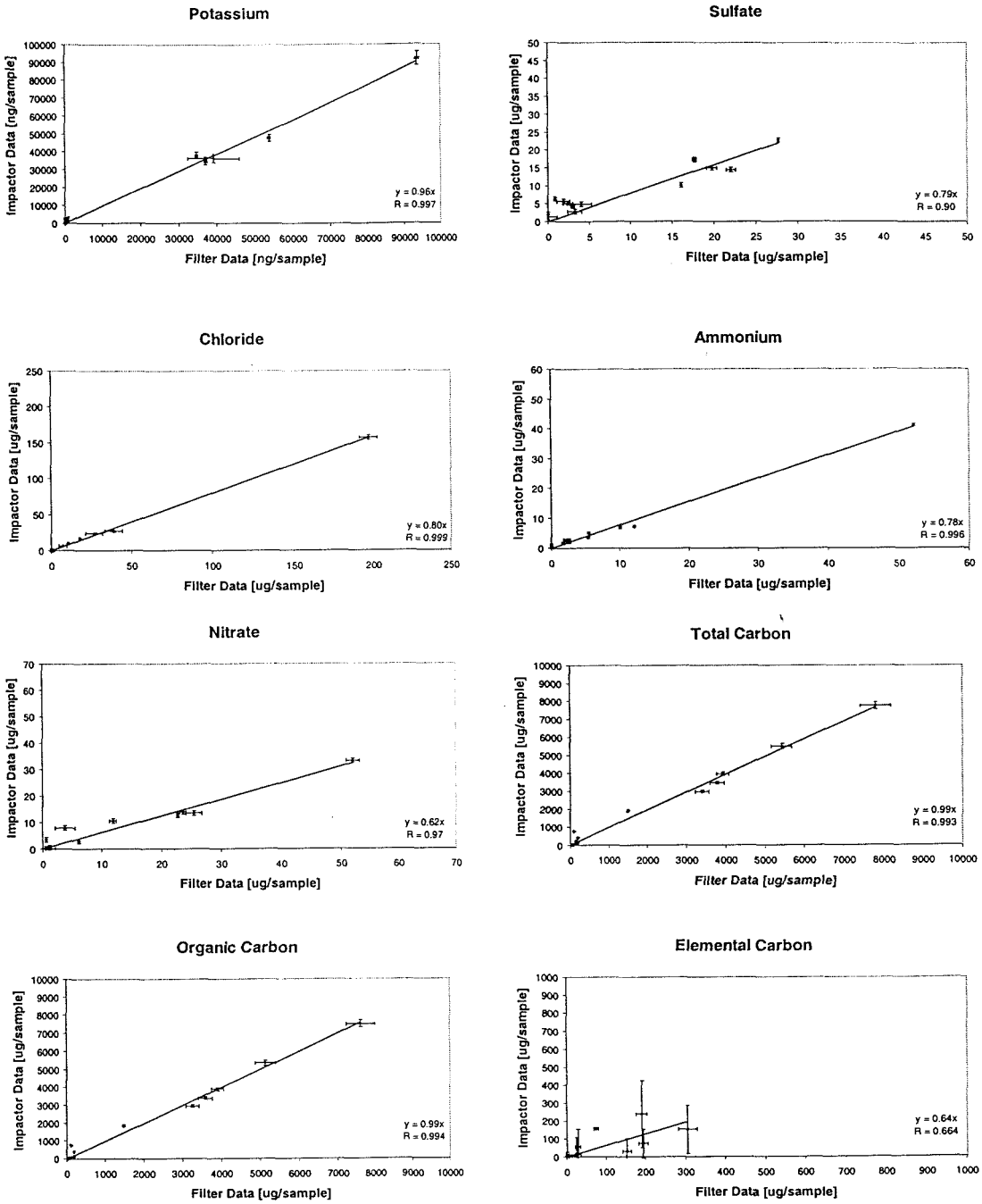

Figure 6.1:
Summation of collections on impactor substrates compared to filter-based measurements of potassium, sulfate, chloride, ammonium ion, nitrate, total carbon, organic carbon, and elemental carbon taken during source tests of motor vehicle exhaust as well as meat charbroiling, wood combustion, and cigarette smoke. For a complete description of on-vehicular source tests see [11, 12, 13].

and filter-based measurements for this species is likely due to additional evaporation of nitrate from the Teflon impaction media.

The amounts of total carbon and organic carbon measured by the impactor are almost exactly equal to that measured by the filter-based sampler. Since the MOUDI impactor also uses a quartz fiber after filter downstream of the last impaction stage, it is expected that the absorption artifact included within the sum of the impaction stages plus after filter will be comparable to that for the filter-based samples. A comparison of elemental carbon concentrations measured on foil impaction substrates to those measured on quartz fiber filters reveals that elemental carbon concentrations measured from the impactor samples are approximately 64% of those measured from the filters. The elemental carbon content of most of the source samples collected in the current study amounted to only 1-2% of the total particle carbon collected. Therefore, a small error in the pyrolysis correction applied when measuring the amount of organic carbon in a sample could lead to large relative changes in the apparent amount of elemental carbon in the sample, while in an absolute sense the analytical error would be quite small.

6.4 Results and Discussion

The size and composition distributions of particles emitted from each of the motor vehicle types tested in the current study are shown in Figures 6.2, 6.3 and 6.4. The results shown are averaged over the several vehicles of each type that were tested within each motor vehicle category. The upper panel of each figure displays the results of the particle size distribution measurements made with the OPC (0.09-3 μm particle diameter) and DMA / CNC combination (0.02-0.25 μm particle diameter) while the lower panel displays the particle chemical composition measurements made using the cascade impactors. Or-

ganic compound concentrations shown in Figures 6.2, 6.3 and 6.4 are derived from organic carbon measurements multiplied by a factor of 1.2 based on the quantification of individual organic compounds measured in primary vehicle exhaust as described by Schauer et al. [9, 8]. Particle size distribution results shown in Figures 6.2, 6.3 and 6.4 have been normalized to display the volume distribution of 1 μcm^3 of emitted aerosol and the mass distribution of 1 μg of emitted fine particles. Absolute fine particle mass emissions rates during these tests have already been reported by Schauer et al. [9, 8]. Impactor results have been converted from measured particle aerodynamic diameter to the particle physical diameter values shown in Figures 6.2, 6.3 and 6.4 based on an approximate particle density of 1.5 g cm^{-3} as would be appropriate for atmospheric particles composed mainly of organic compounds with small amounts of elemental carbon [20].

In addition to organic compounds and elemental carbon, trace concentrations of ionic and metallic species also were quantified in particles emitted from the sources considered in the current analysis. These species are not visible in Figures 6.2, 6.3 and 6.4 because of their relatively small concentrations, yet they are still important. Ionic species influence the initial hygroscopic nature of the particles released to the atmosphere. Metallic species present in fine particles can catalyze heterogeneous chemical reactions within fog droplets [21, 22] and may cause adverse health effects [23]. Separate plots of the size distribution of trace species measured in each of the source tests are shown in Figures 6.5, 6.6 and 6.7. Error bars representing one standard deviation of each measured value also are included in each species plot. When constructing the mass balance diagrams in the lower frames of Figures 6.2, 6.3 and 6.4, trace metallic species shown in Figures 6.5, 6.6 and 6.7 were converted to their common oxides using the conversion factors shown

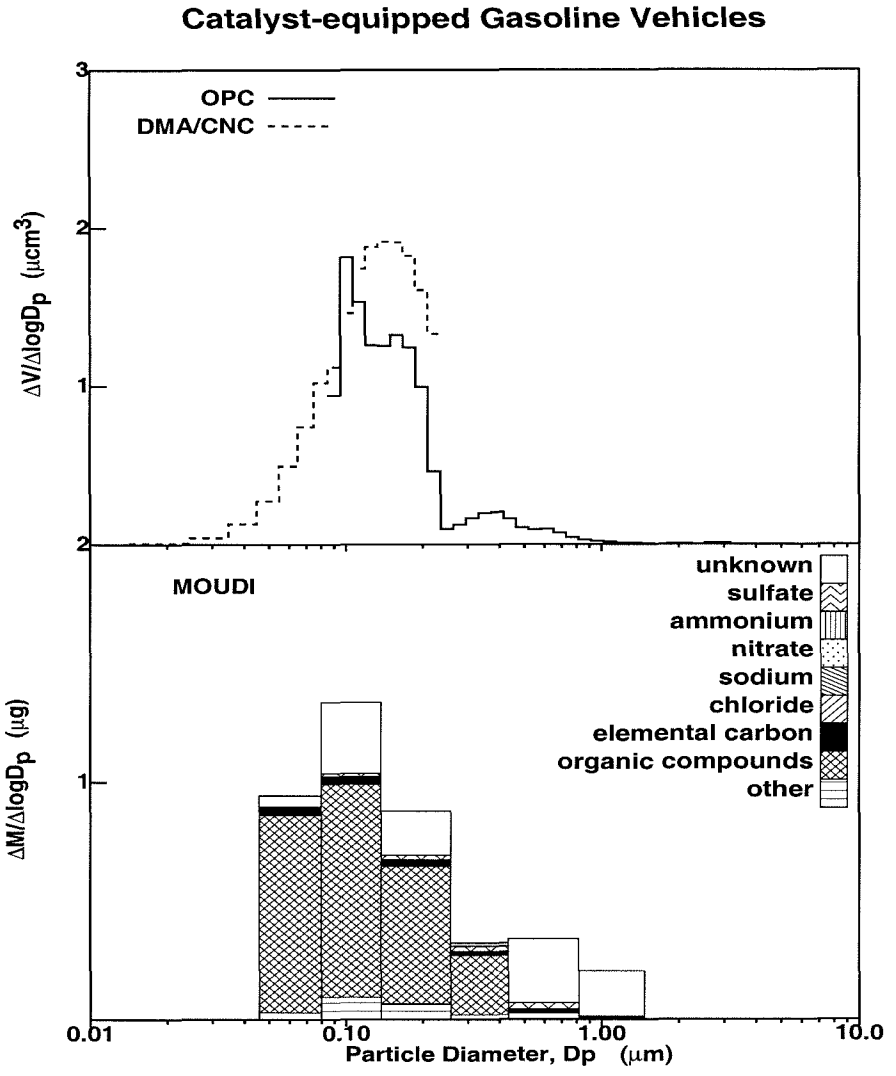

Figure 6.2:
Size and chemical species distribution of fine particles (dp < 1.8 μm) emitted from catalyst-equipped gasoline-powered vehicles. The upper panel shows the size distribution of 1 μcm^3 of fine particulate matter emitted from catalyst-equipped gasoline-powered vehicles as measured by an OPC and DMA / CNC combination. The lower panel shows the size and composition distribution of 1 μg of fine particulate matter emitted from this source as measured by MOUDI impactors.

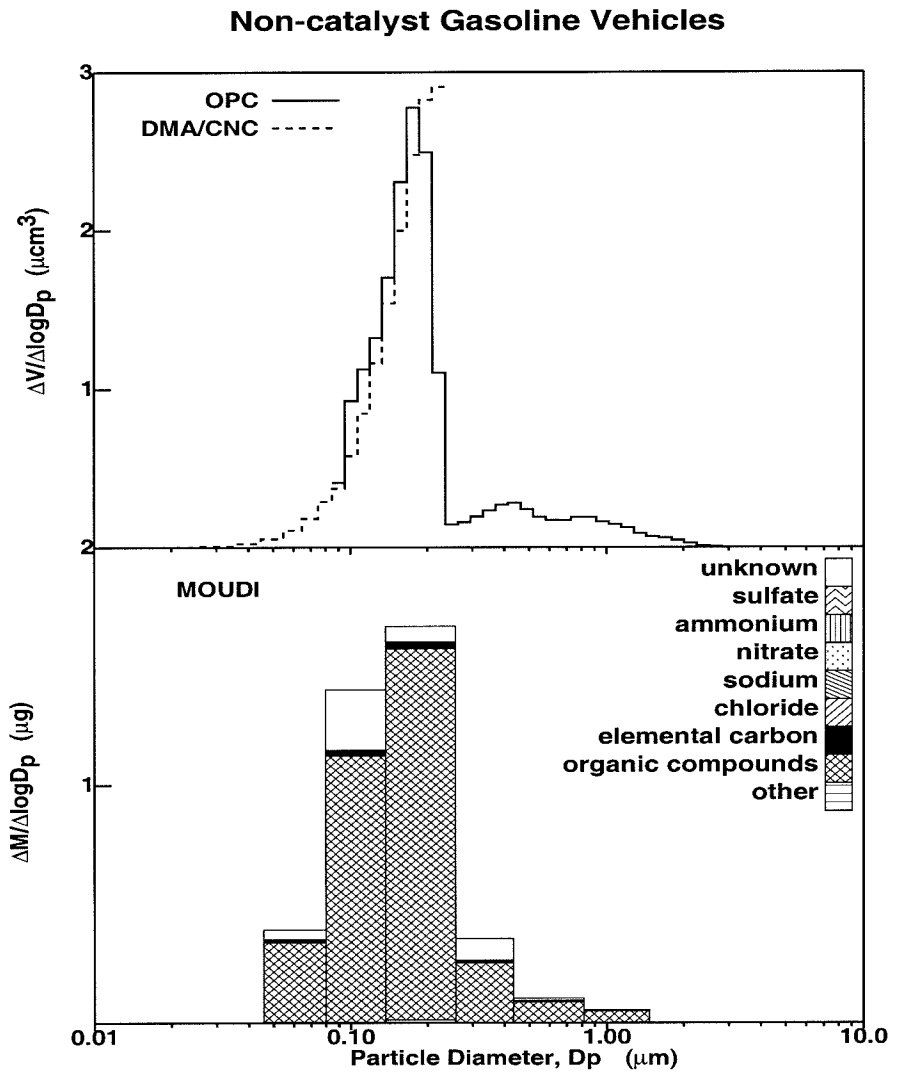

Figure 6.3:
Size and chemical species distribution of fine particles (dp < 1.8 μm) emitted from non-catalyst-equipped gasoline-powered vehicles. The upper panel shows the size distribution of 1 μcm^3 of fine particulate matter emitted from catalyst-equipped gasoline-powered vehicles as measured by an OPC and DMA / CNC combination. The lower panel shows the size and composition distribution of 1 μg of fine particulate matter emitted from this source as measured by MOUDI impactors.

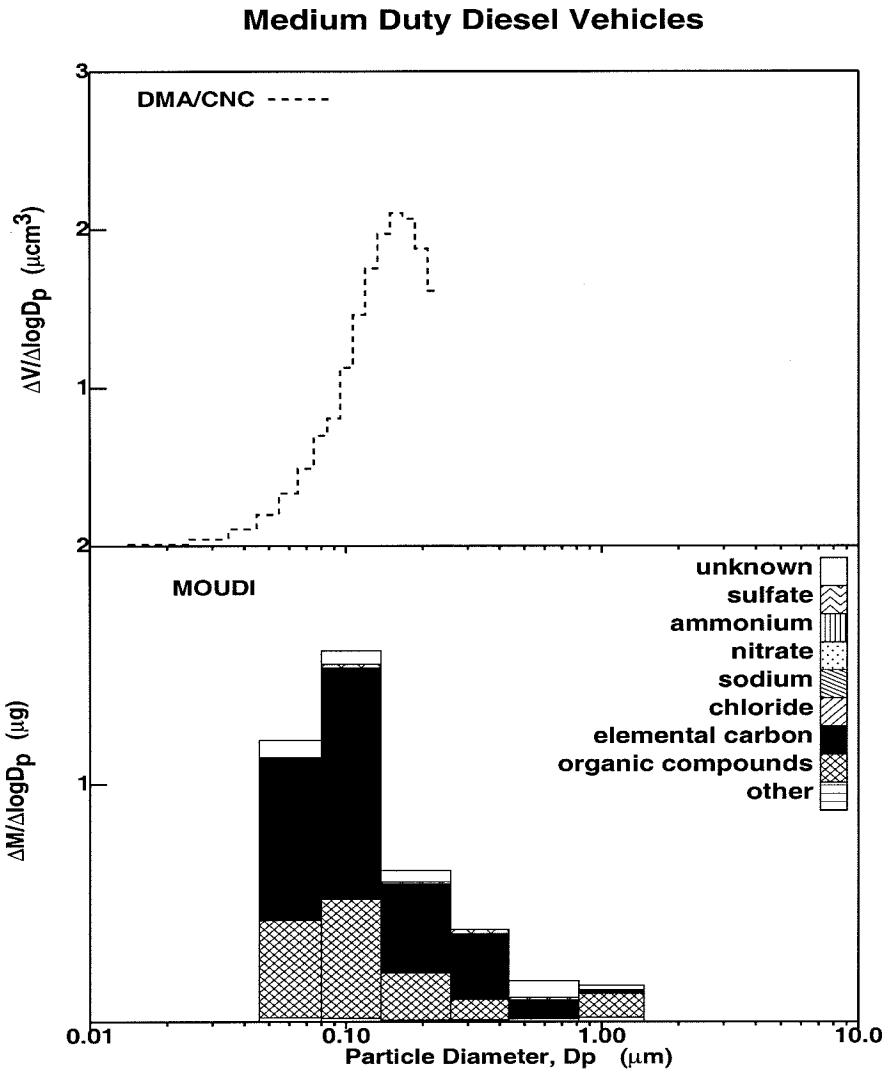

Figure 6.4:
Size and chemical species distribution of fine particles (dp < 1.8 μm) emitted from medium-duty diesel vehicles. The upper panel shows the size distribution of 1 μcm^3 of particulate matter emitted from medium-duty diesel vehicles as measured by a DMA / CNC combination. The lower panel shows the size and composition distribution of 1 μg of fine particulate matter emitted from this source as measured by MOUDI impactors.

Table 6.1: Factors Used to Convert Trace Elements Mass to the Mass of their Common Oxides

Trace Metal	Common Oxide	Conversion Factor
Al	Al_2O_3	1.90
Fe	Fe_2O_3	1.43
Ba	BaO	1.12
Cd	CdO	1.14
Cr	CrO_3	1.92
K	K_2O	1.20
Mn	Mn_2O_7	2.02
Sb	Sb_2O_5	1.33
Ti	TiO_2	1.67
V	V_2O_5	1.78
Zn	ZnO	1.24

in Table 6.1.

Gravimetric and chemical analysis of impactor substrates showed a significant amount of organic material on the impactor afterfilter for all of the mobile sources tested; however, particle size distributions measured with the DMA / CNC combination did not support this finding. It has been concluded that the material observed on the after filters was largely due to an adsorption or absorption artifact and so the afterfilter data have been discarded for the mobile sources considered in the present analysis. Test procedures and results specific to each mobile source category are described in the sections below.

6.4.1 Catalyst-Equipped Gasoline-Powered Vehicles

The size and composition of the fine particulate matter emitted, averaged over all of catalyst-equipped gasoline-powered vehicles tested, is shown in Figure 6.2. The particle mass distribution peaks at approximately 0.1-0.2 μm

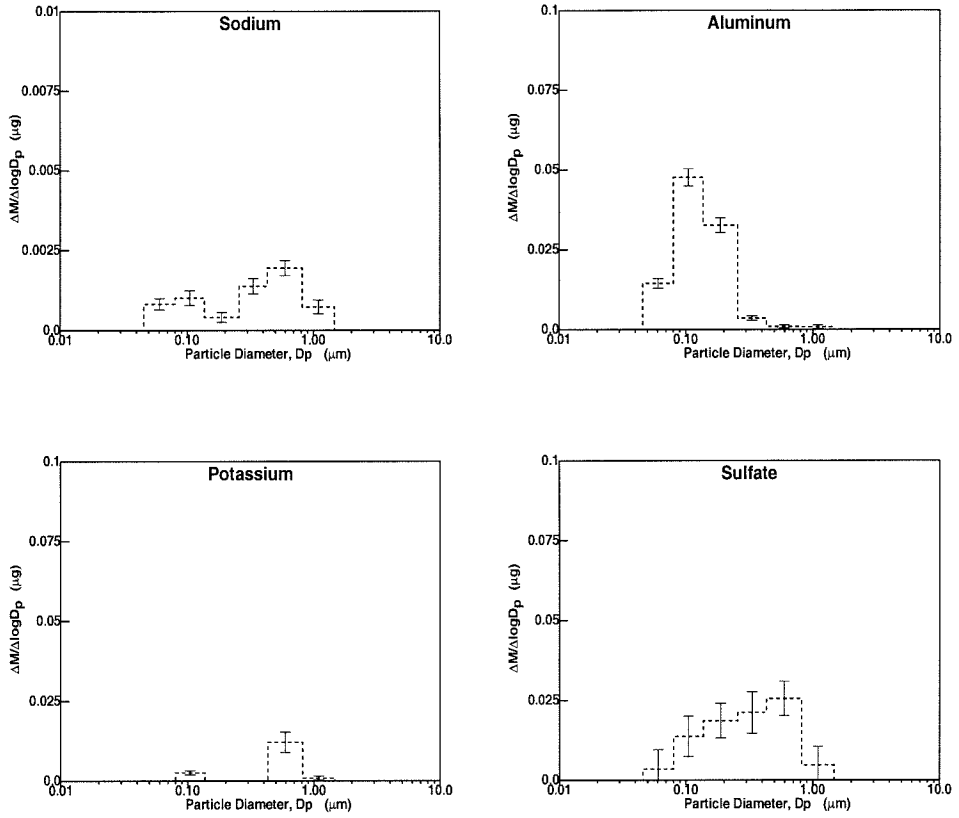

Figure 6.5:
Size distribution of trace species emitted in fine particles (dp $<$ 1.8 μm) from catalyst-equipped gasoline-powered vehicles. Error bars represent one standard deviation.

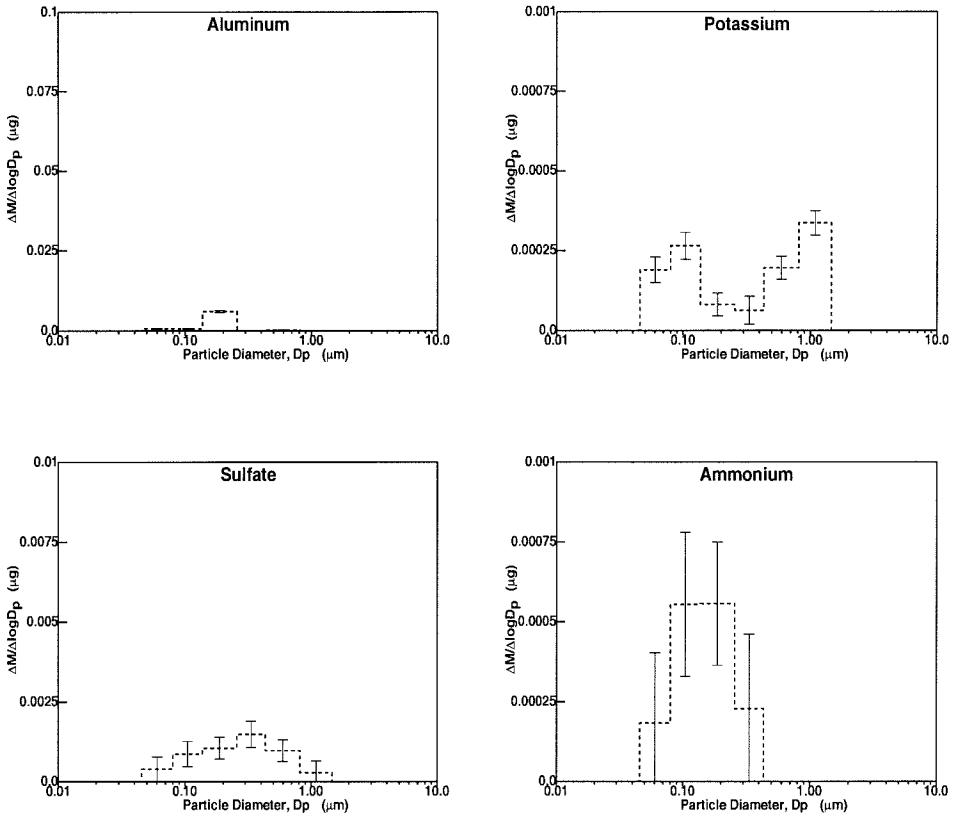

Figure 6.6:
Size distribution of trace species emitted in fine particles (dp $<$ 1.8 μm) from non-catalyst-equipped gasoline-powered vehicles. Error bars represent one standard deviation.

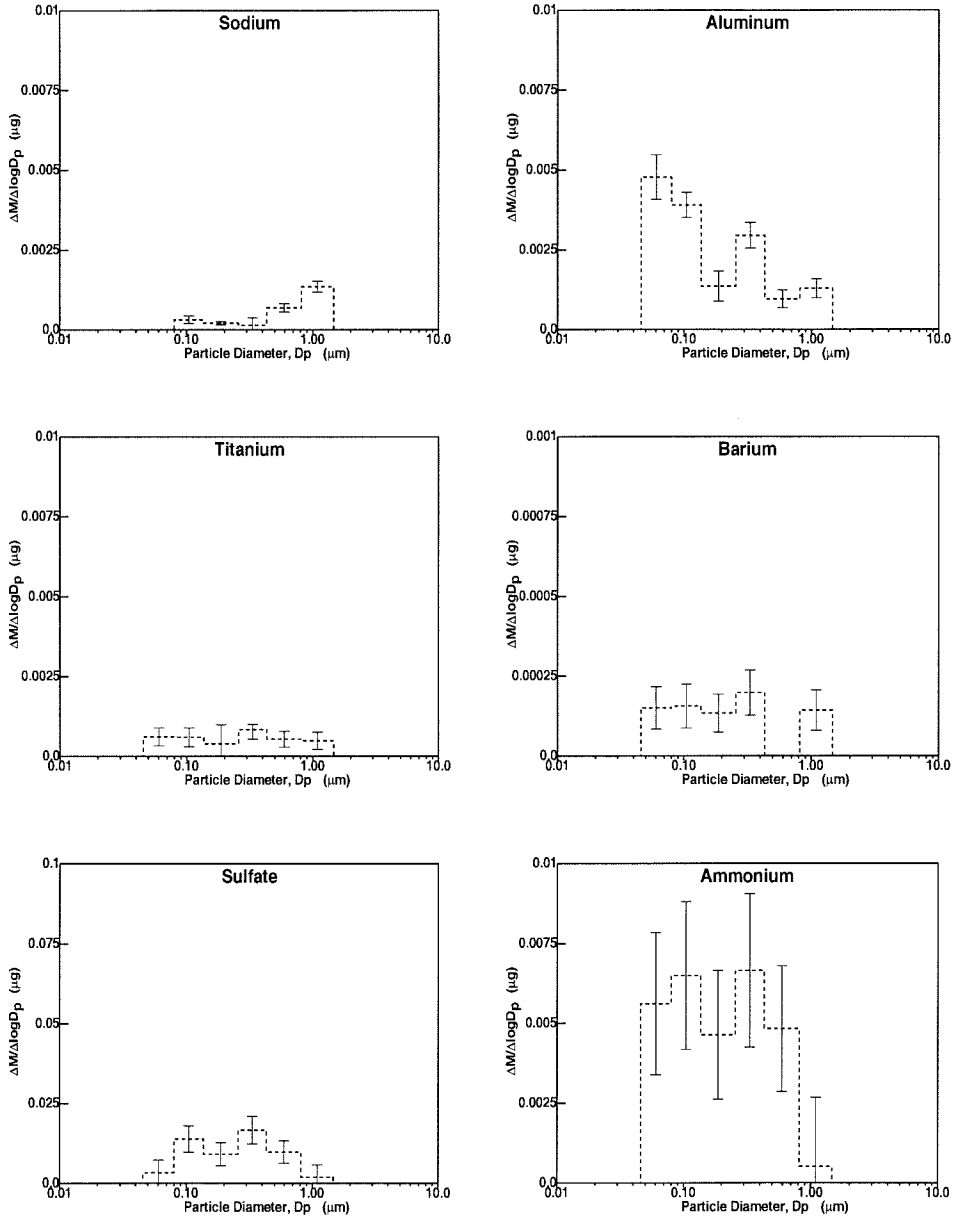

Figure 6.7:
Size distribution of trace species emitted in fine particles (dp < 1.8 μm) from medium-duty diesel vehicles. Error bars represent one standard deviation.

particle diameter and is mainly composed of organic compounds accompanied by small amounts of elemental carbon, sulfates and trace elements (shown as "other" chemical species in Figure 6.2).

The size distributions of trace species measured in particles emitted from catalyst-equipped gasoline-powered vehicles are shown in Figure 6.5. Significant quantities of aluminum were detected peaking at 0.1 μm particle diameter. Potassium also was observed although in extremely small concentrations. Trace levels of sodium were measured that showed a bimodal size distribution peaking at 0.1-0.2 μm particle diameter and at 0.7-0.8 μm particle diameter. Little if any nitrate, chloride or ammonium ion was detected in particles emitted directly from catalyst-equipped gasoline-powered vehicles. Sulfate was found in trace quantities in particles emitted from this source peaking at approximately 0.7μm particle diameter. The sulfur content of the gasoline used to fuel the catalyst-equipped vehicles tested was analyzed to be 71.6 ppm. This is slightly greater than the target of 50 ppm specified in the California Phase II standard for reformulated gasoline.

6.4.2 Non-Catalyst-Equipped Gasoline-Powered Vehicles

The size and composition distribution of fine particles (dp $<$ 1.8 μm) collected from the non-catalyst-equipped gasoline powered vehicles is shown in Figure 6.3. The peak in the mass distribution occurs between 0.1-0.2 μm particle diameter as shown by the DMA / CNC, OPC and MOUDI measurements. Particle composition analysis reveals that fine particles of all sizes emitted from non-catalyst-equipped gasoline vehicles are chiefly composed of organic compounds.

The size distribution of trace species measured in fine particles emitted from the non-catalyst-equipped gasoline-powered vehicles is shown in Fig-

ure 6.6. Trace composition analysis shows measurable quantities of aluminum peaking at approximately 0.2 μm particle diameter. Sulfate and ammonium ion were measured in fine particles originating from this source with a size distribution peaking at approximately 0.3-0.4 μm particle diameter. Potassium was also detected with a bimodal size distribution peaking at 0.1 μm particle diameter and 1.0 μm particle diameter. Concentrations of nitrate and chloride in primary fine particles emitted from non-catalyst-equipped gasoline-powered vehicles were not statistically different from zero.

The size distribution of fine particles emitted from non-catalyst gasoline-powered vehicles shown in Figure 6.3 differs from the results shown in Figure 8 of Hildemann et al. [3]. In the previous measurements by Hildemann et al., the submicron aerosol mass distribution from non-catalyst gasoline-powered vehicles was found to be much broader, with significant mass still apparent at the upper end of the particle diameter range considered (1 μm). Chemical composition analysis of these same particles summarized in Figure 4c of Hildemann et al. [4] indicates that particles emitted from non-catalyst gasoline-powered vehicles measured during that previous work had significant lead content, which is not surprising given that low-lead rather than unleaded fuel was in general use in the mid-1980's when Hildemann et al.'s source tests were conducted. One possible explanation for the differences seen in the particle size distributions between the earlier work and the present experiments is that lead deposits which had accumulated in the exhaust systems of the non-catalyst gasoline-powered vehicles tested by Hildemann et al. would occasionally flake off, producing particles with relatively large diameters. In the current study, the non-catalyst gasoline-powered vehicles which were tested had almost ten additional years of driving time to deplete the accumulated lead from their exhaust systems relative to the vehicles tested

by Hildemann et al. [4, 3] in the mid-1980's. Chemical analysis of bulk fine particle filter samples collected from the exhaust of the non-catalyst gasoline-powered vehicles tested in the current study revealed that only 0.03% of the fine particle mass was composed of lead while Hildemann et al. found that 8.7% of the fine particle mass collected from the exhaust of non-catalyst gasoline-powered cars in the mid-1980's was composed of lead [4].

6.4.3 Diesel Powered Vehicles

The size and composition distribution of particles collected from medium-duty diesel-powered vehicles is shown in Figure 6.4. Particle size distribution measurements made by the electronic instruments are reported only from the DMA / CNC combination because the optical particle counter is not calibrated to measure light absorbing soot particles accurately. The particle mass distribution for this source peaks at approximately 0.1 μm particle diameter and consists of almost equal amounts of elemental carbon and organic compounds.

The size distributions of trace species emitted in fine particles from diesel-powered vehicles are shown in Figure 6.7. Trace composition analysis of samples collected on Teflon substrates indicates noticeable concentrations of aluminum present in particles emitted from this source peaking at or below approximately 0.1 μm particle diameter with a second peak located between 0.3-0.4 μm particle diameter. Other trace elements detected include titanium, chromium and barium, with the size distributions as shown in Figure 6.7. Trace ionic species whose mass emissions rates are statistically different from zero include sodium, ammonium and sulfate. Each of these species displays a bimodal size distribution with the first mode found at approximately 0.1 μm particle diameter and the second mode between 0.3-

1.0 μm particle diameter. The sulfur content of the fuel used during the diesel vehicle source tests was measured to be 33 ppm. No direct emissions of particle-phase nitrate were detected from diesel-powered vehicles.

The two medium-duty diesel vehicles tested in the current study had significantly different engine designs and were built to comply with different pollutant emissions standards. The Izuzu engine tested was rated not to exceed 0.11 g $BHP^{-1}hr^{-1}$ of emitted particulate matter while the GMC engine was rated not to exceed 0.2 g $BHP^{-1}hr^{-1}$ of emitted particulate matter. Recent studies have suggested that the mass emissions of suspended particulate matter may not be the only factor that should be considered when judging the possible health consequences of the particulate emissions from alternative diesel engine designs. Particles trapped in the human lung are cleared by alveolar macrophages; Oberdorster et al. [24] have proposed that the absolute number of inhaled ultra-fine particles (Dp $<$ 0.1 μm) is also an important factor, because it is plausible that high numbers of ultra fine particles trapped in the lung can overwhelm lung clearance mechanisms and that such very small particles may penetrate into the surface tissues of the lung more easily than somewhat larger particles. Electronic size distribution measurements collected by the DMA / CNC and OPC indicate that the number distribution of particles emitted from the Izuzu engine peaked at approximately 30 nm particle diameter while the number distribution of particles emitted from the GMC engine peaked at approximately 50 nm particle diameter. The absolute number of particles emitted from the Izuzu engine over the FTP cycle was roughly four times higher than the number of particles emitted from the GMC engine even though the Izuzu engine was smaller and was built to comply with a lower mass emissions standard than the GMC engine. This result is generally consistent with the findings of

Bagley et al. [25] who noted that the total number of particles in emissions from a more advanced 1991-model Cummins diesel engine was 15 to 35 times greater than the number of particles from a 1988 Cummins diesel engine with less advanced control technology under identical load conditions even though the 1991 engine delivered lower overall particle mass emissions.

6.4.4 Effect of Engine Temperature on Particulate Matter Emitted From Mobile Sources

The FTP urban driving cycle described in Section 6.4.1 can be subdivided into three basic sections. The first 505 sec of the test measures vehicle emissions just after the engine has been started cold. The next 890 sec characterizes vehicle emissions under hot running conditions, followed by 240 sec during which the engine is shut off. The final 505 sec of the test repeats the driving pattern followed during the first 505 sec, but since the engine is now hot, this portion of the FTP urban driving cycle characterizes emissions under hot-start conditions. This methodology is followed because the emission rate of gas-phase pollutants is strongly influenced by the operating temperature of the catalytic converter which warms up during the first several minutes of driving.

Figure 6.8 shows the size distribution of the particulate matter emitted from catalyst-equipped gasoline-powered vehicles, non-catalyst-equipped gasoline-powered vehicles, and diesel vehicles averaged over each portion of the FTP urban driving cycle as measured by the OPC and DMA / CNC combination. The values shown are stated in terms of particle concentrations after the third stage of dilution in the sampling system which varies from vehicle to vehicle in order to keep the instruments on-scale. The relative magnitude of the size distributions for a single vehicle type within different

sections of the FTP driving cycle are directly comparable to each other, however, and so provide some insight into the relationship between engine temperature and particulate emission rates within each single vehicle class.

Particulate matter size distributions measured from both catalyst-equipped gasoline-powered vehicles and non-catalyst-equipped gasoline-powered vehicles show relatively little variation between the cold start and hot start portions of the FTP urban driving cycle, as seen in Figure 6.8. Both types of gasoline-powered vehicles had marginally higher particulate matter release rates during the hot running portion of the test.

A particulate matter size distribution characteristic of medium-duty diesel vehicles under cold start conditions is not available since each diesel vehicle tested was warmed up on the dynamometer prior to the beginning of a test. The particulate matter measured during the first 505 sec of the diesel vehicle test is therefore used to characterize particulate matter emissions from diesel vehicles under hot start conditions. Results shown in Figure 6.8 indicate that fine particulate matter emissions during the hot start portion of the FTP urban driving cycle are marginally higher than those during the hot running portion of the test.

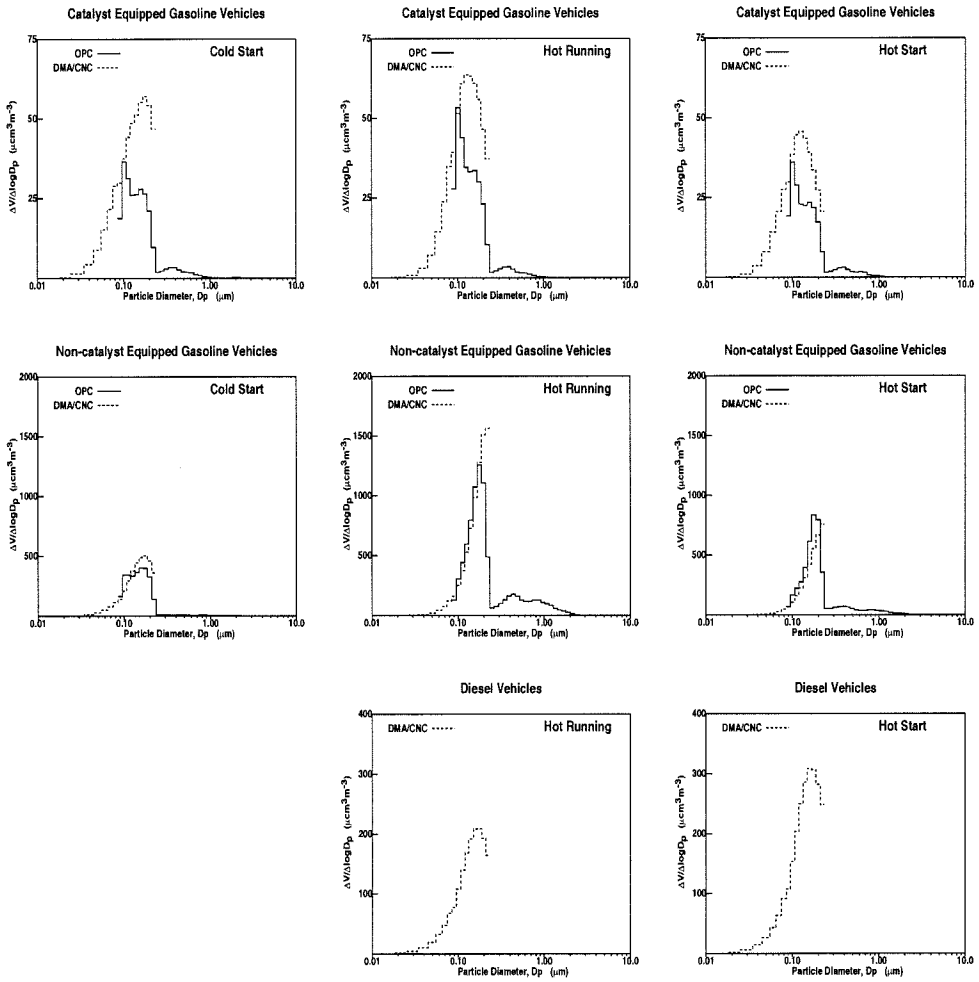

Figure 6.8:
Size distribution of particulate matter emitted from catalyst-equipped gasoline-powered vehicles, non-catalyst gasoline-powered vehicles, and medium-duty diesel vehicles averaged over each portion of the FTP urban driving cycle as measured by an OPC and DMA / CNC combination.

Bibliography

[1] James J. Schauer, Wolfgang Rogge, Lynn M. Hildemann, Monica A. Mazurek, Glen R. Cass, and Bernd R. T. Simoneit. Source apportionment of airborne particulate matter using organic compounds as tracers. *Atmos. Environ.*, 30(22):3837–3855, 1996.

[2] Michael J. Kleeman and Glen R. Cass. Source contributions to the size and composition distribution of urban particulate air pollution. *Atmos. Environ.*, 32:2803–2816, 1998.

[3] Lynn M. Hildemann, Gregory R. Markowski, Michael C. Jones, and Glen R. Cass. Submicrometer aerosol mass distributions of emissions from boilers, fireplaces, automobiles, diesel trucks, and meat–cooking operations. *Aerosol Sci. Technol.*, 14:138–152, 1991.

[4] Lynn M. Hildemann, Gregory R. Markowski, and Glen R. Cass. Chemical composition of emissions from urban sources of fine organic aerosol. *Environ. Sci. Technol.*, 25:744–759, 1991.

[5] Chandra Venkataraman, James M. Lyons, and Sheldon K. Friedlander. Size distributions of polycyclic aromatic hydrocarbons and elemental carbon. 1. Sampling, measurement methods and source characterization. *Environ. Sci. Technol.*, 28:555–562, 1994.

[6] Antonio H. Miguel, Thoms W. Kirchstetter, and Robert A. Harley. On-road emissions of polycyclic aromatic hydrocarbons and black carbon

from gasoline and diesel vehicles. *Environ. Sci. Technol.*, 32:450–455, 1998.

[7] Veli-Natti Kerminen, Timo E. Makela, Christina H. Ojanen, Risto E. Hillamo, Juha K. Vilhunen, Leena Rantanen, Nicole Havers, Alex Von Bohlen, and Dieter Klockow. Characterization of the particulate phase in the exhaust from a diesel car. *Environ. Sci. Technol.*, 31:1883–1889, 1997.

[8] James J. Schauer, Michael J. Kleeman, Glen R. Cass, and Bernd R. T. Simoneit. Measurement of emissions from air pollution sources. 5. C_1-C_{32} organic compounds from gasoline-powered motor vehicles. *Environ. Sci. Technol.*, to be submitted for publication, 1998.

[9] James J. Schauer, Michael J. Kleeman, Glen R. Cass, and Bernd R. T. Simoneit. Measurement of emissions from air pollution sources. 2. C_1-C_{29} organic compounds from medium-duty diesel trucks. *Environ. Sci. Technol.*, submitted for publication, 1998.

[10] Lynn M. Hildemann, Glen R. Cass, and Gregory R. Markowski. A dilution stack sampler for collection of organic aerosol emissions: Design, characterization and field tests. *Aerosol Sci. Technol.*, 10:193–204, 1989.

[11] James J. Schauer, Michael J. Kleeman, Glen R. Cass, and Bernd R. T. Simoneit. Measurement of emissions from air pollution sources. 1. C_1-C_{29} organic compounds from meat charbroiling. *Environ. Sci. Technol.*, submitted for publication, 1998.

[12] James J. Schauer, Michael J. Kleeman, Glen R. Cass, and Bernd R. T. Simoneit. Measurement of emissions from air pollution sources. 4. C_1-

C_{29} organic compounds from fireplace combustion of wood. *Environ. Sci. Technol.*, to be submitted for publication, 1998.

[13] James J. Schauer, Michael J. Kleeman, Glen R. Cass, and Bernd R. T. Simoneit. Measurement of emissions from air pollution sources. 6. C_1-C_{29} organic compounds from environmental tobacco smoke. *Environ. Sci. Technol.*, to be submitted for publication, 1998.

[14] J. J. Huntzicker, R. L. Johnson, J. J. Shaw, and R. A. Cary. Analysis of organic and elemental carbon in ambient aerosols by a thermal-optical method. In G.T. Wolff and R.L. Klimisch, editors, *Particulate Carbon: Atmospheric Life Cycle*, Plenum, New York, 1982.

[15] M. E. Birch and R. A. Cary. Elemental carbon-based method for monitoring occupational exposures to particulate diesel exhaust. *Aerosol Sci. Technol.*, 25:221–241, 1996.

[16] Michael J. Kleeman, James J. Schauer, and Glen R. Cass. Size and composition distribution of fine particulate matter emitted from wood burning, meat charbroiling and cigarettes. *Environ. Sci. Technol.*, to be submitted for publication, 1998.

[17] W. T. Bolleter, C. T. Bushman, and P. W. Tidwell. Spectrophotometric determinations of ammonium as indophenol. *Analytical Chemistry*, 33:592–594, 1961.

[18] Ilhan Olmez. Instrumental neutron activation analysis of atmospheric particulate matter. In J.P. Lodge, editor, *Methods of Air Sampling and Analysis*, Lewis Publishers Inc., Chelsea, MI, 1989.

[19] Walter John and Georg Reischl. A cyclone for size-selective sampling of ambient air. *J. Air Pollut. Control Assoc.*, 30:872–876, 1980.

[20] Susan M. Larson, Glen R. Cass, Kevin J. Hussey, and Frederick Luce. Verification of image processing based visibility models. *Environ. Sci. Technol.*, 22:629–637, 1988.

[21] Yigal Erel, Simo O. Pehkonen, and Michael R. Hoffmann. Redox chemistry of iron in fog and stratus clouds. *J. Geophys. Res.*, 98:18423–18434, 1993.

[22] Michael R. Hoffmann and Jack G. Calvert. *Chemical Transformation Modules for Eulerian and Deposition Models, Volume II: The Aqueous Phase Chemistry.* Technical Report EPA 600/3–85/036, U. S. Environmental Protection Agency, Research Triangle Park, NC, 1985.

[23] K. L. Dreher, R. H. Jaskot, J. R. Lehmann, J. H. Richards, J. K. McGee, A. J. Ghio, and D. L. Costa. Soluable transition metals mediate residual oil fly ash induced acute lung injury. *Journal of Toxicology and Environ. Health*, 50:285–305, 1997.

[24] G. Oberdorster, J. Ferin, R. Gelein, S. C. Soderholm, and J. Finkelstein. Role of the alveolar macrophage in lung injury, studies with ultrafine particles. *Environ. Health Perspect.*, 97:193–199, 1992.

[25] Susan T. Bagley, Kirby J. Baumgard, Linda D. Gratz, John H. Johnson, and David G. Leddy. *Characterization of Fuel and Aftertreatment Device Effects on Diesel Emissions.* Technical Report 76, Health Effects Institute, Cambridge, MA, 1996.

7 Size and Composition Distribution of Fine Particulate Matter Emitted From Wood Burning, Meat Charbroiling and Cigarettes

7.1 Introduction

Mechanistic air quality models are being developed that seek to predict the size and chemical composition distribution of atmospheric particulate matter. These models solve an initial value problem in which the size and composition of particles are specified at the time of release to the atmosphere followed by transformation of the particles as they participate in atmospheric chemical reaction processes. The accuracy of model results is limited by the various links in the chain of calculations, including the need to know the initial properties of the size-resolved particulate matter emissions at their source.

Emissions inventories for particulate matter compiled by air pollution control agencies typically specify only particle mass emission rates for all particles smaller than a stated size (e.g., emissions of PM10 mass). In a few exceptional cases, agencies such as the California Air Resources Board (CARB) describe the release rate of particulate material from individual sources and specify size and chemical composition profiles which transform these bulk emissions into size- and chemically-resolved particulate emissions.

The library of stationary source profiles provided by CARB is based largely on the work of Taback et al. [1] in which the chemical composition of particulate emissions from stationary sources was measured using either an EPA method 5 sampling system or a Source Assessment Sampling System (SASS) sampling train in which particles are sized through collection in a sequence of cyclone separators and filters, followed by bulk chemical analysis. In both of these systems, particulate matter samples are collected using techniques which do not allow for the partitioning of condensible organic vapors onto the particles prior to sampling. Information on particle size is obtained from measurements made using sequential cyclone separators which divide the aerosol into only three particle size ranges below 10 μm particle diameter and that provide no information at all on the shape of the particle size distribution below 1 μm diameter. Since many of the source size and composition profiles are based on the results of source tests conducted approximately 20 years ago, it would be useful in any case to examine present day emissions.

Hildemann et al. [2, 3] conducted a series of source tests in the late 1980's using a dilution source sampling system designed to measure the size distribution and chemical composition of particulate emissions from the major urban sources in Southern California. During these source tests, the source effluent was diluted with pre-cooled purified air prior to sample collection in order to simulate the condensation of organic vapors onto pre-existing solid particles that will occur as hot exhaust plumes are released to the atmosphere. This dilution source testing procedure included high resolution particle size-distribution measurements made using an electrical aerosol analyzer. Chemical analysis of the fine particulate matter emissions was based on fine particle filter samples, however, and so to use these data as inputs to aerosol processes air quality models it must be assumed that all particles

smaller than 2.5 μm diameter have a chemical composition like that of the bulk fine particle filter sample. While the results of this source test program greatly improve the accuracy of the source profiles available to transform bulk particulate emissions into a description of size- and chemically-resolved particulate emissions, the detailed distribution of chemical species between fine particles of different sizes remains unknown.

A source testing program is undertaken in the present work that seeks to obtain high resolution data on the size distribution of the individual chemical species found in the fine particle emissions from urban air pollution sources. To accomplish this objective, the dilution source sampling system of Hildemann et al. [2, 3] is augmented with two multiple orifice uniform deposit impactors (MOUDIs), a laser optical particle counter (OPC), and a scanning differential mobility analyzer (DMA) / condensation nucleus counter (CNC) system. The sources tested with this system and reported in the present chapter include wood burning fireplaces (pine, oak, eucalyptus), meat charbroiling, and cigarettes. In further work, the particulate emission characteristics of motor vehicles will be discussed.

The architecture and operation of the upstream stages of the dilution source sampling system used have been described extensively by Hildemann et al. [2, 3] and Schauer et al. [4, 5, 6, 7, 8] and so only a brief summary will be presented here. The sampler consists of a stainless steel dilution tunnel followed by a residence time chamber from which cooled and diluted pollutant source exhaust is withdrawn for chemical analysis. A diagram of the dilution tunnel and residence time chamber is shown in Figure 1a of Hildemann et al. [2]. In the present study, two sampling trains were operated in parallel downstream of the residence time chamber to quantify the emissions of semivolatile organic compounds from each of the sources tested. A third unit was

used to collect samples of fine particulate matter, carbonyls, organic acids and gas-phase hydrocarbons. The results of the bulk fine particle, semi-volatile organic, inorganic and trace metals measurements taken with the first three sampling trains are presented by Schauer et al. [4, 5, 6, 7, 8]. The purpose of the present study is to discuss measurements made using a fourth sampling train designed to measure size-resolved aerosol properties in the pollutant exhaust stream. In the following sections, a detailed description is provided of the size distribution measurements taken with the electronic particle sizing equipment and cascade impactors.

7.2 Experimental Methods

Particulate emissions from each of the sources considered in the present study were measured with four separate instruments. A differential mobility analyzer (DMA) (TSI model 3071) was used in conjunction with a condensation nucleus counter (CNC) (TSI model 3760) to measure particle number concentrations between 0.02-0.250 μm particle diameter. This instrument was operated as a scanning differential mobility analyzer [9] with automated data aquisition over the particle size range specified every 60 sec or 90 sec depending on the variability of the source being tested. Electronic measurements of particle number concentrations also were made using a laser optical particle counter (OPC) (Particle Measuring Systems model ASASP-100X) which was capable of counting and sizing particles with diameters in the range 0.09-3 μm. Both of the instruments described above measured particle number concentrations between 0.09-0.25 μm particle diameter; agreement in this region of overlap was good but not perfect because the DMA / CNC uses electrical mobility to size particles while the OPC uses light scattering. Each technique reacts differently to variations in particle shape, size and compo-

sition, leading to small differences in the measured particle size distribution.

Two 10-stage multiple orifice uniform deposit impactors (MOUDIs) (MSP model 100) were used to measure particle chemical composition as a function of size. The first impactor was equipped with aluminum foil substrates (47 mm diameter, MSP) and a quartz fiber after filter (37 mm diameter, Pallflex 2500 QAO). This instrument was dedicated to the analysis of carbonaceous aerosol species. The foil substrates and quartz fiber after filters were baked at 550°C for 48 hrs prior to use in order to lower their carbon blank values. After collection, samples were analyzed for elemental and organic carbon content using the thermal-optical carbon analysis method of Huntzicker et al. [10] as modified by Birch and Cary [11]. Correction for pyrolytic formation of elemental carbon during organic carbon determination was accomplished using the methodology described in Section 7.3 of the present chapter.

The second impactor used in the source test procedure was equipped with Teflon substrates (47 mm diameter, Gelman Sciences Teflo, 2 μm pore size) and a Teflon after filter (37 mm diameter, Gelman Sciences, Zefluor, 2 μm pore size). Gravimetric analysis was conducted on all impactor substrates and Teflon after filters by weighing each substrate or after filter in a temperature and humidity controlled room (20-24°C, 35-40% RH) several times before and after the sample was collected using a micro balance (Mettler model M-55-A). Each sample next was cut in half to allow for flexibility in the types of chemical analysis techniques used. The first half of each sample collected on a Teflon substrate was analyzed for sulfate, nitrate and chloride using ion chromatography (Model 2020i, Dionex Corp.), and for ammonium ion using a modified indophenol colorimetric method [12] using a rapid-flow analyzer (Model RFA-300, Alpkem Corp.). The second half of each of these

samples was analyzed for trace elements using neutron activation analysis [13].

Particle bounce within the impactors was not a problem for the source tests described in the current study. Coarse particles that are prone to bounce were removed from the sample stream prior to entering the impactor by a cyclone separator with a cut size of 1.8 μm particle diameter [14]. Stages 0-4 from each impactor were not analyzed for chemical composition since any particles which would have accumulated on these stages were removed by the cyclone separator. The fine combustion particles collected in size ranges below 1.8 μm diameter were generally sticky enough to adhere to the impaction surface. Anti-bounce grease coatings were not used on impactor substrates so that sample contamination could be avoided.

7.3 Carbon Analysis

In order to measure the size-resolved emission rates of particulate elemental carbon (EC) and organic carbon (OC) collected with the MOUDI impactor, an analysis method was needed which could quantify EC and OC accumulations on aluminum impactor substrates. Total carbon can be measured easily on this type of collection media by heating the sample to evolve the carbon, burning the carbon to form CO_2, converting the CO_2 to methane, and then quantifying the result with a flame ionization detector (FID). Following the methodology of Birch and Cary [11], this process is carried out in a pure helium atmosphere during the initial stages of heating until little if any further organic material can be evolved by increasing the temperature. The carbon measured in this first stage of the analysis is defined as organic carbon. A small amount of oxygen (2%) is then introduced into the sample chamber to promote the evolution of any remaining carbon. The intended purpose

of this latter stage of analysis is to obtain a separate measurement of the high-temperature-resistant black elemental carbon present in the sample.

It has been noted by many researchers [15] that during the first phase of the thermal evolution method described above, a portion of the organic carbon present on the substrate is pyrolized to form black carbon which then remains on the collection media. Without appropriate correction measures, this material evolves during the latter stages of the analysis and is mistakenly added to the elemental carbon fraction of the sample. In an attempt to quantify and correct for this behaviour when analyzing quartz fiber filter samples, the optical transmissivity of the filter is monitored throughout the procedure. This transmissivity generally decreases during the initial stages of heating as some fraction of the organic carbon is pyrolized to form black (light absorbing) carbon, and then increases during the latter stages of the procedure as the elemental carbon also is evolved from the sample. The black carbon which evolves before the transmissivity of the sample returns to its original value is identified as the amount of carbon necessary to correct for pyrolysis during the early stages of analysis and is added to the organic carbon fraction of the sample. The carbon which evolves as the transmissivity of the sample increases above its original value is defined as the corrected amount of elemental carbon.

While the procedure described above works well for samples collected on quartz fiber filters, the transmissivity of the deposit collected on opaque aluminum impactor substrates cannot be measured and so cannot be used to distinguish between the organic and elemental carbon fractions. In order to correct for the amount of organic carbon on aluminum impactor substrates which pyrolizes during the initial stages of the analysis, a fine particle filter sample collected on quartz fiber media during the same source test first

was analyzed using identical test procedures to determine the point in the analytical cycle at which all of the organic carbon had been evolved from the sample (with appropriate corrections for pyrolysis). It was then assumed that organic carbon would evolve from the impactor samples in a manner similar to that which was observed for the filter sample, accompanied by a proportionately similar pyrolysis correction.

7.4 Results and Discussion

The size and composition distributions of particles emitted from wood combustion (pine, oak, eucalyptus), meat charbroiling, and cigarette smoking are shown in Figures 7.1-7.3, 7.7 and 7.9 respectively. The upper panel of each figure displays the results of measurements made with the OPC and DMA / CNC combination while the lower panel displays the results of the chemical analysis of the MOUDI measurements. Organic compound concentrations shown in Figures 7.1-7.3, 7.7 and 7.9 are derived from organic carbon measurements multiplied by a factor of 1.4 based on the results of organic speciation analysis of filter-based samples taken during the same source tests as described by Schauer et al. [4, 6, 8]. Results shown in Figures 7.1-7.3, 7.7 and 7.9 have been normalized to display the size distribution of 1 μcm^3 (top frame of each pair) or 1 μg (bottom frame) of particulate matter emitted from the source in question. The size bins used to display impactor results have been adjusted from the measured aerodynamic diameter to the estimated physical diameter of the particles using an approximate particle density of 1.5 g cm^{-3}.

Concentrations of trace species measured in particulate matter emitted by the sources studied in the current analysis generally are not visible in Figures 7.1-7.3, 7.7 and 7.9 due to the abundance of carbonaceous species

in the particle phase. The size distribution of these trace species is still an important factor, however, since the current state of the art mechanistic air quality models rely exclusively on the aerosol fraction composed of ionic salts (e.g., $(NH_4)_2SO_4$, NH_4NO_3) to predict the hygroscopic behaviour of particles released to the atmosphere. Similarly, trace concentrations of transition metals found in particles play a key role in model calculations by catalyzing the oxidation of sulfur species in the aqueous aerosol phase during fog events. Thus, the size distribution of trace species measured in particulate emissions can greatly influence the predicted behaviour of aerosol emissions released to the atmosphere.

Separate plots of the size distribution of trace species measured in each of the source tests discussed in the present study are shown in Figures 7.4-7.6, 7.8 and 7.10. Error bars representing one standard deviation of the measured values are shown in each species plot. The procedures used to conduct specific source tests and the results of those tests are described in the sections below.

7.4.1 Wood Combustion

Measurements of the size and chemical composition of particles emitted from wood combustion in a residential fireplace were made by sampling from a port installed 5 m above the fireplace grate in the chimney flue at the second floor level of a house. In the present analysis, results are reported from three separate tests which were conducted using pine (17.2 kg burned in 189 min), oak (15.4 kg burned in 165 min), and eucalyptus (18.9 kg burned in 218 min) wood purchased from a commercial firewood distributor in Southern California. Kindling for each test was obtained by splintering a log of the wood being burned and igniting a small amount of newspaper. A more

complete description of the experimental procedures used during the wood burning tests, the fine particle mass emission rates per unit wood burned, and the results of the bulk fine particle filter-based analysis of the organic speciation and elemental composition of the particles emitted may be found in Schauer et al. [6].

The size and composition distributions of particles emitted from the combustion of pine, oak, and eucalyptus are shown in Figures 7.1-7.3 respectively. Particles emitted from the combustion of wood have mass distributions which peak at 0.1-0.2 μm particle diameter. Particles emitted from the combustion of all of the woods tested in the current study are chiefly composed of organic compounds with lesser amounts of elemental carbon also apparent.

The size distributions of trace species found in particles emitted from the combustion of pine, oak, and eucalyptus wood are shown in Figures 7.4-7.6, respectively. Analysis reveals similar size distributions of sulfate, nitrate, chloride, ammonium, potassium, and bromine in particles emitted from these woods. Differences in other trace metals detected in particles emitted from burning different woods likely result from differences in soil composition and climate where the wood grew. Particles emitted from the combustion of pine were found to contain measurable quantities of titanium, iron and rubidium. Particles emitted from the burning of oak had trace quantities of aluminum, iron, zinc and barium. Particles emitted from the combustion of eucalyptus wood contained measurable quantities of aluminum, titanium, iron, rubidium, strontium and barium.

Elevated concentrations of salts such as sodium and chloride may indicate that the eucalyptus wood tested in the current study originated from a coastal ocean environment. Non-uniformity in the types and quantities of trace elements released from the combustion of wood may lead to problems in

receptor modeling studies which attempt to compare elemental "fingerprints" for wood smoke to ambient concentrations in order to determine the source origin of ambient particulate air pollution.

7.4.2 Meat Charbroiling

The size and composition distribution of particles emitted from meat charbroiling operations was measured at an institutional scale kitchen that is in current commercial use. Samples were collected from the ventilation system servicing the charbroiling grill downstream of the grease extractors and immediately prior to particle release to the atmosphere. In the present analysis, results are shown from a single test in which 112 pre-formed, thawed hamburger patties (114g meat each, 20% fat) were cooked on a natural gas-fired charbroiler in batches of 8 over a 72 minute period. A more complete description of the experimental procedures specific to the meat charbroiling test, the fine particle mass emission rates per unit meat cooked, the detailed organic chemical speciation of these emissions, and the bulk elemental composition as determined from filter samples collected during that test are given by Schauer et al. [4].

The size and composition distribution of particles measured during the meat charbroiling source test is shown in Figure 7.7. Particles emitted from this source have a mass distribution which peaks between 0.1-0.2 μm particle diameter, but with some particles emitted at larger sizes. Most of the particles are composed of organic compounds.

The size distributions of trace species found in particles emitted from meat cooking operations are shown in Figure 7.8. Nearly all ionic species commonly encountered in the atmosphere were present in detectable amounts including sodium, potassium, sulfate, nitrate and chloride. Ammonium con-

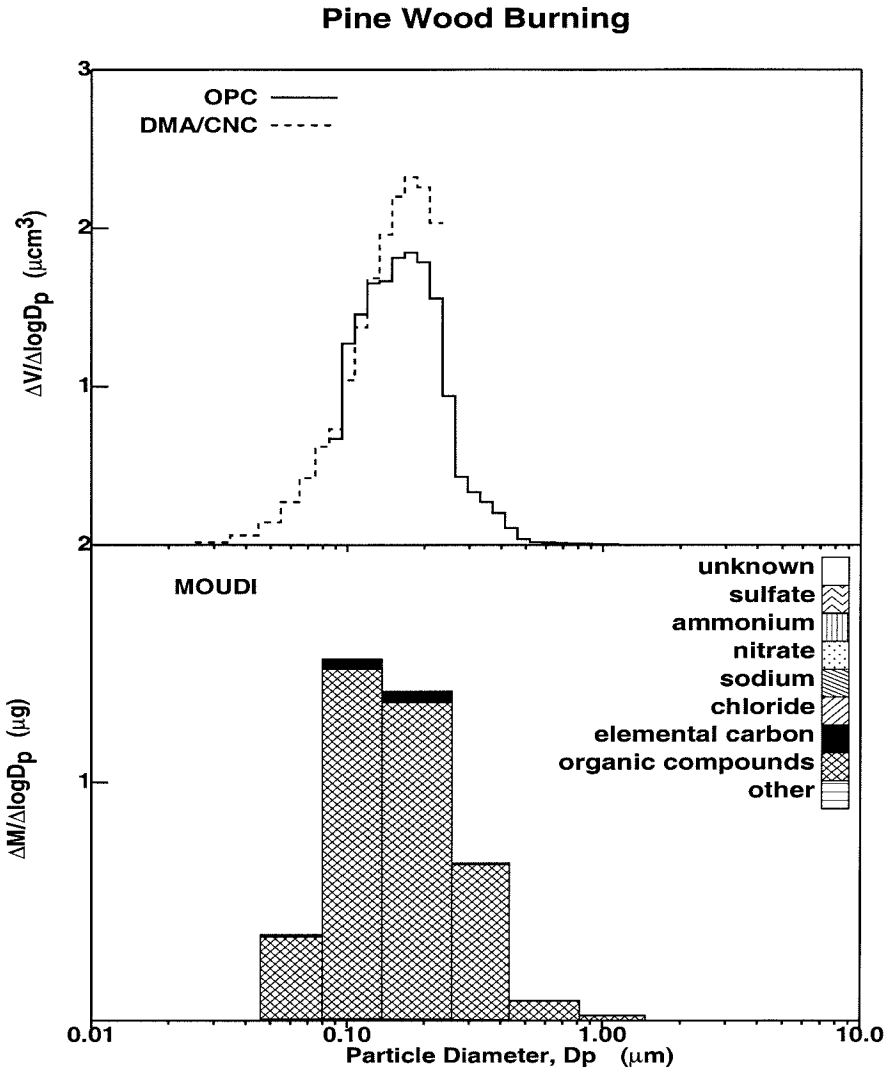

Figure 7.1:
Size and chemical species distribution of fine particles (dp < 1.8 μm) emitted from burning pine wood. The upper panel shows the size distribution of 1 μcm^3 of particulate matter emitted from pine wood smoke as measured by an OPC and DMA / CNC combination. The lower panel shows the size and composition distribution of 1 μg of fine particulate matter emitted from this source as measured by MOUDI impactors.

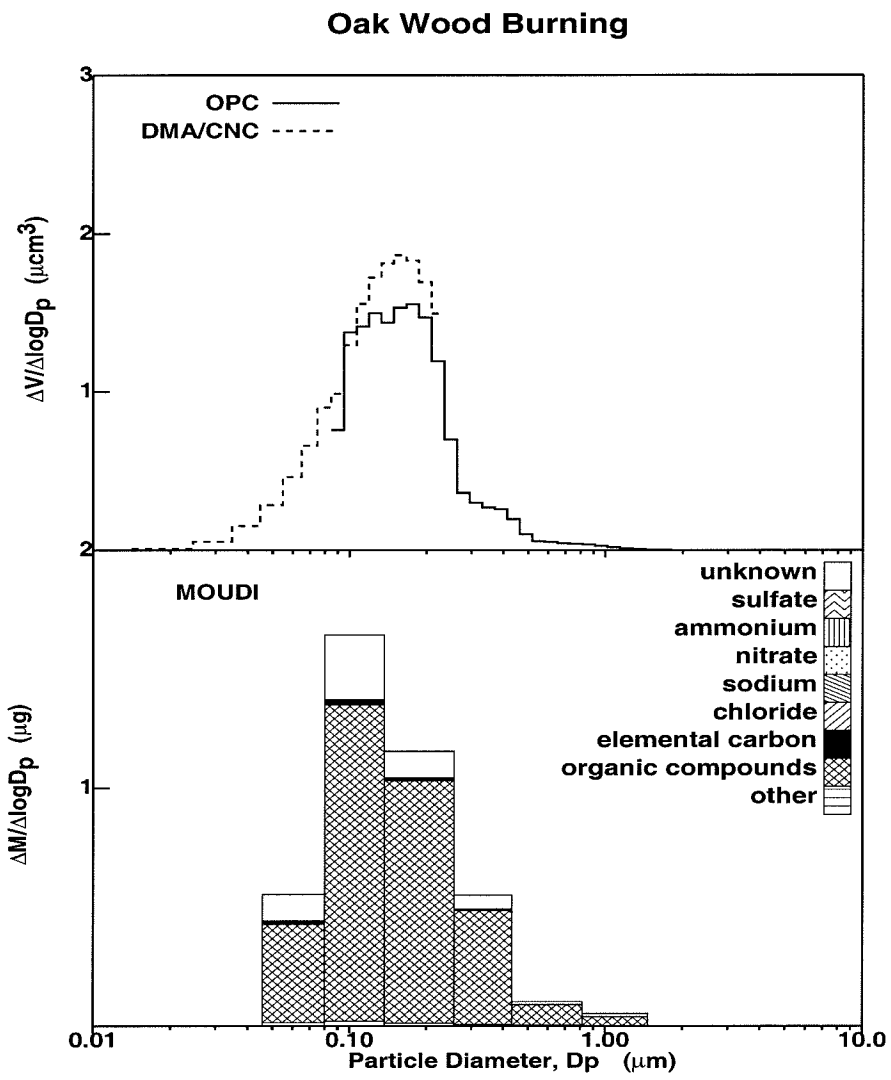

Figure 7.2:
Size and chemical species distribution of fine particles (dp < 1.8 μm) emitted from burning oak wood. The upper panel shows the size distribution of 1 μcm^3 of particulate matter emitted from oak wood smoke as measured by an OPC and DMA / CNC combination. The lower panel shows the size and composition distribution of 1 μg of fine particulate matter emitted from this source as measured by MOUDI impactors.

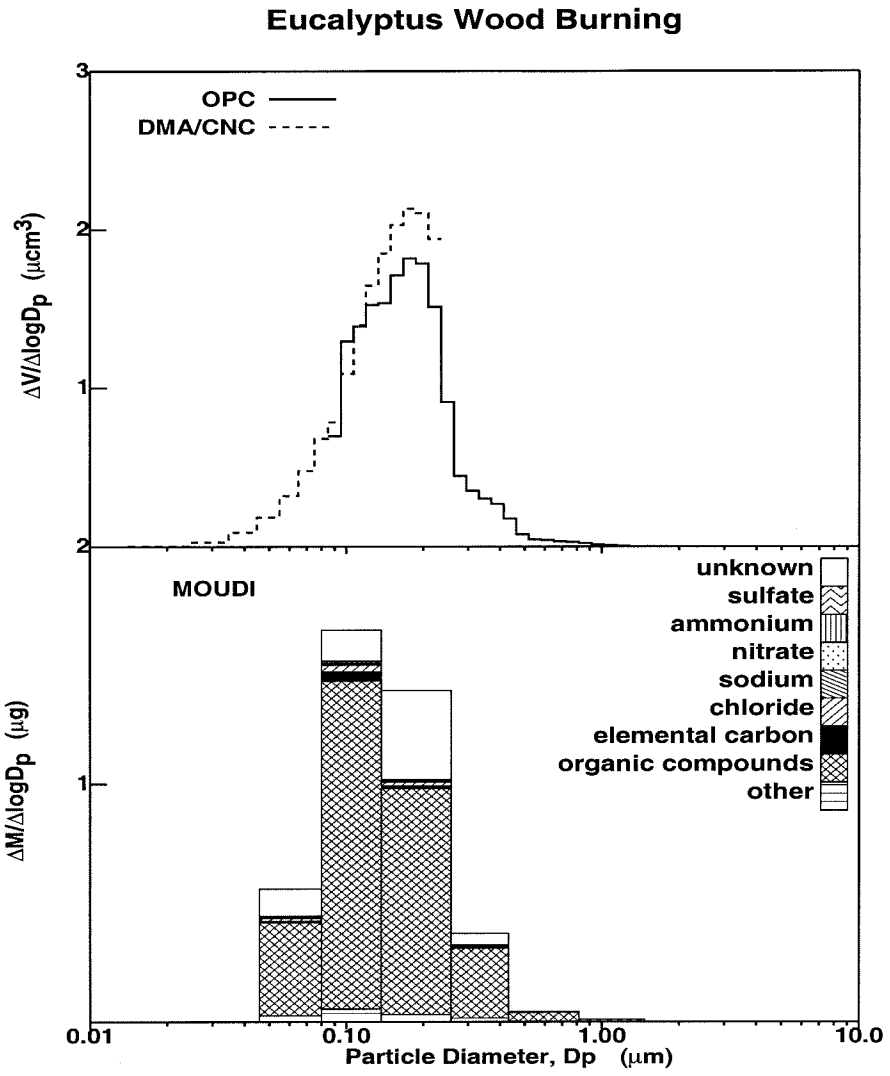

Figure 7.3:
Size and chemical species distribution of fine particles (dp < 1.8 μm) emitted from burning eucalyptus wood. The upper panel shows the size distribution of 1 μcm^3 of particulate matter emitted from eucalyptus wood smoke as measured by an OPC and DMA / CNC combination. The lower panel shows the size and composition distribution of 1 μg of fine particulate matter emitted from this source as measured by MOUDI impactors.

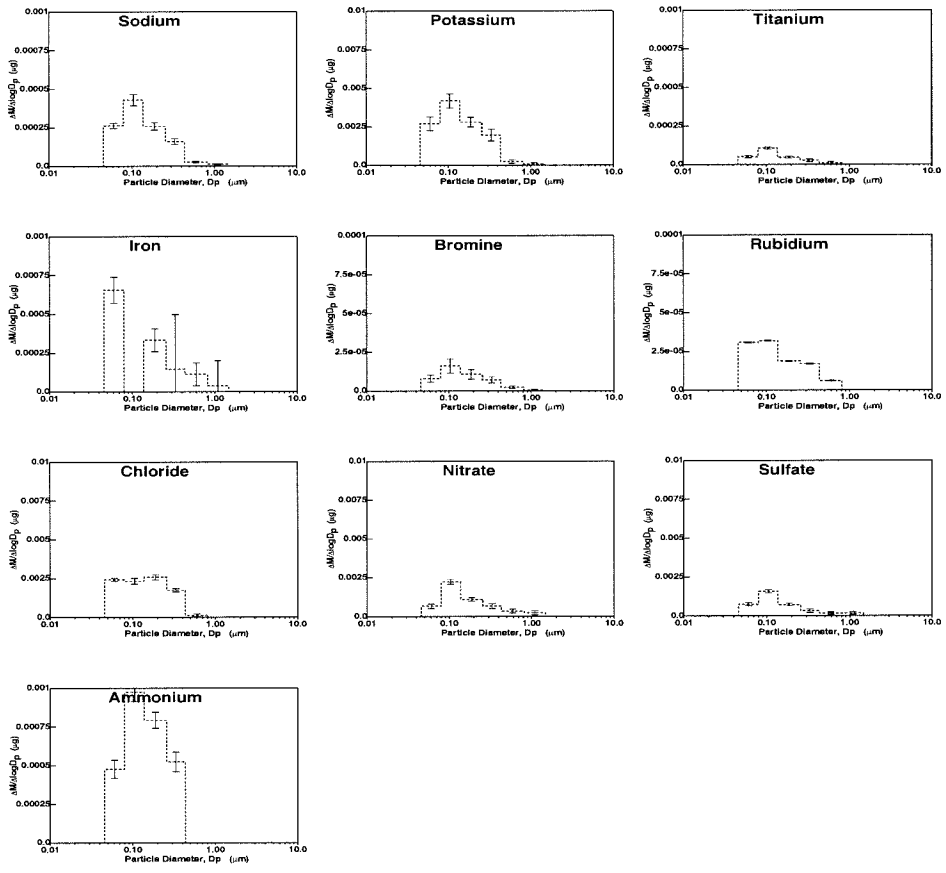

Figure 7.4:
Size distribution of trace species in fine particles (dp < 1.8 μm) emitted from burning pine wood. Error bars represent one standard deviation. Each graph shows the fraction of one μg of fine particulate matter that consists of the trace species indicated.

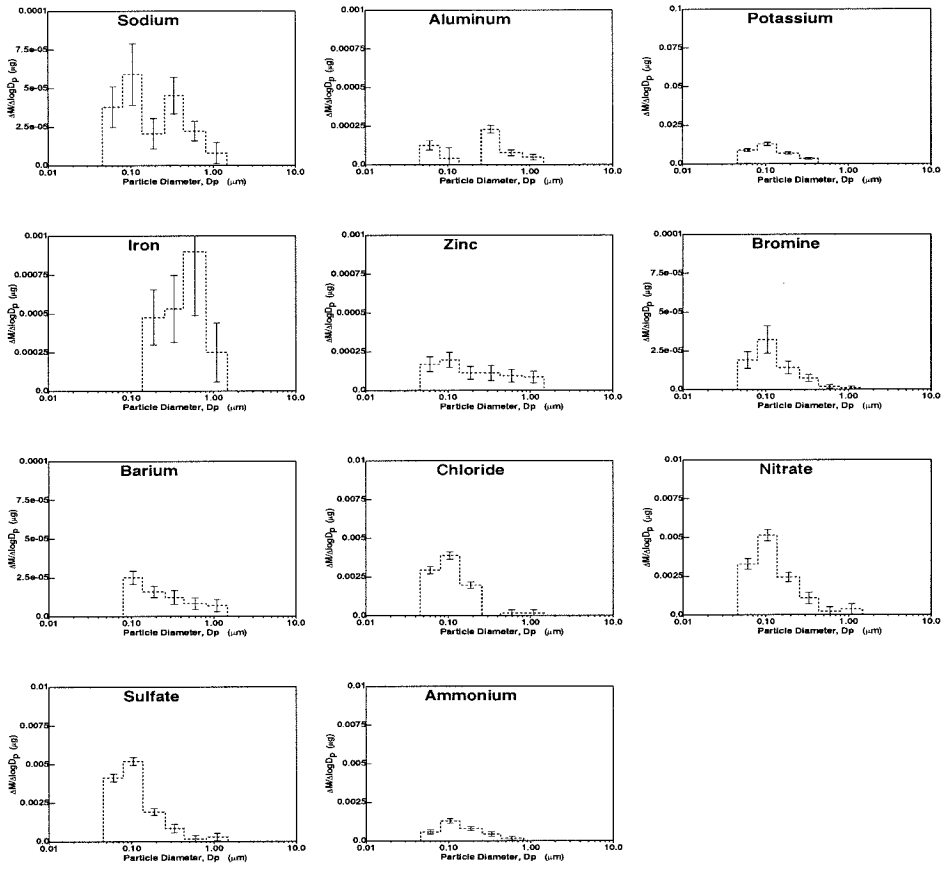

Figure 7.5:
Size distribution of trace species in fine particles (dp < 1.8 μm) emitted from burning oak wood. Error bars represent one standard deviation. Each graph shows the fraction of one μg of fine particulate matter that consists of the trace species indicated.

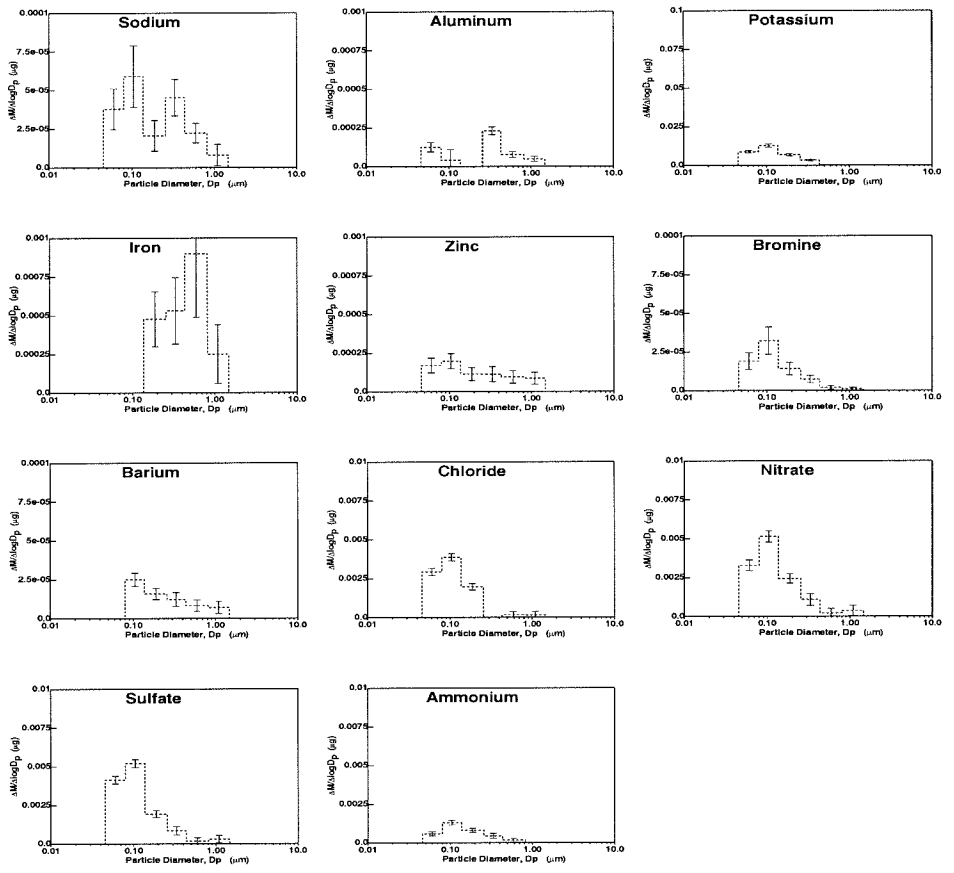

Figure 7.6:
Size distribution of trace species in fine particles (dp < 1.8 μm) emitted from burning eucalyptus wood. Error bars represent one standard deviation. Each graph shows the fraction of one μg of fine particulate matter that consists of the trace species indicated.

centrations measured in particles emitted from this source were not statistically different from zero at any particle size. Trace elements observed include aluminum, strontium and barium. Since air from the kitchen where the charbroiling occurred contained background particles, it is possible that some of the trace species concentrations observed are actually the result of ambient particulate matter drawn through the kitchen, out the exhaust hood, and into the sampler.

7.4.3 Cigarettes

The size and composition distribution of particles emitted from cigarettes was measured by sampling from a chamber occupied by a human smoker which was being flushed with purified air. Sampling began 30 sec prior to the lighting of a cigarette, and continued until 60 sec after the last cigarette was extinguished. During the test, the smoking subject inhaled / exhaled normally and paused between inhalation cycles, resulting in an elapsed time of approximately 5 min for each cigarette smoked. A more complete description of the experimental procedures used during the cigarette tests, the fine particle mass emissions rate per cigarette smoked, and the results of the organic species and bulk fine particle filter-based chemical analysis of samples from these tests are described by Schauer et al. [8].

The size and composition distribution of particles emitted from smoking cigarettes is shown in Figure 7.9. The particle mass distribution peaks between 0.3-0.4μm particle diameter with particles chiefly composed of organic compounds with a lesser amount of elemental carbon.

The size distributions of trace species measured in particles emitted from cigarettes are shown in Figure 7.10. Trace metals detected include sodium, potassium, vanadium, manganese, bromine, antimony, lanthanum, and cerium.

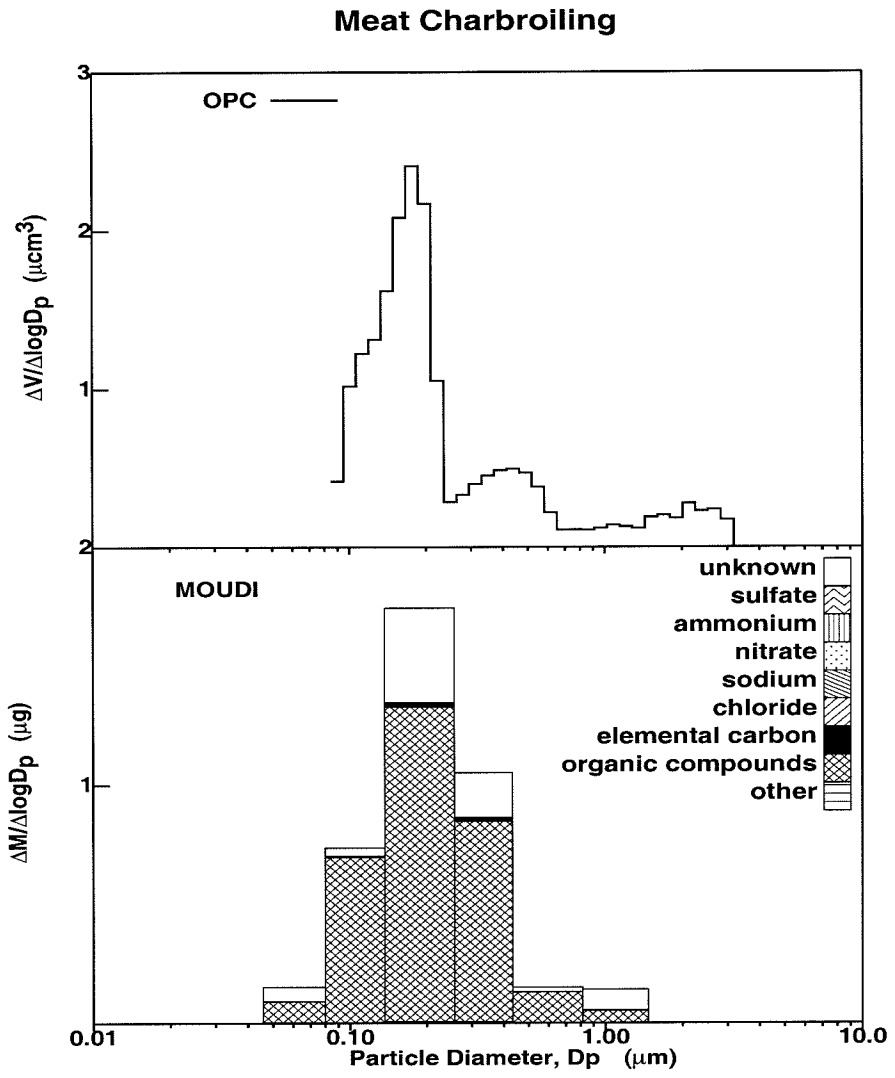

Figure 7.7:
Size and chemical species distribution of fine particles (dp < 1.8 μm) emitted from meat charbroiling. The upper panel shows the size distribution of 1 μcm^3 of particulate matter emitted from meat charbroiling as measured by an OPC. The lower panel shows the size and composition distribution of 1 μg of fine particulate matter emitted from this source as measured by MOUDI impactors.

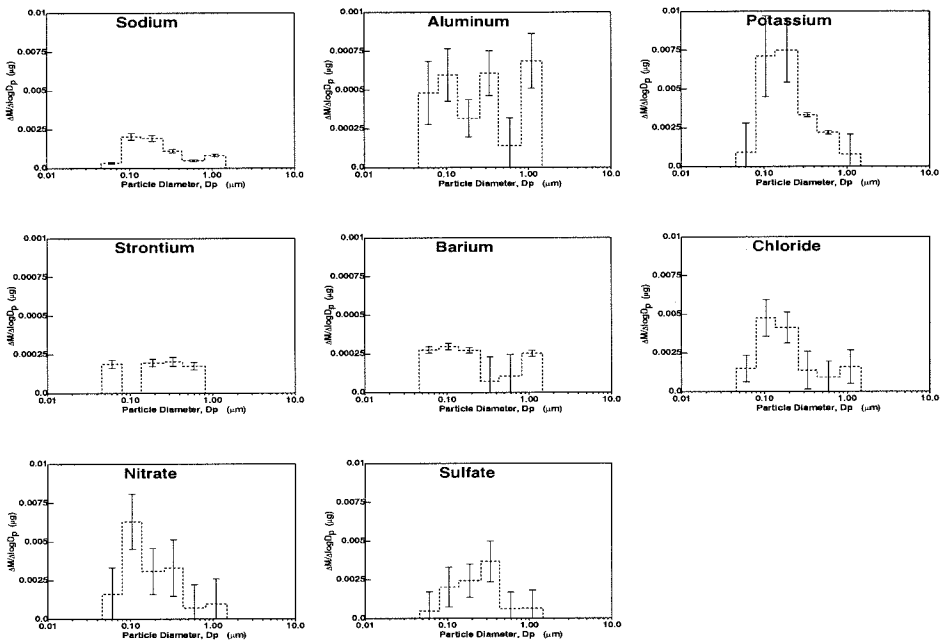

Figure 7.8:
Size distribution of trace species in fine particles (dp < 1.8 μm) emitted from meat charbroiling. Error bars represent one standard deviation. Each graph shows the fraction of one μg of fine particulate matter that consists of the trace species indicated.

Ionic species detected in particles emitted from cigarettes include chloride, nitrate, sulfate and ammonium. Nearly all trace species measured have a size distribution with a single mode peaking between 0.3-0.4μm particle diameter.

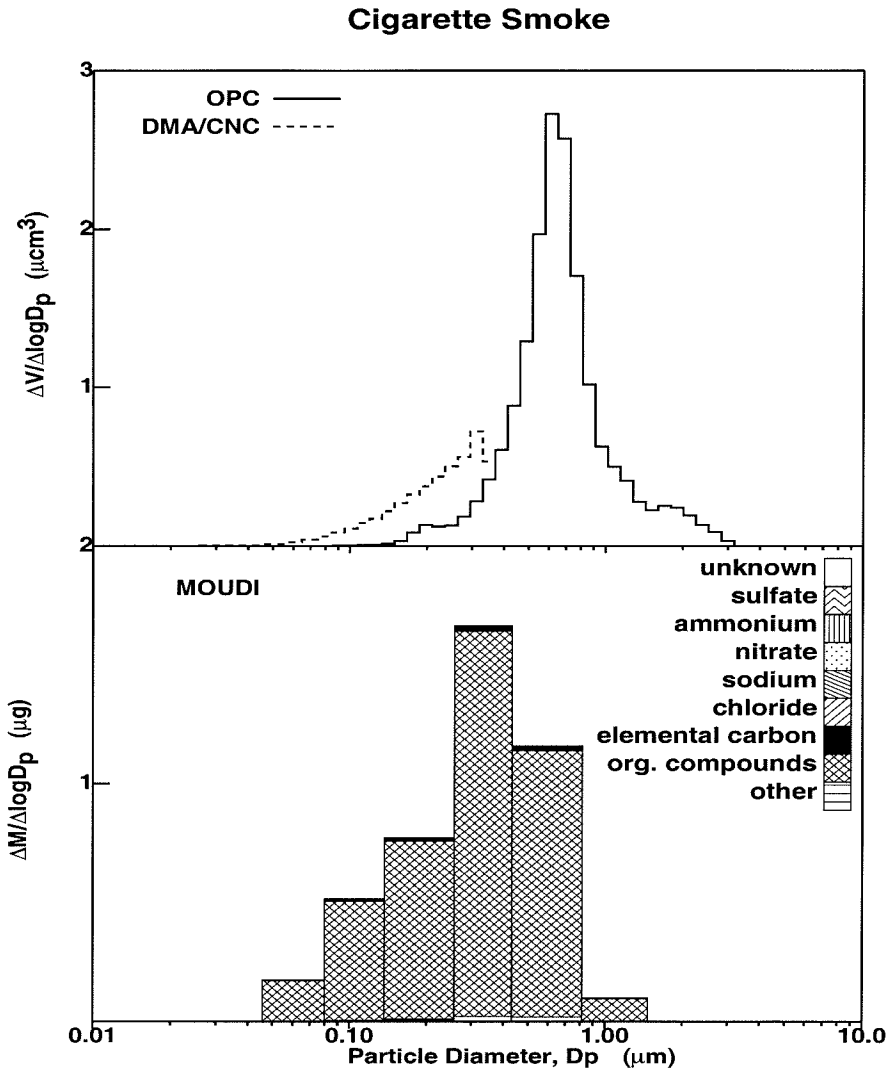

Figure 7.9:
Size and chemical species distribution of fine particles (dp < 1.8 μm) emitted from a cigarette smoked by a human subject. The upper panel shows the size distribution of 1 μcm^3 of particulate matter emitted from cigarette smoke as measured by an OPC and DMA / CNC combination. The lower panel shows the size and composition distribution of 1 μg of fine particulate matter emitted from this source as measured by MOUDI impactors.

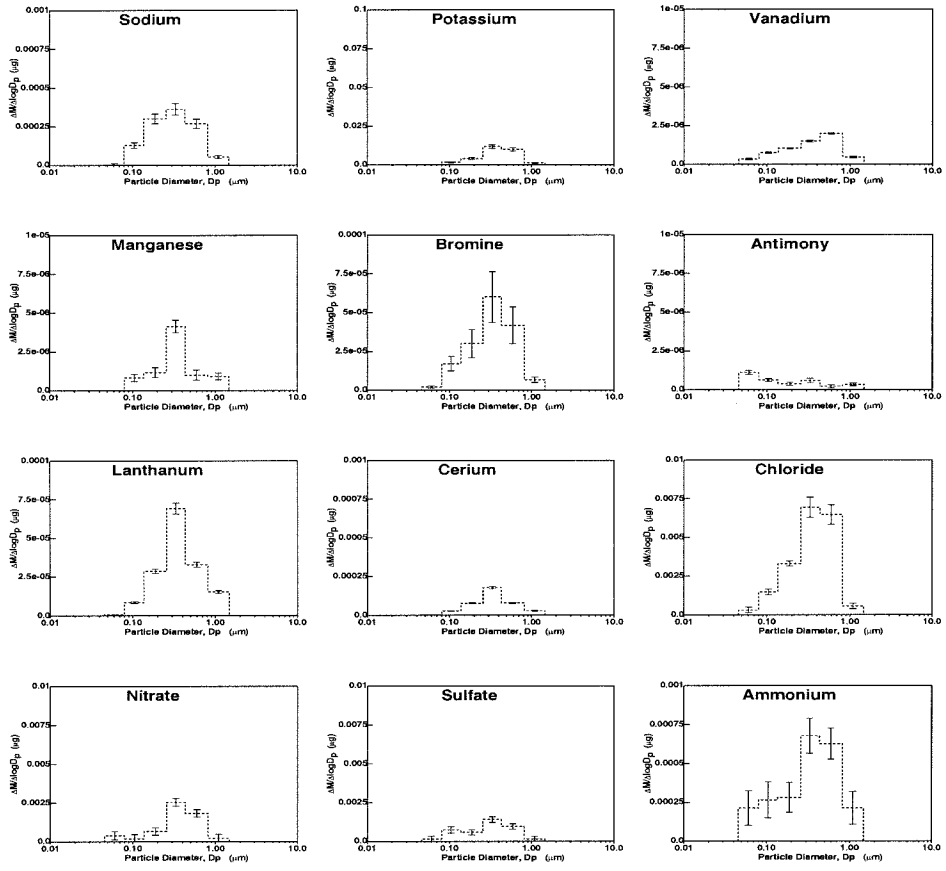

Figure 7.10:
Size distribution of trace species emitted in fine particles (dp < 1.8 μm) from cigarette smoke. Error bars represent one standard deviation. Each graph shows the fraction of one μg of fine particulate matter that consists of the trace species indicated.

Bibliography

[1] H. J. Taback, A. R. Brienza, J. Macko, and N. Brunetz. *Fine Particle Emissions from Stationary and Miscellaneous Sources in the South Coast Air Basin.* Technical Report, California Air Resources Board contract A6–191–30, KVB, Inc., Research–Cottrell, Tustin, California, 1979.

[2] Lynn M. Hildemann, Gregory R. Markowski, and Glen R. Cass. Chemical composition of emissions from urban sources of fine organic aerosol. *Environ. Sci. Technol.*, 25:744–759, 1991.

[3] Lynn M. Hildemann, Gregory R. Markowski, Michael C. Jones, and Glen R. Cass. Submicrometer aerosol mass distributions of emissions from boilers, fireplaces, automobiles, diesel trucks, and meat–cooking operations. *Aerosol Sci. Technol.*, 14:138–152, 1991.

[4] James J. Schauer, Michael J. Kleeman, Glen R. Cass, and Bernd R. T. Simoneit. Measurement of emissions from air pollution sources. 1. C_1-C_{29} organic compounds from meat charbroiling. *Environ. Sci. Technol.*, submitted for publication, 1998.

[5] James J. Schauer, Michael J. Kleeman, Glen R. Cass, and Bernd R. T. Simoneit. Measurement of emissions from air pollution sources. 2. C_1-C_{29} organic compounds from medium-duty diesel trucks. *Environ. Sci. Technol.*, submitted for publication, 1998.

[6] James J. Schauer, Michael J. Kleeman, Glen R. Cass, and Bernd R. T. Simoneit. Measurement of emissions from air pollution sources. 4. C_1-C_{29} organic compounds from fireplace combustion of wood. *Environ. Sci. Technol.*, to be submitted for publication, 1998.

[7] James J. Schauer, Michael J. Kleeman, Glen R. Cass, and Bernd R. T. Simoneit. Measurement of emissions from air pollution sources. 5. C_1-C_{32} organic compounds from gasoline-powered motor vehicles. *Environ. Sci. Technol.*, to be submitted for publication, 1998.

[8] James J. Schauer, Michael J. Kleeman, Glen R. Cass, and Bernd R. T. Simoneit. Measurement of emissions from air pollution sources. 6. C_1-C_{29} organic compounds from environmental tobacco smoke. *Environ. Sci. Technol.*, to be submitted for publication, 1998.

[9] S. C. Wang and Richard C. Flagan. Scanning electrical mobility spectrometer. *Aerosol Sci. Technol.*, 13(2):230–240, 1989.

[10] J. J. Huntzicker, R. L. Johnson, J. J. Shaw, and R. A. Cary. Analysis of organic and elemental carbon in ambient aerosols by a thermal-optical method. In G.T. Wolff and R.L. Klimisch, editors, *Particulate Carbon: Atmospheric Life Cycle*, Plenum, New York, 1982.

[11] M. E. Birch and R. A. Cary. Elemental carbon-based method for monitoring occupational exposures to particulate diesel exhaust. *Aerosol Sci. Technol.*, 25:221–241, 1996.

[12] W. T. Bolleter, C. T. Bushman, and P. W. Tidwell. Spectrophotometric determinations of ammonium as indophenol. *Analytical Chemistry*, 33:592–594, 1961.

[13] Ilhan Olmez. Instrumental neutron activation analysis of atmospheric particulate matter. In J.P. Lodge, editor, *Methods of Air Sampling and Analysis*, Lewis Publishers Inc., Chelsea, MI, 1989.

[14] Walter John and Georg Reischl. A cyclone for size-selective sampling of ambient air. *J. Air Pollut. Control Assoc.*, 30:872–876, 1980.

[15] Judith C. Chow, John G. Watson, Lyle C. Pritchett, William R. Pierson, Clifton A. Frazier, and Richard G. Purcell. The DRI thermal/optical reflectance carbon analysis system: Description, evaluation and applications in U.S. air quality studies. *Atmos. Environ.*, 27A(8):1185–1201, 1993.

8 Source Contributions to the Size and Composition Distribution of Atmospheric Particles: Southern California in September, 1996

8.1 Introduction

In order to formulate effective pollution control strategies, it is necessary to first understand the factors which influence pollutant concentrations in the present day atmosphere. For this purpose, mechanistic air quality models must be continuously refined and evaluated against ambient data. Data sets required for use in testing mechanistic air quality models are extremely expensive and difficult to obtain, since they must include simultaneous measurements of meteorological parameters, gas-phase pollutant concentrations, particle size and composition distributions, accompanied by detailed emissions inventories used as model inputs. The Southern California Air Quality Study (SCAQS) was a large cooperative air quality measurement program carried out in Southern California in 1987 which was designed to collect data for the evaluation of air quality models [1]. The SCAQS data set has proved to be tremendously useful in the development and evaluation of many different air quality models [2, 3, 4, 5]; however, these data are now more than 10 years old.

In an effort to acquire a data set more representative of the current nature of urban air pollution in the greater Los Angeles area, and to take advantage of new real-time aerosol characterization techniques that now are available, a comprehensive air quality measurement program was undertaken during the late summer and early fall of 1996. This experiment included measurements taken at one offshore background site and three inland receptor sites in the South Coast Air Basin surrounding Los Angeles using electronic particle size distribution monitors, inertial impactors, filter-based samplers, and aerosol time of flight mass spectrometers [6]. The purpose of this chapter is to describe the application of an aerosol processes photochemical trajectory model [5, 7, 8] to this data set in an effort both to evaluate the performance of models for an externally mixed aerosol and to understand the factors which influence ambient pollutant concentrations in the Los Angeles area during the study period. In the sections below, the formulation of the photochemical aerosol processes model will be described, along with the input data that document the air quality episode under consideration. Model predictions for ambient pollutant concentrations then will be compared to measurements taken at Long Beach, CA, on September 24, 1996, Fullerton, CA, on September 24, 1996, and at Riverside, CA, on September 25, 1996.

8.2 Model Description

The structure of the aerosol processes trajectory model used in the current study has been described in detail elsewhere [5, 7, 8] and so only a brief summary is presented here. In this model, the airborne particle complex is represented as a source-oriented external mixture of particles that initially are released to the atmosphere as a countable number of discrete particles of 15 different sizes between 0.01-10 μm diameter, each with a chemical compo-

sition determined at its source. Each particle interacts with a common gas phase but otherwise evolves separately from other particles in the atmosphere while retaining information on the source from which it was originally emitted. The host framework for the aerosol calculations is the CIT trajectory model for photochemical air pollution which incorporates the Carter90 [9] gas-phase photochemical mechanism, a modified version of the AIM aerosol thermodynamics module [10, 5], a fog chemistry model based on the work of Jacob [11, 12], and a secondary organic aerosol formation module [3] which has been revised to represent absorption of semi-volatile organic compounds into the particle phase [13, 8]. This formulation provides an accurate representation of the composition of an urban atmosphere, and it also allows for the determination of the contribution which different sources make to the size and composition distribution of suspended particulate matter at downwind receptor locations.

8.3 Model Application

The geographical region of interest for the current modeling study is shown in Figure 8.1, along with the calculated air parcel trajectory path terminating at Riverside, CA, on September 25, 1996, at 1600 hours PST. The target air parcel passes over the Fullerton monitoring station at approximately 1600 PST on September 24, 1996, and just north of the Long Beach monitoring station at 1300 PST on September 24, 1996. Model calculations consider the emissions, vertical mixing, dry deposition and chemical transformation of pollutants within air parcels having a base area of 5 km by 5 km and a height of 1 km. Five vertical layers are represented within the air parcel, with heights (beginning at the ground and proceeding upward) of 34.5 m, 105.5 m, 140 m, 330 m, and 390 m.

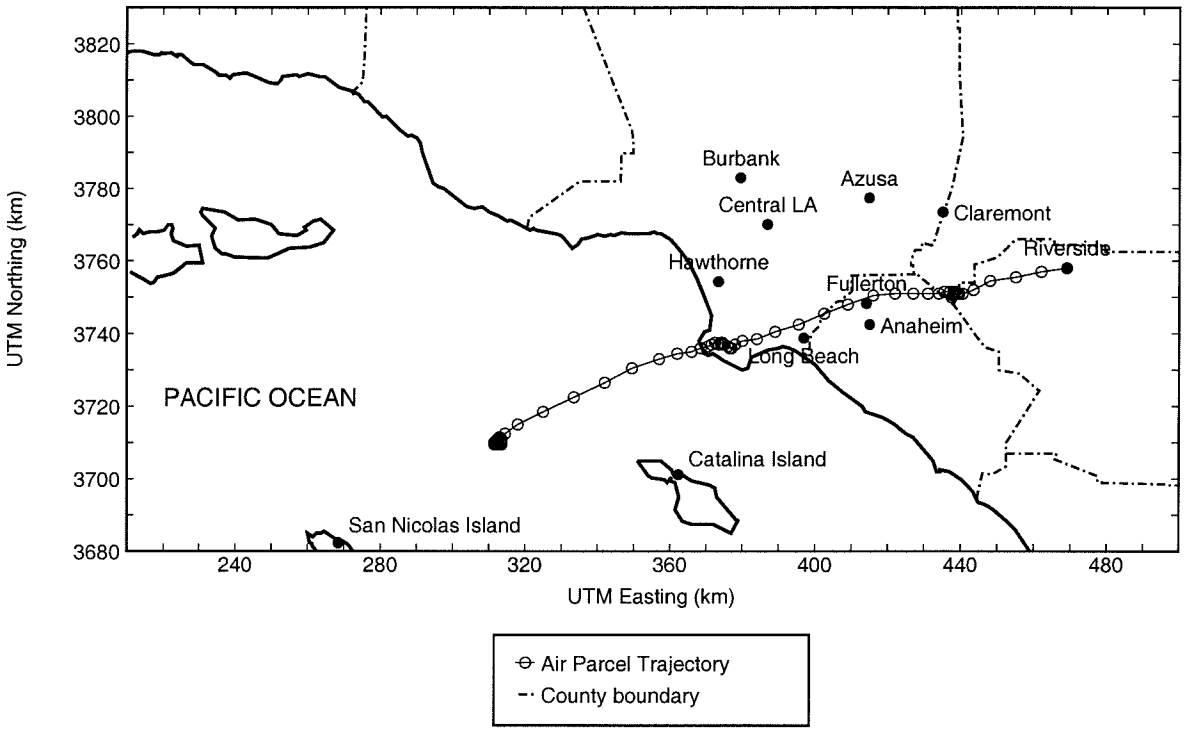

Figure 8.1:
Three day air parcel trajectory path terminating at Riverside, CA, at 1600 PST on September 25, 1996. The target air parcel passes over the Fullerton monitoring station at approximately 1600 PST on September 24, 1996, and just north of the Long Beach monitoring station at 1300 PST on September 24, 1996.

8.3.1 Emissions Model

In order to carry out a detailed simulation of air quality in an urban atmosphere, it is necessary to first characterize the anthropogenic pollutant emissions which serve in large part to drive the problem.

EMISSIONS OF VOC, NO_x, SO_x, CO, AND PM

Compilation of the emissions data for use with the model begins with spatially and temporarily resolved emissions inventories for the South Coast Air Basin of Southern California supplied by the South Coast Air Quality Management District (SCAQMD). An inventory describing the release of pollutants from mobile emissions sources specific to Sept. 21-26, 1996, first was produced using modeled traffic patterns and emissions factors predicted by the California Air Resources Board's emissions model EMFAC-7G. The description of pollutants released from area and general point sources begins with the 1995 average-day emissions inventory supplied by the SCAQMD. Many of the larger point sources for NO_x and SO_x in the South Coast Air Basin of Southern California are regulated under the RECLAIM emissions permit market program. Emissions from RECLAIM sources are described using the 1997 average-day inventory supplied by the SCAQMD.

The base emissions inventories described above list the hourly emissions rate of total volatile organic compounds mass (VOCs), NO_x, SO_x, CO, and particulate matter mass from the many hundreds of sources located in the South Coast Air Basin. Emissions of VOC mass within the base inventory next are further speciated into 28 explicit plus lumped organic compound categories using source-specific emissions profiles according to the treatment of Harley et al. [14, 15, 2]. Emissions of total suspended particulate matter mass released from each source are transformed into size- and composition-

resolved particulate emissions using the emissions model described by Eldering and Cass [4] and Kleeman et al. [5]. New source profiles that describe the size and composition distribution of fine particles emitted from catalyst-equipped gasoline-powered vehicles, non-catalyst-equipped gasoline-powered vehicles, diesel vehicles, meat smoke and wood smoke are employed in this work for the first time, based on source tests conducted for this purpose by Kleeman et al. [16, 17].

Emissions of Ammonia

Emissions of gas-phase ammonia in Southern California are important in the prediction of the amount of particulate ammonium nitrate formed in the ambient atmosphere. Since ammonia is not itself a regulated pollutant, accurate inventories describing the emissions of gas-phase ammonia generally are not available from state and local air pollution control agencies. Gharib and Cass [18] developed a comprehensive ammonia emissions inventory for the South Coast Air Basin of Southern California for the year 1982 that included contributions from 54 different source categories. In the present study, the emissions data for those sources which make significant contributions to daily ammonia emissions and which could potentially have changed since 1982 are updated to the year 1996.

Information describing the daily vehicle miles travelled (VMT) by catalyst-equipped light-duty vehicles within the SoCAB was used in conjunction with ammonia emissions rates measured by Fraser and Cass [19] to calculate the ammonia emissions from mobile sources during the study period. An increase in the daily vehicle miles travelled by light-duty catalyst-equipped vehicles between 1982 and 1996, coupled with a higher measured ammonia emissions factor result in a predicted ammonia emission rate of 30.7 tons day^{-1} from

the catalyst-equipped vehicle fleet in the South Coast Air Basin. This is significantly higher than the 2.4 tons day^{-1} of ammonia estimated to be released from catalyst-equipped light-duty vehicles in 1982.

Semi-annual fertilizer use statistics for the counties included within the South Coast Air Basin were obtained from the California Department of Food and Agriculture [20]. Calculations indicate that ammonia emissions from this source have decreased only slightly from 8.9 tons day^{-1} to 7.7 tons day^{-1} between 1982 and 1996.

Emissions from livestock waste decomposition were found to be the largest single source of ammonia in 1982, accounting for 52% of the ammonia released in the South Coast Air Basin in that year. In the present study, livestock head counts for the counties within the South Coast Air Basin were obtained from the 1992 Census of Agriculture [21]. Using the new livestock head counts and the methods of Gharib and Cass [18], ammonia emissions were recalculated for the mid 1990's. As was the case for fertilizer use, calculations indicate that emissions of ammonia from livestock waste decomposition have decreased only slightly from 84.9 tons day^{-1} to 77 tons day^{-1} between 1982 and the mid-1990's.

Emissions of Biogenic Hydrocarbons

Emissions of biogenic hydrocarbon vapors (i.e., those emitted from vegetation) in the study region were represented using the biogenic emissions inventory developed for the late August episode of the Southern California Air Quality Study. This inventory should be reasonably accurate since the amount and type of vegetation located in the South Coast Air Basin in the late summer and early fall likely does not change significantly from year to year.

8.3.2 Meteorological Inputs

Hourly data describing wind speed (29 sites), wind direction (29 sites), temperature (10 sites), relative humidity (10 sites), total solar radiation (4 sites) and ultraviolet solar radiation (1 site) were obtained from the routine measurements made by the South Coast Air Quality Management District. Supplemental data describing temperature (5 sites), relative humidity (5 sites), cloud cover (6 sites), and the presence of fog events (6 sites) at airports within the greater Los Angeles area were obtained from the National Climatic Data Center. Measurements of temperature and relative humidity also were collected at Long Beach, Fullerton and Riverside as part of the intensive air monitoring experiments conducted to describe this episode by Hughes et al. [6].

Interpolated surface meteorological fields with hourly time resolution were constructed over a grid system of 5 km by 5 km cells that covers the region shown in Figure 8.1 using the procedures developed by Harley et al. [2] and the interpolation scheme described by Goodin et al. [22]. Air parcel trajectories ending at target receptor sites then were back calculated through the resultant wind fields to their starting positions over the Pacific Ocean.

Hourly profiles of upper level wind speed, wind direction, and temperature measured using a lower atmospheric radar profiler located at Los Angeles International Airport (LAX) were obtained from the South Coast Air Quality Management District. Inversion base heights at inland locations were calculated from the vertical temperature profile measured at LAX and the interpolated surface temperature at each grid cell of interest using Holtzworth's method [23]. Overnight inversion base heights throughout the study period were typically quite high (on the order of 100-500 m). As a result, model predictions for ambient pollutant levels during the evening hours are

lower than they would be if surface-based temperature inversions had occurred at night.

ATMOSPHERIC MIXING AT NIGHT

Atmospheric mixing during the evening hours is reduced as wind speeds decrease and the ground radiates energy to space. Under these conditions, the original versions of the CIT trajectory and airshed models predict very little mixing in the atmosphere. The formulation of the vertical mixing algorithm in these models [24] was developed based largely on experiments conducted in sparsely populated locations and does not account for the additional atmospheric mixing in urban areas caused by urban heat island effects and mechanical mixing generated by vehicle traffic and other activity in the city. In an effort to better paramaterize the mixing caused by these urban effects, the algorithm used to calculate vertical turbulent diffusivity coefficients in the current model application was modified to enforce a neutral to slightly unstable mixing condition up to the base of the elevated temperature inversion during the night. This ensures that emissions of atmospheric pollutants become mixed to the height of the base of the elevated temperature inversion over a reasonable time scale.

8.3.3 Initial Conditions

Measurements of background gas- and particle-phase pollutant concentrations over the Pacific Ocean were made for the purpose of specifying the initial conditions at the start of the air parcel trajectories studied here. The size and composition distribution of the airborne particles was measured upwind of the study area at Santa Catalina Island on September 21-22, 1996, using filter-based samplers and MOUDI impactors as described by Hughes et al. [6]. Ozone concentrations at Santa Catalina Island were measured using a

Table 8.1: Gas Phase Pollutant Concentrations Measured at Santa Catalina Island between September 21-22, 1996

Species	Concentration [ppb]
HNO_3	0.0
NH_3	0.4
SO_2	0.1
O_3	57.0
CO	117.0
Methane	1836.0
Ethane	0.9
Ethene	0.2
Propane	0.4
Propene	0.2
Acetylene	0.5
Benzene	0.1
Isoprene	0.2
Formaldehyde[a]	0.8
Acetaldehyde[a]	0.7
Higher Aldehydes[a]	1.4

[a] aldehyde concentrations are the average of measurements made at San Nicolas Island in September, 1993, by Grosjean et al. [25].

Dasibi model 1003 photometric ozone monitor. An instantaneous grab sample of the organic vapor composition of the atmosphere at Santa Catalina Island also was obtained in a 6 L stainless steel cannister which was then analyzed for total non-methane organic compounds and individual gas-phase organic compounds. Concentrations of aldehydes in the background atmosphere were estimated based on data collected during September of 1993 at San Nicolas Island [25]. Gas-phase pollutant concentrations in the offshore background air are shown in Table 8.1

It is assumed in the current analysis that coarse particles composed of sodium chloride generated through the action of breaking waves exist separately in the atmosphere from the smaller sulfur-containing particles, as shown in Figure 8.2. Therefore, the trajectory model is supplied with an externally mixed aerosol as its initial condition. Trajectory model simulations are initialized over the Pacific Ocean with fine sulfur-containing background particle concentrations as measured at the Santa Catalina Island sampling site on September 21-22 with their size distributions shaped according to measurements made near the coast at Long Beach on the day of interest in the current analysis, which is September 24, 1996. The size-resolved particle concentrations shown in Figure 8.2 are stated in terms of particle physical diameter after having transformed cascade impactor data based on an assumed particle density of 1.7 g cm^{-3}.

Background sodium chloride particles are injected into each trajectory air mass it crosses the surf zone at the coast, since this is where particle generation by breaking waves will be most pronounced. As described by Hughes et al. [6], a fine particle cyclone separator was operated upstream of each MOUDI impactor to prevent particles larger than 1.8 μm particle diameter from entering the instrument to reduce particle bounce within the impactor. Coarse particle sodium, chloride, and nitrate values shown in Figure 8.2 at sizes greater than 1.8 μm are based on the difference between fine particle vs total suspended particulate filter samples taken at Santa Catalina Island with concentrations distributed approximately evenly between 1-10 μm particle diameter for lack of any more detailed size distribution data for coarse particles.

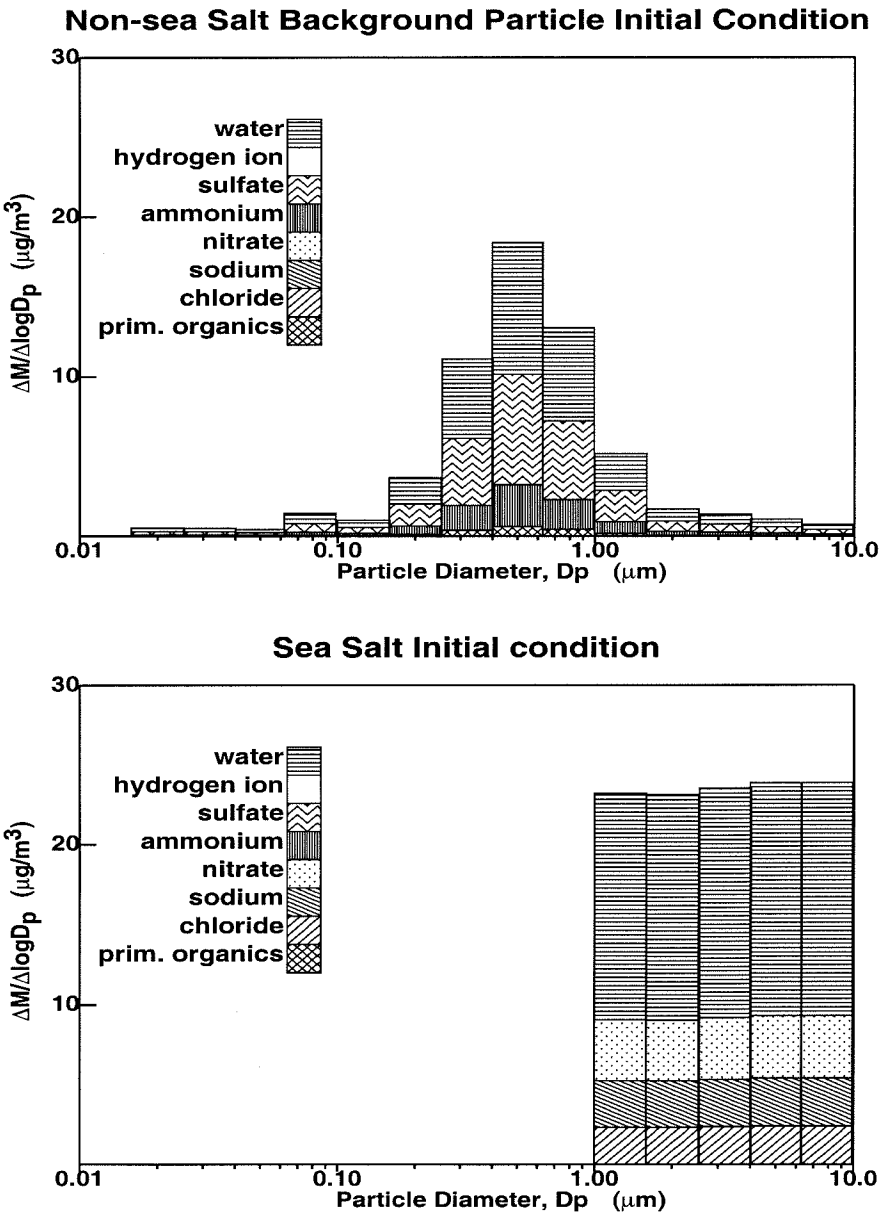

Figure 8.2:
Model initial conditions based on ambient particle size and composition distributions measured at Santa Catalina Island between September 21-22, 1996.

8.4 Model Results

In this section, model results are presented for the September 24, 1996, episode at Long Beach, CA, the September 24, 1996, episode at Fullerton, CA, and the September 25, 1996, episode at Riverside, CA. Intensive particle-phase and gas-phase ambient measurements were collected at Long Beach, Fullerton and Riverside between 600-1000 PST, 1000-1400 PST, and 1400-1800 PST respectively on each day under consideration. Model predictions will be compared to ambient measurements of bulk particle chemical composition, size-distributed particle-phase chemical composition, and gas-phase pollutant concentrations. The predicted contribution which different source categories make to the size and composition distribution of airborne particles at each of the monitoring sites also will be examined.

8.4.1 Bulk Particle-Phase Species

The time series of predicted fine particle mass concentrations and chemical composition at Long Beach, CA, on September 24, 1996, Fullerton, CA, on September 24, 1996, and Riverside, CA, on September 25, 1996, are shown in Figures 8.3, 8.4 and 8.5 respectively. The predicted mass of airborne particles with diameters smaller than 1.8 μm (PM1.8) matches the observed particle mass concentrations well, with a general increase in mass concentrations as air parcels move further inland. As expected, model predictions for the mass of airborne particles with diameters less than 10 μm (PM10) are smaller than the observed mass of total suspended particulate matter (TSP).

Model predictions for PM1.8 sulfate ($SO_4^=$) almost exactly match ambient measurements at all sites. Concentrations of $SO_4^=$ aerosol are relatively constant at approximately 8 μg m^{-3} at all sampling sites. This confirms the results of previous studies which show that the majority of the sulfate aerosol

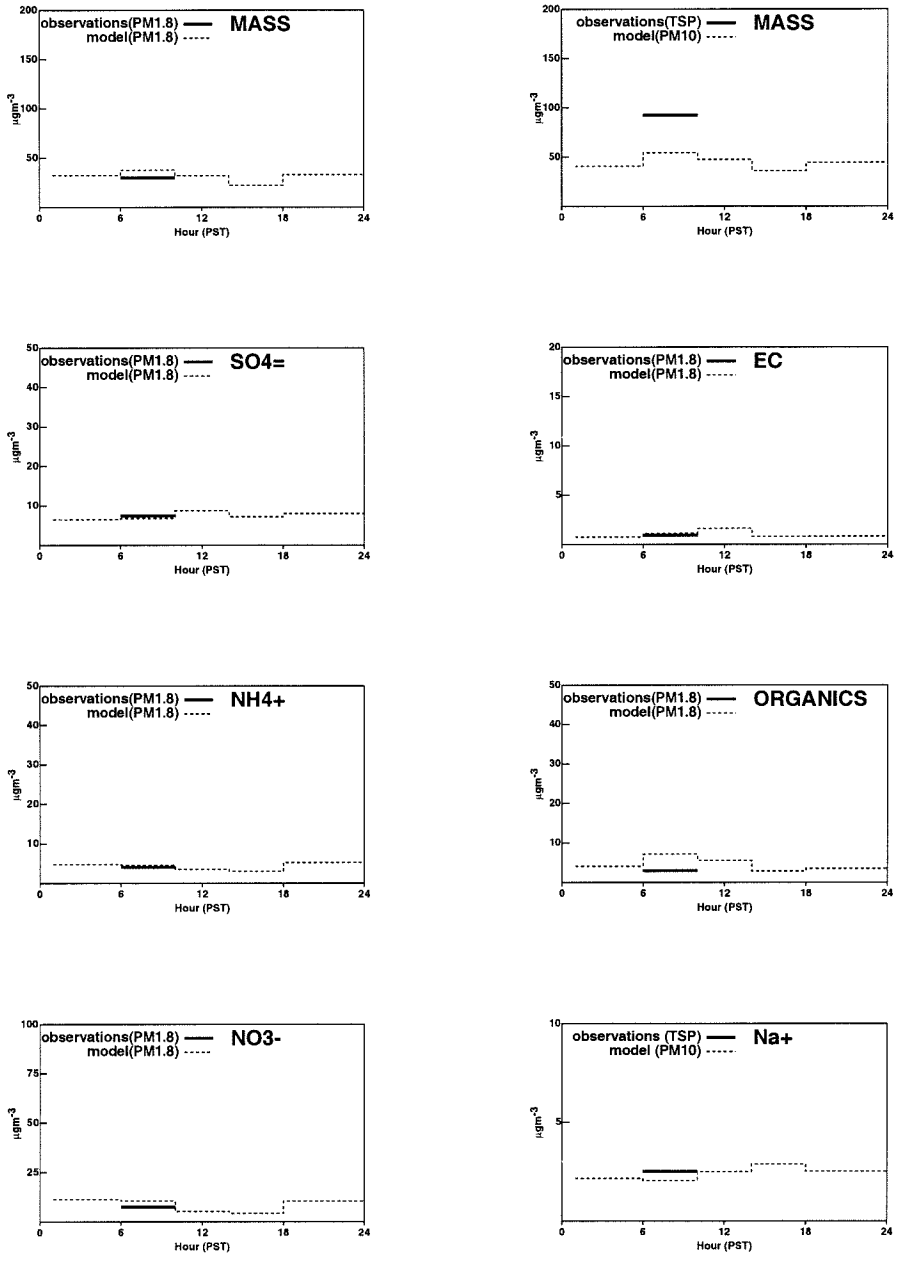

Figure 8.3:
Model predictions vs observations for total mass of particles with diameter less than 1.8 μm, total suspend particulate mass vs model PM10 mass, sulfate, ammonium ion, nitrate, sodium, elemental carbon, and organic compounds at Long Beach, CA, on September 24, 1996.

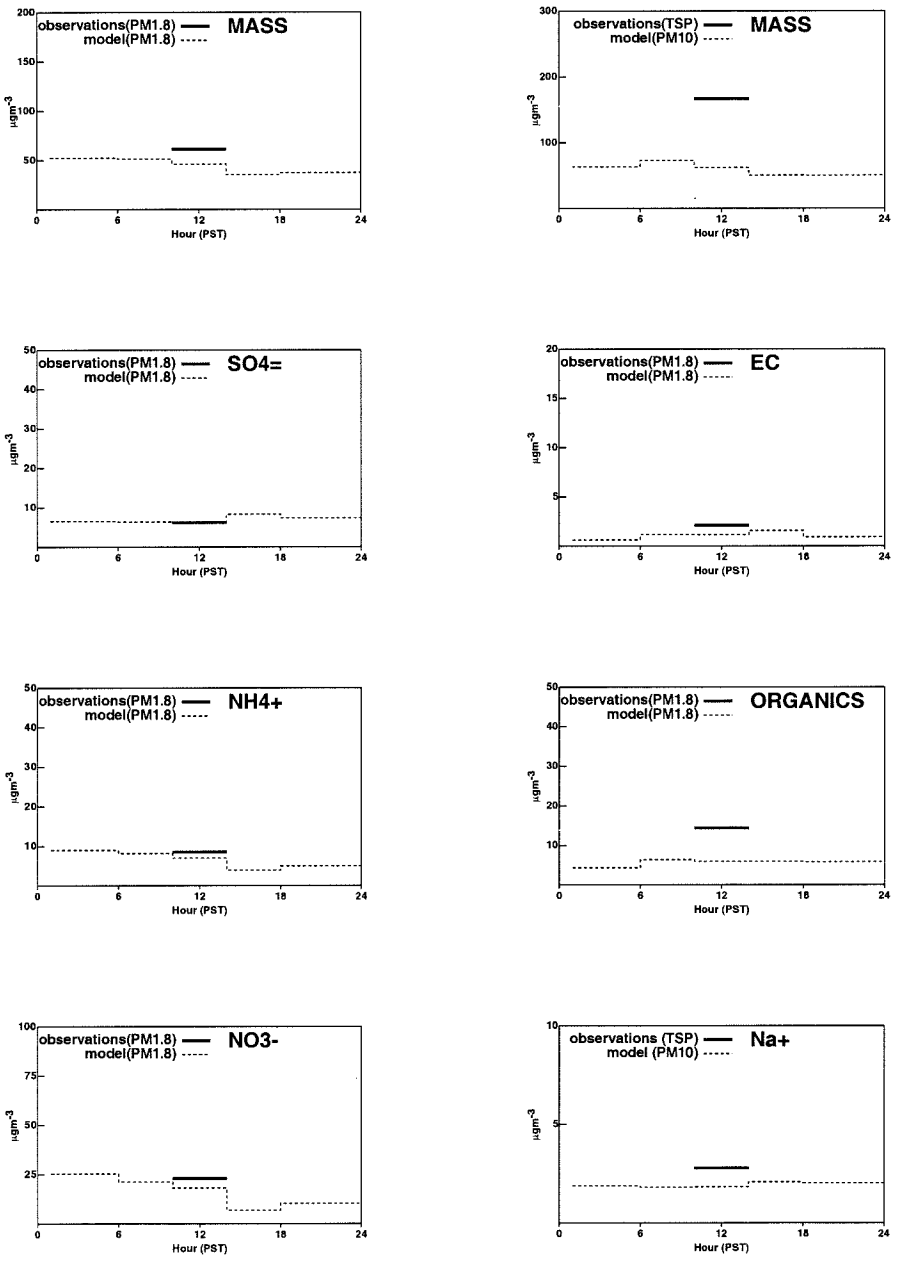

Figure 8.4:
Model predictions vs observations for total mass of particles with diameter less than 1.8 μm, total suspend particulate mass vs model PM10 mass, sulfate, ammonium ion, nitrate, sodium, elemental carbon, and organic compounds at Fullerton, CA, on September 24, 1996.

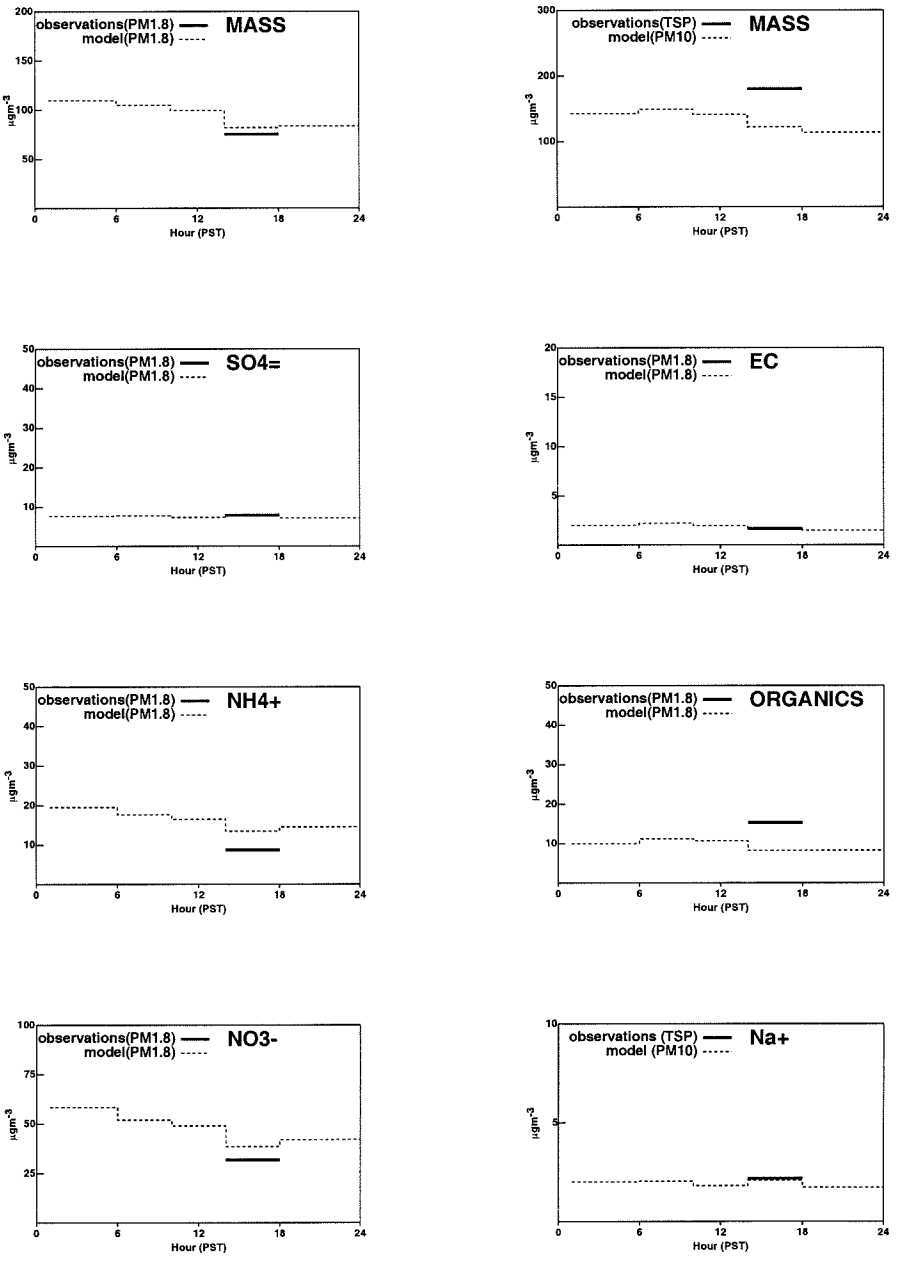

Figure 8.5:
Model predictions vs observations for total mass of particles with diameter less than 1.8 μm, total suspend particulate mass vs model PM10 mass, sulfate, ammonium ion, nitrate, sodium, elemental carbon, and organic compounds at Riverside, CA, on September 25, 1996.

in the Los Angeles area in recent years is advected into the urban region from over the Pacific Ocean [7, 8]. The trend reflects the strict controls on SO_2 emissions which have been adopted in the South Coast Air Basin.

Predicted concentrations of ammonium ion (NH_4^+) and nitrate ion (NO_3^-) contained in particles with diameters smaller than 1.8 μm at Long Beach and Fullerton match observations at each of those sites very well. Calculated and observed concentrations of PM1.8 NH_4^+ and NO_3^- are seen to increase as air parcel trajectories proceed inland. Predictions of PM1.8 NH_4^+ and NO_3^- at Riverside are slightly above observed values. To reach the Riverside sampling site, air parcel trajectories must traverse an agricultural area in western Riverside and San Bernardino counties. High emissions of ammonia and sharp concentration gradients occur in that area due to the presence of dairy farms and other similar activities, making it difficult to predict ammonium nitrate concentrations farther downwind.

Model predictions for aerosol sodium (Na^+) contained in particles with diameters less than 10 μm (PM10) closely match measured values of total suspended particulate (TSP) sodium at all three sampling sites. Airborne particles containing sodium are produced almost exclusively by the action of breaking waves at the coast. As described in Section 8.3.3, background TSP Na^+ concentrations measured at Santa Catalina Island are used to define the model PM10 Na^+ initial condition that is injected into each air parcel as it crosses the coastline. This leads to good agreement between model PM10 predictions and measured TSP Na^+ concentrations at inland receptor sites. As was the case for particulate sulfate, concentrations of Na^+ at all three air quality monitoring sites are relatively constant over time, reflecting the widespread background source for this aerosol constituent.

Observed values of elemental carbon (EC) contained in particles with

diameters less than 1.8 μm (PM1.8) show good agreement with model predictions of PM1.8 EC at the Long Beach and Riverside sampling sites, with a slight over-prediction at the Fullerton sampling site. Atmospheric concentrations of EC are less than 3 μg at all locations, with little trend observed between coastal versus inland receptor sites. EC is not formed in the atmosphere but rather is directly emitted from anthropogenic sources (primarily diesel engines), mixed vertically by turbulent diffusion, and removed at the earth's surface by dry deposition processes. The ability of the model to accurately predict ambient EC concentrations verifies the performance of the emissions inventories and transport algorithms used in the current study.

Model predictions of organic compound (ORGANICS) concentrations contained in particles with diameters smaller than 1.8 μm (PM1.8) are higher than observed values at the Long Beach sampling site and lower than observed values at the Fullerton and Riverside sampling sites. PM1.8 ORGANICS concentrations measured with quartz fiber filters are expected to differ from model calculations since it is generally recognized that 20-30% of the organic material collected by quartz fiber filters is affected by adsorption or desorption of gas-phase organic species.

8.4.2 Impactor Measurements

The predicted size distribution of the major particle-phase chemical species is shown along with impactor measurements made at Long Beach, CA, between 600-1000 PST on September 24, 1996, Fullerton, CA, between 1000-1400 PST on September 24, 1996, and Riverside, CA, between 1400-1800 PST on September 25, 1996, in Figures 8.6, 8.7 and 8.8 respectively. Measurements of the size distribution of aerosol components are only available below 1.8 μm particle diameter since a cyclone separator was used upstream of

each impactor [6]. The measured size distributions shown in each subplot of Figures 8.6-8.8 have been converted from aerodynamic diameter to particle physical diameter according to an assumed particle density of 1.7 μg cm^{-3}.

Because two impactors (one loaded with aluminum substrates and one loaded with Teflon substrates) were operated at each monitoring station, there are two independent measurements of the size distribution of ambient particle mass available for comparison to model predictions. Mass distributions measured with impactors are more accurate at higher particle concentrations because the analysis method employed involves calculating the difference between impactor substrate weights before and after sampling. In conditions where airborne particulate concentrations are low (typical at coastal locations), this mass difference may be very small and thus hard to measure accurately.

In the particle diameter ranges considered (0.01-1.8 μm), a single mode between 0.2-0.8 μm particle diameter is observed in the ambient mass distribution at all monitoring stations. Particle mass concentrations increase towards the eastern end of the air basin. Model predictions for the size distribution of suspended particle mass match this trend well. Both the location and magnitude of the predicted peak in the particle mass distribution at Riverside (the most polluted site) match that feature of the size distribution measured by both impactors very accurately. At the Long Beach and Fullerton sampling sites (where lower particle concentrations lead to greater uncertainty in impactor mass measurements) model predictions for the size distribution of aerosol mass show reasonable agreement with impactor measurements.

Ambient concentrations of particulate sodium (Na^+) peak at sizes above 1 μm particle diameter because these particles are generated by mechanical

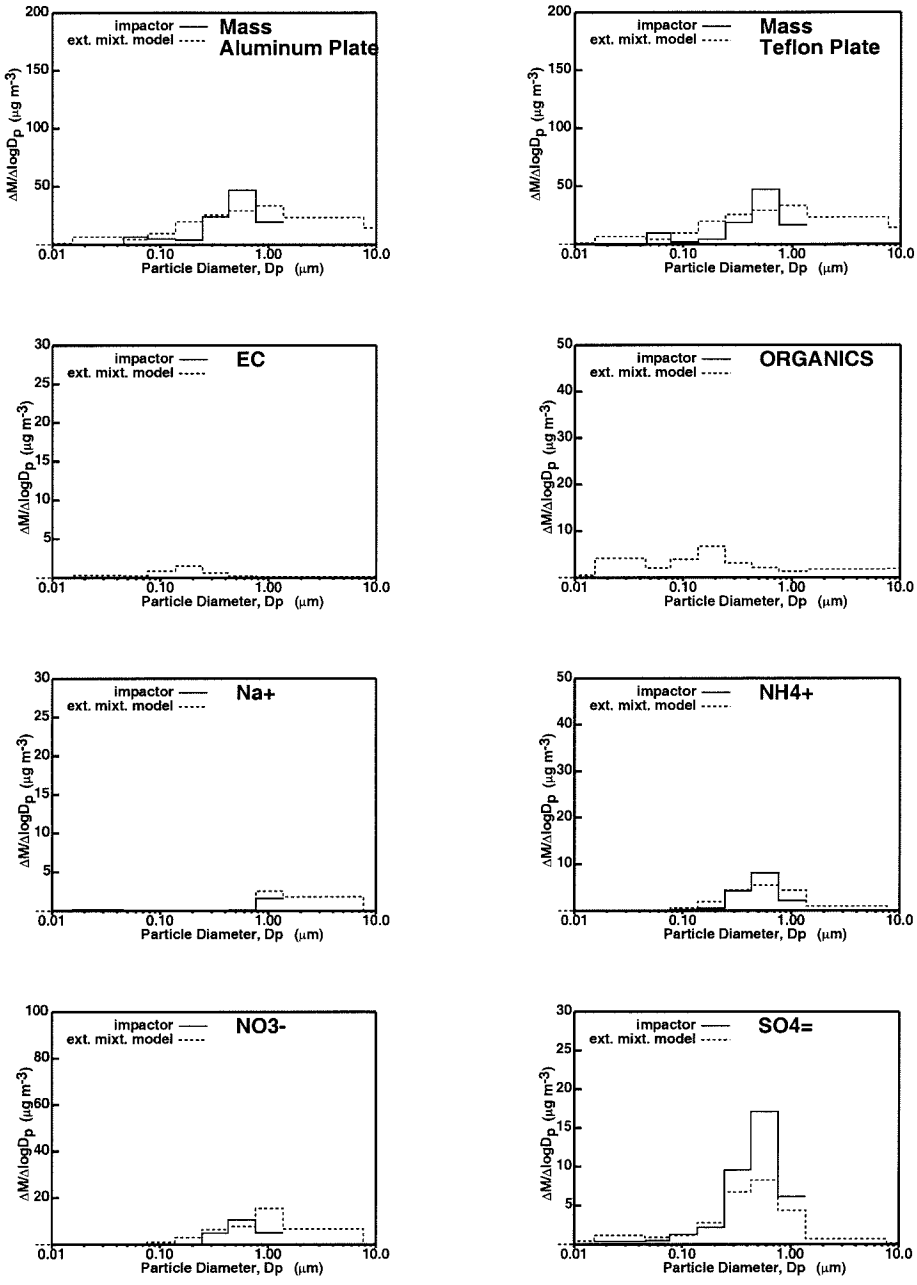

Figure 8.6:
Model predictions vs observations for the size distribution of particle-phase mass, elemental carbon, organic compounds, sodium, ammonium ion, nitrate, and sulfate at Long Beach, CA, on September 24, 1996, between 600-1000 PST.

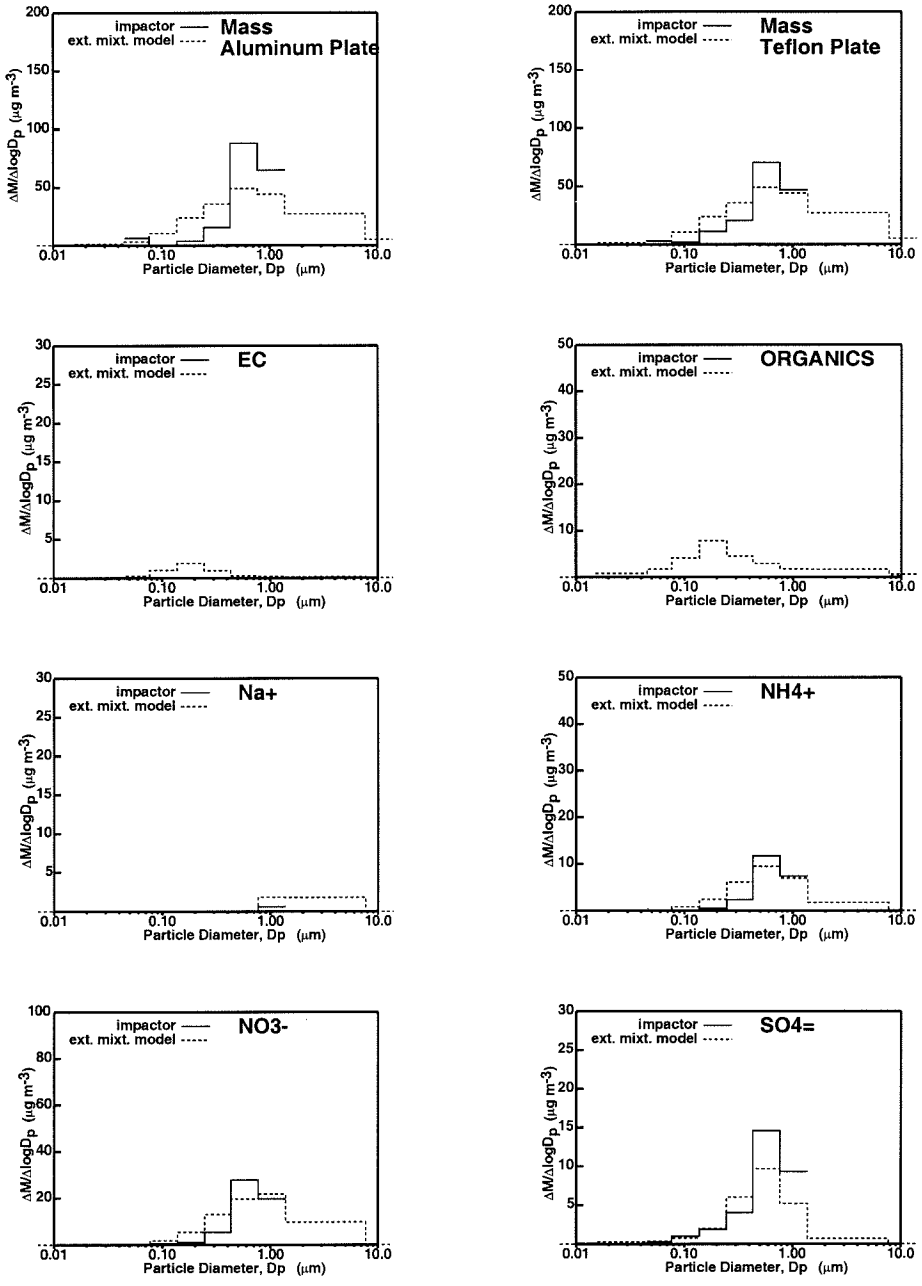

Figure 8.7:
Model predictions vs observations for the size distribution of particle-phase mass, elemental carbon, organic compounds, sodium, ammonium ion, nitrate, and sulfate at Fullerton, CA, on September 24, 1996, between 1000-1400 PST.

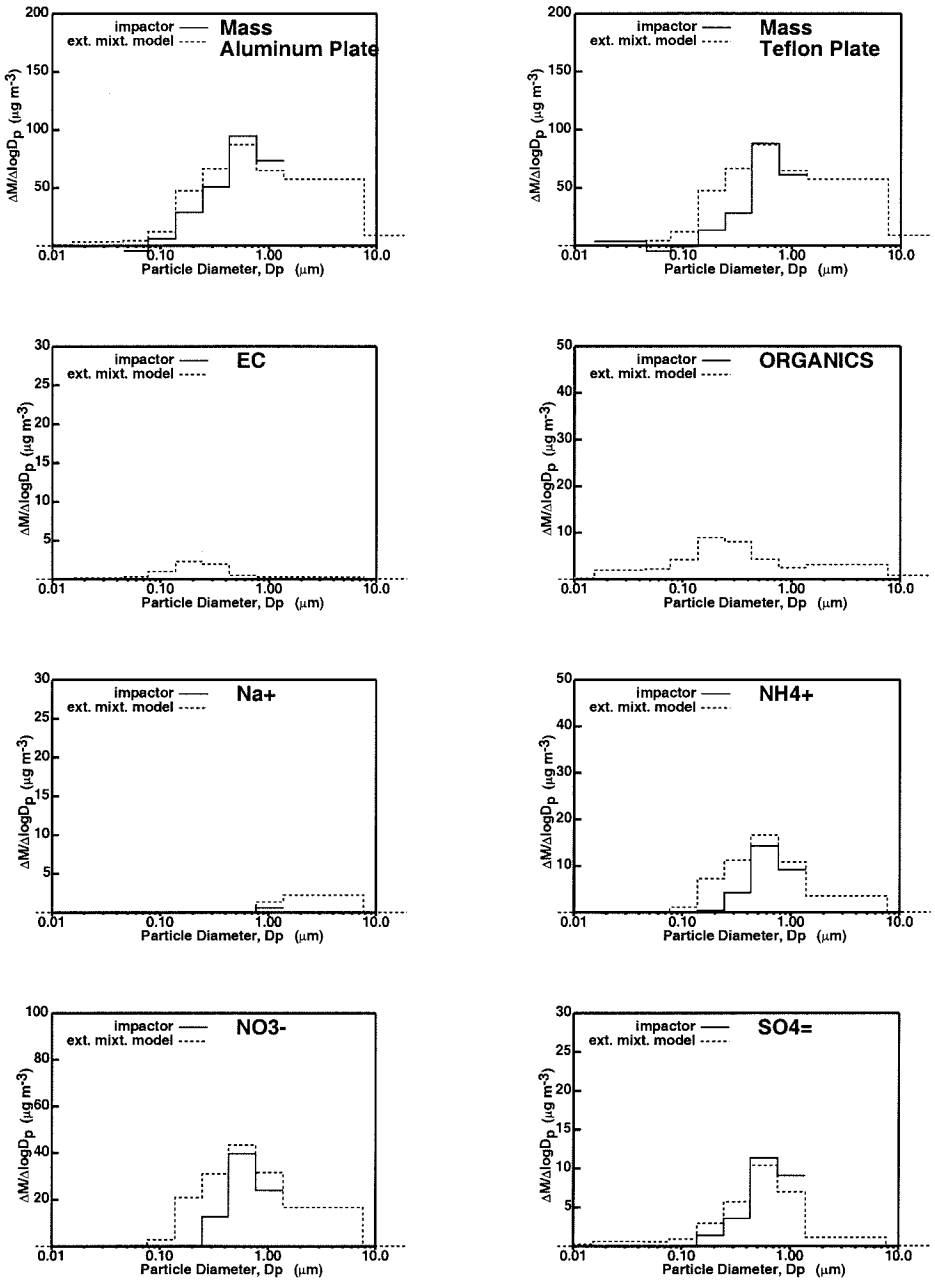

Figure 8.8:
Model predictions vs observations for the size distribution of particle-phase mass, elemental carbon, organic compounds, sodium, ammonium ion, nitrate, and sulfate at Riverside, CA, on September 25, 1996, between 1400-1800 PST.

forces (breaking waves). Since impactor measurements do not extend beyond approximately 1.8 μm particle diameter, only the smallest particles within the measured size distribution of particulate Na^+ may be compared to model predictions. These data show that model calculations slightly over-predict Na^+ concentrations in particles with diameters between 0.8-1.5 μm for all monitoring stations. The results shown in Figures 8.3, 8.4, and 8.5 indicate that the total amount of Na^+ predicted to be in the atmosphere generally matches the total amount of Na^+ measured using filter-based samplers. This suggests that the shape of the size distribution shown in Figure 8.2 for background sea salt particles should be adjusted to reduce the concentration of particles with diameters between 1-2 μm and to increase the concentrations of particles with larger diameters.

Model results for both particulate nitrate (NO_3^-) and ammonium ion (NH_4^+) size distributions show good agreement with impactor measurements at each of the monitoring sites. The size distributions of NH_4^+ and NO_3^- at all receptor sites have a single mode which peaks between 0.3-1.0 μm particle diameter. The magnitude of the peak in the measured distribution of particulate NH_4^+ and NO_3^- generally increases as the air parcels move farther inland, and is highest at the Riverside sampling site which is downwind of a major source of ammonia emissions.

Model predictions for the size distribution of particulate sulfate ($SO_4^=$) are dominated by background particles advected into the study region. As discussed in Section 8.3.3, the initial condition of background sulfate particles is based on measurements made at Santa Catalina Island on September 21-22, 1998, shaped according to the size distribution measured at Long Beach, CA, on September 24, 1998. The shape of the size distribution of particulate $SO_4^=$ matches the distribution of $SO_4^=$ measured by impactors at all three mon-

itoring stations, with a single mode between 0.3-0.8 μm particle diameter. The predicted magnitude of the peak in the size distributions at Fullerton and Riverside matches observations well, but is slightly below the impactor measurement at the Long Beach sampling site. Since the model predictions for PM1.8 $SO_4^=$ concentrations at Long Beach match filter-based measurements well (see Figure 8.3), it is possible that the impactor measurements are biased slightly high.

Concentrations of elemental carbon (EC) and organic compounds (ORGANICS) measured on impactor substrates are not available for comparison to model predictions because they have not yet undergone a correction for pyrolysis effects as discussed in [17]. Model calculations for the size distribution of particulate EC show a single mode between 0.1-0.3 μm particle diameter at Long Beach and Fullerton, and between 0.1-0.5 μm particle diameter at Riverside. This result is consistent with the size distribution of EC emissions from diesel engines. The ambient size distribution of particulate ORGANICS predicted by model calculations shows a single mode between 0.1-0.4 μm particle diameter at the Fullerton and Riverside sampling sites. At the Long Beach sampling site, a bimodal shape is predicted for the size distribution of particulate ORGANICS, with the smaller mode predicted between 0.01-0.05 μm particle diameter, and the larger mode between 0.1-0.3 μm particle diameter.

8.4.3 Gas-Phase Species

The time series of predicted gas-phase pollutant concentrations at Long Beach, CA, on September 24, 1996, Fullerton, CA, on September 24, 1996, and Riverside, CA, on September 25, 1996, are shown in Figures 8.9, 8.10 and 8.11 respectively. Continuous measurements of ozone (O_3) and nitrogen

dioxide plus those species that are measured as if they were NO_2 by chemiluminescent NO_x monitors (NO_2^*) are available throughout each day, while measurements of nitric acid (HNO_3) and ammonia (NH_3) concentrations are available during the four-hour intensive monitoring sessions carried out at each station. Measurements of O_3 and NO_2^* at the "Fullerton" site shown in Figure 8.10 were actually taken at the nearby Anaheim air monitoring station maintained by the South Coast Air Quality Management District (see Figure 8.1).

Peak concentrations of ozone (O_3) measured at all three monitoring sites occur during the early afternoon hours of each sampling period. Peak O_3 concentrations at Long Beach and Fullerton are predicted well by model calculations, while O_3 concentrations at Riverside are under-predicted between 1400-1600 PST on September 25, 1996, when measurements indicate that the peak should have occurred. Analysis of the trajectory paths back calculated from the Riverside sampling site show that the air parcels which arrive at Riverside between 1400-1600 PST on September 25, 1996, stagnated over a large NO_x source during a previous evening. If these trajectories had passed a few kilometers to either side of this large point source (an outcome which is well within the range of uncertainties on the actual path followed by the air parcel), then the O_3 profiles shown in Figure 8.11 would likely match observations well.

Predicted concentrations of nitrogen dioxide and related species ($NO_2^* = NO_2 + HNO_3$) at Long Beach and Fullerton are roughly equal at 50 ppb. Measurements of NO_2^* are not available at Long Beach or Fullerton, but measurements of NO_2^* taken at Anaheim show reasonable agreement with predictions at the nearby Fullerton monitoring station. Predicted concentrations of NO_2^* at Riverside are higher than measured values. This trend

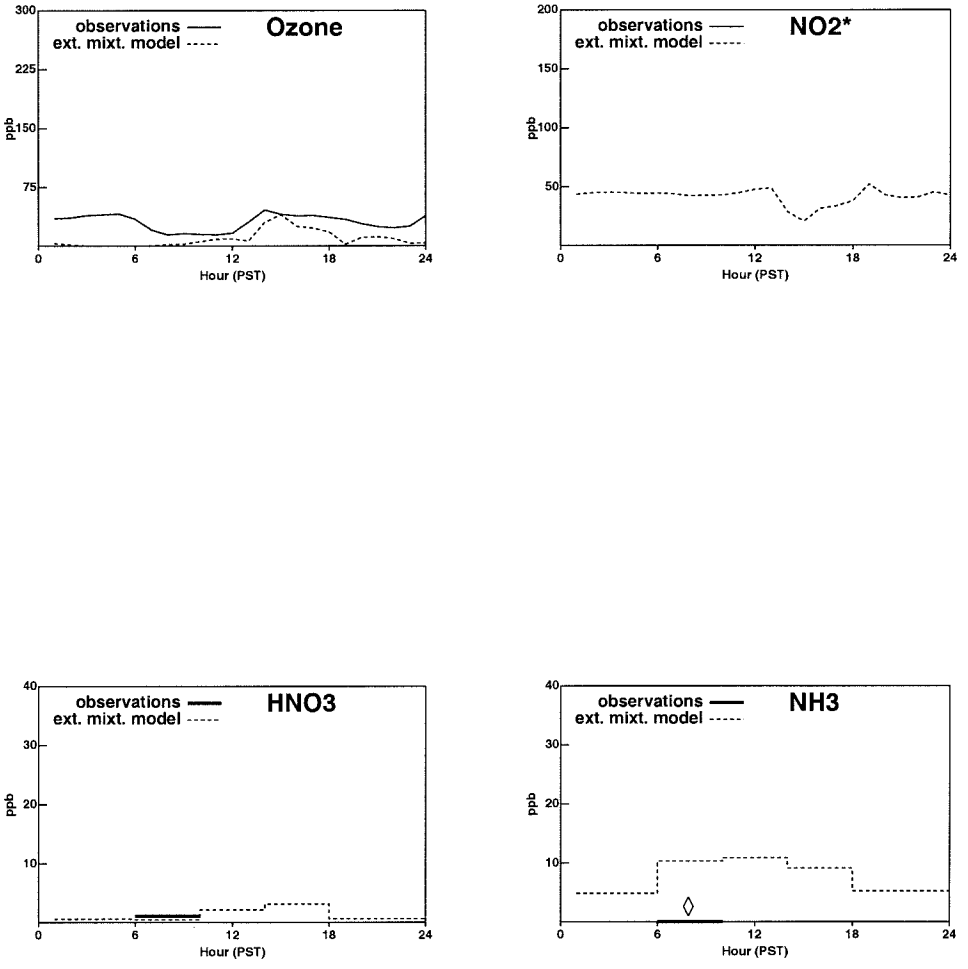

Figure 8.9:
Model predictions vs observations for ambient concentrations of O_3, NO_x, HNO_3, and NH_3 at Long Beach, CA, on September 24, 1996. Values marked with a $\diamond$ show inconsistencies with other measurements.

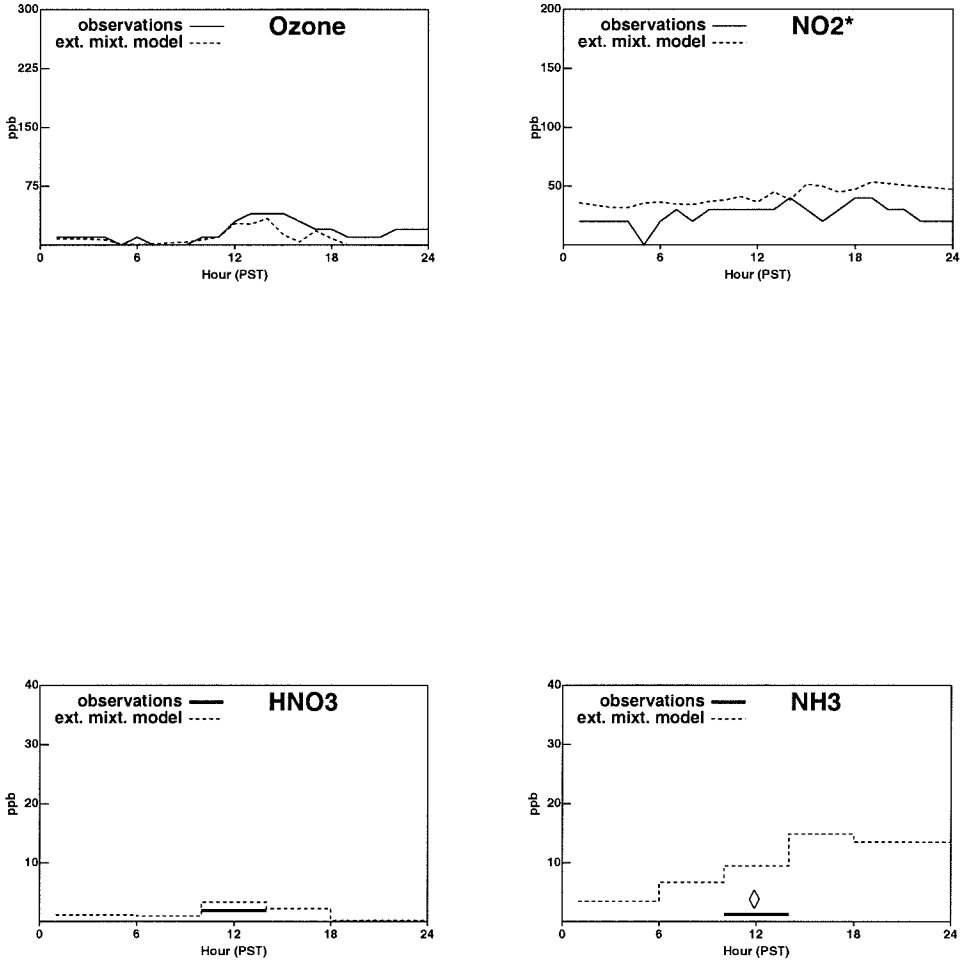

Figure 8.10:
Model predictions vs observations for ambient concentrations of O_3, NO_x, HNO_3, and NH_3 at Fullerton, CA, on September 24, 1996. Values marked with a $\diamond$ show inconsistencies with other measurements.

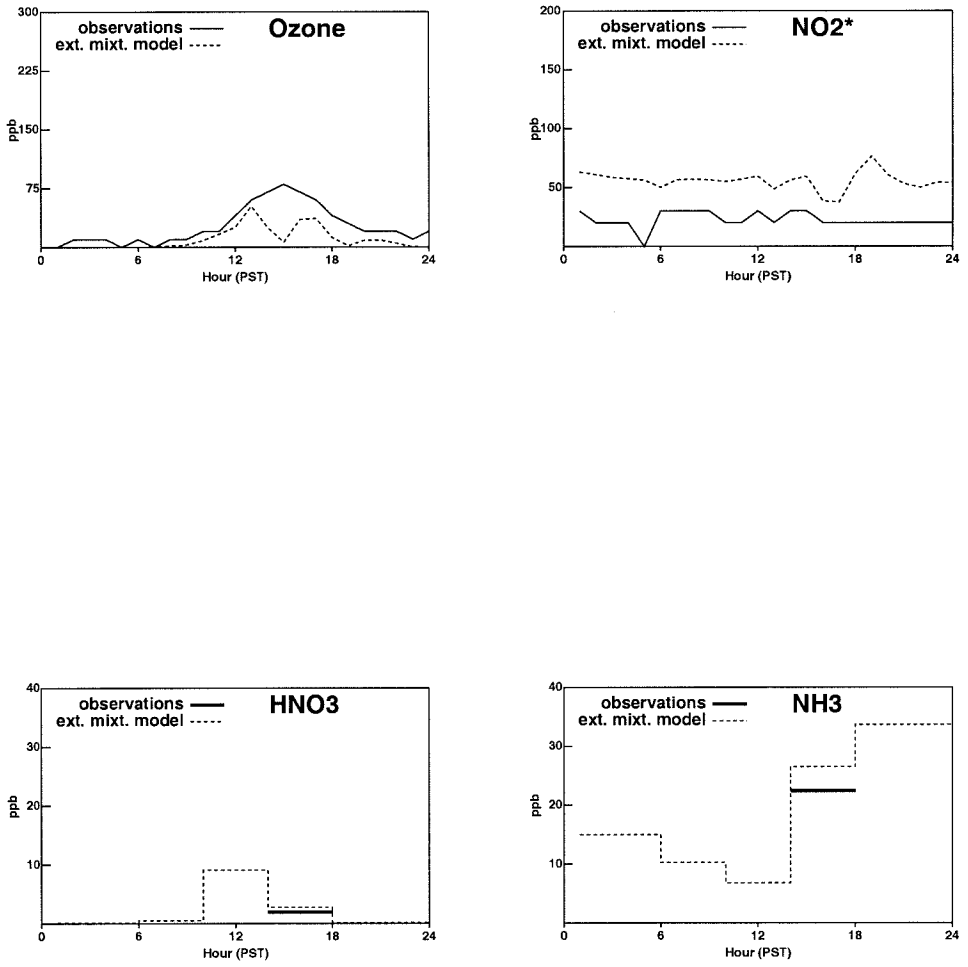

Figure 8.11:
Model predictions vs observations for ambient concentrations of O_3, NO_x, HNO_3, and NH_3 at Riverside, CA, on September 25, 1996.

is consistent with the suppression of the O_3 concentrations discussed above, and is caused by emissions of NO_x from large point sources around the Los Angeles harbor.

Predicted concentrations of gas-phase nitric (HNO_3) acid show good agreement with measured values at all of the target receptor sites. Likewise, predicted concentrations of ammonia (NH_3) at Riverside show good agreement with measured values. NH_3 concentrations at Riverside are very high because this site is located downwind of dairies and farming operations which have large NH_3 emissions. Measurements of ammonia (NH_3) at Long Beach and Fullerton are very close to zero, while model predictions for NH_3 are greater than zero. These NH_3 measurements are inconsistent with coincident filter-based measurements which indicate that particle-phase ammonium nitrate was present in the atmosphere at both Long Beach and Fullerton at the times of interest. The observed concentration product for NH_3 * HNO_3 is 0 ppb^2 and 2 ppb^2 at Long Beach and Fullerton, respectively. These values are well below the concentration product necessary to form particle-phase ammonium nitrate at the temperatures and relative humidities recorded during the sampling period, yet filter-based and impactor measurements indicate that ammonium nitrate aerosol was present. Model results which match the measurements for particulate ammonium, particulate nitrate, and gas-phase nitric acid vapor well, predict gas-phase NH_3 concentrations of 10.3 ppb and 4.5 ppb at Long Beach and Fullerton respectively.

8.4.4 Source Contributions to Ambient Particle Concentrations

One of the primary advantages of the mechanistic air quality model used in the present study is that it can separately quantify the size and composition distribution of particles released from different sources as they reach a down-

wind receptor site. Figures 8.12, 8.13 and 8.14 show the predicted size and composition distribution of particles originally released from crustal sources (other than paved road dust), paved road dust, diesel engines, food cooking operations, non-catalyst-equipped gasoline-powered engines, catalyst-equipped gasoline-powered engines, high sulfur content fuel combustion, other primary particle sources, and background particles advected into the study region at the Long Beach, Fullerton, and Riverside sampling stations respectively. The concentrations shown in each figure represent the 24 hour average for each day of interest.

Figures 8.12-8.14 show that primary particles released from paved road dust and crustal sources other than paved road dust have a mass distribution which peaks at particle diameters larger than 2.5 μm. Little secondary aerosol nitrate or sulfate is predicted to be associated with the large and generally hydrophobic particles emitted from these sources. Particles emitted from diesel engines and non-catalyst-equipped gasoline-powered engines are predicted to contribute significantly to the ambient particle size and composition distribution between 0.1-0.3 μm particle diameter. Particles originally released from diesel engines account for most of the elemental carbon predicted to be in the atmosphere. Particles originally released from both diesel engines and non-catalyst-equipped gasoline engines are seen to accumulate significant coatings of ammonium nitrate, especially at the Riverside sampling site.

Calculations indicate that primary particles originating from catalyst-equipped gasoline engines and sulfur bearing particles from fuel combustion and industrial processes make only very minor contributions to ambient particulate concentrations at the Long Beach, Fullerton, and Riverside receptor sites.

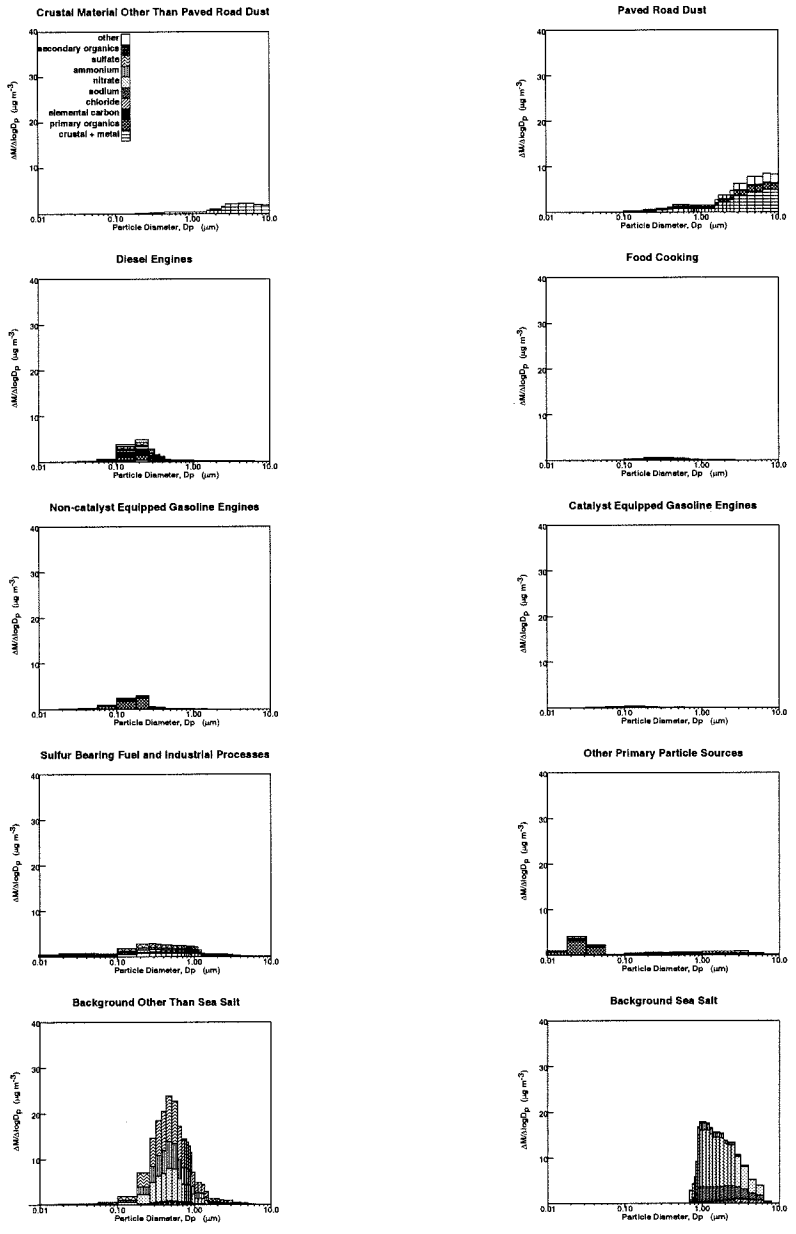

Figure 8.12:
Individual source contributions to the airborne particle size and chemical composition distribution at Long Beach, CA, averaged over each hour of the day on September 24, 1996. Each subplot shows the primary seed particles originally released from the indicated source along with the gas-to-particle conversion products that have accumulated on those seed particles between their time of release to the atmosphere and their arrival at the receptor site.

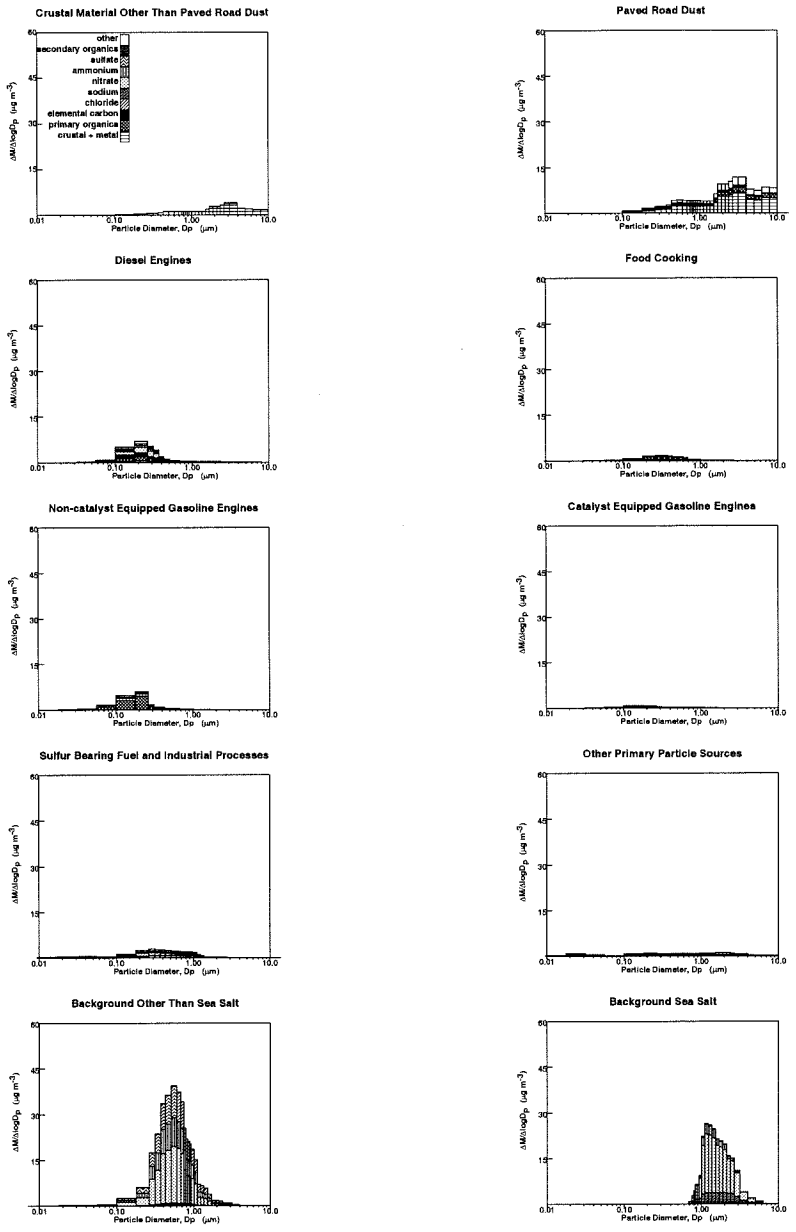

Figure 8.13:
Individual source contributions to the airborne particle size and chemical composition distribution at Fullerton, CA, averaged over each hour of the day on September 24, 1996. Each subplot shows the primary seed particles originally released from the indicated source along with the gas-to-particle conversion products that have accumulated on those seed particles between their time of release to the atmosphere and their arrival at the receptor site.

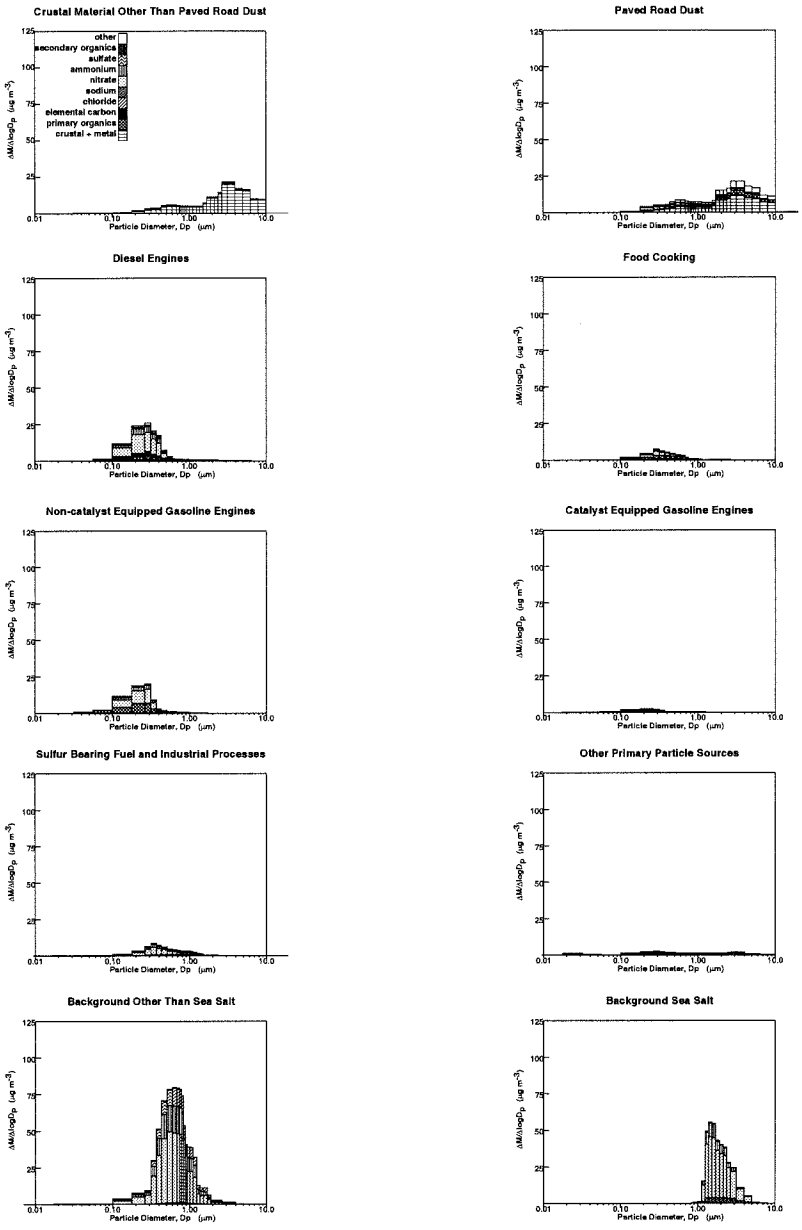

Figure 8.14:
Individual source contributions to the airborne particle size and chemical composition distribution at Riverside, CA, averaged over each hour of the day on September 25, 1996. Each subplot shows the primary seed particles originally released from the indicated source along with the gas-to-particle conversion products that have accumulated on those seed particles between their time of release to the atmosphere and their arrival at the receptor site.

Background particles which are advected into the study region and then transformed by gas-to-particle conversion processes occurring in the urban atmosphere are predicted to make a major contribution to PM2.5 concentrations at all three sampling sites. Water-soluble sulfate-containing background particles (other than sea salt) are predicted to accumulate large amounts of secondary ammonium and nitrate during transit from the ocean across the urban area to Fullerton and Riverside, making the single largest contribution to ambient PM2.5 concentrations during the study period. This result is consistent with the findings summarized in Chapter 4 in which it was observed that for cases where primary particle concentrations are relatively low, significant secondary aerosol formation occurs on the non-sea salt sulfate-containing background particles advected into the South Coast Air Basin from over the Pacific Ocean. In addition, sea salt particles advected into the study region are predicted to be completely transformed by chemical reaction from sodium chloride to produce sodium nitrate.

The predicted source contributions to 24-hour average PM2.5 particulate matter concentrations at Long Beach on September 24, 1996, Fullerton on September 24, 1996, and Riverside on September 25, 1996, are shown in Tables 8.2, 8.3, and 8.4, respectively. The average PM2.5 mass concentrations increase progressively as the air parcels move inland, reaching a peak concentration of 106 μg m^{-3} at Riverside on September 25, 1996. The PM2.5 mass concentration at Riverside described in Table 8.4 is almost a factor of two higher than the 24-hour average PM2.5 concentration standard of 60 μg m^{-3} recently set by the United States Environmental Protection Agency. As was the case for previous calculations conducted for Claremont, CA, during the summer of 1987 [7], non-sea salt sulfate-containing background particles advected into the Los Angeles area from over the Pacific Ocean that

subsequently have been transformed by gas-to-particle conversion processes during transit across the air basin make the largest contribution to PM2.5 concentrations at Riverside on September 25, 1996. These particles while still over the ocean were composed primarily of sulfate and ammonium ion, and they account for the majority of the particulate sulfate in the atmosphere of the South Coast Air Basin. Secondary formation of particulate sulfate does occur within the urban atmosphere; however, sulfate production within the urban atmosphere accounts for only 30-40% of the PM2.5 $SO_4^=$ concentrations observed during the 1996 episode studied here.

The overwhelming majority of PM2.5 ammonium nitrate at all three receptor sites is secondary in nature, with concentrations at Riverside accounting for 65% of the PM2.5 mass. The non-sea salt sulfate-containing background particles acquire large additions of ammonium nitrate due to atmospheric chemical reactions during transit to all sites, with significant nitrate formation also seen on particles originally released from diesel engines and non-catalyst equipped gasoline engines at the polluted Riverside site.

Tables 8.2-8.4 show that most of the particulate organic carbon at Long Beach, Fullerton, and Riverside is released as primary particles from upwind emissions sources, with secondary organic aerosol formation playing a relatively minor role during the episode studied here. Studies of Southern California during the 1980's [7, 8] showed that food cooking and diesel engines were the most significant sources of particulate organic compounds, with small contributions from gasoline-powered engines. In contrast, Tables 8.2-8.4 show that, during the 1996 episode, non-catalyst equipped gasoline-powered engines make the largest contribution to PM2.5 particulate organic compound concentrations. This is chiefly caused by the increasing emissions factors for non-catalyst equipped gasoline-powered motor vehicles as these cars get older

Table 8.2: Source Contributions to 24-hour Average PM2.5 Particulate Matter Concentrations at Long Beach, CA, September 24, 1996

Source type	PM2.5[a]	$SO_4^=$		NH_4^+		NO_3^-		Cl^-		Organics	
	(μg m^{-3})	Prim[b]	Sec[c]	Prim[b]	Sec[c]	Prim[b]	Sec[c]	Prim[b]	Sec[c]	Prim[b]	Sec[c]
Paved road dust	2.00	0.02	0.02	0.00	0.03	0.00	0.04	0.00	0.00	0.31	0.00
Other crustal material	0.56	0.00	0.00	0.00	0.00	0.00	0.01	0.00	0.00	0.01	0.00
Diesel engines	2.60	0.01	0.27	0.00	0.18	0.01	0.25	0.01	0.00	0.52	0.00
Food cooking	0.46	0.00	0.01	0.00	0.01	0.00	0.02	0.00	0.00	0.30	0.00
Catalyst gasoline engines	0.29	0.01	0.01	0.00	0.01	0.00	0.01	0.00	0.00	0.16	0.00
Non-cat gasoline engines	1.60	0.00	0.05	0.00	0.05	0.00	0.09	0.00	0.00	1.21	0.00
S-bearing fuel+ind	3.50	0.94	0.19	0.00	0.45	0.01	0.49	0.00	0.02	0.15	0.00
Other sources	2.87	0.21	0.03	0.00	0.02	0.06	0.03	0.06	0.00	1.58	0.00
NaCl initial cond.	8.43	0.00	0.12	0.00	0.51	2.26	3.54	1.38	-1.12	0.00	0.00
non-NaCl initial cond.	13.14	4.22	1.39	1.58	1.68	0.00	3.74	0.00	0.15	0.36	0.01
Total	35.45	5.41	2.09	1.59	2.93	2.34	8.20	1.46	-.95	4.61	0.02

[a] Concentration increment includes both primary particle core plus net accumulation of secondary aerosol due to atmospheric chemical reactions. Source contributions without secondary reaction products can be computed by subtracting secondary components listed in columns 3, 5, 7, 9, and 11. [b] Concentration increment due to primary particle emissions or pre-existing aerosol (μg m^{-3}). [c] Net concentration increment due to atmospheric chemical reaction within trajectories crossing the air basin (μg m^{-3}).

Table 8.3: Source Contributions to 24-hour Average PM2.5 Particulate Matter Concentrations at Fullerton, CA, September 24, 1996

Source type	PM2.5[a]	$SO_4^=$		NH_4^+		NO_3^-		Cl^-		Organics	
	(μg m^{-3})	Prim[b]	Sec[c]	Prim[b]	Sec[c]	Prim[b]	Sec[c]	Prim[b]	Sec[c]	Prim[b]	Sec[c]
Paved road dust	5.13	0.06	0.02	0.00	0.10	0.01	0.24	0.01	0.00	0.77	0.00
Other crustal material	1.55	0.00	0.01	0.00	0.02	0.00	0.06	0.00	0.00	0.04	0.00
Diesel engines	3.87	0.01	0.28	0.00	0.35	0.01	0.82	0.01	0.00	0.75	0.01
Food cooking	1.22	0.00	0.01	0.00	0.03	0.00	0.10	0.01	-.01	0.76	0.00
Catalyst gasoline engines	0.69	0.01	0.01	0.00	0.03	0.00	0.06	0.00	0.00	0.37	0.00
Non-cat gasoline engines	3.12	0.00	0.07	0.00	0.13	0.00	0.34	0.00	0.00	2.21	0.01
S-bearing fuel+ind	2.79	0.58	0.15	0.00	0.41	0.01	0.72	0.00	0.01	0.11	0.01
Other sources	1.68	0.05	0.03	0.00	0.04	0.01	0.09	0.02	0.00	0.52	0.00
NaCl initial cond.	9.14	0.00	0.10	0.00	0.87	1.90	4.66	1.16	-1.02	0.00	0.00
non-NaCl initial cond.	20.73	4.18	1.52	1.57	3.40	0.00	9.48	0.00	0.16	0.36	0.05
Total	49.91	4.91	2.20	1.58	5.39	1.95	16.57	1.21	-.86	5.88	0.09

[a] Concentration increment includes both primary particle core plus net accumulation of secondary aerosol due to atmospheric chemical reactions. Source contributions without secondary reaction products can be computed by subtracting secondary components listed in columns 3, 5, 7, 9, and 11. [b] Concentration increment due to primary particle emissions or pre-existing aerosol (μg m^{-3}). [c] Net concentration increment due to atmospheric chemical reaction within trajectories crossing the air basin (μg m^{-3}).

Table 8.4: Source Contributions to 24-hour Average PM2.5 Particulate Matter Concentrations at Riverside, CA, September 25, 1996

Source type	PM2.5[a]	$SO_4^=$		NH_4^+		NO_3^-		Cl^-		Organics	
	(μg m^{-3})	Prim[b]	Sec[c]	Prim[b]	Sec[c]	Prim[b]	Sec[c]	Prim[b]	Sec[c]	Prim[b]	Sec[c]
Paved road dust	9.07	0.09	0.04	0.00	0.46	0.02	1.43	0.01	0.00	1.15	0.03
Other crustal material	6.45	0.01	0.02	0.00	0.20	0.01	0.66	0.01	0.00	0.13	0.01
Diesel engines	13.31	0.02	0.48	0.01	2.03	0.02	6.30	0.02	0.02	1.39	0.13
Food cooking	3.79	0.01	0.03	0.00	0.36	0.00	1.20	0.02	-.01	1.53	0.03
Catalyst gasoline engines	1.75	0.02	0.02	0.00	0.17	0.00	0.55	0.00	0.00	0.62	0.01
Non-cat gasoline engines	9.72	0.01	0.13	0.00	1.20	0.00	3.91	0.00	0.02	3.76	0.10
S-bearing fuel+ind	4.80	0.47	0.16	0.00	0.89	0.01	2.40	0.00	0.01	0.12	0.03
Other sources	2.94	0.08	0.03	0.00	0.20	0.02	0.62	0.02	0.00	0.83	0.01
NaCl initial cond.	14.36	0.00	0.13	0.00	2.29	1.51	9.19	0.92	-.85	0.00	0.02
non-NaCl initial cond.	39.75	4.13	1.87	1.55	7.69	0.00	23.75	0.00	0.17	0.36	0.25
Total	105.94	4.82	2.91	1.56	15.51	1.58	50.00	1.00	-.63	9.89	0.62

[a] Concentration increment includes both primary particle core plus net accumulation of secondary aerosol due to atmospheric chemical reactions. Source contributions without secondary reaction products can be computed by subtracting secondary components listed in columns 3, 5, 7, 9, and 11. [b] Concentration increment due to primary particle emissions or pre-existing aerosol (μg m^{-3}). [c] Net concentration increment due to atmospheric chemical reaction within trajectories crossing the air basin (μg m^{-3}).

combined with reductions from newer diesel engines sold in recent years.

8.4.5 Evolution of the Ambient Aerosol During Transport Across the South Coast Air Basin

Figure 8.15 shows the evolution of the ambient aerosol size and composition distribution within approximately the same air mass as it is advected across the South Coast Air Basin surrounding Los Angeles. The primary particle contributions from different source categories are displayed separately from one another in Figure 8.15, while all sulfates, nitrates, ammonium ion, and secondary organics that have accumulated on primary particles are plotted separately. The most striking feature apparent in this figure is the large amounts of secondary ammonium nitrate that is both predicted and observed to form during transit between Fullerton and Riverside as the air parcel stagnated overnight in an area with high ammonia emissions as was explained earlier. Ambient particles with diameters greater than 2.5 μm also increase substantially between Fullerton and Riverside during the study period, and are seen to originate primarily from paved road dust and other crustal sources.

8.5 Conclusions

A comparison between air quality model predictions and pollutant concentration measurements made at three receptor sites in Southern California during September of 1996 shows that the aerosol processes photochemical trajectory model used in the current study can successfully predict the size-resolved features of the airborne particle complex at widely separated sites across the South Coast Air Basin. Calculations show that background non-sea salt sulfate-containing particles advected into Southern California from over the

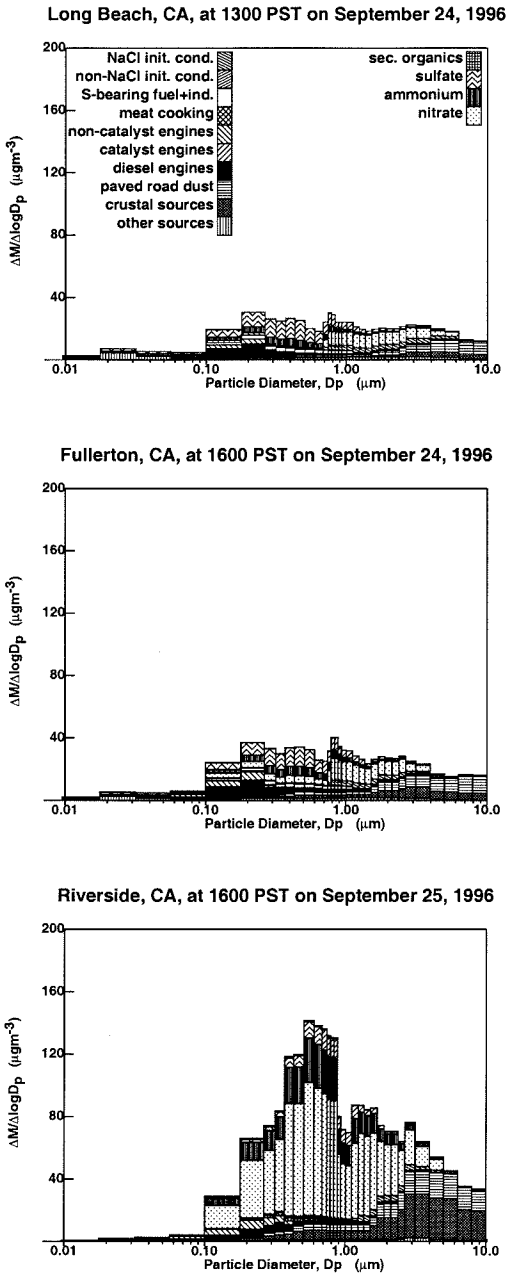

Figure 8.15:
Evolution of the calculated ambient aerosol within approximately the same air mass crossing the South Coast Air Basin of Southern California between September 24-25, 1996. The trajectory path terminating at Riverside, CA, on September 25, 1996, at 1600 PST is shown in Figure 8.1.

ocean upwind are greatly transformed by the accumulation of secondary ammonium nitrate in the urban atmosphere. These transformed background particles account for the majority of the PM2.5 mass measured throughout the South Coast Air Basin during the September 1996 episode studied here. These background sulfate particles have a size distribution centered around 0.4-0.6 μm particle diameter, making them very efficient at scattering light. As a result, it is likely that a significant portion of the visibility degradation observed throughout the study period was attributable to transformation of these non-sea salt background particles as they interact with pollutant gases in the Los Angeles atmosphere.

Bibliography

[1] Douglas R. Lawson. The Southern California Air Quality Study. *J. Air Waste Manage. Assoc.*, 40:156–165, 1990.

[2] Robert A. Harley, Armistead G. Russell, Gregory J. McRae, Glen R. Cass, and John H. Seinfeld. Photochemical modeling of the Southern California Air Quality Study. *Environ. Sci. Technol.*, 27:378–388, 1993.

[3] Spyros N. Pandis, Robert A. Harley, Glen R. Cass, and John H. Seinfeld. Secondary organic aerosol formation and transport. *Atmos. Environ.*, 26A:2269–2282, 1992.

[4] Annmarie Eldering and Glen R. Cass. Source–oriented model for air pollutant effects on visibility. *J. Geophys. Res.*, 101(D14):19343–19369, 1996.

[5] Michael J. Kleeman, Annmarie Eldering, and Glen R. Cass. Modeling the airborne particle complex as a source-oriented external mixture. *J. Geophys. Res.*, 102(D17):21355–21372, 1997.

[6] Lara S. Hughes, Jonathan O. Allen, Michael J. Kleeman, Robert J. Johnson, Glen R. Cass, Deborah S. Gross, Eric Gard, Markus Gaelli, Christopher A. Noble, D-Y Liu, P. Silva, Brad Morrical, David P. Fergenson, Tas Dienes, and Kimberly A. Prather. The size and composition distribution of atmospheric particles in southern California. *Environ. Sci. Technol.*, submitted for publication, 1998.

[7] Michael J. Kleeman and Glen R. Cass. Source contributions to the size and composition distribution of urban particulate air pollution. *Atmos. Environ.*, 32:2803–2816, 1998.

[8] Michael J. Kleeman and Glen R. Cass. Effect of emission control strategies on the size and composition distribution of urban particulate air pollution. *Environ. Sci. Technol.*, submitted for publication, 1998.

[9] William P. L. Carter. A detailed mechanism for the gas–phase atmospheric reactions of organic compounds. *Atmos. Environ.*, 24A:481–518, 1990.

[10] Anthony S. Wexler and John H. Seinfeld. Second-generation inorganic aerosol model. *Atmos. Environ.*, 25A:2731–2748, 1991.

[11] Daniel J. Jacob. Chemistry of OH in remote clouds and its role in the production of formic acid and peroxymonosulfate. *J. Geophys. Res.*, 91(D9):9807–9826, 1986.

[12] Daniel J. Jacob, Elaine W. Gottlieb, and Michael J. Prather. Chemistry of a polluted boundary layer. *J. Geophys. Res.*, 94(D10):12975–13002, 1989.

[13] Jay R. Odum, Donald Dabdub, and John H. Seinfeld. Observations on modeling and measuring ambient carbonaceous aerosol. *Environ. Sci. Technol.*, submitted for publication, 1998.

[14] Robert A. Harley, Michael P. Hannigan, and Glen R. Cass. Respeciation of organic gas emissions and the detection of excess unburned gasoline in the atmosphere. *Environ. Sci. Technol.*, 26:2395–2408, 1992.

[15] Robert A. Harley, Armistead G. Russell, and Glen R. Cass. Mathematical modeling of the concentrations of volatile organic compounds: Model performance using a lumped chemical mechanism. *Environ. Sci. Technol.*, 27:1638–1649, 1993.

[16] Michael J. Kleeman, James J. Schauer, and Glen R. Cass. Size and composition distribution of fine particulate matter emitted from mobile sources. *Environ. Sci. Technol.*, to be submitted for publication, 1998.

[17] Michael J. Kleeman, James J. Schauer, and Glen R. Cass. Size and composition distribution of fine particulate matter emitted from wood burning, meat charbroiling and cigarettes. *Environ. Sci. Technol.*, to be submitted for publication, 1998.

[18] S. Gharib and G.R. Cass. *Ammonia Emissions in the South Coast Air Basin, Open file report 84–2.* Environmental Quality Laboratory, Calif. Inst. of Technol., Pasadena, 1984.

[19] Mathew P. Fraser and Glen R. Cass. Detection of excess ammonia emissions from in-use vehicles and the implications for fine particle control. *Environ. Sci. Technol.*, 32(8):1053–1057, 1998.

[20] California Department of Food and Agriculture. *Fertiling Materials Tonage Report: July-December 1996.* Technical Report, California Department of Food and Agriculture, Sacramento, CA, 1996.

[21] United States Bureau of the Census. *1992 Census of Agriculture.* Technical Report AC92-A-5, United States Bureau of the Census, Washington, DC, 1992.

[22] William R. Goodin, Gregory J. McRae, and John H. Seinfeld. A comparison of interpolation methods for sparse data: Application to wind and concentration fields. *J. Appl. Met.*, 18:761–771, 1979.

[23] G. C. Holtzworth. Mixing depths, wind speeds, and air pollution potential for selected locations in the United States. *J. Appl. Met.*, 6:1029–1044, 1967.

[24] Gregory J. McRae. *Mathematical Modeling of Photochemical Air Pollution.* PhD thesis, California Institute of Technology, 1981.

[25] Eric Grosjean, Daniel Grosjean, Mathew P. Fraser, and Glen R. Cass. Air quality model evaluation data for organics. 2. C_1-C_{14} carbonyls in Los Angeles air. *Environ. Sci. Technol.*, 30:2687–2703, 1996.

9 Conclusion

9.1 Summary

A mechanistic air quality model has been constructed which is capable of representing the atmospheric aerosol as a source-oriented external mixture of particles. A source-oriented external mixture is created when particles are released to the atmosphere from sources having distinctly different particle size and composition distributions. Within this model, particles are allowed to age by chemical reaction in the atmosphere in a realistic fashion. Processes represented in the model include advection, turbulent diffusion, gas-phase photochemistry, diffusion of reactants and products to and from the particles, aerosol thermodynamics, heterogeneous chemical reactions within fogs, and dry deposition. This model represents the nature of particles suspended in an urban atmosphere more accurately than previous models which treat all ambient particles with the same diameter as if they have exactly the same chemical composition and which instantaneously average freshly emitted particles into the composition distribution of the aged ambient aerosol. The new aerosol processes model is applied to two air quality episodes in Southern California to study the contribution which specific emissions sources make to the size and composition distribution of suspended particulate matter at urban locations.

9.1.1 Representation of the Ambient Aerosol as a Source-Oriented External Mixture

The Lagrangian air quality model developed represents the airborne particle complex as a source-oriented external mixture. In a source-oriented external mixture, particles of the same size can evolve to display different chemical compositions that depend on the chemical and hygroscopic properties of the primary seed particles initially emitted from different sources. In contrast, previous models represent the airborne particle size distribution as an internal mixture in which all particles of the same size are assumed to have the same chemical composition. Test cases show that representation of the aerosol as an internal mixture can distort the predicted particle composition and concentration in the $HNO_3/NH_3/HCl/H_2SO_4$/aerosol $Cl^-/SO_4^=/NO_3^-/NH_4^+/Na^+$ system when Na^+ and $SO_4^=$ exist in separate particles, as may occur when sea spray coexists with long-distance transport of anthropogenic sulfates. Tests also indicate that the external mixture model can predict the evolution of a nearly monodisperse aerosol into a bimodally distributed aerosol as relative humidity increases, qualitatively matching observations. Calculations for August 28, 1987, at Claremont, CA, predict an aerosol mass distribution that is distinctly bimodal in the size range from 0.1 μm to 1.0 μm particle diameter, matching field observations at that time and place.

9.1.2 Source Contributions to Ambient Particle Size and Composition Distributions

The formulation of the mechanistic air quality model next was extended to represent the ambient aerosol as a source-oriented external mixture which is allowed to age in a more realistic fashion than can be accomplished when

fresh particle-phase emissions are averaged into the pre-existing atmospheric aerosol size and composition distribution. Particles emitted from the following source types were tracked separately through the atmosphere: catalyst-equipped gasoline engines, non-catalyst equipped gasoline engines, diesel engines, food cooking, paved road dust, crustal material from sources other than paved road dust, and sulfur-bearing particles from fuel burning and industrial processes. All remaining anthropogenic particle emissions were lumped together into an eighth category. In addition, background sea salt particles and background sulfur-containing particles (not sea salt) were tracked separately in the source-oriented external mixture. Discrete primary seed particles from each of these source types were emitted into a simulation of atmospheric transport and chemical reaction. The individual particles evolved over time in the presence of gas-to-particle conversion processes while retaining information on the initial sources from which they were emitted. Model predictions for August 28, 1987, at Claremont, CA, indicated that the observed mode in the ambient aerosol size distribution between 0.2-0.3μm particle diameter is shaped by transformed emissions from diesel engines and food cooking operations with lesser contributions from gasoline-powered vehicles and other fuel burning. The larger mode observed at 0.7-0.8μm particle diameter is due to background sulfur-containing particles which are advected into the study region and then further transformed by fog and other gas-to-particle conversion processes. Smaller contributions to the mode located at 0.7-0.8μm particle diameter are made by food cooking and by the fine particle fraction of paved and unpaved road dust.

9.1.3 Changes in Ambient Particle Size and Composition Distributions in Response to Emissions Control

The predicted behavior of the size- and chemical-composition distribution of airborne particles in the Los Angeles area was examined as it changes in response to specific emissions control strategies. Model calculations indicated that strategies currently envisioned to control the emissions of primary particles in the Los Angeles area effectively reduce the atmospheric concentrations of particles between 0.1-0.3 μm particle diameter and above 2.5 μm particle diameter but do little to reduce particulate concentrations between 0.6-0.8 μm particle diameter. Calculations revealed that particles in this size range between 0.6-0.8 μm diameter begin as water-soluble sulfur-containing background particles which are advected into the Los Angeles area from upwind and which then are transformed by significant accumulation of gas-to-particle conversion products during transport across the urban area. Control of primary particulate emissions alone does not reduce the amount of secondary aerosol which forms in the atmosphere and may even serve to redistribute this secondary material to particles with diameters that scatter light more efficiently. Combined strategies which specify control of both primary particle emissions and specific gas-phase emissions appear to provide the most effective method to reduce ambient particulate matter concentrations. The simultaneous use of all gas-phase and particle-phase emissions control measures studied here would reduce atmospheric particle concentrations by 46% at Claremont, CA, relative to the base case 1987 summer conditions.

9.1.4 Improving the Resolution of the Source-Oriented External Mixture Model

A procedure was demonstrated that greatly expands the number of sources whose contribution to ambient particle levels can be followed separately within an aerosol processes trajectory model without significantly increasing the computational burden of the problem. Particles emitted from different sources within the same general class can be differentiated from each other with this technique; for example, particles emitted by on-road diesel vehicles can be distinguished from particles emitted by diesel railroad locomotives, and particles emitted from identical sources at different locations can be distinguished from each other as well.

The method developed was illustrated by application to the air quality situation in Southern California. The contributions of more than 50 types of air pollution sources to primary particle concentrations at Claremont, CA, were separated from each other by post-processing the output from the aerosol processes trajectory model for an externally mixed aerosol developed previously by Kleeman and Cass [1, 2].

9.1.5 Particulate Matter Source Profiles for On-Road Vehicles

A dilution source sampling system was augmented to measure the size distributed chemical composition of fine particle emissions from motor vehicles. Measurements were made using an optical particle counter (OPC), a differential mobility analyzer (DMA) / condensation nucleus counter (CNC) combination, and a pair of micro-orifice uniform deposit impactors (MOUDIs). The sources tested with this system include catalyst-equipped gasoline-powered light-duty vehicles, non-catalyst gasoline-powered light-duty vehicles, and medium-duty diesel trucks. Chemical composition analysis demonstrated

that particles emitted from the gasoline-powered vehicles tested were largely composed of organic compounds while particles emitted from diesel engines contained roughly equal amounts of organic compounds and elemental carbon. The particle mass distributions from all mobile sources tested had a single mode which peaks at approximately 0.1-0.2 μm particle diameter. This result supersedes the size distribution profile for particles emitted from non-catalyst gasoline-powered vehicles in the mid-1980's as measured by Hildemann et al.[3]. The newer profile described in the current study showed a shift to smaller particle sizes which accompanies the current use of unleaded gasoline and the reduction in emissions from lead deposits in the non-catalyst vehicles' exhaust system relative to the vehicles tested in the previous work. Electronic measurements of emitted particle number concentrations indicated that diesel engines incorporating control technology designed to reduce the mass emission rate of particulate matter may in fact release greater numbers of smaller particles to the atmosphere. Particle size distribution measurements taken throughout the FTP urban driving cycle used to test all of the vehicles described in this work revealed that particulate mass emission rates and particulate size distributions from the vehicles tested here were similar during the cold start and hot start segments of the driving cycle.

9.1.6 Particulate Matter Source Profiles for Stationary Sources

A dilution source sampling system was augmented to measure the size distributed chemical composition of fine particle emissions from several stationary air pollution sources. Measurements were made using a laser optical particle counter (OPC), a differential mobility analyzer / condensation nucleus counter (DMA / CNC) combination, and a pair of micro-orifice uniform deposit impactors (MOUDIs). The sources tested with this system included

wood smoke (pine, oak, eucalyptus), meat charbroiling, and cigarettes. The particle mass distributions from all wood smoke sources had a single mode which peaks at approximately 0.1-0.2 μm particle diameter. The smoke from meat charbroiling showed a major peak in the particle mass distribution at 0.1-0.2 μm particle diameter, with some material present at larger particle sizes. Particle mass distributions from cigarettes peak between 0.3-0.4 μm particle diameter. Chemical composition analysis reveals that particles emitted from all of the sources tested were largely composed of organic compounds. Noticeable concentrations of elemental carbon were found in the particles emitted from wood burning. The size distributions of the trace species emissions from these sources also were determined, including data for Na, K, Ti, Fe, Br, Ru, Cl, Al, Zn, Ba, Sr, V, Mn, Sb, La, Ce, as well as sulfate, nitrate and ammonium ion when present in statistically significant amounts.

9.1.7 Particulate Air Pollution in Southern California in 1996

The air quality model and the new emissions measurements described in previous chapters of this work were combined to predict ambient air quality at three sites in Southern California during September of 1996. Calculations show that concentrations of primary particles released from sources such as on-road vehicles and food cooking operations have generally fallen relative to 1987 summertime conditions, but concentrations of background (non-sea salt) sulfate particles advected into the Los Angeles area remain high. These background non-sea salt particles continue to act as efficient collectors of gas-to-particle conversion products; they draw these secondary aerosol products into a particle size range that will scatter light very efficiently. Given the reduction in primary particle concentrations in the 0.1-0.2 μm size range

relative to conditions during the 1987 SCAQS experiments and maintenance of secondary aerosol growth on the non-sea salt background particles which generally peak above 0.5 μm particle diameter, the September 1996 ambient aerosol was both predicted and observed to show a single mode in its size distribution between 0.1-1.0 μm particle diameter.

9.2 Suggestions for Future Research

The results of research presented in this work reveal that non-sea salt background sulfate aerosol which is advected into the Los Angeles area acts as a principal site for the accumulation of secondary ammonium nitrate aerosol. These transformed background particles are shown to contribute significantly to the concentrations of airborne particles with diameters between 0.3-0.8 μm in the Los Angeles atmosphere. As emissions of anthropogenic primary particles are reduced through control programs, the relative contribution of the transformed non-sea salt background sulfate particles will become even more pronounced.

The effect of the presence of non-sea salt background sulfate particles will play an important role when considering how to improve visibility in the Los Angeles area, since particles with diameters close to 0.5 μm scatter visible light very efficiently. Evidence suggests (see Chapter 4) that further application of primary particle emissions controls could lead to the accumulation of additional amounts of semi-volatile ammonium nitrate onto the non-sea salt sulfate background particles. Light scattering calculations should be performed to calculate the contribution which transformed non-sea salt background particles make to visibility reduction in the Los Angeles area and to calculate how different emissions control strategies could be expected to affect visibility.

Future work should attempt to identify the initial source(s) of the background sulfate particles, so that the factors which control pollutant concentrations in the Los Angeles atmosphere can be better understood. There are several possible sources of these particles. Ships at sea typically burn high-sulfur content fuel along the California coastline. Gaseous SO_2 contained in the emissions from these ships is oxidized over time to form sulfate aerosol that will contribute in some part to the background particulate sulfate concentrations observed. It is also possible that high sulfur content fuel burned on-shore (but outside the South Coast Air Basin surrounding Los Angeles) leads to the formation of anthropogenic sulfate aerosol which is advected out over the ocean and then circulated into the Los Angeles atmosphere by large scale weather patterns. Finally, biological activity in coastal surface waters has been shown to produce dimethyl sulfide which is oxidized in the atmosphere to form sulfate aerosol.

Recently, aerosol time of flight mass spectrometers (ATOFMS) have been developed which are able to measure the size and composition of individual airborne particles [4]. With such instruments, it is possible to more accurately characterize the types of particles in the atmosphere because information describing the heterogeneity of particle composition at the same particle size can be obtained directly. The modeling tools which have been developed in the present research represent the atmospheric aerosol as a source-oriented external mixture which also tracks the aerosol as a countable number of discrete particles that have different chemical compositions at the same physical diameter. By using these new measurement and modeling techniques together, it will soon be possible to compare both predictions and direct observations of the size and composition of atmospheric particulate matter at the single particle level. The 1996 field study that formed the basis of the

model evaluation effort reported in Chapter 8 of this work included single particle measurements taken by aerosol time of flight mass spectrometers that will form the basis for such a comparison in the near future.

Eulerian implementations of photochemical aerosol processes air quality models provide increased spatial and temporal resolution at the cost of a larger computational burden relative to Lagrangian models. As the power of computer systems continues to increase, however, it will soon be feasible to perform detailed calculations for source-oriented externally mixed atmospheric aerosols such as those described in the present work using a grid-based model.

Bibliography

[1] Michael J. Kleeman and Glen R. Cass. Source contributions to the size and composition distribution of urban particulate air pollution. *Atmos. Environ.*, 32:2803–2816, 1998.

[2] Michael J. Kleeman and Glen R. Cass. Effect of emission control strategies on the size and composition distribution of urban particulate air pollution. *Environ. Sci. Technol.*, submitted for publication, 1998.

[3] Lynn M. Hildemann, Gregory R. Markowski, Michael C. Jones, and Glen R. Cass. Submicrometer aerosol mass distributions of emissions from boilers, fireplaces, automobiles, diesel trucks, and meat–cooking operations. *Aerosol Sci. Technol.*, 14:138–152, 1991b.

[4] Christopher A. Noble and Kimberly A. Prather. Real-time measurement of correlated size and composition profiles of individual atmospheric aerosol particles. *Environ. Sci. Technol.*, 30(9):2667–2680, 1996.